Characterization, Structure and Mechanism of Sulfide:quinone oxidoreductase (SQR) from *Acidithiobacillus ferrooxidans*

by

Yanfei Zhang

A thesis submitted in partial fulfillment of the requirements for the degree of

Doctor of Philosophy

Department of Biochemistry
University of Alberta

Abstract

A key enzyme in maintaining sulfide homeostasis is the membrane-associated flavoenzyme sulfide:quinone oxidoreductase (SQR) found in nearly all domains of life (except plants). SQR maintains a critical equilibrium between sulfide (H_2S, HS^- and S^{2-}) and elemental sulfur (S^0), coupling the oxidation of sulfide to the reduction of ubiquinone via a non-covalent FAD cofactor. SQR interacts with the membrane via two amphipathic helices and the Q-pool through a conserved hydrophobic domain. The active site of SQR includes three cysteines (Cys160, Cys356 and Cys128) and the FAD in close juxtaposition to the ubiquinone binding site. To understand the sulfide oxidation mechanism, we expressed the wild-type *sqr* gene from *Acidithiobacillus ferrooxidans,* as well as several variants of conserved, catalytically important amino acids in *E. coli* BL21(DE3) and purified soluble, active, His-tagged SQR. The purified wild-type SQR and the variants were subjected to extensive kinetic (pre-steady state and steady state) and structural analysis (X-ray crystallography). We also monitored SQR activity *in vivo* by detecting the H_2S produced by growing *E. coli* transformed with wild-type and variant SQR. Our catalytic activity analysis and structural determination led us to propose two alternative mechanisms: (1) A nucleophilic attack mechanism that involves Cys356–S–S^- as a nucleophile which attacks the C^{4A} atom of FAD; or (2) A radical mechanism of direct electron transfer from Cys356 disulfide to FAD. The growing polysulfide is held between Cys160 and Cys356. The role of Cys128 (most likely in the form of a disulfide) is confined to the release of the polysulfur product. We further investigated the role of the FAD and the conserved Cys and His residues using a combination of kinetics and EPR spectroscopy. Using steady state kinetics of Na_2S-dependent decylubiquinone (DUQ) reduction we measured a k_{cat} of 6.5 s^{-1} and a K_m (Na_2S) of 3.0 mM and a K_m (DUQ) of 3.4 mM. Variants of Cys160, Cys356 and His198 had greatly

diminished DUQ reduction activity whereas variants of Cys128 and His132 were less affected. A neutral flavin semiquinone was observed in the EPR spectrum of SQR reduced with Na_2S which was enhanced in the Cys160Ala variant suggesting the presence of a Cys356-S^{γ}-S-C^{4A}-FAD adduct. Potentiometric titrations of the FAD semiquinone revealed an midpoint potential (E_m) of -139 ± 4 mV at pH 7.0 in wild-type SQR. The E_m of the FAD in $SQR^{Cys160Ala}$ (E_m= -135 ± 5 mV) is similar to that in wild-type SQR. We also combined computational docking and kinetic approaches to analyze quinone binding. SQR can reduce both benzoquinones and naphthoquinones. The alkyl side chain of ubiquinone derivatives enhances binding to SQR but limits the enzyme turnover. Pentachlorophenol and 2-*n*-heptyl-4-hydroxyquinoline-*N*-oxide are potent inhibitors of SQR with apparent inhibition constants (K_i) of 0.46 μM and 0.58 μM, respectively. The highly conserved amino acids surrounding the quinone binding site play an important role in quinone reduction. The phenyl sidechains of Phe357 and Phe391 sandwich the benzoquinone head group and are critical for quinone binding. Importantly, conserved amino acids that define the ubiquinone-binding site also play an important role in flavin reduction.

Preface

This thesis is an original work by Yanfei Zhang (YZ) under the supervision of Dr. Joel H. Weiner (JHW). As the primary author for the following manuscripts, YZ prepared the majority of the materials, executed and analyzed all experiments with collaborator Maia M. Cherney (MMC, the crystal structure part). YZ and JHW designed the experiments and prepared the following manuscripts with collaborators MMC and Michael N. G. James (MNGJ).

Chapter 2 of this thesis has been published as Cherney, M. M.*, Zhang, Y.*, Solomonson, M., Weiner, J. H., and James, M. N. G. (2010) Crystal structure of sulfide:quinone oxidoreductase from Acidithiobacillus ferrooxidans: insights into sulfidotrophic respiration and detoxification. *J Mol Biol* **398**, 292–305. MMC and YZ contributed equally to this study. Matthew Solomonson contributed to gel filtration chromatography and FPLC support.

Chapter 3 of this thesis has been published as Cherney, M. M., Zhang, Y., James, M. N. G., and Weiner, J. H. (2012) Structure-activity characterization of sulfide:quinone oxidoreductase variants. *J. Struct. Biol.* **178**, 319–328. YZ executed the construction, expression, purification and enzymatic activity assay of SQR variants. YZ also partially contributed to the crystallization, data collection and structure refining under the guidance and help from MMC.

Chapter 4 of this thesis has been published as Zhang, Y., and Weiner, J. H. (2014) Characterization of the kinetics and electron paramagnetic resonance spectroscopic properties of Acidithiobacillus ferrooxidans sulfide:quinone oxidoreductase (SQR). *Arch. Biochem. Biophys.* **564**, 110–119. YZ executed the experiments. YZ and JHW designed the experiments and prepared the manuscript.

Chapter 5 of this thesis has been published as Zhang, Y., and Weiner, J. H. (2014) A simple semi-quantitative in vivo method using H_2S detection to monitor sulfide metabolizing enzymes. *Biotech.* **57**, 208–210. YZ carried out the experiments, performed the data analysis, and drafted the manuscript. JHW conceived of the study, supervised the research and helped to draft the manuscript.

Chapter 6 of this thesis has been submitted for publication as Zhang, Y., Qadri, A. and Weiner, J. H. (2014) The Quinone-Binding Site of *Acidithiobacillus ferrooxidans* Sulfide:Quinone Oxidoreductase Controls both Flavin and Quinone Reduction. Ali Qadri, as a summer student under the supervision of YZ and JHW, contributed to the construction, expression, purification and enzymatic activity assay of several SQR variants.

Acknowledgments

First and foremost, I would like to thank my supervisor Dr. Joel H. Weiner for his guidance and support during my years in the lab. Dr. Weiner is an outstanding mentor. He has been motivational and inspirational towards my research and academic training. I am especially grateful for his help in developing my scientific writing and public presentation skills. Over the years, his wisdom, patience, understanding, encouragement and support were greatly appreciated.

I would also like to give a big thank you to Dr. Richard Rothery, who not only taught me how to perform EPR experiments, but also inspired me to taste many outdoor sports and leisure activities. I want to acknowledge Dr. Maia M. Cherney for her contributions to this project, especially in the field of protein crystallography.

I would also like to thank Justin Fedor, Huipo Tang, Glen Zhang and Sally Wu for numerous meaningful comments and discussions. I would also like to thank Gillian McCuaig, Nasim Boroumand, Matt Solomonson, Francesca Sebastian, Michelina Kierzek, Shannon Murphy, Dr. Maryam Zarepour, Dr. Francois Chartier, Dr. Victor Cheng and Dr. Quang Tran for being wonderful co-workers and making my time in the lab enormously enjoyable and memorable. I want to thank my two summer students Peter (Jingyang) Xu and Ali Qadri for their participation in my research project, and for giving me valuable experience in trainee supervision.

I would also like to acknowledge my supervisory committee, Drs. Joanne Lemieux and Mark Glover. Thank you all for your help, guidance and suggestions over the years. I want to thank the Department of Biochemistry at the University of Alberta for a truly wonderful graduate student experience.

Finally, and most importantly, I want to thank my family. I thank my parents and parents-in-law who gave me their trust, patience and ever-lasting support. Thank you all and I love you all! I thank my son Alex for being my exceptional most successful gene recombination experiment ever; and my wife Qiqi, who has always been by my side through the ups and downs of life as a graduate student. Thank you for your support, encouragement and understanding of my weekend and late night experiments.

Table of Contents

List of Tables

List of Figures

List of Abbreviations

AMD	acid mine drainage
ANSO	anthraquinone sulfonate
At. f or *A. ferrooxidans*	*Acidithiobacillus ferrooxidans*
ATCC	American Type Culture Collection
ATP	adenosine 5'-triphosphate
DDM	n-dodecyl-ß-D-maltoside
DHBQ	2,5-Dihydroxy-1,4-benzoquinone
DNA	deoxyribonucleic acid
DSR	disulfide oxidoreductase family
DUQ	decylubiquinone
e^-	electron
E. coli	*Escherichia coli*
EDTA	ethylenediaminetetraacetic acid
E_h	actual redox potential at a defined pH (mV)
E_m	redox potential
$E_{m,7}$	redox potential at pH7
EPR	electron paramagnetic resonance
FAD/$FADH_2$	flavin adenine dinucleotide (oxidized/reduced)
FCC or FCSD	flavocytochrome c:sulfide dehydrogenase
FMN	flavin mononucleotide
FPLC	fast performance liquid chromatography
H_2S	Hydrogen sulfide
HOQNO	2-*n*-heptyl 4- hydroxyquinoline-*N*-oxide
IPTG	isopropyl β-D-1-thiogalactopyranoside
KBr	potassium bromide
k_{cat}	turnover number
kDa	kilodalton
K_i	apparent inhibition constants
K_m	Michaelis constant

LB	Luria Bertani
MALDI-TOF	matrix-assisted laser desorption/ionisation-time of flight
MOPS	3-(N-morpholino)propanesulfonic acid
NAD	Nicotinamide adenine dinucleotide
OD	optical density
PCP	pentachlorophenol
PCR	polymerase chain reaction
PDB	Protein Data Bank
PMSF	phenylmethylsulfonyl
Q	quinone
Q-pool	quinone pool
Q-site	quinone binding site
r.m.s.d.	root means quare deviation
ROS	reactive oxygen species
SDS-PAGE	sodium dodecyl sulfate polyacrylamide gel electrophoresis
SQR	sulfide:quinone oxidoreductase
TB	Terrific Broth
TCA	trichloroacetic acid
TTFA	thenoyltrifluoroacetone
UQ/UQH2	ubiquinone(oxidized)/ubiquinol(reduced)
UV-VIS	ultraviolet-visible
V_{max}	maximal activity
WT	wild-type

Chapter 1: General Introduction

1.1 Sulfide

1.1.1 Physical and chemical properties of sulfide

Sulfide was first chemically identified by the Swedish Pomeranian pharmaceutical chemist Carl Wilhelm Scheele (1742 - 1786) in 1777 [1; 2]. It exists in three different forms: two anionic forms—— sulfide (S^{2-}), hemisulfide (HS^-) and the gas form—— Hydrogen sulfide (H_2S), which is well-known by its toxic rotten egg smell. H_2S is soluble in water with a solubility of 100 mM atm^{-1} at 25 °C or 80 mM atm^{-1} at 37 °C [3; 4; 5]. H_2S also exhibits a high lipophilicity and is twice as soluble in a lipid membrane compared to water with a partition coefficient ($K_p^{membrane/water}$) of 2.0 ± 0.6 [6] at 25 °C. The higher membrane solubility indicates that H_2S is membrane permeable with the permeability coefficient (P_m) of 3 cm s^{-1} [3]. Aqueous H_2S is also volatile and weakly acidic. Therefore, H_2S equilibrates between the gas phase and the aqueous phase ($H_2S_{(gas)} \rightleftarrows H_2S_{(aqueous)}$). In aqueous solutions, H_2S equilibrates with its anions S^{2-} and HS^- ($H_2S_{(aqueous)} \rightleftarrows HS^- + H^+ \rightleftarrows S^{2-} + 2H^+$). The reported p$K_{a1}$ ranges from 6.97 to 7.06 at 25 °C [4]. Similarly, the published value of pK_{a2} is >12 at 25 °C [5]. At the physiological pH of 7.4, total sulfide distributes 72% as HS^- and 28% as H_2S. At pH 3.8, sulfide solutions can be considered 100% H_2S, as only 0.06% is in the form of HS^- [3]. The high pK_{a2} value indicates that S^{2-} is insignificant in acidic and physiological solutions. In this thesis the term "sulfide" will refer to the total sulfide present in solution including the three different forms: H_2S, HS^- and S^{2-}. The species H_2S, SH^- and S^{2-} will be named specifically as necessary.

Sulfide is a reductant with the lowest oxidation state (-2) of sulfur. Its standard redox potential ($E_{m,7}$) is -270 mV [6]. The bond dissociation energy of the S−H bond in sulfide is 90 kcal/mol [7], which is consistent with that of the S-H bond in thiols (RSH, 92 kcal/mol) [10]. Like thiolate (RS^-), anionic HS^- is also a nucleophile and can initiate chain reactions such as

thio/disulfide exchange (HS^- + R−S−S−R′ → RSS^- + R′SH or $R'SS^-$ + RSH) and protein S-sulfhydration (Cys-SH + HS^- → Cys-SSH) [4; 8; 9; 10]. Hence, the reductive and nucleophilic properties of sulfide are the most principal aspects of sulfide chemistry. It readily engages in 1 and 2 electron redox reactions with oxidants, metals and thiol derivatives. In addition, sulfide radical species (sulfhydryl radicals: $HS^{\bullet}$ / $S^{\bullet-}$) are formed in 1 electron oxidation reactions. The radical species are highly reactive and can initiate chain reactions as well [11].

1.1.2 Biological and physiological aspects of sulfide

Sulfide is involved in a variety of biological processes. In mammals, it is considered as a very toxic molecule, which inhibits mitochondrial ATP production at micromolar concentrations [12]. However, at lower concentrations, sulfide can be used as an electron donor and an energy source through the sulfide oxidation pathway that involves a sulfide quinone oxidoreductase [13; 14]. Interestingly, sulfide is also a newly found signal molecule that takes part in the cell signaling which affects inflammation and cell protection [15; 16]; sulfide also affects ion channels [17], blood pressure and other systemic responses in blood vessels, heart, and nerves [18; 19]. Maintaining the homeostasis of sulfide is a key in deciding whether sulfide is a toxic component or a useful molecule. Several enzymes are involved in sulfide production and removal.

Sulfide is toxic

Sulfide is considered to be toxic for animals and humans due to its inhibitory effect on cytochrome c oxidase, which is the terminal electron acceptor of the mitochondrial respiratory chain. The inhibition, attributed to the binding of sulfide to ferric heme and CuB, is non-competitive towards to either cytochrome c or oxygen [20; 21]. It was reported that respiration of isolated mitochondria or intact cells was inhibited 50% at 10 μM and ~30 μM sulfide,

respectively [22; 23]. However, there is no evidence as yet that endogenous sulfide significantly inhibits respiration *in vivo* [12]. The toxic effects of sulfide are most likely to result from inhalation, which initially causes a loss of sense of smell and consequently becomes serious. Our noses can detect H_2S at concentrations of only 0.0047 part per million (ppm); At 100 ppm, it breaks the olfactory system after 3-5 minutes exposure; At 300 ppm, it breaks breathing; Exposure to 800 ppm for just 5 minutes will lead to death [24].

Sulfide is an energy source

Sulfide in the environment is oxidized by many chemolithotrophic prokaryotes (*e.g. Acidithiobacillus ferrooxidans*, see section 1.3) for both respiration and/or fixation of CO_2 into organic carbon [25]. Oxidation of sulfide (to SO_4^{2-}) can provide up to eight electrons for energy conservation. In practice, microbes that have the sulfur/sulfide-metabolizing trait are used widely in sulfide mineral biomining operations [26]. Additionally, at low concentrations, sulfide is also a substrate for the mitochondrial respiratory chain. It contributes to ATP production by directly donating electrons, and indirectly stimulating oxygen consumption and increasing membrane potential [27; 28].

Sulfide is a signal molecule

In recent years, sulfide has been identified as the third gas signal molecule (also termed as gasotransmitter or gasomediator) along with carbon monoxide (CO) and nitric oxide (NO), and plays prominent roles in cellular physiology and pathophysiology including the regulation of vascular homeostasis, inflammation, apoptosis and cellular stress response. Reports on the biological and physiological effects of sulfide have accumulated in recent years but insights into the mechanism of the cell signaling activity of sulfide are lacking. By analogy with the mechanisms of other gas signal molecules, several possible mechanisms were proposed. The S-

sulfhydration of reactive cysteine residues in target proteins, by yielding a hydropersulfide moiety (Cys–SSH), was recognized as a major mechanism of sulfide signaling [10]. The other proposed alternative mechanisms are modification of prosthetic groups (heme, Cu) of metalloproteins [29], interaction with reactive oxygen species (ROS) [29], interaction with NO & participation in S-nitrosylation of protein [30] and interaction with electrophilic lipid derivatives such as 4-hydroxynonenal which is a strong modulator of oxidative stress, cell proliferation and apoptosis [31].

1.1.3 Endogenous sulfide synthesis and metabolism

Sulfide synthesis

In cells and tissues, sulfide is endogenously produced from cysteine and/or homocysteine by sulfide-generating enzymes (**Figure 1.1**), e.g. cystathionine β-synthase (CBS, EC 4.2.1.22), cystathionine γ-lyase (CSE, EC 4.4.1.1), 3-mercaptopyruvate sulfurtransferase (3-MST, EC 2.8.1.2) teamed with cysteine aminotransferase (CAT, EC 2.6.1.3), cysteine lyase (EC 4.4.1.10) and cysteine desulfurase (IscS or NifS, EC 2.8.1.7) [32; 33; 34; 35]. In prokaryotes, sulfur/polysulfide reductase (EC 1.12.98.4), sulfite reductases (EC 1.8.99.1) and other sulfur metabolism enzymes are involved in generating sulfide. Apart from enzymatic synthesis, non-enzymatic sulfide production is also possible. The pathways include direct reduction of glutathione, elemental sulfur and thiosulfate.

Sulfide catabolism

Sulfide is membrane permeable and highly diffusible in its gas form (H_2S) [3]. The produced sulfide can be removed (or stored) as sulfane-bound sulfur, which is the storage intermediate for sulfide and in turn may release sulfide when cells are under certain

physiological conditions [36]. Sulfide:quinone oxidoreductase (SQR, EC 1.8.5.4), acting as a sulfide remover, catalyzes the oxidation of sulfide to elemental sulfur (polysulfide or octasulfur rings) [37]. Thiol S-methyltransferase (TMT, EC 2.1.1.9) and thiosulfate:cyanide sulfurtransferase (Rhodanese, EC 2.8.1.1) are also involved in removing sulfide via methylation and oxidation, respectively [38; 39].

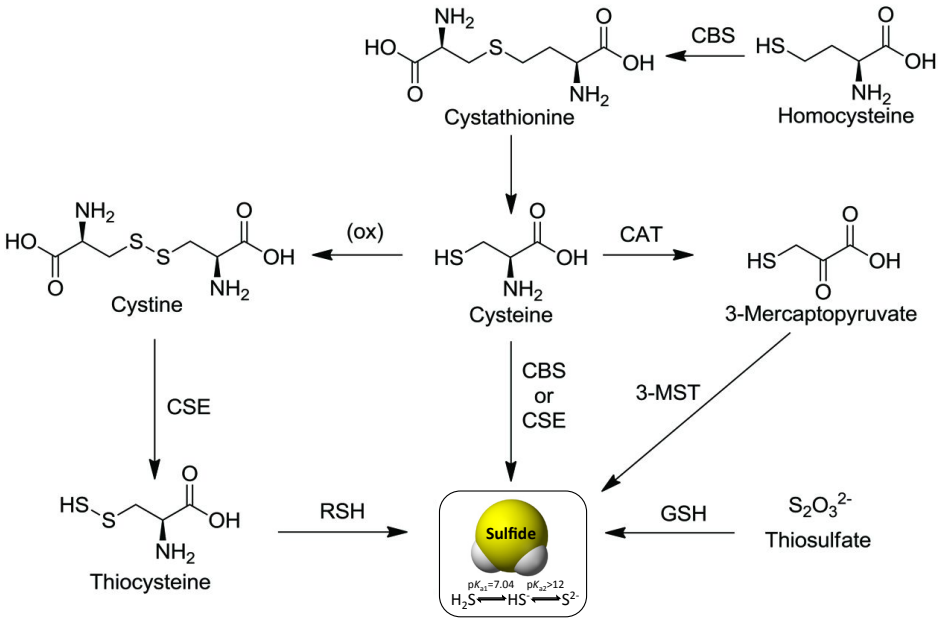

Figure 1.1 Biosynthetic pathways for endogenous sulfide formation in mammalian cells. CAT, cysteine aminotransferase; CBS, cystathionine β-synthase; CSE, cystathionine γ-ligase; 3-MST, 3-mercaptopyruvate sulfurtransferase; RSH, thiol. This figure is adapted and modified from Pluth *et al.*, 2013 [40]

1.2 Quinone

Quinones, the most important lipophilic electron and proton carriers, shuttle electrons and protons between respiratory enzymes via the membrane-bound quinone pool. Quinone/quinol undergoes reversible oxidation-reduction with the release or consumption of $2e^-/2H^+$ via formation of an intermediate radical semiquinone (**Figure 1.2**). The reduced form of the quinone is more polar and the quinol head group is thought to preferentially localize in the polar interphase of the lipid membrane.

Quinones are commonly named with a prefix that indicates the parent aromatic hydrocarbon (*e.g.* "benzo-" for benzene, "naphtho-" for naphthalene, "anthra-" for anthracene) [41]. Different types of natural quinones, comprising mainly benzoquinones, naphthoquinones, anthraquinones and polycyclic quinones, are widely distributed in different organisms (**Figure 1.3**). Animals and plants use ubiquinones (1,4-benzoquinones or *p*-benzoquinone) in their mitochondrial membrane quinone-pool, while bacteria use a mixture of quinones including ubiquinones, naphthoquinones and the derivatives menaquinone and rhodoquinone for the bioenergetic reactions. The distribution of the redox potentials ($E_{m,7}$) of quinones and derivatives range from ~ -400 mV for the non-physiological anthraquinones to ~ +110 mV for the physiological ubiquinones [42]. In general, the redox potential of quinones decreases with the increase of the condensation degree of aromatic rings (the proportion of the condensed aromatic C). A significant shift of the redox potential can be caused by hydroxylation or methylation on the quinone motif. e.g. duroquinone ($E_{m,7}$ = +7 mV), menadione ($E_{m,7}$ = -12 mV), lawsone ($E_{m,7}$ = -119 mV) and plumbagin ($E_{m,7}$ = -40 mV) [43].

Ubiquinone (UQ, also called Coenzyme Q) is a 1,4-benzoquinone and is constituted of a polar head group and a hydrophobic prenyl side chain. The length of the side chain varies among microorganisms from 0 to 12. UQ homologues are soluble in ethanol and most organic solvents but not in water due to their hydrophobic isoprenoid side chains. UQ absorbs light in the ultraviolet region with a maximum at 275 nm in ethanol when in the oxidized form (extinction coefficient $\varepsilon_{275\text{-}Oxi}$= 15 $mM^{-1}\cdot cm^{-1}$) [44]. Coenzyme Q_{10} (CoQ_{10} or UQ_{10}, 2,3-Dimethoxy-5-methyl-6-decaprenyl-1,4-benzoquinone) was discovered to be an essential component of respiratory and photosynthetic chains in most eukaryotes (primarily in mitochondria) and prokaryotes. Its 50-carbon hydrocarbon side chain renders UQ_{10} highly hydrophobic. Therefore, the less

hydrophobic, commercially available analog decylubiquinone (DUQ, 2,3-Dimethoxy-5-methyl-6-decyl-1,4-benzoquinone) (**Figure 1.4**) has been utilized in many *in vitro* experimental studies.

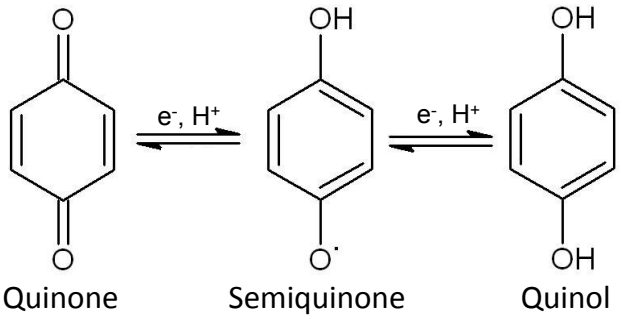

Figure 1.2 The two steps of quinone reduction/quinol oxidation.

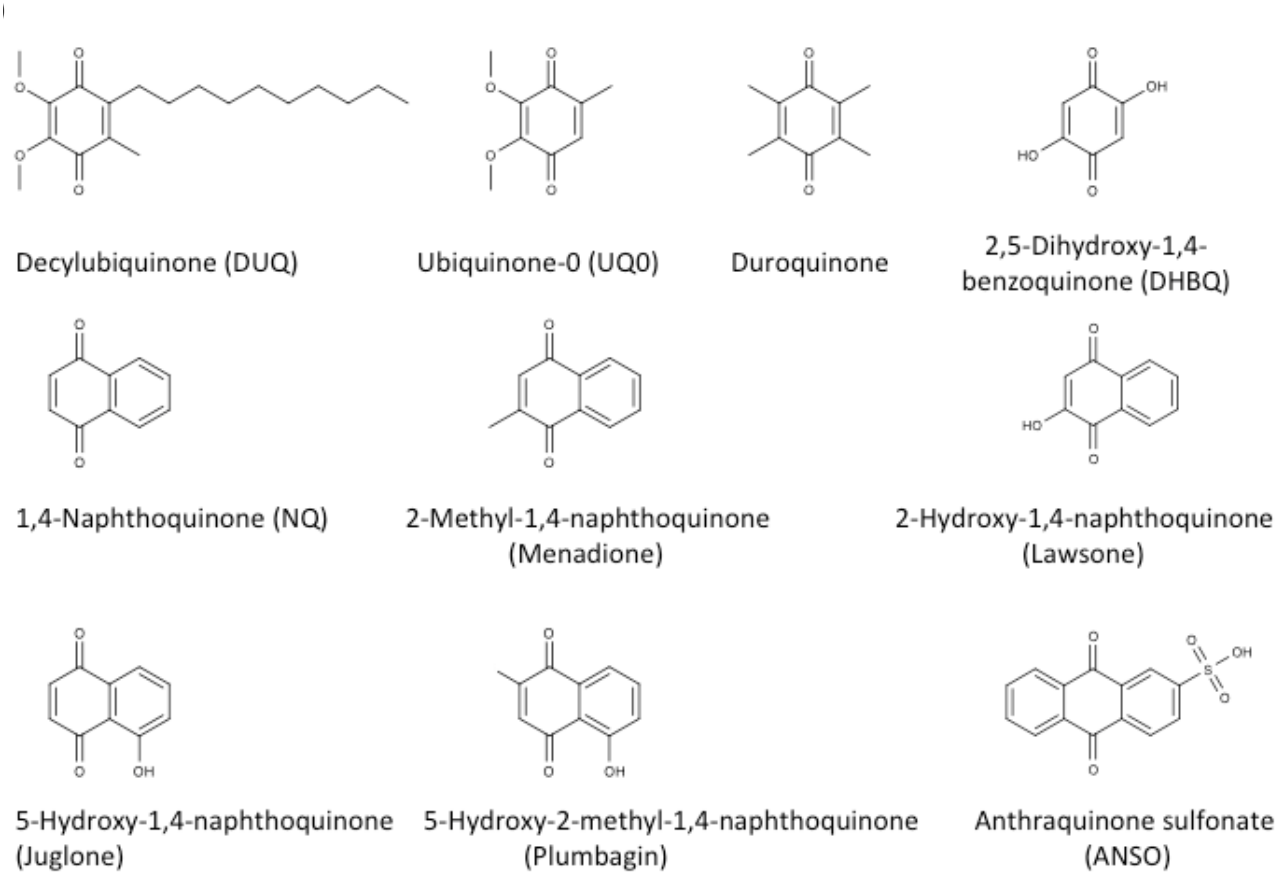

Figure 1.3 Chemical structures of quinones and quinone analogs.
The image was created using the MarvinSketch software package (http://www.chemaxon.com).

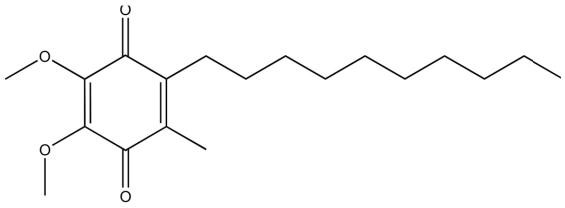

Decylubiquinone (DUQ)
($C_{19}H_{30}O$)

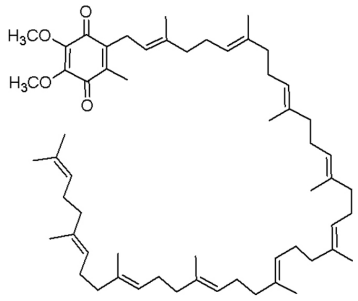

Coenzyme Q_{10}
($C_{59}H_{90}O_4$)

Figure 1.4 Decylubiquinone (DUQ) and Coenzyme Q_{10} (UQ_{10})

1.3 *Acidithiobacillus ferrooxidans*

Acidithiobacillus ferrooxidans (*A. ferrooxidans*, formerly known as *Thiobacillus ferrooxidans* [45]) is a motile, rod-shaped, Gram-negative, acidophilic, mesophilic, chemolithotrophic γ-proteo-bacterium with optimum growth at 30 °C and pH 2.0 [46]. Phylogenetically, it is affiliated with genus *Acidithiobacillus* in the family of *Acidithiobacillaceae*. This organism is usually found in acid environments such as mine dumps, coal deposits and acid mine drainage (AMD) [47]. It participates in one of the key roles of microbial communities by taking part in the bacterial chemical processes of bioleaching or biomining and contributes to the biogeochemical solubilization and recycling of metals and nutrients [48; 49; 50]. It derives energy for growth mainly from oxidative respiration using reduced inorganic compounds such as Fe^{2+}, H_2S, S^{2-} and S^0 that are present in surrounding ores [51]. The major by-products of these energy transductions are ferric iron (Fe^{3+}) and sulfuric acid, which can mobilize and solubilize metals (e.g. copper, zinc and arsenic) in the environment via chemical oxidation [52; 53].

Acidithiobacillus ferrooxidans has been studied as a model organism for probing life in extremely acidic environments, investigating the mechanism of bioleaching and studying the

metabolic mechanism involved including the assimilation and homeostasis of iron, sulfur and sulfide. Studying *A. ferrooxidans* also offers insights into the ancient ways of life in euxinic (sulfidic), acidic Archaean locations and the origin of life [53]. Additionally, *A. ferrooxidans* has been proposed as a potential biomarker to be used when searching for the evidence of extraterrestrial life on a planet other than Earth [53; 54].

The type strain *A. ferrooxidans* ATCC 23270^T, was isolated and descripted by William W. Leathen, Norma A. Kinsel and S. A. Braley in 1954 [55; 56]. Since then, there has been great interest in *A. ferrooxidans* ATCC23270^T due to its participation in bioleaching or biomining processes. Its whole genome sequence was determined and annotated by The Institute for Genomic Research (TIGR, merged into the J. Craig Venter Institute in 2006) in 2003. The genome of *A. ferrooxidans* ATCC 23270^T consists of a single circular chromosome of 2.98×10^6 bp with a G+C content of 58.77% [53]. *A. ferrooxidans* is a chemolithoautotrophic bacterium, it derives energy mainly from the oxidation of ferrous iron (Fe^{2+}) and reduced inorganic sulfur compounds (RISCs). The metabolism models of ferrous iron and RISCs are firstly proposed by a bioinformatics-based genomic analysis and further confirmed and extended by proteomics analysis, quantitative RT-PCR analysis and microarray-based transcriptional profiling experiments (**Figure 1.5**) [53; 57; 58; 59].

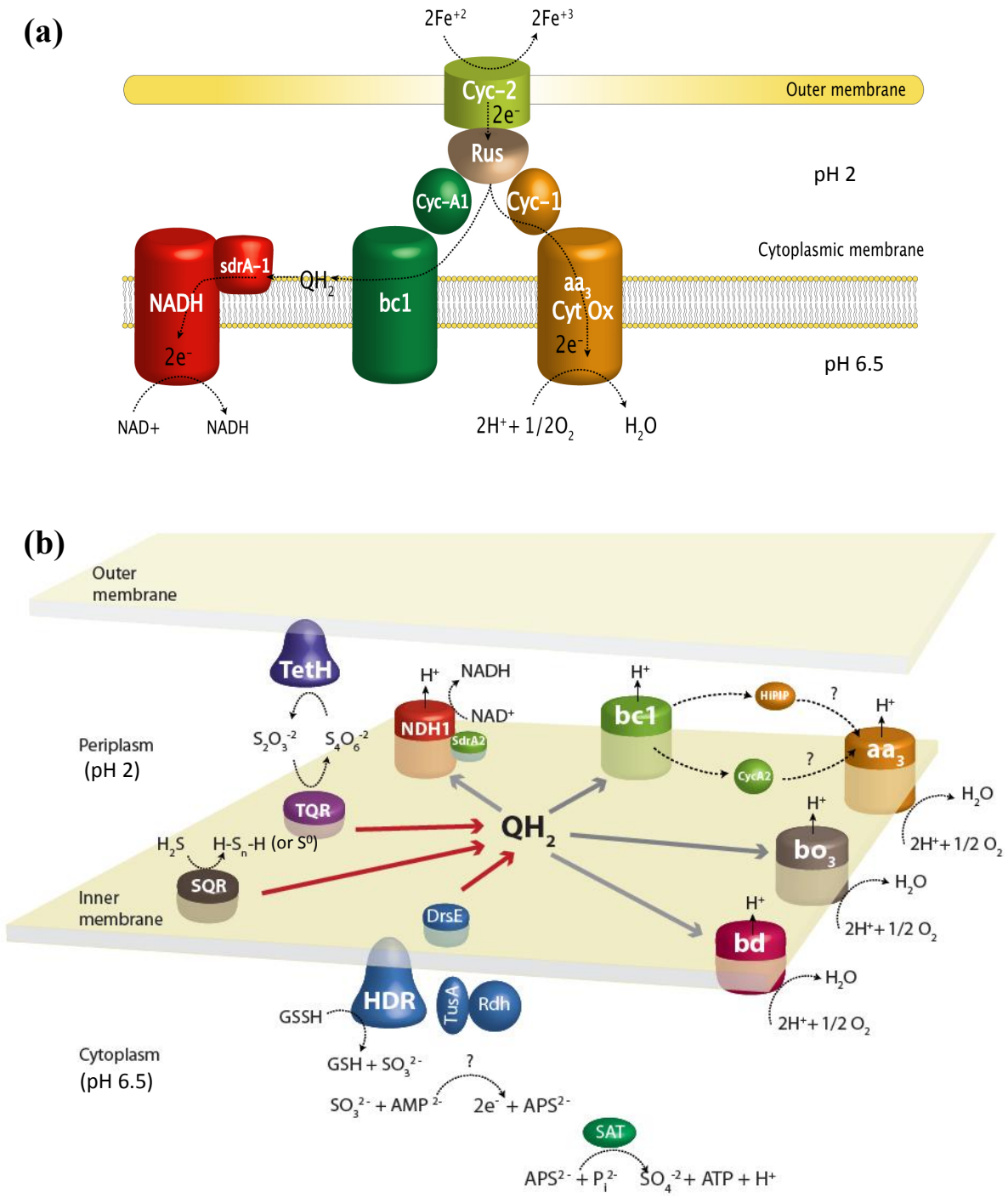

Figure 1.5. Metabolism model of the oxidation of Fe^{2+} (a) and sulfur oxidation (b) in *A. ferrooxidans* ATCC 23270 [53; 59].
The Figures are adapted from Valdés J. *et al.*, 2008 and Quatrini R. *et al.*, 2009 [53; 59].

(1) Metabolic model of the oxidation of Fe^{2+} in *A. ferrooxidans* ATCC 23270

A. ferrooxidans oxidizes Fe^{2+} to Fe^{3+} ($E_{m,2}$ = +770 mV) in acidic environment (pH 2) where Fe^{2+} is soluble and chemical oxidation is much slower than at pH 7. The oxidation of Fe^{2+} occurs at the interface of the cell membrane and the solution environment, where an outer membrane cytochrome *c* (Cyc2) oxidizes Fe^{2+} to Fe^{3+}. The electrons derived from Fe^{2+} oxidation are first transferred to a periplasmic soluble blue copper protein rusticyanin (Rus). From this branch point, some of the electrons are transferred "downhill" to oxygen ($E_{m,7}$ = +1229 mV) through a periplasmic c-cytochrome (Cyc1) and an aa_3-type cytochrome oxidase (aa_3 Cyt Ox). Alternatively, a small proportion of the electrons feed the "uphill electron pathway" to NAD^+ ($E_{m,7}$ = -320 mV) via *c*-cytochrome CycA1, *bc*1 complex, the quinone pool and NADH dehydrogenase (**Figure 1.5a**) [37]. The energy to accomplish the "uphill electron transfer" comes from the proton motive force that naturally occurs across the inner membrane of *A. ferrooxidans*. The pH of the cytoplasm of *A. ferrooxidans* is about pH 6.5. The pH of the periplasmic space of *A. ferrooxidans* is about pH 2.0. The large pH gradient is balanced by a membrane potential (positive inside the cell) [60].

(2) Metabolic model of sulfur oxidation in *A. ferrooxidans* ATCC 23270

Sulfur, due to the existence of the low-lying empty 3d orbital, has multiple oxidation states ranging from -2 to +6. It forms various compounds with most elements except the noble gases. Therefore, the metabolic pathways for sulfur and reduced inorganic sulfur compounds (RISCs) oxidation are more complicated than those for Fe^{2+} oxidation in *A. ferrooxidans*. Various enzymes, redox complexes and a number of electron carriers located in different cellular compartments are proposed to be involved in the oxidation of sulfur and RISCs (**Figure 1.5b**) [53; 59]. Sulfide quinone oxidoreductase (SQR) oxides the sulfide compounds H_2S, HS^- and S^{2-} to

soluble polysulfide chains (H-S_n-H) or to elemental sulfur (S^0) in the form of octasulfur rings [61; 62]. Elemental sulfur (S^0) is poorly soluble in water and cannot enter the cell. It was proposed that extracellular elemental sulfur (S_8) is first converted and mobilized to glutathione persulfide (GSSH) or persulfide sulfane sulfur by special outer-membrane proteins [61]. Sulfur also shows a very great tendency to catenate in all sorts of compounds, e.g. polysulfide ions (S_2^{2-}, S_4^{2-} and S_n^{2-}; Mixture of such ions are formed be dissolving sulfur in a sulfide-ion solution), thiosulfate ($S_2O_3^{2-}$) and tetrathionate ($S_4O_6^{2-}$). The sulfane-sulfur-containing compounds may be further oxidized to sulfite (SO_3^{2-}) by heterodisulfide reductase (HDR). The SO_3^{2-} produced from S^0 oxidation may be converted to adenosine 5'-phosphosulfate (APS), which is then converted to SO_4^{2-} using ATP sulfurylase (Sat) to generate SO_4^{2-} and ATP. A cascade of sulfur transferases (DsrE, TusA and Rhd) is involved in sulfur and sulfur compound trafficking in *A. ferrooxidans*. The interconversion of tetrathionate and thiosulfate are catalyzed by tetrathionate reductase (TetH) and thiosulfate quinone reductase (TQR). Electrons released from the oxidation of sulfide, thiosulfate ($S_2O_3^{2-}$) or sulfane sulfate (GSSH) are transferred via the membrane-bound quinone pool (Q-pool) to NADH complex I (NDH1) and terminal oxidases (*bd*, bo_3 and aa_3) where O_2 reduction takes place. A bc_1 complex and a cytochrome *c* (CycA2) and a high potential iron-sulfur protein (HiPIP) are also involved in the electron shuttling [59].

The absence of the typical sulfur metabolism enzymes sulfur oxygenase/reductase (EC 1.13.11.55), sulfur dioxygenase (EC 1.13.11.18) and the sulfite oxidase (EC 1.8.3.1) in *A. ferrooxidans* indicates that the sulfur oxidation pathways of *A. ferrooxidans* are different from those of most archaea and bacteria, which also stresses the significance of its SQR, TQR and HDR. Overall it makes the study on these enzymes an exciting challenge.

1.4 Riboflavin, FMN and FAD

Flavin (derived from the Latin word "flavous" meaning yellow) is a group of yellow-colored organic compounds with the basic structure of 7,8-dimethyl-10-alkylisoalloxazine. Flavins are ubiquitous in nature and play important roles in many biological reactions as cofactors such as flavin mononucleotide (FMN) and flavin adenine dinucleotide (FAD). The flavin cofactors are synthesized from the precursor riboflavin, which is also known as vitamin B_2 (**Figure 1.6**). FMN is produced from linking one phosphate molecule to the hydroxyl moiety of riboflavin by the action of riboflavin kinase (EC 2.7.1.26). FAD, subsequently, is synthesized by the addition of one adenosine monophosphate (AMP) molecule to FMN.

Flavin cofactors are able to undergo reversible $1e^-/1H^+$ or/and $2e^-/2H^+$ oxidation-reduction reactions through the isoalloxazine moiety of the cofactor. The oxidized flavin cofactors exhibit characteristic yellow color and typical UV-visible absorption with a maxima at ~360 nm and 450 nm. In the reduced state, both the yellow color and the typical spectral feature disappear due to the isoalloxazine moiety hardly absorbs visible light in the electron rich state. The isoalloxazine moiety of flavin cofactors can undertake both one- and two-electron redox reactions with the formation of three redox states (**Figure 1.6**): oxidized flavin, an intermediate radical semiquinone (one electron reduced), and the fully reduced flavin. The flavin free radical semiquinone can exist in cationic, neutral and anionic forms and is detectable by electron paramagnetic resonance (EPR). Neutral and anionic flavin semiquinone forms have been found in flavoproteins. They can be distinguished by different linewidths of the EPR spectra, which is defined as the separation, in gauss (G), between the positive and negative extremes [63]. A 19 G linewidth is characteristic for a neutral flavin semiquinone, a 14~15 G linewidth is the trait of an anionic flavin semiquinone [63].

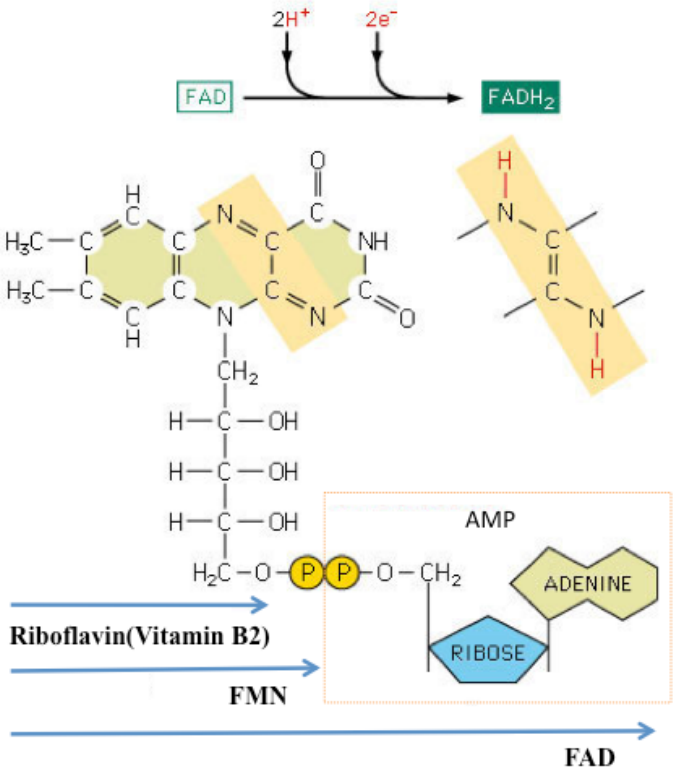

Figure 1.6 Chemical structure of riboflavin, flavin mononucleotide (FMN) and flavin adenine dinucleotide (FAD).
This figure is adapted and modified from B. Alberts, *et. al,* 1998 [64]

1.5 Flavoprotein

Flavoproteins are enzymes using either FMN or FAD as cofactors to catalyze oxidation-reduction reactions. The redox potential (E_m) of the $2e^-/2H^+$ oxidation-reduction of flavin is about -200 mV. In flavoproteins, however, the E_m of the flavin cofactor varies from -400 mV to +60 mV due to modification of the flavin environment in the protein. In general, the proximity of a positive charge or a covalent-bond to FAD molecule are believed to increase the redox potential and a negative charge or a hydrophobic environment are expected to lower it. Therefore, the trait of having the broad redox potential range of the flavin cofactor makes flavoprotein very versatile in terms of substrate and type of reactions.

1.6 Sulfide:quinone oxidoreductases (SQRs)

Sulfide:quinone oxidoreductase (SQR, EC 1.8.5.4) is an ancient flavoprotein of the disulfide oxidoreductase family **(DSR)** that is present in all domains of life (from archaea to humans but not plants). SQR is a peripheral membrane protein and catalyzes the oxidation of sulfide species (H_2S, HS^- and S^{2-}) to elemental sulfur by transferring two electrons from a sulfide ion via the FAD cofactor to the quinone pool in the membrane (**Figure 1.7**).

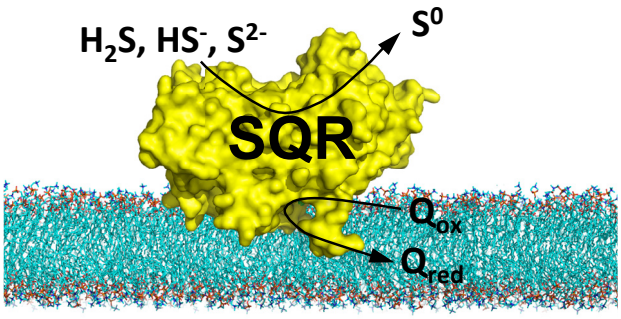

Figure 1.7. Schematic view of sulfide:quinone oxidoreductase (SQR)

The original roles of SQR are involved in the sulfide-dependent respiration and anaerobic photosynthesis [13]. SQR also serves multiple functions including detoxification [62] and heavy metal tolerance [65; 66; 67]. In animals, SQR may participate in maintaining sulfide homeostasis and signaling by controlling the levels of *in vivo* H_2S [15; 16; 68; 69].

1.6.1 Studies on the enzymatic characterization of SQRs

SQR was first identified in autotrophs, then, its homologs were recognized in archaea and eukaryotes (mitochondria) [65; 70; 71]. In the past two decades, several SQRs from different organisms have been purified and/or heterogeneously expressed. Their biochemistry characteristics were studied in some detail by biochemical methods (**Table 1**).

Table 1.1 The biochemical characteristics of SQRs

Organism	Strain	Preparing method	Molecular mass (kDa) Theoretical/Apparent	pH optimum	Temperature optimum (°C)	*Specific activity* (μmol mg^{-1} min^{-1})	k_{cat} (s^{-1})	K_m[Na_2S] (μM)	K_m[Quinone] (μM)	Florescence maxima (nm) (Excitation)/(Emission)	FAD	Reference
Acidithiobacillus ferrooxidans	ATCC 23270	Expressed in *E. coli*	48 (47.4+6His) / 48	7	30	8.1 ± 0.2 (DUQ)* 59.4 ± 5.9 (UQ_0) 42.1 ± 2.8 (NQ)	7.6 ± 0.2 47.7 ± 4.7 33.8 ± 2.2	2.97 ± 0.28	3.4 ± 0.43 (DUQ) 193 ± 15.6 (UQ_0) 76.9 ± 7.1 (NQ)	(280 / 375 / 460) / (520)	Covalently bound	Zhang & Weiner 2014, 2015
Acidithiobacillus ferrooxidans	NASF-1	Purified from membrane	47.4 / 47	7	n.a.	20.6 (Q_2)	n.a.	42	14 (Q_2)	n.a.	Lost	Wakai, 2007
Aquifex aeolicus	VF5	Purified from membrane	47 / 47	n.a.	80	1.4, 3.5 (DUQ at 20 °C)	n.a.	11	5 (DUQ)	n.a.	Yes	Michel, 2010 a,b, 2000
Paracoccus denitrificans	GB17	Purified from membrane		7.3	n.a.	0.3 (DUQ)	n.a.	26 ± 4	3.1 ± 0.6 (DUQ)	n.a.	Yes	Hauska, 1998
Chlorobium limicola		Purified from membrane		na	n.a.	na	n.a.	nd	<20 (PQ-1)	n.a.	Yes	Shahak, 1992
Oscillatoria limnetica		Purified	47 / 57	nd	n.a.	1.89 (Plastoquinone-1)	1.6	8	32 (PQ-1)	(280 / 373 / 461) / (527)	Yes	Padan, 1994
Rhodobacter capsulatus	*DSM 155*	Purified from chromatophores	48 / 55(with polypeptide)	6.3	n.a.	3.5	n.a.	2	2 (DUQ)	(280 / 375 / 458) / (518)	Yes	Hauska, 1997
		Expressed in *E. coli*	48 (47+6His) / 55	6.7	n.a.	50-55	n.a.	5	3 (DUQ)	(280 / 375 / 475) / (525)	Covalently bound	Hauska, 2002,
Acidianus ambivalens		Purified from membrane	45 / ~48	6.5	70	0.47 (DUQ)	2.1 (at 70 °C) 0.4 (at 50 °C)	2	n.a.	n.a.	Covalently bound	Archer, 2009
Caldivirga maquilingensis	IC-167	Expressed in *E. coli*	45 / 45	na	60	~1.2 (DUQ)**	0.6 ± 0.07	77 ± 8	30 ± 1 (DUQ)	n.a.	Noncovalently bound	Gennis, 2013
Human		Expressed in *E. coli*	47 / 47	7	n.a.	95 ± 5 (CoQ_1)	65 ± 2 or 74	315 ± 28	19 ± 2 (CoQ_1) 14 ± 2	n.a.	Noncovalently bound	Jorns, 2012
Schizosaccharomyces pombe	Sp223	Expressed in *E. coli*	52.6 (51.6+6His)/~52	na	n.a.	20.4 (Q_2)***	52	2000	2000 (Q_2)	(280 / 375 / 455) / (520)	Noncovalently bound	Weghe, 1999
Arenicola marina		Expressed in Yeast		9 at 22°C	n.a.	1.5 (DUQ)	n.a.	23	6.4 (DUQ)	n.a.	Yes	Martin, 2008
Urechis unicinctus		Expressed in *E. coli*	50.5/~60	8.5	37	1.75 (Q_2)	n.a.	40.3	15.6 (Q_2)	n.a.	Yes	Li, 2011

*Abbreviation of quinones and Q-ananlogs: 1,4-Naphthoquinone (NQ); Decylubiquinone (DUQ); Ubiquinone-0 (UQ_0); coenzyme Q_2 (Q_2)

** Estimated from k_{cat} (0.6 s^{-1}) using 45 kDa and 50% FAD

***Calculated from the apparent V_{max} of 1.36 μM coenzyme Q_2 reduced per (s•μg) of enzyme in 250-μL reaction volume

In the early 1990s, Shakak and Hauska *et al.* observed the electron transfer reaction from sulfide to quinone in the thylakoid of the filamentous cyanobacterium *Oscillatoria limnetica* [70] and in the membrane of the green sulfur bacterium *Chlorobium limicola* [72], respectively. From their results, they highlighted the membrane-bound sulfide:quinone oxidoreductase (SQR) which catalyzed this reaction.

In 1994, Arieli *et al.* purified SQR in an active form from the thylakoid of *Oscillatoria limnetica* [73]. The purified SQR was composed of a single polypeptide of about 57 kDa. Its catalytic activity is similar to the previously isolated membrane-bond form with a specific activity of 1.89 μmol mg^{-1} min^{-1} (plastoquinone-1). Its Michaelis constant K_m values for Na_2S and plastoquinone-1 are 8 μM and 32 μM, respectively. The UV-Visible absorption and fluorescence spectra of the purified SQR are typical of a flavoprotein. Both the absorption peaks and fluorescence intensities are reduced by sulfide. The sequence of the purified SQR contains the highly conserved fingerprint of the NAD/FAD-binding domain of flavoproteins.

In 1997, Michael Schutz and Gunter Hauska *et al.* purified the SQR from chromatophores of the non-sulfur purple photosynthtic bacterium *Rhodobacter capsulatus* DSM155 [74]. The purified SQR was a monomer with a molecular mass of ~55 kDa. Its absorption and fluorescence spectra, exhibiting typical features of a flavoprotein, are similar to the SQR from *Oscillatoria limnetica*. The Michaelis constant K_m values for Na_2S and DUQ are 2 μM. The V_{max} was 3.5 $\mu mol \cdot mg^{-1} \cdot min^{-1}$. The optimum pH for the electron transfer from sulfide to DUQ was around pH 6.3, which simply reflects a preference of H_2S over HS^- as a substrate for the enzyme. DNA primers based on the sequences of the N-terminus and tryptic peptides of the purified SQR were used to clone the *sqr* gene, which was further functionally expressed in *E. coli* BL21(DE3) [74]. The *sqr* gene encodes a protein of 427 amino acid residues with a theoretical molecular mass of

47 kDa. The heterogeneously expressed SQR showed sulfide:quinone oxidoreductase activity with an apparent molecular weight of 55 kDa in SDS-PAGE.

In 1999, Michael Schutz and Gunter Hauska *et al.* further investigated the localization and the sequence involved in translocation of SQR in *Rhodobacter capsulatus* [75]. An alkaline phosphatase (PhoA) fusion study indicated that the SQR of *R. capsulatus* functions at the periplasmic side of the cytoplasmic membrane and that the C-terminal 38 amino acids of SQR were required for translocation across the cytoplasmic membrane by an unknown mechanism.

In 2002, Hauska *et al.* expressed the *sqr* gene from *R. capsulatus* in *E. coli* BL21(DE3) and purified active N-terminal-His-tagged SQR from the membrane fraction [62]. Surprisingly, a relatively high proportion (30–50%) of soluble SQR was obtained from the non-membrane fraction of *E. coli*. The specific activity of the heterogeneously expressed SQR was ~50 μmol mg^{-1} min^{-1}, which is about 15 times higher than that of the directly purified SQR from *R. capsulatus*. The other enzymatic properties are similar to the purified SQR. Hauska's research group extended many understandings on SQR from *R. capsulatus* in the 1990s. In addition, they also demonstrated SQR activity in the membranes of the chemotrophic bacterium *Paracoccus denitrificans* GB17 [76] and the hyperthermophilic bacterium *Aquifex aeolicus* VF5 [77].

In 2007, Wakai and Kamimura *et al.* first purified the SQR from *Acidithiobacillus ferrooxidans* NASF-1 grown on sulfur medium [78]. The purified SQR was composed of a single polypeptide with an apparent molecular weight of 47 kDa. The Michaelis constant K_m values for Na_2S and ubiquinone-2 (Q_2) are 42 μM and 14 μM, respectively. The optimum pH for the SQR activity was about 7.0. However, their further studies were halted when they attempted the heterogeneous expression of thioredoxin-fused SQR in *E. coli,* which resulted in inactive inclusion bodies with no FAD cofactor assembled.

SQRs from Archaea were studied in the hyperthermoacidophilic archaeon *Acidianus ambivalens* [79] and *Caldivirga maquilingensis* [80], respectively. In 2009, José A. Brito *et al.* reported a detailed biochemical and structural characterization of the SQR isolated from the membranes of *A. ambivalens* [79]. The purified homogeneous SQR is a monomer in solution under the conditions tested, with the molecular mass of ~48 kDa. Its visible absorption spectrum has the typical fingerprints of a flavoprotein with λ_{max} at 454 and 350 nm. The presence of a covalently bound FAD was further confirmed by the X-ray structure. The observed (at pH6.5) sulfide:DUQ oxidoreduction turnover was 2.1 s^{-1} at 70 °C and 0.4 s^{-1} at 50 °C, respectively. At room temperature (25°C) the enzyme was almost inactive with only 3% activity remaining. In 2013, SQR from *Caldivirga maquilingensis* was expressed in *E. coli* and purified from the membrane fraction [80]. The Michaelis constant K_m values for Na_2S and DUQ are 77 ± 8 μM and 30 ± 1 μM, respectively. The turnover was measured as 0.6 s^{-1} at the optimum temperature 60 °C. Their studies demonstrated that it was possible to convert the membrane bound SQR into a water-soluble form with full activity by substituting the non-polar residues in the last C-terminal amphiphilic helix with more polar amino acids. These authors also suggested that the C-terminal amphiphilic helix is important not only for membrane binding but also for creating an entrance pathway for the quinone substrate.

Eukaryotic SQR homologues, sharing relatively low sequence identity (~20%) with prokaryotic and archaea SQRs, are widespread among the mitochondria of the organisms such as nematodes, fruit flies, worms, mice, rats, and humans [65; 71; 81; 82]. In 1999, the first functional mitochondrial SQR from fission yeast *Schizosaccharomyces pombe* was cloned, expressed in *E. coli*, purified and characterized [65]. The *S. pombe* SQR was also named as HMT2 based on its genetic designation *hmt2*$^+$ (a gene related to heavy metal tolerance). The purified recombinant

HMT2 protein was soluble, containing noncovalently bound FAD and was able to catalyze the sulfide:quinone (Q_2) redox reactions with a turnover number of 52 s^{-1}. The apparent K_m values for both Na_2S and Q_2 are 2 mM. This is relatively higher than that of other SQRs which are at micromolar levels. The sulfide-tolerant lugworm *Arenicola marina* can use electrons from sulfide for mitochondrial ATP production. In 2008, Ursula Theissen and William Martin reported the heterologously (in *Saccharomyces cerevisiae*) expressed *A. marina* SQR exhibited cyanide- and thioredoxin-dependent sulfide:quinone oxidoreductase-specific activity. The recombinant SQR purified from yeast mitochondrial membranes reduced DUQ (K_m = 6.4 μM) after the addition of sulfide (K_m = 23 μM) only in the presence of millimolar concentrations of cyanide. This observation was surprising, because bacterial, archaeal SQRs and even the SQR from yeast *S. pombe* require no additional substrate other than sulfide and quinone. Thiocyanate was the end product of the reaction, which suggests a function of SQR is a persulfide donor. When cyanide was substituted by thioredoxin and sulfite, the cyanide-dependent activity dropped to one-tenth. In 2010, SQR from another ocean worm *Urechis unicinctus* was reported to exhibit independent sulfide:quinone oxidoreductase-specific activity which is about 3-fold lower than the cyanide-dependent activity [83]. Diluted and refolded active recombinant *U. unicinctus* SQR (expressed in *E. coli*) exhibited optimal activity at 37 °C and pH 8.5 and K_m for sulfide and CoQ_2 at 40.3 μM and 15.6 μM, respectively. Western blot analysis indicated the *in vivo U. unicinctus* SQR was located in mitochondria and was ~10 kDa heavier than the recombinant protein. This indicated a post-translation modification involved in the mature protein. In 2012, Michael R. Jackson and Marilyn Schuman Jorns *et al.* reported human SQR catalyzes the first step in hydrogen sulfide metabolism and produces a sulfane sulfur metabolite [84]. Human SQR was expressed in *E. coli* and purified from the membrane fraction. Recombinant SQR contains

noncovalently bond FAD and catalyzes sulfide:CoQ_1 redox reaction with cyanide, sulfite, or sulfide as the sulfane sulfur acceptor, which dramatically enhance the apparent reaction turnover. The corresponding end products of the reactions are thiocyanate, thiosulfate, or hydrogen disulfide (H_2S_2), respectively.

In summary, the SQRs from different organisms, except *S. pombe*, exhibited high substrate (sulfide and quinone) affinity with the apparent K_m values falling in a narrow range in the micromolar level ($K_{m\,[sulfide]}$= 2 ~ 42 μM, $K_{m\,[quinone]}$= 2 ~ 22 μM). The turnover rate of the sulfide:quinone redox reaction varied between 0.6 ~ 52 s^{-1}. Studies on the enzymatic properties of SQRs extended the understanding of the enzyme and its function. However, to explore the mechanisms of sulfide oxidation and quinone reduction further studies on its structural characteristics is required.

1.6.2 Studies on the structure and mechanism of SQRs

At the beginning of my thesis research, the crystal structure of SQR was not available. The only related structure used for interpreting SQR was the structure of the flavocytochrome c:sulfide dehydrogenase (FCC or FCSD) from *Allochromatium vinosum* (PDB: 1fcd) that shares 24% sequence identity with SQR. Therefore, investigations of the catalytic mechanism of SQR were mainly focused on product analysis and site-directed mutagenesis of the conserved amino acids in various heterologously expressed SQRs. Hauska *et al.* proposed the first mechanism of the reductive half-reaction of SQR from *R. capsulatus* [62] (**Figure 1.8**): Initially, the oxidized form of SQR contains a disulfide bridge between two cysteines Cys127 and Cys159, or between Cys127 and Cys353 (in *R. capsulatus* numbering); These two disulfide bridges are in equilibrium with each other by thio/disulfide exchange (state 1 and 2 in Figure 1.7). The reductive half-reaction begins with the cleavage of the disulfide bridge between Cys127 and Cys353 by a

sulfide molecule. This step leads to a persulfide at Cys353 and a thiol at Cys127 (state 3). The persulfide at Cys353 is nucleophilically attacked by a second sulfide molecule to form a thiol group at Cys353 and a free persulfide, which is released from the enzyme as the primary product. Simultaneously, a proton from the thiol group of Cys159 is taken by Glu165 and transferred to the oxidized FAD (state 4). Subsequently, the Cys159 thiolate covalently attaches to the C^{4A} atom of FAD, one electron is transferred to FAD (state 5), resulting a half-reduced FAD in the semiquinone form and a disulfide bridge between Cys159 and Cys127 (state 6).

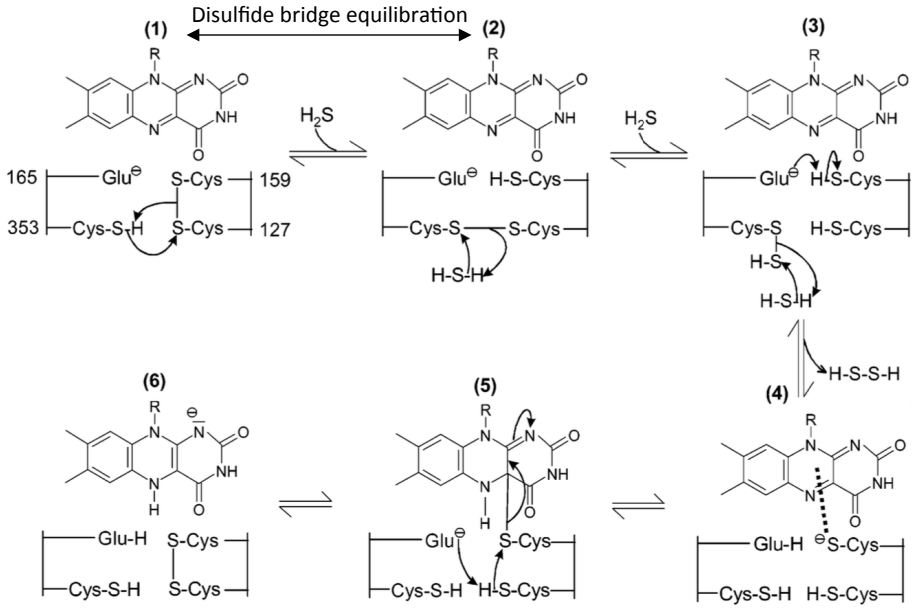

Figure 1.8 Hauska *et al.* proposed the first mechanism of the reductive half-reaction of SQR from *R. capsulatus* [62]. The figure is adapted and modified from Hauska *et al.*, 2002.

The crystal structures of SQRs from three different organisms were resolved successively during the thesis: the archaeal SQR from hyperthermoacidophilic *Acidianus ambivalens* [79], the bacterial SQR from *Aquifex aeolicus* [85] and the SQR from acidophilic, mesophilic, chemolithotrophic γ-proteo-bacterium *Acidithiobacillus ferrooxidans* ($SQR_{A.f.}$, see Chapter 2) [37;

[86]. The available structures shed light on the complex mechanism of sulfide oxidation and electron transfer. Several sulfide oxidation mechanisms were proposed based on the structural information and enzymatic characteristics.

The SQR from *A. ambivalens* shares 27% sequence identity with SQR from *A. ferrooxidans*. Its X-ray structure (PDB: 3h81) was determined to 2.6 Å resolution with no interpretable electron density observed for the last 53 amino acid residues at the C-terminal region of the full-length SQR. The enzyme is a homodimer. The structure revealed that SQR contains two redox active sites: a covalently-bound FAD cofactor, which is bound to Cys129 via the 8-methylene group of the isoalloxazine ring, and an adjacent pair of cysteine residues (Cys178 and Cys350, in *A. ambivalens* numbering) located on the *re*-side of the FAD. The proposed possible mechanism for sulfide oxidation basically agrees with the previously suggested mechanism by Hauska *et al.*: A sulfide molecule nucleophilically attacks the Cys178-S-S-Cys350 disulfide bridge, resulting in cleavage of the disulfide bridge and formation of S persulfide at Cys350 and a thiolate at Cys178 (Cys178-S^-) that attacks the C^{4A} atom of FAD to transfer one electron to it. The polysulfide chain grows on Cys350. The role of the third cysteine of the active site (Cys129) is to maintain the position of the flavin ring of FAD. The presence of two aspartate residues (Asp215 and Asp353) in the vicinity of Cys350 was suggested to stabilize the sulfide molecule and increased the nucleophilicity of the sulfide molecule.

The *A. aeolicus* SQR shares 40% sequence identity with the SQR from *A. ferrooxidans*. *A. aeolicus* SQR is a homotrimeric, periplasmic monotopic membrane protein that inserts into the lipidic bilayer to a depth of approximately 12 Å through the C-terminal amphipathic helices and lipid clamps. Its X-ray structure was determined in the form of "as-purified" (PBD: 3hyv), "substrate-bound" (PBD: 3hyw), and "inhibitor-bound" (PBD: 3hyx) at resolutions of 2.3, 2.0,

and 2.9 Å, respectively [85]. The structure indicated a FAD cofactor is covalently-bound through a disulfide bridge between the 8-methyl group of the isoalloxazine ring and Cys124 (Cys124-S-S-C^{8M}-FAD). The three catalytic related cysteines (Cys124, Cys156 and Cys347) are located at the *re*-side of the isoalloxazine ring, where the sulfide oxidation and sulfur chain elongation occur. The quinone binding site is located in a hydrophobic channel that connects the *si*-side of the cofactor FAD to the membrane. The aromatic ring is situated between the conserved residues Phe385 and Ile346. The structural information agrees with the conventional mechanism including the formation of a Cys156-S-S-C^{4A}-FAD adduct via the Cys156 thiolate nucleophilically attacking the C^{4A} atom of FAD. The polysulfide chain grows on Cys347. The role of the third cysteine of the active site (Cys124) is to maintain the position and the electronic properties of the flavin ring of FAD. Additionally, an alternative mechanism was proposed for *A. aeolicus* SQR. This mechanism involves the formation of a Cys124–S–S^- disulfide species that attacks the C^{8M} atom of FAD. Electron transfer occurs during this step. This leads to the formation of a transient Cys124–S–S^+ cation. The trisulfide bridge Cys124–S–S–S–Cys156 forms after the recombination of the above cation with the Cys156 thiolate. The role of Cys347 is to take over the growing polysulfide chain and, as a result, to recover the Cys156 thiolate.

In the case of *A. ferrooxidans* SQR, although the above-mentioned mechanisms might be applicable, we proposed two alternative mechanisms based on a combination of site-directed mutagenesis, enzymology, X-ray crystallography and electron paramagnetic resonance (EPR) (details see Chapter 2 and 3).

1.7 Research Objectives

With the boost of research on the newly discovered gasotransmitter —sulfide (H_2S, HS^- and S^{2-}), the ancient widespread flavoprotein SQR attracts more and more attention due to its

potential role of maintaining the sulfide homeostasis. The goals of this thesis are to determine the three dimensional structure of SQR from *A. ferrooxidans* and to use $SQR_{At.f}$ as a model system to investigate the enzymatic mechanism of sulfide oxidation and quinone reduction in SQR. The principle objectives of this thesis consist of (1) the expression of the wild-type *sqr* gene from *A. ferrooxidans,* as well as several variants of conserved, catalytically important amino acids in *E. coli* BL21(DE3) and the purification of active, His-tagged SQR for X-ray crystal structural and biochemical characterization analysis; (2) the determination the 3-D structure of wild-type $SQR_{At.f}$ and the variants; (3) the investigation on the mechanisms of sulfide oxidation, quinone binding and reduction in $SQR_{At.f}$; (4) the study on the roles of the catalytically essential residues in the enzymatic mechanism of SQR and (5) the exploration on the interaction between the sulfide oxidation site and the quinone binding site.

A comprehensive understanding of the biochemical characteristics, 3-D structure and catalytic mechanism of $SQR_{At.f}$ will contribute to the clarification of this ubiquitous ancient enzyme as well as its homologue in human.

Chapter 2: Crystal structure of sulfide:quinone oxidoreductase from *Acidithiobacillus ferrooxidans*: insights into sulfidotrophic respiration and detoxification

A version of this chapter has been published in Journal of Molecular Biology.

Cherney, M. M.*, Zhang, Y.*, Solomonson, M., Weiner, J. H., and James, M. N. G. (2010) Crystal structure of sulfide:quinone oxidoreductase from Acidithiobacillus ferrooxidans: insights into sulfidotrophic respiration and detoxification. *J Mol Biol* **398**, 292–305

* CMM and YZ contributed equally to this study.

Acknowledgements : We are very thankful for help with data collection on beamline 9-2 at the Stanford Synchrotron Radiation Laboratory and particularly to Pawel Grochulski on beamline 08ID-1 (Canadian Macromolecular Crystallography Facility) at the Canadian Light Source (Saskatoon). Research in the laboratories of M.N.G.J. and J.H.W. was supported by the Canadian Institutes of Health Research (CIHR FRN-37770, CIHR MOP-15292, and MOP-121065). M.N.G.J. also had funding support from the Alberta Heritage Foundation for Medical Research.

2.1 Introduction.

Acidithiobacillus ferrooxidans (*A. ferrooxidans)* is a Gram negative, acidophilic, chemolithotrophic bacterium that is usually found in acidic environments. It derives energy for growth mainly from oxidative respiration using reduced inorganic compounds such as Fe^{II}, H_2S, S^{2-} S^0 and Cu^I that are present in the surrounding ores; ultimately electrons are moved from these substrates to oxygen [87; 88]. Several redox proteins are involved in the respiratory chains. One of the enzymes responsible for the earlier stages in sulfide oxidation is sulfide:quinone oxidoreductase (SQR). SQR is an ancient flavoprotein of the disulfide oxidoreductase family (DSR) that is present in all domains of life (archaea, bacteria and eukarya) thereby augmenting its original role in respiration. Initially, SQRs were found in sulfidotrophic bacteria. Later SQR-like enzymes (SQRDLs) were also found in the mitochondria of some fungi, as well as in all animal species with known genome sequences [71; 89]. Based on phylogenetic analysis of completed bacterial genomes, SQR genes were classified into at least two clades: type I and type II SQRs. Type I SQRs occur in a diverse range of bacteria, including *A. ferrooxidans* [13; 62; 90]. They participate in respiration or in anaerobic photosynthesis and are characterized by high substrate affinities and high reaction rates [62; 90]. Type II SQRs include those from other bacteria, as well as the mitochondrial SQRDLs. Type II SQRs are mostly involved in detoxification [89], heavy metal tolerance [65; 66] and, presumably, in signaling in higher eukaryotes by controlling the levels of H_2S in the brain [15; 16; 68; 69]. Additionally, the ATP production in mitochondria with sulfides as electron donors has been observed [22; 27; 91].

SQRs are thought to be mainly dimeric, similar to other members of the DSR family, embedded in the cytoplasmic membrane on the periplasmic side [13; 62], but some of them might be trimers [85]. They are considered to be integral monotopic membrane proteins. The molecular mass

of the monomeric enzyme is around 50 kDa. The enzyme usually harbors a covalently bound FAD cofactor in each monomer [79; 85; 92], but the FAD cofactor can also be bound non-covalently (the current structures; there are also reports about the loss of FAD in SQRs during purification) [62]. The enzymatic reaction catalyzed by SQR includes oxidation of reduced sulfur compounds H_2S, HS^- and S^{2-} to soluble polysulfide chains [62] or to elemental sulfur in the form of octasulfur rings [85]. The electrons from the sulfides are transferred through FAD to the ubiquinone or menaquinone pool in the membrane.

The structures of the SQRs from a hyperthermophilic bacterium *Aquifex aeolicus* (*A. aeolicus*, PDB codes 3hyx, 3hyv, 3hyw) and from a hyperthermoacidophilic archeon *Acidianus ambivalens* (*A. ambivalens,* PDB code 3h8l) have recently been reported [79; 85]. *A. ferrooxidans* SQR has 40% and 27% sequence identity with the above mentioned proteins, respectively. A related structure of the flavocytochrome *c*:sulfide dehydrogenase from *Allochromatium vinosum* (FCC, PDB code 1fcd) that was reported about 15 years ago has 24% sequence identity [92]. The available structures shed light on the complex mechanism of electron transfer, but further investigation including structural data of the SQRs from different species is needed for a better understanding of the catalytic events.

Here we present the three-dimensional structures of the *A. ferrooxidans* native unbound enzyme, the acceptor-bound enzyme and the Cys^{160Ala} variant SQR molecule.

2.2 Materials and Methods

2.2.1 Crystallization and data collection

The *A. ferrooxidans* SQR was expressed, purified and crystallized in a tetragonal form as described elsewhere [86]. Small changes in crystallization conditions were used to grow crystals of

the hexagonal crystal form. They were grown in hanging drops from 30% PEG 600, 0.1 M bis-tris pH 5.5 or 6.5, 0.1 M magnesium sulfate and 0.05% DDM. Co-crystals with decylubiquinone (DUQ) were produced from the mixture of the protein at 10 mg/ml concentration and 2 mM DUQ in these same crystallization conditions. Crystals for data collection were flash-cooled in liquid nitrogen. Data were collected on beamline 9-2 at the Stanford Synchrotron Radiation Laboratory (SSRL) and on beamline 08ID-1 at the Canadian Light Source (Saskatoon) using a temperature of 100 K and detectors MAR 325 or MAR 225. The raw data were processed with the HKL-2000 suite [93] and XDS/ XSCALE [94].

2.2.2 Structure determination and analysis

Molecular replacements were performed with MOLREP [95] and Phaser [96]. Refinement of the coordinates and the atomic temperature factors was carried out using the PHENIX package and a maximum likelihood target [97]. Model rebuilding at various refinement stages was performed using Coot [98]. Protein stereochemistry was analyzed by PROCHECK [99]. The program PyMOL [100] was used to calculate r.m.s.d. values between analogous structures and to make figures. Calculations of the buried surface area ($Å^2$) and thermodynamic parameters of the possible assemblies were carried out with the EMBL-EBI PISA server [101].

2.2.3 Enzymatic activity assay

Reduction of DUQ

The activity of sulfide:quinone oxidoreductase was spectroscopically measured by the decrease of absorbance at 275 nm due to the reduction of decylubiquinone (DUQ) as described previously[33]. The reaction mixture contained 25 μg/ml (0.5 μM) protein in 50mM Bis–Tris (pH 6.5), 20mM glucose, 50 μM DUQ, 1 unit of glucose oxidase per mL and 10 units of catalase per mL. Anoxic conditions were established by flushing with N_2. The reaction was started by the

addition of 100 μM freshly prepared Na_2S. One unit of activity was defined as the amount of enzyme that catalyzed the reduction of 1 μmol of DUQ per minute [102]. Absorption spectra during the enzymatic reaction were measured at 275 nm. The differential extinction coefficient determined by the measurement of difference spectra of oxidized and reduced DUQ is 12.5 mM^{-1} cm^{-1}.

Reduction of FAD

The FAD reduction assay was conducted by measuring spectroscopically the decrease in absorbance at 375 nm and 450 nm due to the reduction of FAD. The reaction mixture contained 1 mg/ml protein in 50 mM MOPS, 0.5 mM NaCl at pH 7.0. The mixture was titrated with sodium sulfide to concentrations from 0.12 mM to 1.52 mM. The absorbance was measured in the range from 300 nm to 600 nm.

2.2.4 Accession codes

The coordinates and structure factors have been deposited in the PDB under accession codes 3KPI, 3KPG and 3KPK.

2.3 Results

2.3.1 SQR enzymatic activity assays

Enzymatic activity assays have been carried out for wild type (WT) and the Cys^{160Ala}, Cys^{356Ala} and Cys^{128Ala} variants. The WT protein showed the highest specific activity reported to date: 400-500 [unit (mg protein)$^{-1}$]. The K_m for sulfide has been determined = 2.8 μM and for DUQ = 22 μM. The Cys160Ala variant has no activity. The activity assays conducted for the Cys128Ala variant showed 30-35% activity (~70% activity loss) determined in the DUQ assay. However, in the FAD reduction assay, both the WT and the C128A variant have been similarly

active (100%). This is the first observation that the Cys128 is not involved in the FAD cofactor reduction step.

2.3.2 Structure determination

SQR from *A. ferrooxidans* was overexpressed in *E. coli* and purified to homogeneity, as described elsewhere[20]. Crystals of the acceptor-bound SQR were grown from a solution containing protein and DUQ. The crystals of the native protein grew in the space group $P4_22_12$, whereas the co-crystals of the complex with DUQ, as well as the crystals of the Cys^{160Ala} variant grew in the space group $P6_222$. Soaking of the native crystals with several quinone substrates and inhibitors failed to result in specific quinone binding. The native structure was solved in the tetragonal space group by molecular replacement using as a search model a C-terminally truncated molecule A of the *A. aeolicus* SQR [85]; the SQR structure from *A. ferrooxidans* was refined to R_{work}/R_{free} of 16.7/20.0% (to 2.3 Å resolution). The refined *A. ferrooxidans* SQR coordinates were used to obtain the structural solutions for SQR in the hexagonal space group. The final values of R_{work} and R_{free} for each of these structures were 18.5/23.1% and 17.0/20.9% (to 2.05 Å and 2.3 Å resolution), respectively, for the Cys^{160Ala} variant and for the quinone-bound *A. ferrooxidans* SQR. The details of the data collection and refinement are given in **Table 2.1**.

2.3.3 Structure of *A. ferrooxidans* SQR

The overall structure of *A. ferrooxidans* SQR is characteristic for the DSR family of proteins (**Figure. 2.1**). It is comprised of two tandem Rossmann fold domains and a very flexible C-terminal domain containing two amphipathic helices that are thought to provide for the membrane binding [85; 103]; there also is one noncovalently bound FAD cofactor. The structures determined here are from two different crystal forms, tetragonal (PDB code 3kpi) and hexagonal (PDB code 3kpg). The hexagonal form was grown in the presence of a detergent, DDM, while

the tetragonal form was grown in the absence of detergents. Both crystal forms are physiological, as the protein is equally active in the presence or absence of detergents. The SQR molecules determined in each crystal form are very similar with the r.m.s.d. between the protein molecules of 0.42 Å for 412 C^{α} atom pairs. However, the last amphipathic helix in the hexagonal form (residues 407-427) undergoes a major conformational change. Several residues of the N-terminus of this helix partially unwind and, as a result, it becomes shorter and it changes its orientation. The last amphipathic helix is very flexible even within the same crystal form. The structures solved from several hexagonal crystals showed that the last helix has slightly different conformations in each crystal (data not shown). Its *B*-factors are highly elevated. The last seven residues (tetragonal form) and the last 16 residues (hexagonal form) have no electron density and have not been included in our structural models. It is likely that the flexible part of the SQR molecule keeps mobile in the membrane environment. Superposition of the two structures is shown in **Figure 2.1**.

There are two SQR molecules in the asymmetric unit of the tetragonal crystal form (**Figure 2.2**) and one molecule in the asymmetric unit of the hexagonal crystal form. The crystallographic dimer of the tetragonal asymmetric unit is formed largely by interactions between the hydrophobic C-terminal regions that include the amphipathic helices of each protomer (**Figure 2.2**). Similar dimers interacting by their C-terminal domains have also been observed in the hexagonal crystal form of this protein and in the both *A. aeolicus* and *A. ambivalens* SQR structures. It is very likely that all SQRs dimerize in solution by the largely hydrophobic membrane-interacting surfaces of the molecules. Most probably, these particular dimers are usually found by conventional methods. For the *A. ferrooxidans* SQR, the asymmetric unit dimer has a solvent inaccessible interface of 1154 $Å^2$ per protomer. The solvation free

energy of this interface is -14.8 kcal/mol, which indicates the predominantly hydrophobic nature of the dimer interactions. It has the positive ΔG_{diss} (4.2 kcal/mol) upon its dissociation confirming the stability of this dimer. Calculations of the dissociation constant $K_{diss}=\exp(-\Delta G°_{diss}/RT)$ gives $K_{diss}=10^{-3}$ M, which means that at physiological concentrations (below 0.1 mM = 5 mg/ml) the dimer concentration will be less than 10%; at the protein concentration below 0.01 mM the dimer concentration will be less than 1%. In other words, the equilibrium shifts sharply towards monomers at lower protein concentrations, as it has been confirmed by the size exclusion chromatography (data are not shown). However, these dimers should dissociate for membrane insertion. The thermodynamic analysis of the possible assemblies using the European Molecular Biology Laboratory– European Bioinformatics Institute Protein Interfaces, Surfaces, and Assemblies (EMBL-EBI PISA) server does not find any other stable multimers in solution. The only dimer that would exist in solution at moderate and higher protein concentrations should be the dimer discussed above. However, in the membrane environment, the entropy term ΔS_{diss} should only slightly change for the membrane-bound multimer upon its dissociation and it can be disregarded. Now, the binding energy ΔH will determine the stability of assemblies. The possible multimer should also allow the proper positioning of the amphipathic helices in the membrane.

Based on this requirement and the examination of all interfaces a probable biological dimer (with a common interface in two crystal forms) is suggested (**Figure 2.3**). It is different from the trimer that has been proposed for the *A. aeolicus* SQR [85]. This difference in the oligomeric state of the SQR enzyme in the membrane is not important from the mechanistic point of view. The superposition of the biological dimer structures of two crystal forms (tetragonal and hexagonal) is shown in **Figure 2.3**. The dimer interface buries approximately 620 $Å^2$ (per protomer) of solvent-accessible surface area. It is formed mostly by the β17-strands of an

extended antiparallel β-sheet (residues 247-254) from each protomer, which are related by a crystallographic twofold axis. Each protomer has an elliptical shape with approximate dimensions 45 Å x 67 Å; the longer elliptical axis is almost doubled in the dimer: 54 Å x 126 Å. This arrangement of the protomers in the dimer puts the C-terminal domains with the amphipathic helices on one side of the dimer below the equatorial plane of the ellipsoid, so that they could penetrate into the membrane, whereas the extended β-sheet is situated on the opposite side away from the membrane surface. The amphipathic helices make a sharp angle (~30˚) with the equatorial plane that is perpendicular to the crystallographic twofold axis, but they are very flexible and could easily become parallel to the membrane surface. The most flexible C-terminal segment that protrudes from the protein bends sharply in the direction of the presumptive membrane. The depth of the insertion could be estimated using the supposition that both molecules of the biological dimer are equally inserted and both benzoquinone rings of the substrate determine the top level of the phospholipid bilayer. It has been estimated to be about 20 Å (**Figure 2.3**), which is approximately one half of the membrane thickness [104]. A similar membrane-bound biological dimer likely forms in the *A. ambivalens* SQR, in which the dimerization occurs by the β-strands (residues 51-61) and the amphipathic helices are equally inserted in the membrane. In *A. aeolicus* SQR a dimer of trimers organization allows for the amphipathic helices to be in a hydrophobic environment that mimics the membrane. The amphipathic helices, as well as the whole trimers are almost parallel to the equatorial plane, and consequently, to the presumable membrane surface. It was suggested that they penetrate the membrane to a depth of approximately 12 Å [85].

The SQR multimers (dimers or trimers) do not affect the catalytic mechanism. Their possible role could be to provide stability to the protein orientation in the membrane. A change

in the orientation could put the FAD cofactor and the electron acceptor (ubiquinone or menaquinone) floating in the membrane in unfavorable positions.

The *A. ferrooxidans* SQR structure exhibits an overall fold that is quite similar to those of the other reported homologues. The superposition of the *A. ferrooxidans* SQR structure with the structures of *A. aeolicus* SQR (PDB codes 3hyw, 3hyv, 3hyx, **Figure 2.4**), *A. ambivalens* SQR (PDB code 3h8l), and flavocytochrome c: sulfide dehydrogenase from *A. vinosum* (PDB code 1fcd) shows that the present structure is more closely related to the *A. aeolicus* SQR structure than to the two latter structures with r.m.s.d. values of about 1.3 Å, 2.75 Å and 2.26 Å for 401, 370 and 348 C^{α} atoms, respectively. The largest differences occur in the C-terminal domains containing the amphipathic helices.

2.3.4 Redox active site and bound ligands

The active site of the *A. ferrooxidans* SQR includes two cysteines (Cys160 and Cys356), the FAD cofactor and, possibly, a third cysteine residue (Cys128) (**Figure 2.5**). The FAD cofactor plays a central role in the catalytic mechanism. It accepts electrons from a sulfide species and transfers them to the acceptor molecules (ubiquinone or menaquinone). The cofactor position in the *A. ferrooxidans* SQR structure is similar to that in other DSR proteins; it is bound in the first Rossmann fold domain. It makes a network of van der Waals contacts with the protein, 11 of these contacts are hydrogen-bonding and electrostatic interactions. The most important interactions involve the isoalloxazine ring (atoms O4 and O2), oxygen atoms of the phosphate groups (atoms O^{1P}, O^{2P} and O^{2A}), the ribose moiety (atom O^{3B}) and the adenine moiety (atoms N^{1A} and N^{6A}) of the FAD. They form hydrogen bonds with the main chain nitrogen atoms of Thr11, Gly12, Ala78, Ile302, Gly322, and Phe357, with the main chain oxygen atom of Ala78, and with the side chain nitrogen and oxygen atoms of Lys391 and Ser34. The O^{1P} atom of the

phosphate group is also involved in the capping interaction with the N-terminus of the a1 helix (Gly12); this interaction is due to the dipole moment of the helix that is positively charged at N-terminus. It makes an electrostatic interaction with the negatively charged phosphate group. As a result of the multiple interactions with the enzyme, the average B-factor of the FAD molecule is very low; in fact, it is lower than the average *B*-factor for the protein molecule (**Table 2.1**). Interestingly, the second Rossmann fold domain does not bind a second nucleotide (as it was discussed previously) [79] in contrast to some of the related oxidoreductases (for instance, the lipoamide dehydrogenase, PDB code 1lvl). The latter binds FAD and NAD cofactors simultaneously. However, in SQR, the binding of the second nucleotide is prevented by the loop (residues 155-160) that occupies the space where the second nucleotide would bind. This loop contains one of the active site cysteine residues, Cys160.

The mode of the FAD binding in *A. ferrooxidans* is different from those in other DSR proteins. The three most closely-related structures contain a covalently bound FAD cofactor (via its C^{8M} atom) that connects to the Cys128 (hereafter in the *A. ferrooxidans* numbering unless specifically mentioned) sulfur atom directly [79; 92] or through a disulfide bridge [85]. In the *A. ferrooxidans* SQR the cofactor has no covalent bond to Cys128, even though the Cys128 S^{γ} atom is 3.86 Å from C^{8M}. This fact was also confirmed in another experiment in which FAD was removed from the trichloroacetic-acid-treated protein by dialysis (data not shown).

The cofactor is also situated in the vicinity of the two active site cysteines Cys160 and Cys356. The distance between the C^{4A} atom of the isoalloxazine ring of the FAD cofactor and the S^{Y} atoms of Cys160 or Cys356 is ~ 5 Å. These two cysteine residues are positioned on a line that is almost parallel to the plane of the isoalloxazine ring, on its *re*-side (**Figure 2.5**). The electron density of the thiol groups of Cys160 and Cys356 extends in both crystal forms to form

adducts with additional sulfur atoms. Cys356 has been modeled as a disulfide covalently connected to a tetrasulfide at Cys160 (in the hexagonal form) or a trisulfide (in the tetragonal form). The resulting arrangement of sulfur atoms can also be considered as a branched penta or tetrasulfide molecule covalently attached to both cysteines (**Figures 2.5, 2.9, 2.10**). The occupancy of the sulfur atoms in the tetragonal form refined to an average of 0.58, whereas in the hexagonal form the occupancy varies from 0.5 to 1.0 with the S5 atom having the highest occupancy.

A species (tentatively determined as sulfide, based on an occupancy 1.0, to fit the spherical $| f_o |-| f_c |$ electron density peak at 15.8 σ) was found bound in the pocket close to Cys128 in the tetragonal crystal form and in some hexagonal crystals. It makes a network of hydrogen bonds with the N^{δ} atom of His132, the O^{γ} atom of Ser126, and the backbone N atoms of Thr129 and Cys128. However, it does not make a covalent bond with Cys128; it is situated at a distance of 4 Å from S^{γ} atom of Cys128. It may form a Cys128 disulfide at some point in the catalytic cycle. The role of the Cys128 and its possible disulfide is discussed more in the "Discussion".

Additional electron density peaks that have probably originated from the expression and purification in *E. coli* were present in all structures. Based on the shape of the electron density several of them have been modeled as glycols (1,3-butanediol or 1,2-propanediol). Several flat oval blobs were stacked against aromatic rings of tryptophan and tyrosine residues (Trp52, Tyr195, Tyr223 and Tyr383) on the molecular surface, indicating an affinity for aromatic rings and possible additional sites for ubiquinone binding. Several putative sulfate binding sites have been identified in the tetragonal crystal form. No sulfate ions have been detected in the hexagonal form. The DUQ binding is discussed more fully below.

2.3.5 Cys^{160Ala} variant

Crystals of the Cys^{160Ala} variant are isomorphous with those co-crystallized with DUQ. The structure of the Cys^{160Ala} variant (PDB code 3kpk) is very similar to those of the native protein. Superposition of the variant structure with the structures of the native protein in complex with DUQ or with the native protein in the tetragonal crystal form gives r.m.s.d. values of approximately 0.28 Å for 418 C^{a} atom pairs and 0.49 Å for 412 C^{α} atom pairs, respectively. The distance between C^{β} atoms of Ala160 and Cys356 (9.2 Å) in the variant structure is slightly larger than the average equivalent distance for the Cys160 and Cys356 residues in the native protein structures (8.8 Å). There are no additional electron density peaks other than that for the methyl group in the vicinity of the Ala160 C^{α} atom. However, some positive electron density appeared in close proximity to the S^{γ} atom of Cys356 and it was modeled as a disulfide at Cys356. The sulfur atom of the disulfide was refined with occupancy 1.0 at the S-S covalent bond distance (2.08 Å) from the S^{γ} atom of Cys356 in alternative conformations. The density indicates that the sulfide substrate can interact with Cys356 directly in the absence of the redox active disulfide bridge, but the reaction stops there. Three water molecules are located within a hydrogen-bonding distance from the Cys356 disulfide. No polysulfide chains were detected and there was no catalytic activity associated with the Cys^{160Ala} variant (data not shown).

2.3.6 Complex with decylubiquinone

Soaking pregrown hexagonal native crystals with DUQ did not result in quinone binding despite the fact that the last amphipathic helix is highly flexible. The soaked and not soaked crystals revealed an electron density peak close to the isoalloxazine ring of FAD that was not consistent with the DUQ structure (data not shown). The quinone-binding site has been determined from the structure of SQR that was co-crystallized with DUQ. The co-crystals

belonged to the hexagonal crystal form, space group $P6_222$ and were isomorphous with the hexagonal, unbound native protein (not reported here) and the Cys^{160Ala} variant crystals (**Table 2.1**). DUQ has atomic occupancy factors of 1.0 in the binding site. The quinone position is slightly different from that in the *A. aeolicus* SQR-quinone structure. The majority of the contacts of the atoms of DUQ with the atoms of the protein are hydrophobic. The aromatic ring of the quinone moiety is situated between the two benzene rings of Phe394 and Phe357 (**Figure 2.6**). Out of a total of 18 contacts at a distance of 3.6 Å, 10 contacts are made to these two phenylalanine residues. The other contacting residues are Phe41, Pro43, Gly322, Tyr323, Asn353 and Tyr411. The benzoquinone head is also close to the isoalloxazine ring; the distance between the O4 atom of the quinone and the O2 atom of FAD is less than 3 Å (**Figure 2.5**). The hydrophobic decyl chain points backwards from the amphipathic helices. It makes very few contacts with the protein (residues Tyr323, Asn353 and Tyr411). Superposition of the co-crystallized SQR-DUQ complex structure with the native tetragonal form crystal structure showed that the side chain of Met418, a residue situated at the C-terminus of the second amphipathic helix, would occupy the benzoquinone position, whereas Leu415 would have very close contacts (1.7-2.1 Å) with the quinone tail. This observation indicates that the second amphipatic helix of the tetragonal form would have to rearrange to allow quinone binding.

2.3.7 Electrostatic surface and channels

Electrostatic surface analysis shows that the molecule of SQR is divided into positively and negatively charged regions that are situated on opposite sides of the molecule (**Figure 2.7a,b**). The positively charged region of the SQR molecule (**Figure 2.7b**) mostly contains both of the amphipathic helices and other segments of protein that potentially interact with the negatively charged region of the phospholipid bilayer. The membrane-binding part contains a

large number of Arg, Lys and His residues and is rich in hydrophobic residues that are necessary to maintain the protein inside the hydrocarbon layer of the membrane.

The electrostatic surface representation also reveals several channels that connect the interior of the molecule to the outside neighbouring environment. The largest of these channels contains the FAD cofactor, its isoalloxazine ring is located deep in the interior of SQR (**Figure 2.7a**). This channel is much wider than is required to accommodate the FAD, so the rest of the channel is filled with series of ordered solvent molecules. Cys128 is close to this channel, but its sulfhydryl group is turned away from it. The sulfide species bound in the pocket close to Cys128 has no direct access to the channels, but it is separated from the bulk solvent by only an imidazole ring of His132. Both active site cysteine residues, Cys160 and Cys356, as well as the important proton acceptor Glu166, have access to smaller sulfide channels. Cys160 is more solvent accessible than Cys356. The sulfide channels in *A. ferrooxidans* SQR are slightly different from those in *A. ambivalens* and *A. aeolicus*. DUQ and dodecyl maltoside (DDM, the detergent) are located in two other channels. One of these channels occupied by DDM in the hexagonal crystal form is hydrophobic; it would open into the internal part of the membrane and it could possibly serves as a product release pathway. The hydrophobic tail of DDM points into the interior of the protein molecule and comes very close to Cys356 and the polysulfur product. The distance between the C^{α} atom of Cys356 and the C12 atom of DDM is less than 4 Å. The hydrophilic head of DDM sticks out of the channel, exposed to the bulk solvent (**Figure 2.7b**). The DUQ is oriented in a different way; its polar head is inserted deep into the protein interior, whereas its hydrophobic tail points to the outside of the molecule. This is the region of the enzyme that is proposed to be inserted into the membrane.

2.4 Discussion

The molecular mechanism of the electron transfer reaction catalyzed by SQR is not fully understood due to the complexity of the mechanism and the scarcity of the structural information. Three cysteine residues (Cys160, Cys356 and Cys128) have been shown to be necessary components of the enzymatic reaction. Substitution of any of the two residues (Cys160 or Cys356 (data not shown)) leads to a complete loss of activity; substitution of the third residue, Cys128, causes a substantial loss (~70%) of activity. Several hypotheses concerning the catalytic mechanism of electron transfer by SQRs have been suggested. The conventional mechanism includes the formation of a Cys160 thiolate [62; 79] or a Cys160-S-S$^-$ disulfide [85] that attacks the C^{4A} atom of FAD. The polysulfide chain is growing on Cys356. The role of the third cysteine of the active site, Cys128, is to maintain a redox active disulfide bridge with Cys160, and/or to maintain the position of the flavin ring of FAD [62; 79; 85]. An alternative mechanism was suggested for the *A. aeolicus* SQR; this mechanism involves the formation of a Cys128-S-S$^-$ disulfide species that attacks the C^{8M} atom of FAD. The electron transfer occurs during this step [85]. This leads to the formation of a transient Cys128-S-S$^+$ cation. The trisulfide bridge Cys128-S-S-S-Cys160 forms after recombination of the above cation with Cys160 thiolate. The role of Cys356 is to take over the growing polysulfide chain and, as a result, to recover the Cys160 thiolate. However, this mechanism is not applicable to FCC.

A. ferrooxidans SQR shares many structural and biological properties with other SQRs and with FCC, particularly with *A. aeolicus* SQR. The relative spatial positions of the three essential cysteines are similar to a certain degree in all four homologues (**Figs 2.8, 2.9**). The largest structural difference is found in FCC. The equivalent cysteine residue to Cys128 in FCC is Cys42; it is covalently attached to FAD and is situated on the other side of the isoalloxazine

ring. Cys42 of FCC does not directly participate in sulfur polymerization. In SQR from *A. ferrooxidans* Cys128 and Cys160 are situated on loop segments that are separated from the N-termini of corresponding helices by one (for Cys160) or two (for Cys128) residues; Cys356 is located in the middle of a β-strand. The initial redox active disulfide bridge may be located between Cys160 and Cys356 similarly to FCC, where the equivalent to the Cys160-S-S-Cys356 disulfide bridge was actually observed.

Although the previously suggested conventional mechanisms [79; 85] might be applicable in the case of *A. ferrooxidans* SQR (with the Cys160 thiol/disulfide being the nucleophile), we propose an alternative mechanism that involves Cys356-S-S$^-$ as the most probable nucleophile for attacking the C^{4A} atom of FAD. The details of this mechanism are presented in **Figure 2.10**. The initial nucleophilic attack of S^{2-} on the Cys160-Cys356 disulfide bridge leads to a thiol at Cys160 and a disulfide at Cys356 (**Figure 2.10, Ia,b**); the latter attacks the C^{4A} atom of the isoalloxazine moiety. The Cys356-S-S-C^{4A} adduct is formed and one electron is transferred to the isoalloxazine ring (**Figure 2.10, Ic**). The Cys160-S$^-$ thiol then attacks the Cys356-S-S-C^{4A}-FAD adduct releasing the FAD cofactor and forming a trisulfide bridge between Cys160 and Cys356 (Cys356-S-S-S-Cys160, **Figure 2.10 Ic,d**); a second electron is transferred in this step to the isoalloxazine ring that is now fully reduced. Protons that are added to the reduced cofactor likely come from solvent. Repetition of the above described steps leads to the elongation of the polysulfide chain that is growing on Cys160 (**Figure 2.10 II-VIII**). The elongation reaction stops when the stereochemical constraints prevent further incorporation of sulfur atoms. The octasulfur ring is released from Cys160 as depicted (**Figure 2.10, IX**). The role of Cys128 (most likely in the form of the disulfide) is confined to the release of the polysulfur product. The sulfide species observed in the pocket near Cys128 might produce the Cys128 disulfide that can

reach the S^{γ} atom of Cys160. The release of the hydrophobic polysulfur product could likely proceed as it was proposed [85] through the hydrophobic channel occupied by the DDM in the present structures or less likely through the sulfide channel that connects Cys160 with the exterior of the molecule. The other sulfide channel going to Cys356 is much narrower, and only water and sulfide ions can move through this channel.

The unique point of this hypothesis is that the S^- atom of the Cys356-S-S^- disulfide is the nucleophile that attacks C^{4A} at the start of each cycle. This hypothesis is supported by the fact that the distance of the S^- atom of the Cys356 disulfide to the C^{4A} atom of flavin is around 3.2-3.5 Å, whereas the distances between any other potential nucleophilic sulfur atom of Cys160 or Cys356 or the Cys160-S-S^- disulfide and the C^{4A} atom of flavin are too long for such a nucleophilic attack (**Figure 2.5**). It makes the Cys160 a less likely, although not impossible, candidate for the role of the nucleophile. The finding that the octasulfur ring in *A. aeolicus* SQR [85] is attached to the Cys160 also supports our proposed mechanism in which the polysulfide is growing on the Cys160. As the Cys^{128Ala} variant retains full activity in the FAD reduction assay it should be excluded as a potential nucleophile in the electron transfer to FAD. The fact that it is impaired in the DUQ assay indicates that the reaction stops when the polysulfur product accumulates on the Cys160, so the reaction turnover is diminished.

The abstraction of protons from hydrogen sulfide molecules and the consequent addition of protons to the reduced cofactor presumably occur either from active site base (the highly conserved Glu166) or from the proximity of abundant water molecules [79; 85]. For the protonation of the reduced ubiquinone two candidate residues could be proposed, Tyr411 and Lys391. Tyr411 is situated on the last mobile helix; its hydroxyl group is close to the benzoquinone ring and it is at a hydrogen-bonding distance from a water molecule. Lys391 is positioned farther

away, on the other side of the DUQ; the N^{ζ} atom of Lys391 is at the 4.6 Å distance from the closest atom of the benzoquinone head (and at 2.7 Å distance from the O4 atom of FAD), and it is close to water molecules. Both Tyr411 and Lys391 could potentially transfer protons from water to DUQ. Glu326 and Lys391 have been suggested as possible proton donors for reduced ubiquinone in *A. aeolicus* [85]. However, in the structures presented here, the carboxyl group of Glu326 is oriented differently, and it is unlikely to be the proton donor to ubiquinole.

The intermediate products observed in the structures here were modeled as a trithiosulfurous acid (four sulfur atoms, tetragonal form) or a branched pentasulfane (five sulfur atoms, hexagonal form) covalently attached to the S^{γ} atoms of Cys160 and Cys356 as schematically shown in **Figure 2.10** (boxed structures). The branching of the polysulfur moiety was also observed in the *A. aeolicus* SQR in which the octasulfur ring is covalently attached to Cys160.

The sulfur derivatives of the *A. ferrooxidans* SQR expressed in *E. coli* have been formed in the absence of any added sulfides. The *E. coli* expression host has been shown to produce sulfides endogenously in reductive environments [105].

The superposition of the active sites from *A. ferrooxidans* and *A. aeolicus* SQRs is shown in **Figure 2.9**. Evidently, they represent different moments in the catalytic cycle. The polysulfur product in *A. ferrooxidans* SQR structure is smaller than that in *A. aeolicus* SQR structure, consequently, the Cys160-Cys356 distances are significantly different for these structures. It appears possible for the Cys160 and Cys356 in *A. ferrooxidans* to move slightly from each other during stepwise polysulfide chain elongation. The alternative could be formation of smaller polysulfide chains that can rearrange into stable octasulfur rings outside the protein.

The difference among the several proposed mechanisms of electron transfer reaction from sulfides to FAD lies in assigning the nucleophile that attacks the flavin moiety. According to the other proposed mechanisms, the thiol group of Cys160 nucleophilically attacks the C^{4A} atom of flavin [62; 79; 85], or Cys128 indirectly attacks the C^{8M} atom of flavin via a persulfate species [85]. Definitely, more studies are needed to answer the remaining questions and uncertainties.

2.5 Tables

Table 2.1. Data collection and refinement statistics

	SQR native (PDB code 3kpi)	SQR-DUQ (PDB code 3kpg)	SQR C160A (PDB code 3kpk)
Data collection			
Space group	$P4_22_12$	$P6_222$	$P6_222$
Cell dimensions			
a, *b*, *c* (Å)	131.7, 131.7, 208.9	150.8, 150.8, 82.0	150.1, 150.1, 81.7
a, b, g (°)	90, 90, 90	90, 90, 120	90, 90, 120
Temperature (K)	100	100	100
Wavelength	0.97946	0.97950	0.97946
Resolution (Å)	50.0-2.30 (2.38-2.30)	20.0-2.30 (2.36-2.30)	50.0-2.05 (2.12-2.05)
R_{sym}	0.097 (0.986)	0.113 (0.987)	0.058 (0.814)
R_{rim}	0.104 (1.058)	0.116 (1.01)	0.063 (0.948)
R_{pim}	0.037 (0.384)	0.025 (0.218)	0.025 (0.566)
I / sI	19.5 (1.94)	23.7 (4.08)	31.7 (1.55)
Completeness (%)	100 (100)	99.7 (100)	98.1 (85.5)
Redundancy	8.0 (7.6)	21.4 (21.5)	6.6 (3.8)
Refinement			
Resolution (Å)	40.7-2.3	19.91-2.3	34.6-2.1
No. reflections	82001	24844	33789
R_{work} / R_{free}	16.7/20.0	17.0/20.9	18.5/23.1
Numbers of atoms[a]	7371	3643	3596
Protein	6564	3209	3202
FAD	106	53	53
DDM	-	35	35
Sulfur	13	7	2
DUQ	-	23	-
Ions/other	55/12	-	5
Water	621	316	299
B-factors (Å^2)			
Protein	56.5	46.6	50.4
FAD	43.2	30.5	31.6
DDM	-	42.7	46.5
Sulfur	67.7	58.6	72.0
DUQ	-	81.1	-
Ions	108.8	-	-
Water	60.8	50.3	50.5
Average	57.1	46.9	50.1
R.m.s. deviations			
Bond lengths (Å)	0.014	0.004	0.007
Bond angles (°)	1.625	0.910	1.183

Values in parentheses are for the highest-resolution shell.

[a] Number of nonhydrogen atoms present in the asymmetric unit.

[b] "Ions/other" includes SO_4, 1,3-butanediol, or 1,2-propanediol.

2.6 Figures

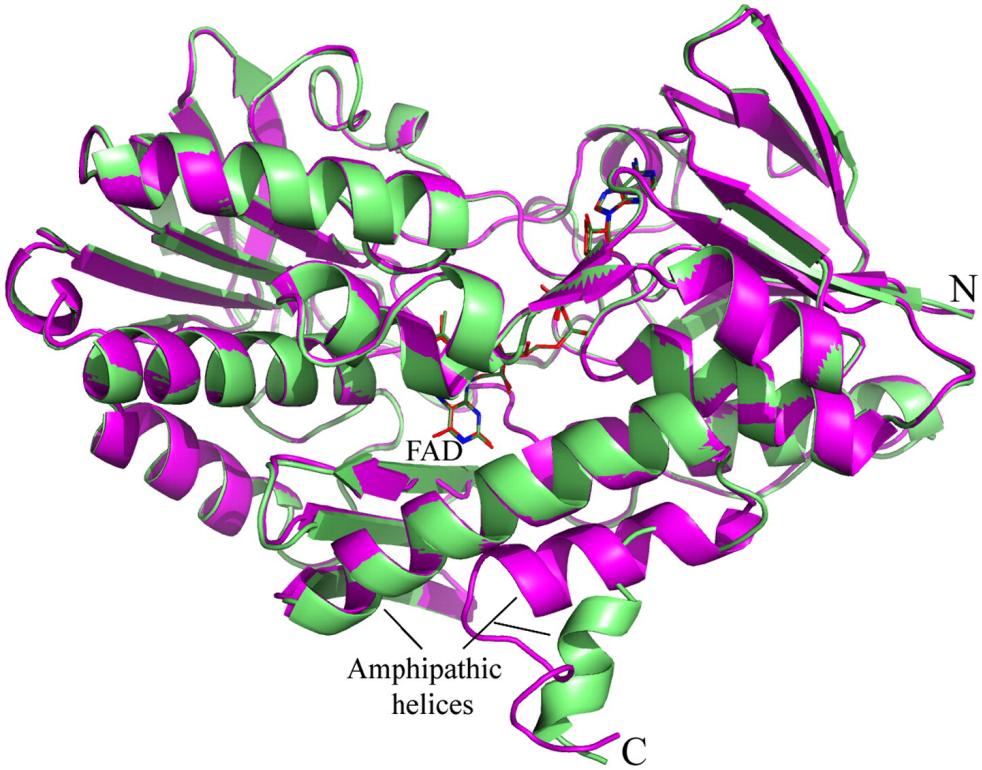

Figure 2.1. Superposition of the structures of the tetragonal (magenta) and hexagonal (green) crystal forms of *A. ferrooxidans* SQR.
The major conformational differences are observed in the C-terminal region; the N-terminal few residues of the last amphipathic helix of the hexagonal form of SQR partially unwind and the helix changes its orientation.

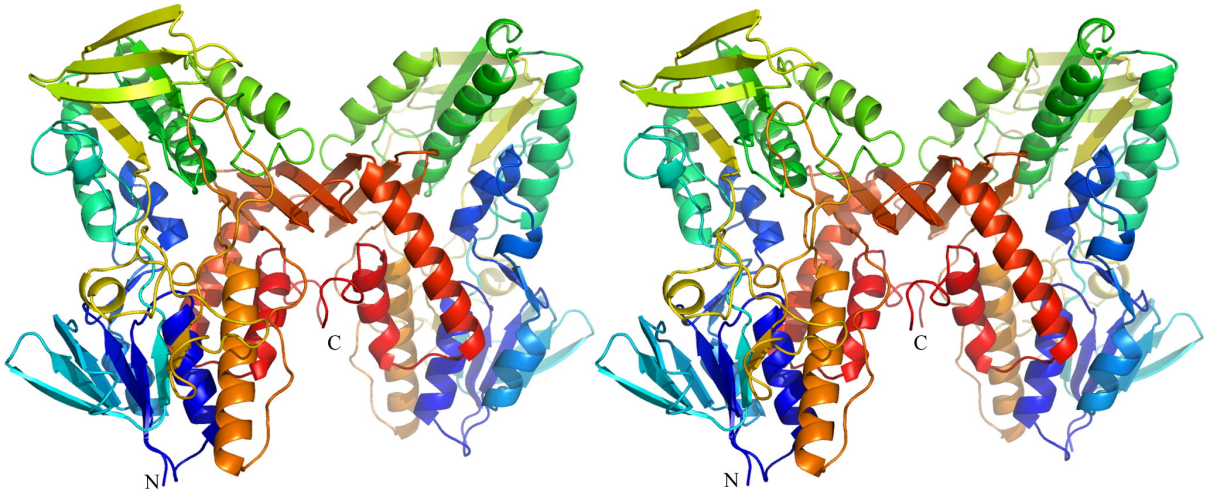

Figure 2.2. The crystallographic dimer of *A. ferrooxidans* SQR in the tetragonal crystal form. Each protomer is represented in rainbow colors: blue at the N-terminus, passing to red at the C-terminus. The majority of contacts across the dimer interface occur between the putative membrane-interacting segments of the enzyme. As a result, this dimer cannot exist in the membrane.

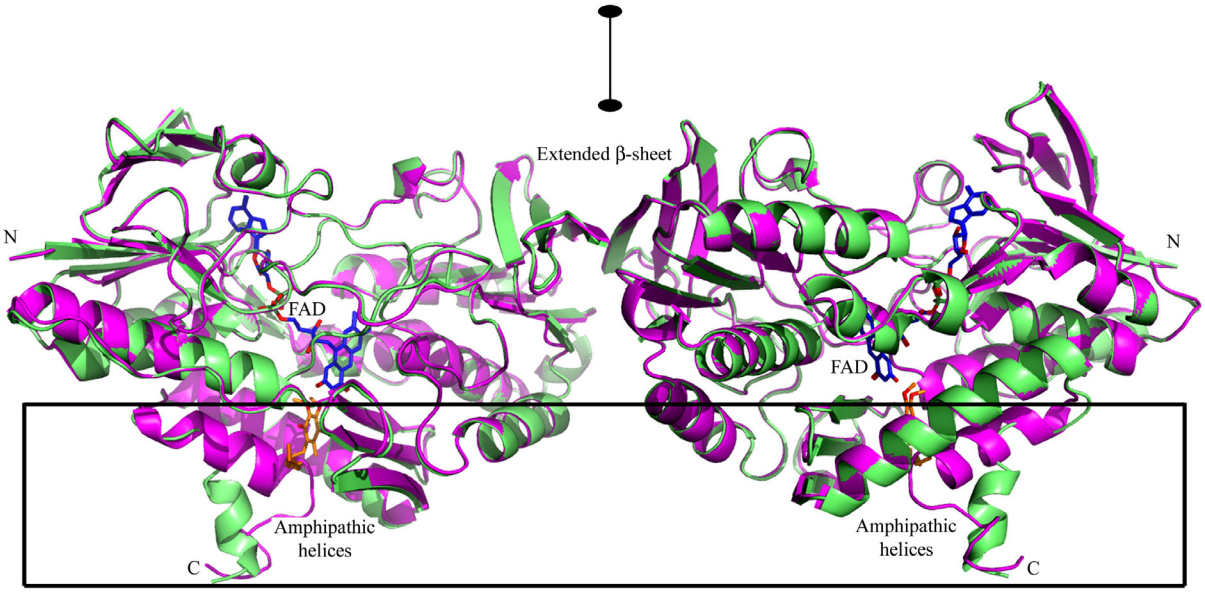

Figure 2.3. The biological dimer present in both crystal forms: tetragonal (magenta) and hexagonal (green).
The two protomers are related by a crystallographic two-fold axis. Two β-sheets, one from each protomer, align in an extended b-sheet on the top of the dimer. DUQ (shown in orange below the FAD cofactor) delimits the upper surface of the membrane. The two amphipathic helices penetrate into the membrane (shown as a rectangle) by about 20 Å (the height of the rectangle).

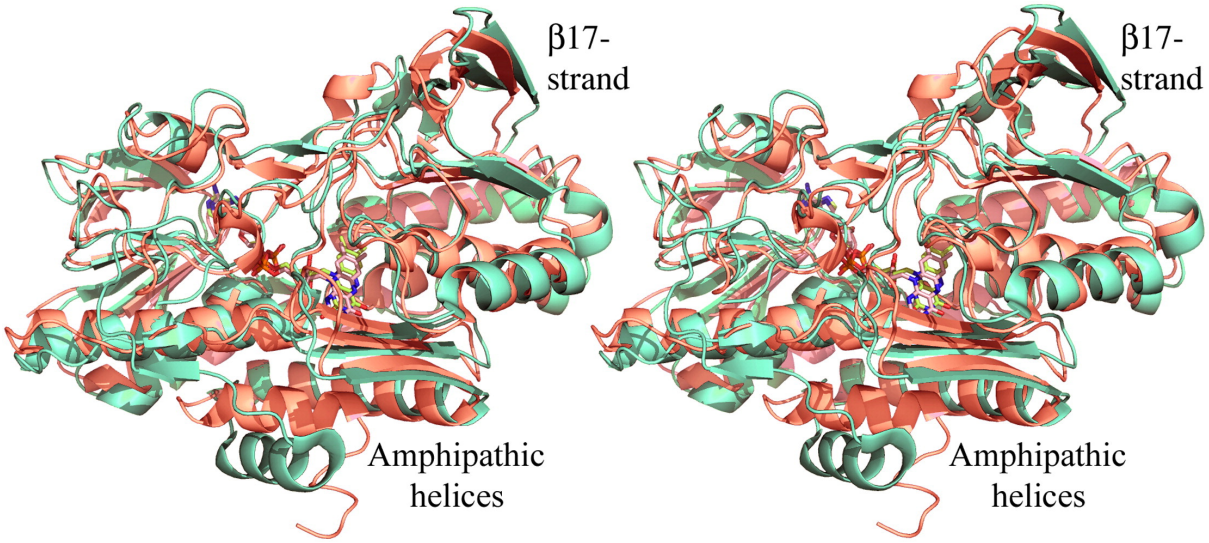

Figure 2.4. Superposition of the SQR structure from *A. ferrooxidans* (salmon) with that from *A. aeolicus* (green).
The FAD cofactors are represented by sticks. The major difference between two structures occurs in the C-terminal domains containing amphipathic helices. The b17 strand forms a dimer interface in the *A. ferrooxidans* SQR.

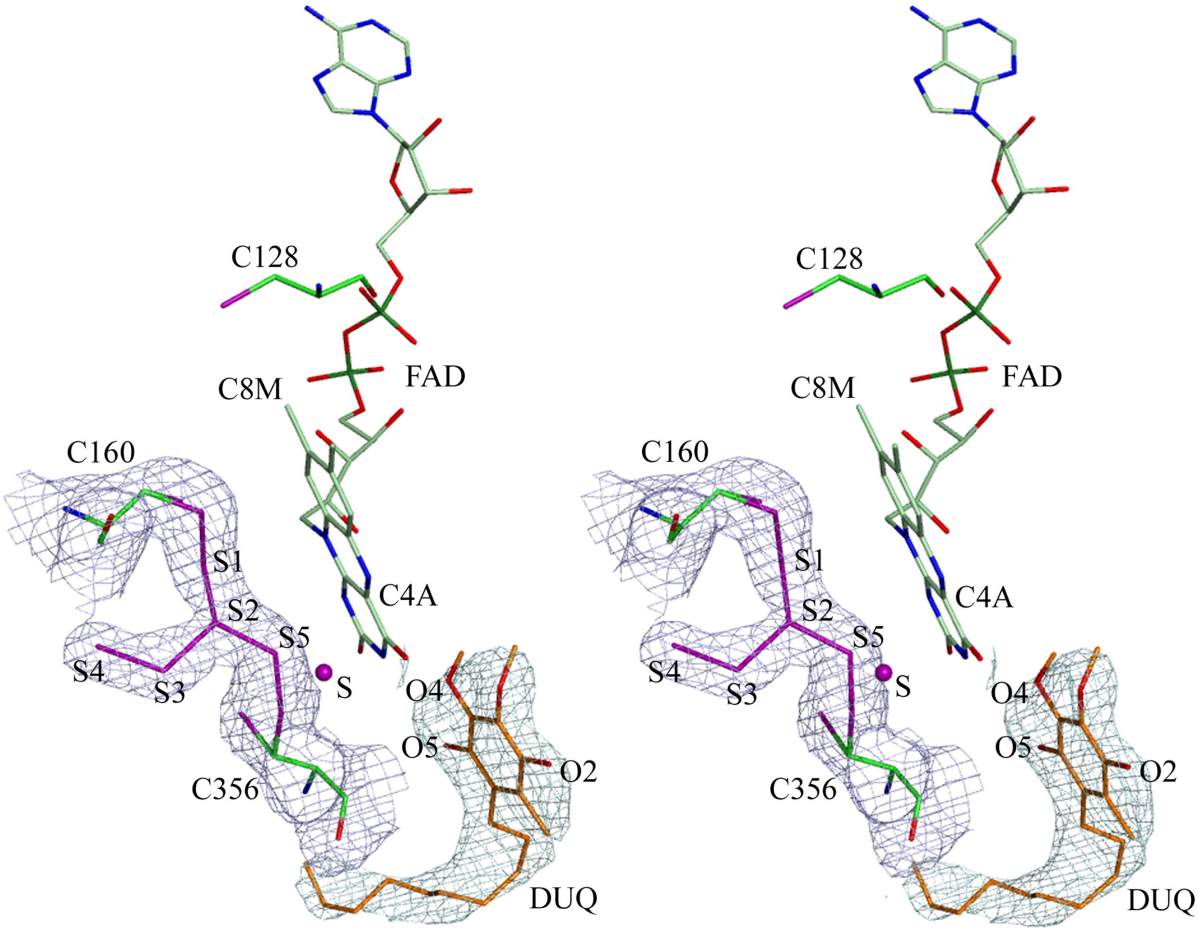

Figure 2.5. The redox active site and the ligands in the SQR-DUQ complex.
Two active site cysteines (Cys160 and Cys356; green carbon atoms) lie on the *re* side of the isoalloxazine ring of FAD (lime carbon atoms), the decylubiquinone (DUQ, orange sticks) is located on the *si* face of the isoalloxazine ring of FAD. Cys128 (green carbon atoms) is not modified. Sulfur atoms (magenta) form a branched pentasulfane that is covalently bound to both cysteines. The S^5 atom covalently attached to Cys356 is close to C^{4A} atom of FAD (distance is less than 3.5 Å). A putative sulfur atom (S) is at a hydrogen-bonding distance from Cys356 and Glu166 (not shown). The latter is thought to be the general base for abstracting protons from hydrogen sulfide. The $2|F_o|-|F_c|$, a_c electron density omit map is contoured at the 0.8s level in the region of DUQ, Cys160 and Cys356.

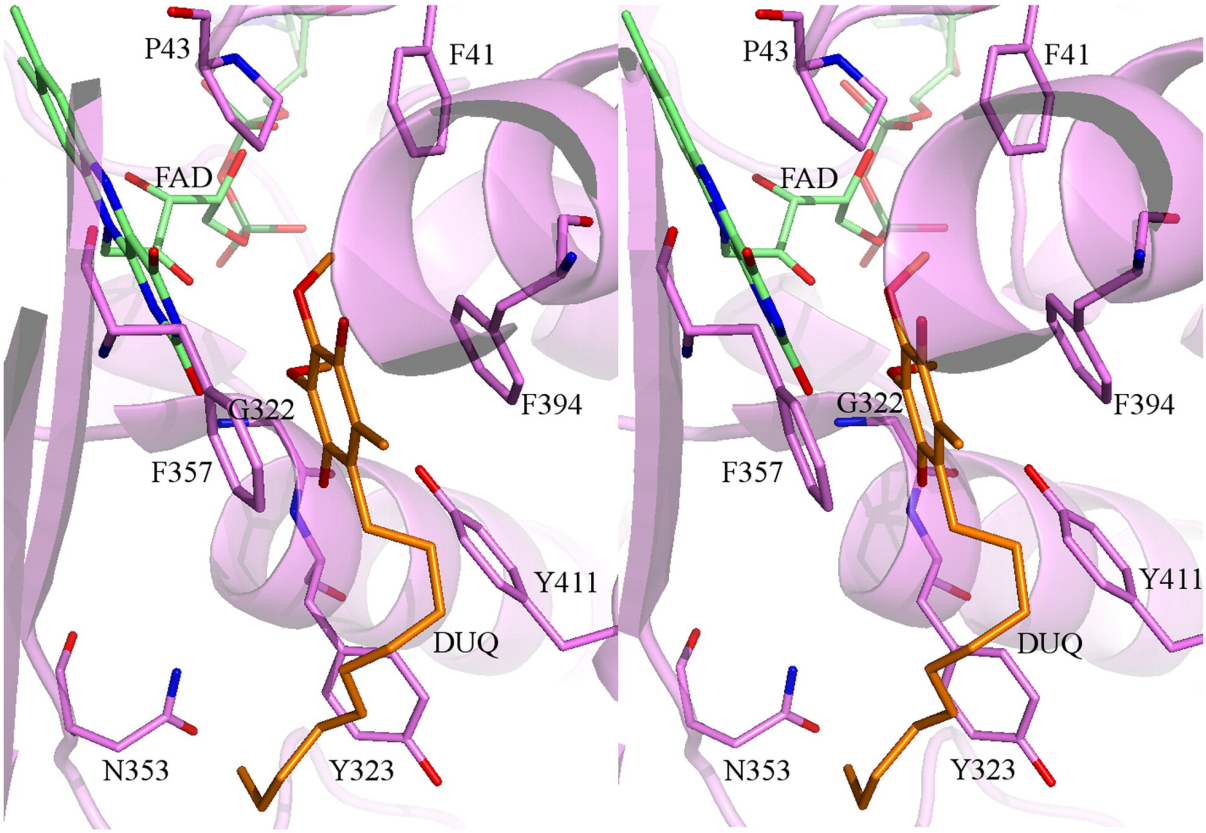

Figure 2.6. The aromatic ring of decylubiquinone (DUQ, orange sticks) is sandwiched between two benzene rings of Phe357 and Phe394 (green).

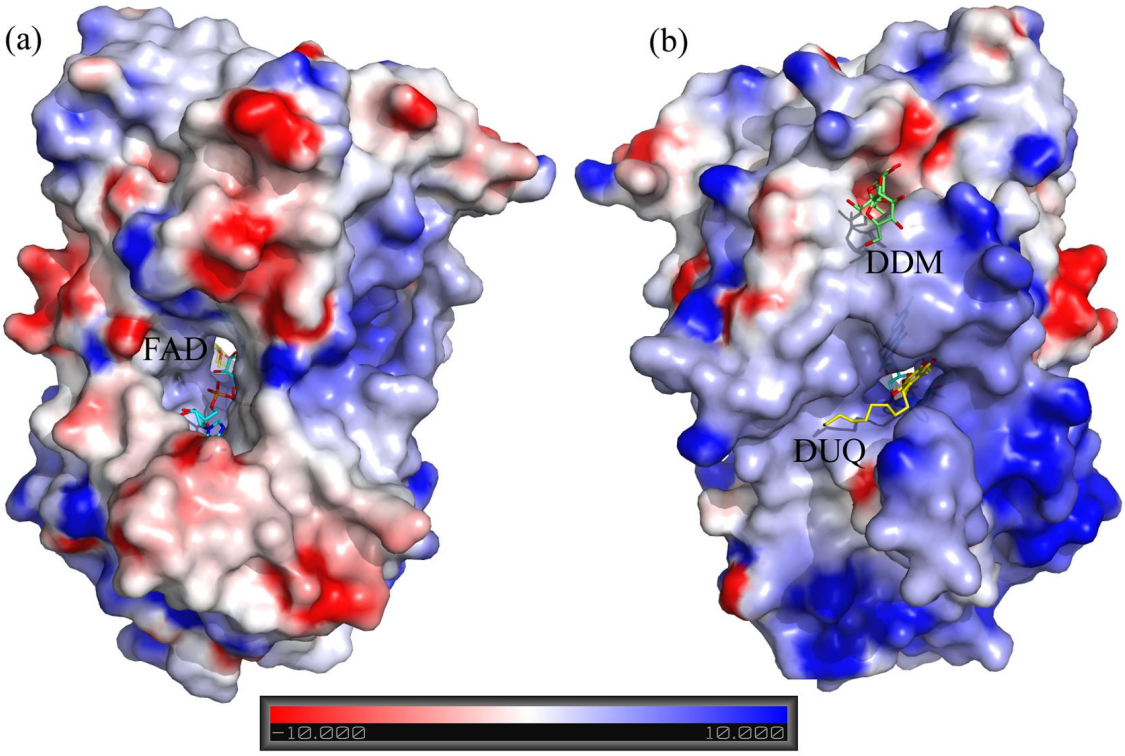

Figure 2.7. The electrostatic surface of SQR and channels through the molecule calculated by the program GRASP.
(a). One side of the SQR molecule has a largely negative (red) surface. The adenine moiety of the FAD cofactor is seen (cyan sticks) in the opening of the largest channel. (b). The opposite side of the molecule has a largely positive (blue) surface. The DUQ (yellow sticks) and DDM (the detergent, green sticks) are located in smaller channels that are connected to the large channel occupied by FAD.

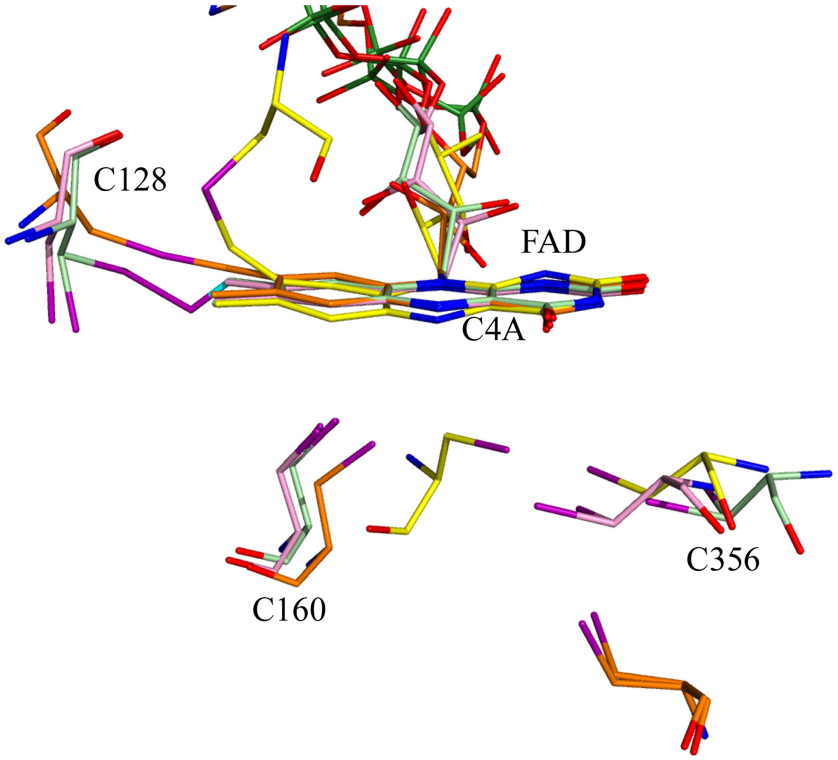

Figure 2.8. Superposition of active sites of four analogous sulfide-oxidizing enzyme structures. Only the atoms of the FAD cofactors were used for the superposition. The distance between the C^{a} atoms of Cys160 and Cys356 in *A. ferrooxidans* SQR (pink) is 2 Å shorter then in *A. aeolicus* SQR (pale green), and it is similar to the equivalent distance in *A. ambivalens* SQR (orange). The equivalent residues in *Allochromatium vinosum* FCC (yellow) are present as a disulfide bridge. The FAD cofactor is covalently attached to Cys128 in homologous SQRs from *A. ambivalens* and *A. aeolicus*, as it is to the equivalent cysteine in FCC (Cys42 in FCC numbering). It is thought that Cys42 of FCC is not involved in the catalytic mechanism. The polysulfide bridges between Cys160 and Cys356 are not shown (Sulfur atoms are depicted in magenta).

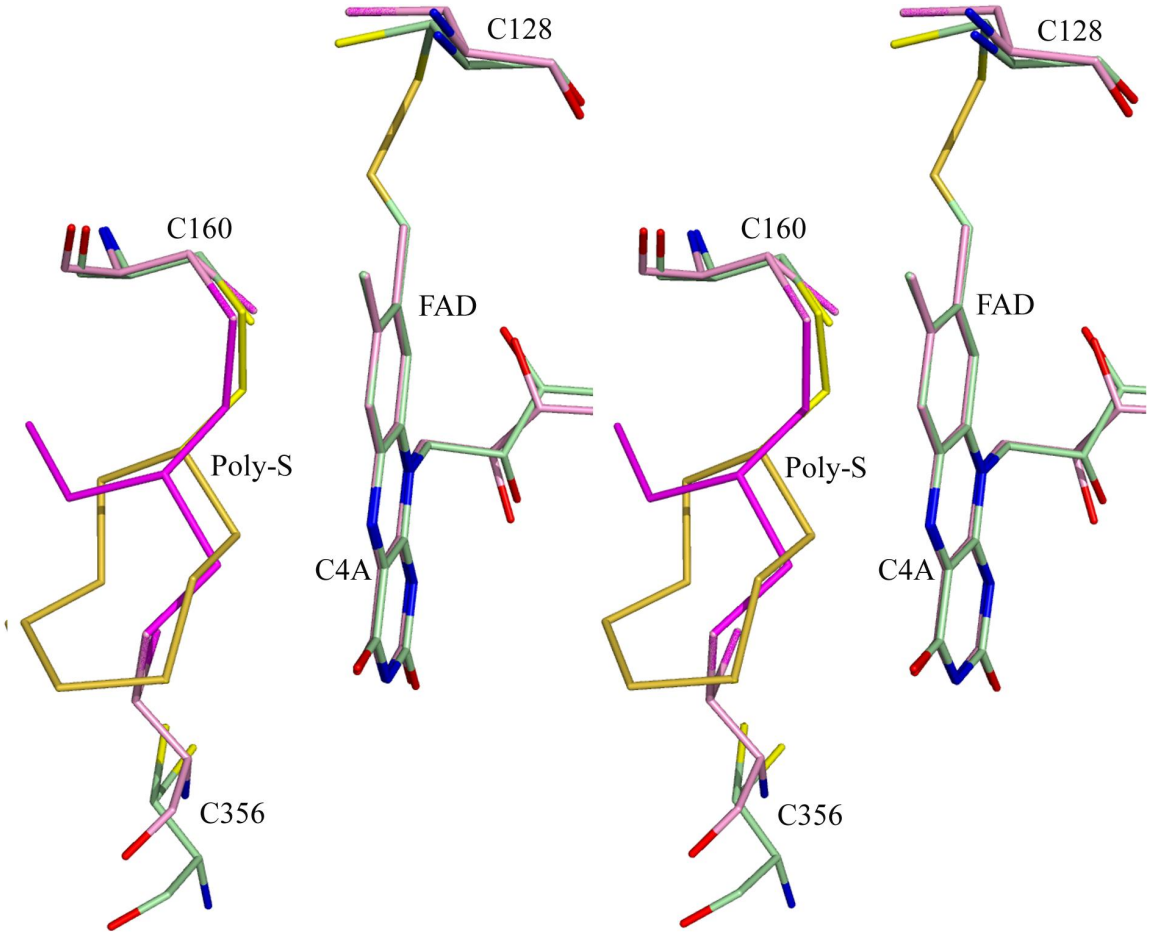

Figure 2.9. A detailed comparison of the active sites of *A. ferrooxidans* SQR (pale pink, sulfur atoms are colored in magenta) and *A. aeolicus* SQR (cyan, sulfur atoms are colored in yellow). Only the atoms of the FAD cofactors were used for this superposition. The positions of Cys128 and Cys160 are very similar, whereas Cys356 is slightly moved away by 2 Å from the Cys160 in *A. aeolicus* SQR. The Cys160 and Cys356 are connected by a branched polysulfide bridge. These cysteines are not bridged in *Aq. aeolicus*.

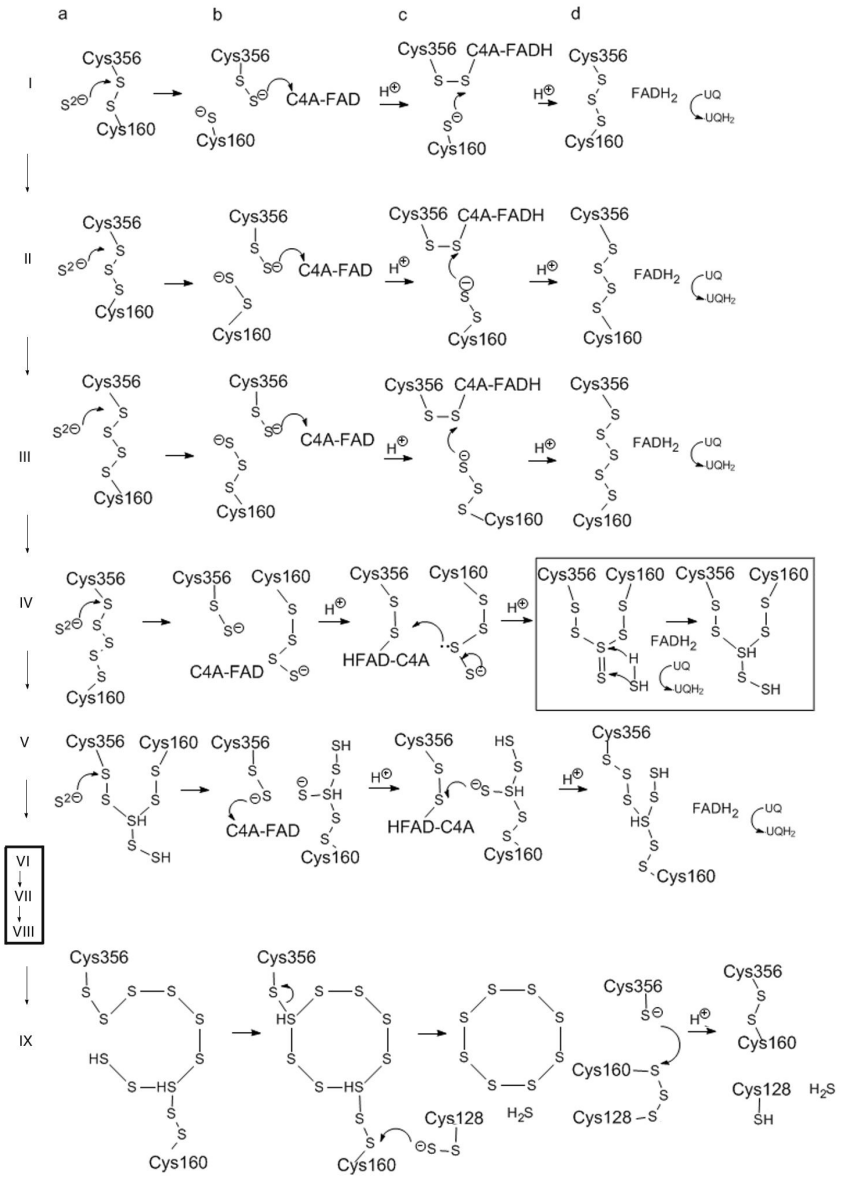

Figure 2.10. The proposed mechanism of sulfur reduction:
a sulfide ion attacks S^{γ} of Cys356 in each elongation cycle (I-VIII) resulting in a transfer of two electrons to FAD and an attachment of a sulfur atom into the polysulfide bridge. Cycle I. A sulfide ion attack on Cys356-S^{γ} breaks the disulfide bridge, consequently producing a disulfide on Cys356 and a thiol on Cys160. Cys356 disulfide attacks the C^{4A} atom of FAD forming a covalent adduct with C^{4A}-FAD and one electron is transferred to the isoalloxazine ring. Cys160-thiol attacks the adduct and releases FAD. A second electron is transferred. FAD is now fully reduced and will transfer the electrons to the ubiquinone pool in the membrane. Cycles II-VIII repeat the steps of cycle I (details of cycles VI-VIII are not shown). The polysulfide chain is growing on Cys160. The sulfur atom of the polysulfide chain nucleophilically attacks the covalent adduct of Cys356-disulfide with FAD. Formation of the branched polysulfide bridge may occur as shown in the cycle IV. The boxed intermediate products are consistent with the structures determined here. A possible octasulfur ring formation and its separation from Cys160 involves a nucleophilic attack most like from Cys128 disulfide.

Chapter 3: Structure-activity characterization of sulfide:quinone oxidoreductase variants

A version of this chapter has been published in Journal of Structural Biology.

Cherney, M. M., Zhang, Y., James, M. N. G., and Weiner, J. H. (2012) Structure-activity characterization of sulfide:quinone oxidoreductase variants. *J. Struct. Biol.* **178**, 319–328

Acknowledgments This research was supported by the Natural Sciences and Engineering Research Council Grant 171410-07 to J.H.W. Y.Z. was supported by a Ph.D. Entrance Scholarship from the Faculty of Medicine and Dentistry. Research described in this paper was performed at the Canadian Light Source, which is supported by the Natural Sciences and Engineering Research Council of Canada, the National Research Council Canada, the Canadian Institutes of Health Research, the Province of Saskatchewan, Western Economic Diversification Canada, and the University of Saskatchewan. Especially we are thankful to Shaun Labiuk and Julien Cotelesage for data collection.

3.1 Introduction

Acidophilic, chemolithotrophic bacteria derive energy for their growth from oxidative respiration using electron-rich inorganic compounds such as reduced sulfur or metal ions (i.e. Cu^{I}, Fe^{II}). The electrons are transferred from these compounds to the quinone pool in the membrane and, ultimately, to oxygen. Several enzymes are involved in chemolithotrophic respiration, including sulfide:quinone oxidoreductase (SQR). SQRs are considered to be monotopic membrane proteins [70]. Initially found in sulfidotrophic bacteria, they play a key role in the sulfide-dependent respiration and anaerobic photosynthesis, sulfide detoxification, heavy metal tolerance, and in mammals, in controlling optimal levels of hydrogen sulfide [62; 65; 66; 69; 77; 89]. Hydrogen sulfide was considered poisonous for mammals, but recently it has been identified as a widespread and biologically relevant signalling molecule [15; 19]. It also has significant cardio-protective activity due to its anti-apoptotic, anti-inflammatory and antioxidant effects [106; 107]. SQRs are ancient flavoproteins of the disulfide oxidoreductase (DSR) family. Recently several SQR structures, particularly SQRs from *Acidianus ambivalens* (*A. ambivalens*) [79], *Aquifex aeolicus* (*A. aeolicus*) [85], and *Acidithiobacillus ferrooxidans* (*A. ferrooxidans*) [37] have been determined; in addition, new biochemical data have been reported [108]. SQRs consist of 50 kDa subunits that can be monomers or can assemble into dimers or trimers in solution. SQRs contain one flavin adenine dinucleotide (FAD) cofactor per monomer. In different SQRs the FAD can be covalently-bound to a conserved, catalytically essential cysteine (Cys128 in the *A. ferrooxidans* numbering) or non-covalently bound *e.g. A. ferrooxidans* SQR [37]. SQRs also contain a redox-active polysulfide bridge formed between two other catalytic cysteine residues, Cys160 and Cys356. The three essential cysteines and the FAD cofactor together form the active site of SQRs.

SQR catalyzes sulfide oxidation to elemental sulfur by transferring two electrons from a sulfide ion via the FAD cofactor to the quinone pool in the membrane. However, the two-part enzymatic mechanism of SQR is not completely understood. The reductive part of the enzymatic reaction has been investigated in several structural and biochemical studies [37; 62; 79; 85]. The common feature of the proposed mechanisms is that a sulfide ion reduces the initial redox-active disulfide bridge; then one of the reduced cysteine residues, in the form of a thiolate or a disulfide, nucleophilically attacks the target atom on the isoalloxazine ring of FAD and forms a covalent adduct. The remaining cysteine residue as a thiol or a disulfide attacks the newly formed bond of the adduct and releases the reduced cofactor. As a result, FAD receives two electrons from a sulfide ion, whereas the sulfide ion is oxidized to elemental sulfur that becomes incorporated into a polysulfur chain connected to one or both catalytic cysteines via their sulfhydryl groups. Proton abstraction or addition is facilitated by surrounding residues or by water molecules. The polysulfur chain grows with each redox cycle until it cannot fit in the active site; then the polysulfur product (likely in the form of octasulfur) is released [85]. In the several mechanisms, different catalytic cysteines are proposed as nucleophiles; they attack different target atoms in FAD, C^{4A} or C^{8M}. The differences between the four proposed mechanisms have been summarized in **Table 3.1**. Notably, the transient adduct via the C^{4A} atom has never been observed. Even less is known about the oxidative part of the reaction that includes the transfer of electrons from FAD to quinones. To address important questions about the catalytic mechanism, in particular, which cysteine residues are directly involved in the electron transfer to FAD, a number of *A. ferrooxidans* SQR variants have been produced and their X-ray structures have been determined.

As selenides are homologous to sulfides in chemical properties, it was interesting to investigate whether SQR can interact with selenides. Selenide ions are considerably larger than sulfides so it is easier to identify selenides in the crystal structure. They also give an anomalous signal at a wavelength that is usually used for data collection at synchrotrons (around 1 Å). It is well-known that gold (I) complexes have an affinity for sulfur compounds. They form covalent bonds with sulfur that can substitute the ligands from gold (I) complexes. In proteins gold (I) compounds bind to thiol groups of cysteine residues. Herein we also present the structures of SQR complexes with gold (I) cyanide and with sodium selenide.

3.2 Materials and Methods

3.2.1 Construction and expression of SQR variants.

Construction of the site-directed mutants was carried out following the QuikChange method (Stratagene) using pLM1::SQR plasmid [86] as the template for mutagenesis. Mutants were verified by DNA sequencing carried out by the Department of Biochemistry DNA Core Facility at the University of Alberta.

Wild-type and mutant plasmids were transformed into *E. coli* BL21 (DE3) cells. The cells were grown at 37 ºC in 2 L of Terrific Broth (TB) medium [109] containing ampicillin (100 mg/liter) to an OD_{600} of 0.8. At this point, the cells were incubated at 25 ºC with the addition of 0.3 mM isopropyl ß-D-1-thiogalactopyranoside (IPTG) for 22 h with shaking at 180 rpm.

3.2.2 Purification of SQR variants

Cells were harvested and washed by centrifugation and resuspended in buffer containing 50 mM MOPS (pH 7.0), 500 mM NaCl, 0.2 mM PMSF and 10 mM imidazole (buffer A). The cells were ruptured in an EmulsiFlex high-pressure cell homogenizer (Avestin) at ~15,000 p.s.i. and ultracentrifuged at 40,000 rpm for 90 min at 4 °C. The supernatant was filtered through a

0.45 μm filter (Sartorius) and loaded on a 20 ml $NiSO_4$-charged chelating sepharose resin FPLC column (GE Healthcare) equilibrated in buffer A. Following sample loading, the column was washed with buffer A and SQR_{His6} was eluted with the same buffer containing 300 mM imidazole. The purified enzyme fractions were washed and concentrated to 5 mg/ml using a YM-30 Centricon tube (Amicon). All steps of protein purification subsequent to the initial thawing of cells were performed at 4 °C.

3.2.3 Enzymatic activity assayed by reduction of FAD

The FAD reduction assay was performed in the absence of decylubiquinone (DUQ) by monitoring the reduction of FAD absorption at 375 nm and 450 nm after 0.03 μM Na_2S was added [62]. The reaction mixture contained 50 mM Bis-Tris (pH 6.5), 20 mM glucose, 1 unit of glucose oxidase per mL and 10 units of catalase per mL. Anoxic conditions were established by flushing with N_2.

3.2.4 Enzymatic activity assayed by reduction of DUQ

The DUQ reduction activity of SQR was measured as described previously [110] as the decrease of absorbance at 275 nm due to the reduction of decylubiquinone (DUQ). The reaction mixture contained 50 mM Bis-Tris, pH 6.5, 20 mM glucose, 50 μM DUQ, 1 unit of glucose oxidase per mL and 10 units of catalase per mL. The pre-mixture (50 mM Bis–Tris, pH 6.5, 20 mM glucose) was first flushed with N_2 to establish anoxic conditions, and the reaction was started by the addition of 100 μM of freshly prepared Na_2S. One unit of activity was defined as the amount of enzyme that catalyzed the reduction of 1 μmol of DUQ per minute [102]. The millimolar differential extinction coefficient (12.5 mM^{-1} cm^{-1}) was determined by the measurement of difference spectra of oxidized and reduced DUQ.

3.2.5 Crystallization and data collection

The *A. ferrooxidans* wild-type SQR and variants were crystallized according to the previously published protocol [37; 86]. Briefly, the crystals grew at a protein concentration of 10 mg/ml in hanging drops from 30% polyethylene glycol 600, 0.1 M Bis-Tris buffer (pH 5.5), 0.1 M $MgSO_4$, and 0.05% DDM. In some cases DDM was not added to the mother liquor. The cocrystals of the complexes with DUQ or sodium sulfide or sodium selenide were produced by adding 2 mM of these compounds to the mother liquor in the same crystallization conditions. Crystals for data collection were flash-cooled in liquid nitrogen. Data were collected on beamline 08ID-1 at the Canadian Light Source (Saskatoon) using a temperature of 100 K. Raw data were processed with HKL-2000 [93], Mosflm [111] and Scala [112].

3.2.6 Structure determination

The structures of the wild-type and the variant SQR complexes were refined using the PHENIX package and a maximum likelihood target [113]. Model rebuilding at different refinement stages was performed with Coot [98]. Pymol was used for viewing the structures and for generating figures [100].

3.2.7 Accession numbers

Coordinates and structure factors have been deposited in the Protein Data Bank with accession numbers: 3SX6, 3SXI, 3T14, 3T2K, 3SZW, 3SY4, 3SYI, 3SZF, 3SZ0, 3SZC, 3T0K, 3T2Y.

3.3 Results

3.3.1 Enzymatic activity assays

In order to investigate the role of several highly conserved residues including the three cysteine residues [62] that might be critical for SQR activity, a number of singly substituted

variants were generated and their enzymatic activity determined. The variants were over-expressed in *Escherichia coli* and purified to homogeneity. The activity assays were designed to monitor the reduction and oxidation steps separately. The reduction of FAD (FAD assay) was monitored spectroscopically in the absence of decylubiquinone (DUQ) at 375 nm and 450 nm after sulfide was added, whereas the reduction of DUQ (DUQ assay) was measured by the decrease in absorbance at 275 nm, also after the addition of sulfide. The activity results are summarized in **Table 3.2**. The Cys^{356Ala} variant exhibited complete loss of FAD reduction, whereas the Cys^{160Ala} variant retained approximately 32% of the FAD reduction activity. All of the variants showed either decreased activity or complete loss of activity in the DUQ reduction assay. The Cys^{356Ala} variant lacked the DUQ reduction activity due to its inability to reduce FAD, whereas the Cys^{160Ala} variant lacked the DUQ reduction activity despite its ability to retain one third of the FAD reduction activity. The remaining variants showed full activity in the FAD reduction assay and reduced activities in the DUQ reduction assay compared with the activity of the wild-type enzyme.

3.3.2 Crystallization and structure determination of SQR variants

Variants were crystallized in the presence of the detergent n-dodecyl β-D-maltoside (DDM) in space group $P6_222$ using the protocols [37] reported previously for the wild-type protein and the Cys160Ala variant. The substrates, Na_2S and/or the electron acceptor DUQ, were added in some crystallization conditions. The variant structures were solved by refinement using the wild-type SQR structure (PDB ID 3T31) as the starting model. Superposition of each of the variant structures on the wild-type protein structures (PDB code 3T31 and 3T2Z) gave r.m.s.d.s in the range 0.15 to 0.20 Å for 390-406 C^{α} atom pairs and 0.19 to 0.27 Å for 375-390 C^{α} atom

pairs, respectively. The data collection and refinement details are presented in **Supplementary Tables 3.1, 3.2 and 3.3**.

3.3.3 Structure of the Cys356Ala variant

The active site of this variant is lacking the catalytic cysteine residue, Cys356. As a result, the activity tests showed no enzymatic activity for both steps (FAD reduction and DUQ reduction)(Table 2). Crystals of the variant were obtained in the presence and in the absence of Na_2S. They were isomorphous with the previously described hexagonal crystals (space group $P6_222$) of the wild-type SQR in complex with DUQ and DDM and with the crystals of all *A. ferrooxidans* SQR variants. The Cys^{356Ala} variant structure has well-defined electron density for more than 90% of the sequence; the final C-terminal helix is partially unwound and is poorly defined. The last 16 residues are completely disordered.

The structure of the Cys^{356Ala} variant showed some positive electron density on the S^{γ} atom of Cys160; it was modeled as a disulfide bonded to the S^{γ} atom of Cys160 (Cys160-S^{γ}-S-SH, **Figure 3.1**). The positive electron density on S^{γ} atom was present with and without addition of Na_2S due to the fact that the *E. coli* expression host produces sulfides exogenously in reductive environments [105]. The occupancies of the persulfide sulfur atoms were refined to about 0.5. The density for the S^{γ} atom shows no alternate conformations. The distance between the C^{β} atoms of Cys160 and Ala356 differs very insignificantly from the distance between corresponding atoms of residues Cys160 and Cys356 in the wild-type protein. The sulfur atom of Cys128 is in the same position relative to the isoalloxazine ring of FAD as it is in the wild-type and the C160A variant. The distance between S^{γ} atom of Cys128 and C^{8M} atom of FAD is approximately 4 Å. The isoalloxazine ring of the FAD cofactor does not form a covalent adduct with the Cys160-S^{γ}-S-SH residue. When 2 mM Na_2S was added to the crystallization mother

liquor contained 2 mM Na_2S, some additional positive electron density for solvent molecules (water and/or sulfide ions) appeared in the active site region (**Figure 3.1**). One of these additional solvent molecules (W, **Figure 3.1**) is situated at a very short distance from the O^4 atom of FAD (about 2.4 Å). It also makes hydrogen bonds with the N^5 atom of FAD, the carbonyl oxygen of Phe357 and three waters. This cluster of solvent molecules connects to a narrow solvent channel passing in the vicinity of Glu166, Pro43 and Trp47. It is also situated close to Ala356 so that in the wild-type protein the sulfide ions would be accessible to Cys356.

DUQ (not shown in **Figure 3.1**) has a defined electron density only for the ring moiety, whereas the hydrocarbon tail is disordered. The position of the aromatic ring of DUQ has changed slightly compared to the previously reported wild-type SQR-DUQ complex [37], but it is still confined in the hydrophobic space between Phe357, Phe394, Pro43, Phe41, and the isoalloxazine moiety of FAD.

3.2.4 Structures of the partially active variants, Cys^{128Ala}, Cys^{128Ser}, Ser^{126Ala}, His^{132Ala} and His^{198Ala}

These partially active variants all crystallized in the hexagonal space group $P6_222$. All crystals were isomorphous among all variants and the wild-type protein in this space group and had very similar structures. The common problem of all structures described in this paper is the C-terminal helix, one of the two amphipathic helices that are proposed to penetrate into the membrane; it is partially unwound and poorly defined as is the case in all structures in the hexagonal crystal form. On the other hand, this helix is well defined in the structure of the wild-type protein in the tetragonal crystal form [37]. The isoalloxazine ring of the FAD cofactor is slightly bent when refined with loose planar restraints. In order to detect differences in the

intermediate products of the catalytic cycle several crystals of each variant were used for data collection; the data sets from each crystal were processed separately.

Ser^{126Ala}, His^{132Ala} and His^{198Ser}

A number of SQR structures of the wild-type and variants showed a sulfide ion located in the vicinity of Cys128. The sulfide binding pocket includes residue Ser126 (**Figure 3.2**). The O^{γ} atom of Ser126 makes a hydrogen bond with the sulfide ion in the wild-type protein. The Ser^{126Ala} variant was made in order to determine the effect of the loss of this hydrogen bond on SQR activity and to observe the state of the Cys128 sulfhydryl group by X-ray structure determination. The Ser^{126Ala} variant had significantly impaired DUQ reduction activity; it retained only 30% activity. However, it showed full activity in the FAD reduction assay. The crystal of this variant diffracted to 1.91 Å resolution. In order to detect the anomalous signal from sulphur atoms a second dataset from a crystal of this variant was collected at 7.0 keV; the crystal diffracted to 2.35 Å resolution. The anomalous map calculated from the second dataset confirmed the presence of a sulfide ion in the sulfide binding pocket (**Figure 3.2**) despite the lack of one hydrogen bond (Ser126-O^{γ} – sulfide ion). Both sulfur atoms (the sulfide ion and the S^{γ} atom of Cys128) exhibited anomalous scattering (**Figure 3.2**, magenta mesh). The sulfide ion makes two hydrogen bonds with the N^{δ} atom of His132 (2.8 Å), and with the main chain N atom of Cys128 (3.2 Å). There are also several additional van der Waals contacts with the carbon atoms in the side chains of Leu109, Cys128, His132, and Ser126. The distance between the S^{γ} atom of Cys128 and the sulfide ion is 4.1 Å.

The His^{132Ala} variant also showed reduced activity in the DUQ reduction assay but no decrease in the FAD reduction assay. The structure of this variant was determined to 2.5 Å resolution. The electron density for the final amphipathic helix was not observable, so the C-

terminus was cut off at the residue 407 (there are 434 residues in *A. ferrooxidans* SQR). The sulfide binding site did not have a bound sulfide ion, likely due to lack of the hydrogen bond in the His132Ala variant.

His198 is highly conserved among SQRs. The His^{198Ala} variant was 40% less active in DUQ reduction than the wild-type protein (**Table 3.2**). The crystal of this variant diffracted to 2.1 Å resolution. It showed no differences in the protein folding or in the active site of SQR. However, this variant lacks a hydrogen bond and a salt bridge between His198 and Glu310 that in the wild-type SQR connect two loops. The loss of these interactions could possibly affect the overall stability of the protein.

Cys^{128Ala} and Cys^{128Ser}

The third essential residue of the SQR active site, Cys128, was replaced by an Ala or by a Ser in two of the variants. They were fully active in the FAD reduction assay. The Cys^{128Ala} variant showed almost one third of the DUQ reduction activity. Three crystals (1, 2 and 3) of the Cys^{128Ala} variant were used for data collection, processing and refinement. They diffracted to 2.1 Å, 2.35 Å and 2.5 Å resolution, respectively. Crystal 1 was co-crystallized with DUQ, whereas crystals 2 and 3 did not contain DUQ in the mother liquor. All three crystals of this variant showed different structures of the active site (**Figures. 3.3a, 3.4a, 3.4b**). More detailed description of their active sites, as well as of other partially active variants is given below, in the section titled "Sulfide oxidation site".

The Cys^{128Ser} variant showed complete loss of activity in the quinone reduction assay (**Table 3.2**). Only one crystal of the Cys^{128Ser} variant (grown with DUQ) showed useful diffraction. The data from this crystal were processed and refined to 2.3 Å.

Sulfide oxidation site

The structures of all of the partially active variants showed additional electron density peaks associated with the sulfhydryl groups of the catalytic residues, Cys160 and Cys356, in the $2|F_o|-|F_c|$ and the $|F_o|-|F_c|$ electron density omit maps. At least three typical electron density intermediate states were found in the active sites of these variants. The most prevalent intermediate state (intermediate state I, **Figures 3.3a-c**) could be described by the presence of persulfide groups on both redox-active cysteines. However, the electron density between the persulfide groups is not continuous, so they are not covalently bonded. The other striking feature is the presence of a free hydrogen sulfide ion in close proximity to both persulfide groups, but it is not covalently connected to either of them. The distance between the sulfide ion and the persulfide sulfur of Cys356 is 3.1 to 3.2 Å, whereas the distance from the sulfide ion to the persulfide sulfur of Cys160 is longer, in the range of 3.6 to 4.0 Å (values are from 3 structures, **Figures. 3.3a-c**). A solvent molecule (likely water) usually accompanies the sulfide ion due to several hydrogen bonding interactions with the main chain oxygen (Ser159, Leu199) and nitrogen (Phe167) atoms. It is situated within a hydrogen bonding distance from the sulfide ion. Interestingly, the anomalous map calculated for the Ser^{126Ala} variant (data collected at 7.0 keV) showed large peaks for the persulfide group on Cys160 and a small peak for S^{γ} thiol of Cys356 (not shown; in addition there are peaks on the Cys128 thiol and the sulfide ion in the sulfide binding pocket, **Figure 3.2**). No other anomalous peaks for the sulfur atoms in the sulfide oxidation site were observed, likely due to the high *B*-factors for those sulfur atoms.

Another active site intermediate state (intermediate state II) is shown in **Figure 3.4a**. It was observed in one of the crystals of the Cys^{128Ala} variant and in one crystal of the His^{132Ala} variant. In this intermediate state, the electron density peak on the $2|F_o|-|F_c|$ omit map extends from the S^{γ} atom of Cys356 beyond the persulfide sulfur indicating that a third sulfur atom is

covalently attached to the persulfide group at Cys356, thus forming a trisulfide group; the Cys160 residue remains as the persulfide. Cys160 and Cys356 are not connected as can be seen by the non-continuous electron density.

In the third active site intermediate state (intermediate state III), a pentasulfide bridge covalently connects the two redox-active cysteines, in which two sulfur atoms belong to the mentioned cysteines and a trisulfide is inserted into the bridge (**Figure 3.4b**).

Some structures of the active sites show an overlap of intermediate states, for example, state I and state III (**Figure 3.4c**). This was interpreted initially, as a branched tetrasulfide [37]. The branching of polysulfurs was observed in the active site of *A. aeolicus* SQR [85]. In that structure the branched polysulfur was not planar. However, in the structures of the *A. ferrooxidans* SQR shown in **Figure 3.4c** the omit electron density is planar in the view from the top (not shown). Sulfur, in general, has very versatile bonding abilities in terms of bond length, bond angles and hybridizations. However, the planar tetrasulfur arrangement that is bonded to two sulfhydryl groups of Cys160 and Cys356 is not known in sulfur chemistry. Overlapping of two (or three) intermediate states in which sulphur atoms have partial occupancies could explain the branched configuration of the electron density. The refined occupancies of the sulfurs vary in the range of 0.3 to 0.6 for several different crystal structures, which would allow for two alternate intermediate states.

In all of these intermediate states the sulfur atom that makes a covalent bond to the thiol of Cys356 is also very close to the N5 and C4 atoms of the isoalloxazine ring (3.2-3.8 Å). The S^{γ} atom of Cys356 has alternate conformations; as does the persulfide sulfur on Cys356 (**Figure 3.5**).

The three intermediate states were observed in the wild-type protein (tetragonal and hexagonal crystal forms) and in the variants. They likely represent three different stages in the catalytic reaction.

3.3.5 Active site of the wild-type SQR complex with sodium selenide

Selenides, the selenium versions of sulfides, could be potential substrates or inhibitors of SQR. The wild-type SQR was co-crystallized with Na_2Se, with and without DUQ. The crystals grew in the hexagonal space group $P6_222$ (**Supplementary Table 3.2**) and they were isomorphous with the other hexagonal crystals of SQR and its variants. The S^{γ} atom of Cys356 had, as usual, two alternative conformations with high B factors. Strong anomalous signals for the selenium atoms were observed in the anomalous map of the active site (**Figure 3.5a**). As in the case of the two overlapping conformations described for the SQR complexes with sulfides, there are two overlapping conformations with the selenide ligands in the active site. One conformation (conformation A) represents the intermediate state I in which Se atoms are bound to S^{γ} sulphurs of Cys160 and Cys356 (equivalent of persulfides); the other conformation is the intermediate state III (**Figure 3.4c**). In this conformation (conformation B), the selenium atoms form a tri-selenide bridge that is covalently inserted between the S^{γ} atoms of both active site cysteines (Cys160-S^{γ}-Se-Se-Se-S^{γ}-Cys356). Selenium atoms bonded to Cys356 are situated at 3.2Å to 3.3Å distances from the C^4 and N^5 atoms of FAD, respectively. This is the same distance as for the persulfide sulfur on Cys356 that is involved in the catalytic reaction. Superposition of the active sites of SQR with polyselenide and with polysulfide in similar intermediate states is shown in **Fig 3.5b**. The distance between the C^{α} atoms of redox active cysteines (Cys160 and Cys356) increased by 0.4 Å in the polyselenide complex (conformation B) whereas the distance between the corresponding C^{β} atoms increased by 0.5 Å. This increase is consistent with the

larger covalent radius of selenium compared with that of sulfur (0.2 Å). The structure of this complex confirms that selenide is a substrate involved in the same redox reactions as sulfide.

3.3.6 Active site of the wild-type SQR complex with gold (I) cyanide

Gold (I) cyanide, $Au(CN)_2^-$, reacts with thiol groups of cysteines to form gold thiolates. Gold (I) usually has two ligands that form a linear complex with the gold atom between them. It was interesting to see how the cysteine residues of the active site react with gold (I). The wild-type SQR crystals were soaked with 2 mM sodium gold (I) cyanide over night. The structure of the active site showed a large anomalous peak (22 σ) for gold at Cys128 and a smaller split peak (4 σ and 4.5 σ) at Cys160 (**Figure 3.6**). The occupancy of the gold atom at Cys128 is approximately 65%. The bond length between the S^{γ} atom of Cys128 and the gold atom is 2.3 Å; the latter is positioned at a distance of 3.7 Å from the C^{8M} atom of FAD. The gold atom in this structure has only one ligand, the S^{γ} atom; no second ligand is seen in the 2|Fo|-|Fc| electron density map.

The S^{γ} atom of Cys160 has two alternative conformations. The anomalous peak for the gold atom at Cys160 also has two conformations; however they are of low occupancies of 24% and 18%. In one of the conformations, the gold atom is positioned between the thiol group of Cys160 and the sulfide ion (the distances are 2.5 Å, the angle S-Au-S is 132°). The normal Au(I)-S bond length (the sum of the covalent radii) is 2.36 Å, the S-Au(I)-S angle is close to 180°. In the other conformation, the gold atom has two ligands; one ligand with a shorter bond (the thiol group of Cys160, 2.4 Å) and the other ligand at a longer distance (the persulfide sulfur of Cys356, 2.7 Å); the S-Au-S angle is 160°. However, the gold peaks are not well defined. No anomalous peak for gold was observed at Cys356. The difference in the gold binding by cysteine

residues of the active site can be attributed to the poor accessibility of a large gold cyanide complex $Au(CN)_2^-$ to the sulfur atoms of Cys160 and, especially, of Cys356.

The persulfide group of Cys356 has one conformation. A sulfur species is positioned at approximately 2.6 Å distance from the persulfide sulfur atom on Cys356. This distance is longer than the average single S-S bond (2.06 Å), but it is shorter than the van der Waals distance between sulfur atoms (~3.4 Å) indicating some weak bonding.

3.4 Discussion

The mechanism of SQR remains ambiguous despite several recent publications of structural and biochemical studies. A cysteine triad, Cys128, Cys160 and Cys356, is essential for enzymatic activity [62]. Several different catalytic mechanisms of SQR involving these cysteines have been proposed (**Table 3.1**). To understand better the role of each essential cysteine and other conserved residues in the active site, several variants of *A. ferrooxidans* SQR have been produced and their structures have been determined. The structures showed that the spatial positions of the three catalytic cysteines, or their substitutes, have not changed relative to each other in comparison to the wild-type protein. There were no significant changes in the distance between the C^{α} atoms of Cys160 and Cys356 or equivalent residues. The S^{γ} atom of Cys128 was never modified by additional electron density in the His^{198Ala}, Ser^{126Ala}, His^{132Ala} and Cys^{356Ala} variants, neither was it modified in the previously reported variant Cys160Ala.

The several proposed SQR mechanisms (**Table 3.1**) were all based on the formation of a transient covalent adduct between one of the active cysteines and the isoalloxazine ring of FAD (directly or via a persulfide linkage). We had hoped to trap this covalent adduct by preventing the next catalytic step. For that purpose, each of the three catalytic cysteines was substituted with alanine or serine residues in the variants Cys^{160Ala}, Cys^{356Ala}, Cys^{128Ala} and Cys^{128Ser}. In one of

these variants it was hoped that the first step involving the nucleophilic attack of an essential cysteine (Cys160 or Cys356) on the C^4 atom of FAD would have taken place, but that the next step would be disabled due to the substitution of the other catalytically important cysteine residue. However, these covalent adducts have not been observed in the structures of any of the SQR variants. Neither has the thiolate-FAD covalent bond been detected in the numerous structures of disulfide reductases including different variants and complexes with substrates. As a result, none of the previously proposed mechanisms could be structurally verified (the previously proposed thiolate-FAD adducts of disulfide reductases were based on spectrophotometric data). The nucleophilic attack mechanism could still be valid, assuming the covalent adducts with FAD are very unstable and are hydrolysed by other nucleophiles in solution. Without experimental confirmation of the covalent adduct of an active site cysteine with FAD, alternative mechanisms should also be considered.

It is well known that cysteines can be involved in a number of reactions other than nucleophilic attack including thiol-disulfide exchange and radical reactions, metal ion transfer, oxygen atom transfer, hydrogen atom transfer, electron transfer, proton transfer, and hydride transfer [114]. The direct electron transfer can be an alternative option to the nucleophilic attack mechanism. As will be reported elsewhere, activity assays (for two separate reaction steps) carried out on the wild-type protein and the Cys^{128Ala} variant excluded Cys128 as the redox active cysteine [115]. The other two essential cysteines (Cys160 and Cys356) proved to be the most likely catalytic residues. The variants that had Cys160 and Cys356 substituted with alanine lost all or a substantial portion of activity in the flavin reduction step and, consequently, in the DUQ reduction step. The location of these redox-active cysteines at a short distance below the *re* face of the isoalloxazine ring puts at least one of them (Cys356) in a favourable position for an

electron transfer to the isoalloxazine ring of FAD (**Figure 3.7**). An anionic radical mechanism for the formation of elemental sulfur (S_8) from sulfides in industrial processes (non-enzymatically) has been described in detail [116]. In this mechanism a number of intermediate anionic radicals as well as polysulfide anions appear during the elongation process. However, in the enzymatic mechanism of the formation of elemental sulfur from sulfides, the catalytic cysteine residues must be involved. Here we propose a tentative radical mechanism of SQR enzymatic activity that can be an alternative to the nucleophilic attack mechanism (**Figure 3.8**). The pKa values of Cys-$(S)_n$-SH in the particular environment of the SQR active site are not known, but these groups are likely deprotonated at pH 7.0, the pH optimum for catalysis [78]. One electron can be transferred from the persulfide anion Cys356-SS^- to the isoalloxazine ring with formation of a neutral radical Cys356-$SS^\bullet$. At this pH the sulfide ion likely exists in solution as HS^-. We speculate that a reaction between Cys356-$SS^\bullet$ and HS^- results in the formation of an anionic radical Cys356-$SS(^{\bullet-})$SH. The disulfide anionic radicals were observed in irradiated cysteine hydrochloride crystals [117] and in ribonucleotide reductases [118]. They are negatively charged molecules with a three-electron bond between two sulfurs. A similar species might form as a transient intermediate. After the subsequent transfer of the unpaired electron to FAD and deprotonation the Cys356-trisulfide anion Cys356-SSS^- is formed (**Figures. 3.3a, 3.4b**, intermediate state II). Another electron can be transferred to FAD resulting in the trisulfide radical R-$SSS^\bullet$. This is consistent with the finding that the Cys160Ala variant retained a portion (approximately 32.5%) of the FAD-reducing activity. The proximity of the Cys160-SS^- to the radical R-$SSS^\bullet$ would cause an interaction between them and the formation of a pentasulfide bridge between the two redox-active cysteines (**Figures. 3.3b, 3.4c**, intermediate state III).

The three intermediate states observed in the active sites of the SQR variants (**Figures 3.3, 3.4**) are schematically presented in **Figure 3.8**. Subsequent reactions with sulfide ions and transfers of electrons to FAD result, likely in the formation of more elongated polysulfur adducts. For every reaction with the sulfide HS^- ion two electrons are transferred to FAD, one proton is released to solvent and one sulfur atom is incorporated in the polysulfide complex with SQR.

The wild type SQR can also use selenides as a substrate. A strong anomalous signal from selenium atoms was located in the space between two cysteines, Cys160 and Cys356, confirming their redox-active role. Interestingly, we did not find longer polysulfide (polyselenide) species in the structures of *A. ferrooxidans* SQR such as were observed in the structures of the *A. Aeolicus* SQR (likely due to the crystal lattice preferences). Nonetheless, they likely form in *A. ferrooxidans* SQR. We hypothesize that the role of Cys128 is in releasing the polysulfur (S_8) molecule from Cys160 as proposed by Cherney *et al*. [37].

It is noteworthy that we have not observed the redox-active disulfide bridge between Cys160 and Cys356 (Cys160-S^{γ}-S^{γ}-Cys356) in any of our structures, including another crystal form reported earlier [37]. The average distance between corresponding C^{α} atoms (10 Å) is approximately 2.5-3 Å longer than that for the flavocytochrome C sulfide dehydrogenase (PDB code 1FCD), the only closely SQR related structure in which such a redox-active disulfide bridge was observed. Cys160 located on a loop close to the N-terminus of a helix might be more mobile, whereas Cys356 located in the middle of a β-strand is likely to be less mobile. It appears possible for Cys160 to move towards Cys356 to form the disulfide bridge Cys160-S^{γ}-S^{γ}-Cys356 at the beginning of the reaction cycle or in the opposite direction, towards Cys128, when it is needed to accommodate a bigger polysulfur chain during elongation reactions. As we have not observed

the disulfide bridge in these SQR structures we chose to start the reaction from Cys356-S^{γ}-S^{-} /Cys160-S^{γ}-S^{-} persulfides.

Similarly, as we have not observed in our structures bigger polysulfur intermediates and their relative spatial positions in regards to Cys128, we can only hypothesize the role of Cys128. It can be in releasing the polysulfur (S_8) molecule from Cys160 as proposed by Cherney *et al*. [37]. Another role might be in the electron transfer reaction to quinones. It has been shown that the environment in the proximity of flavins has a great effect on their redox potential [119]. Protein side chains, as well as the backbone significantly influence the redox potentials of flavins, but also of quinones. The balance between the redox potentials of the two systems determines the electron transfer occurrence and direction. The changes in the DUQ reduction activities of different SQR variants (**Table 3.2**) reflect those influences. The Cys^{128Ser} variant showed that Ser128 has a stronger negative effect on the DUQ reduction than the Ala128 in the Cys^{128Ala} variant.

The wild type SQR can also use selenides as a substrate. A strong anomalous signal from selenium atoms was located in the space between two cysteines, Cys160 and Cys356, confirming their redox-active role.

3.5 Tables

Table 3.1. Summary of proposed enzymatic mechanisms of SQR

Mechanism number	I	II	III	IV	V
Source of SQR	*R. capsulatus*[a]	*A. ambivalens*[b]	*A. aeolicus*[c]	*A. aeolicus*[c]	*A. ferrooxidans*[d]
Nucleophile	Cys160-S^-	Cys160-S^-	Cys160-S-S^-	Cys128-S-S^-	Cys356-S-S^-
Target atom of FAD	C^{4A}	C^{4A}	C^{4A}	C^{8M}	C^{4A}

a Griesbeck *et al.* (2002).
b Brito *et. al.*, (2009)
c Marcia *et. al*. (2009)
d Cherney *et. al.* (2010)

Table 3.2. Summary of FAD reduction and DUQ reduction activity of SQR variants

	FAD Reduction Assay [a] (%)	DUQ Reduction Assay (units) [b]
Wild-type	40±3	0.5
Ser^{126Ala}	40±3	0.15
Cys^{128Ala}	40±3	0.15
Cys^{128Ser}	40±3	0
His^{132Ala}	40±3	0.2
Cys^{160Ala}	13±3	0
His^{198Ala}	40±3	0.3
Cys^{356Ala}	0	0

[a] FAD reduction corresponds to the % reduction of FAD fluorescence by 0.03 μM Na_2S.

[b] One unit of DUQ reduction based activity was defined as the amount of enzyme that catalyzed the reduction of 1 μmol of DUQ per minute.

3.6 Figures

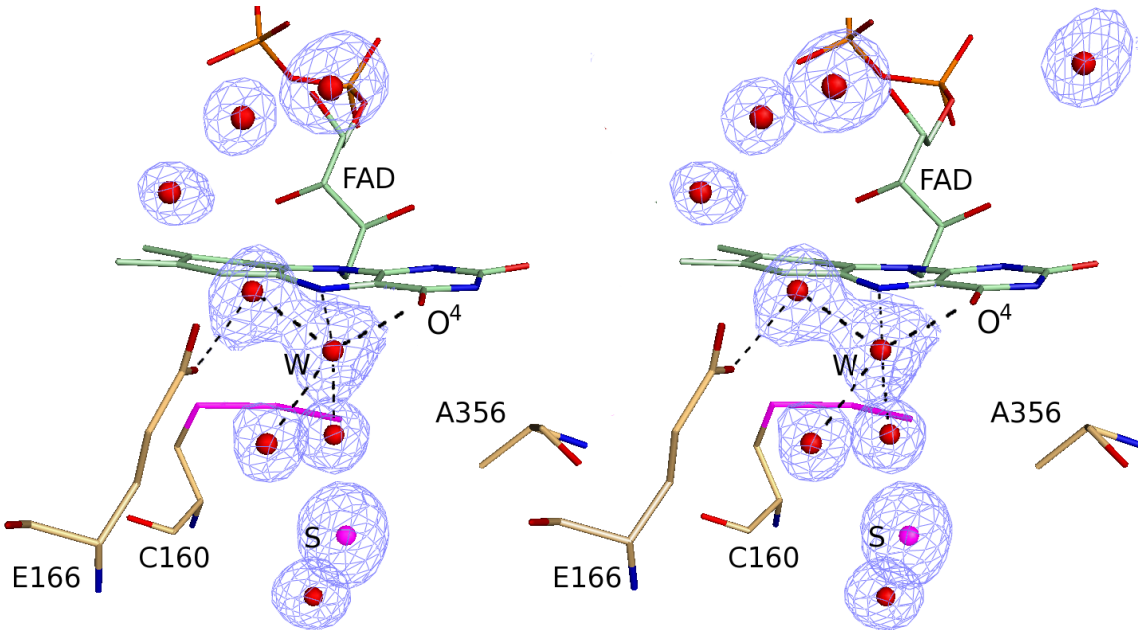

Figure 3.1. Active site region of Cys^{356Ala} variant soaked with 2 mM Na_2S.
The disulfide is bonded to the S^{γ} atom of Cys160 forming a trisulfide. The $2|F_o|-|F_c|$ electron density map (contoured at 1 σ; blue mesh) depicts solvent molecules (most of them are likely sulfide ions with partial occupancies) accumulate in the active site. They represent one of the solvent channels carrying sulfides to the active site. This channel was not noticeable in other crystals of this variant in which sulfide was not soaked (data not shown). The accumulation of sulfide clusters happens only in this variant, as the reaction with sulfides cannot proceed in the absence of reactive sulfhydryl group of Cys356. The electron transfer reaction to FAD cannot proceed for this variant.

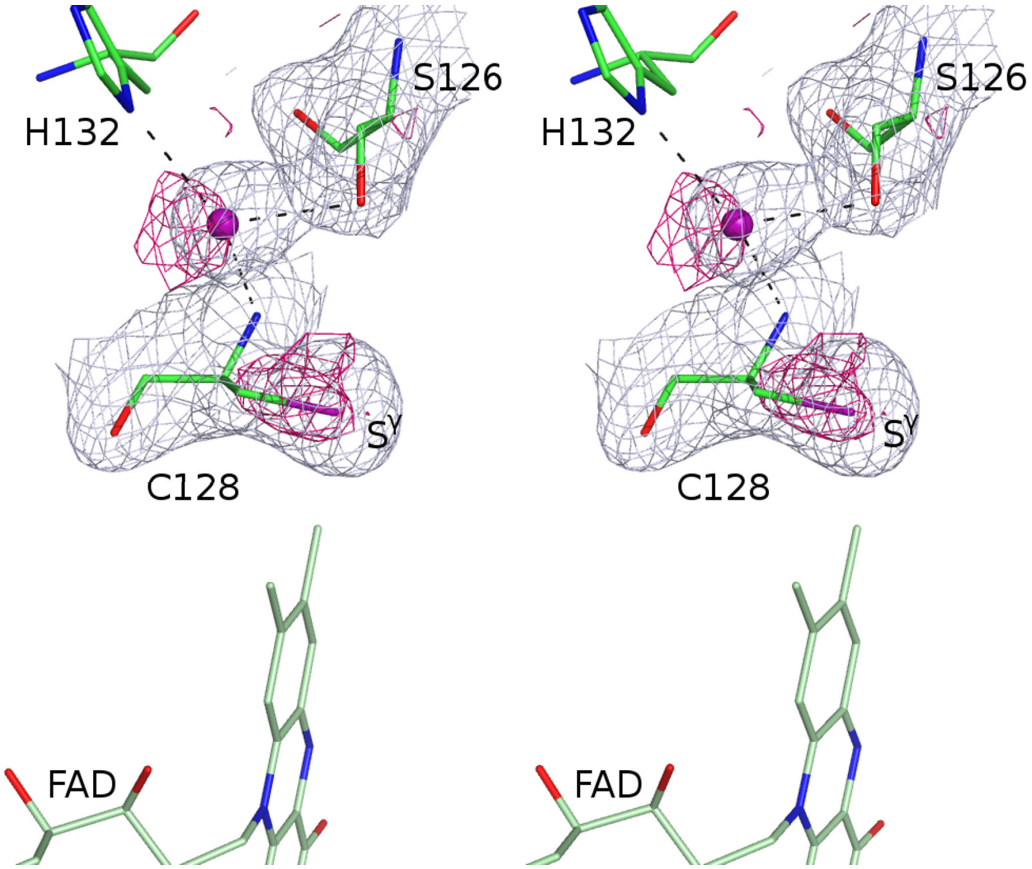

Figure 3.2. The sulfide binding pocket of the wild-type SQR.
A sulfide ion (magenta sphere) makes hydrogen bonding interactions (broken lines) with the side chain atoms of residues Ser126 (2.85 Å), His132 (2.86 Å) and the main chain nitrogen atom of Cys128 (3.06 Å) (Distances are measured in the structure 3T2Z.pdb). The $2|F_o|-|F_c|$ electron density map is contoured at 1σ (blue mesh); also shown is the superposed anomalous difference map for sulfur contoured at 2.8σ (magenta mesh); the anomalous dataset was collected at 7.0 keV (corresponding to λ=1.7712 Å) from the crystal of the Ser^{126Ala} variant.

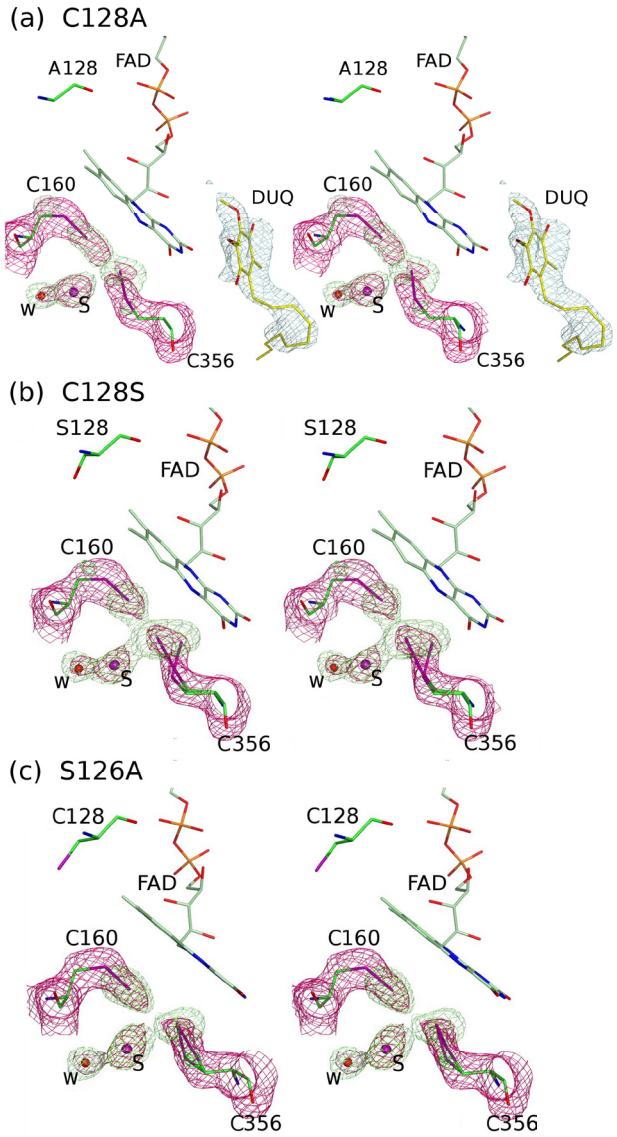

Figure 3.3. Electron densities in the sulfide oxidation site of the SQR variants in intermediate state I.

The $2|F_o|-|F_c|$ electron density omit maps are contoured at 1σ (magenta mesh); the $|F_o|-|F_c|$ electron density omit maps are contoured at 3σ (light green mesh). The active-site cysteines (Cys160 and Cys356, green carbon atoms, magenta sulfur atoms) form persulfides that are separated by a gap in the electron density. A sulfide ion (magenta sphere) is situated at approximately 3.1-3.2 Å (average from the three structures shown in this figure) from the persulfide sulfur atom of Cys356. A water molecule (red sphere) forms hydrogen bonds to the sulfide ion and to two carbonyl oxygen atoms of Leu199 and Ser159 and the main chain nitrogen of Phe161 (not shown). (a) Cys^{128Ala} variant, crystal 1 (Table 3); it was co-crystallized with DUQ (yellow sticks, $2|F_o|-|F_c|$ electron density map contoured at 1σ, blue mesh). (b) Cys^{128Ser} variant. (c) Ser^{126Ala} variant. "W" is water, "S" is sulfur.

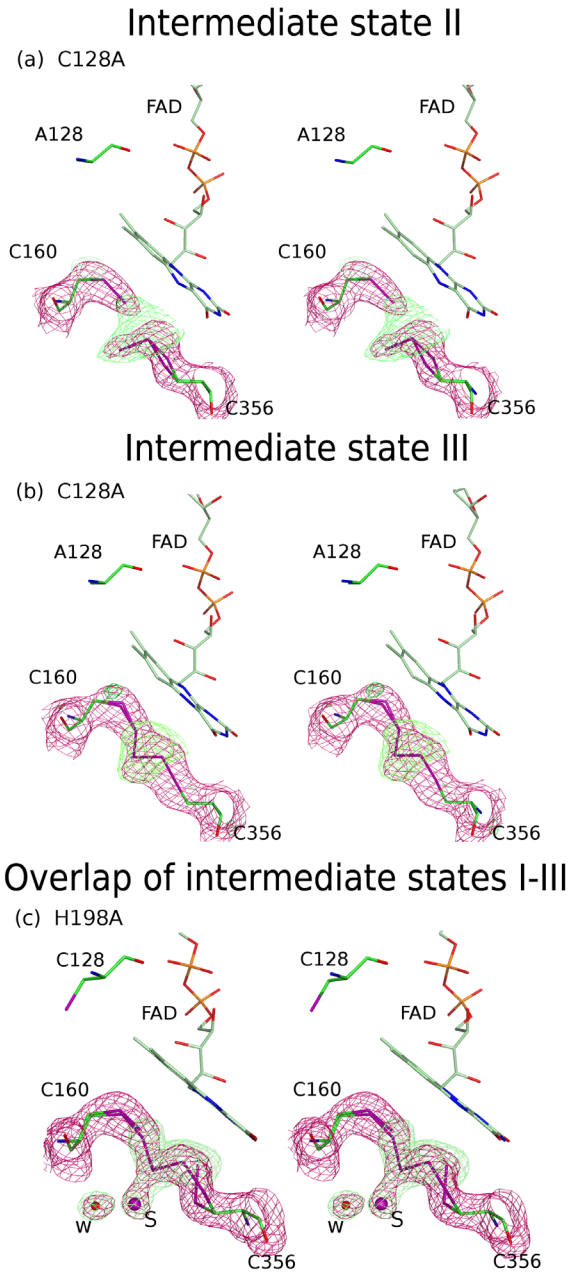

Figure 3.4. Electron densities in the sulfide oxidation site of the SQR variants in intermediate states II and III.

The $2|F_o|-|F_c|$ electron density omit maps are contoured at 1σ (magenta mesh); the $|F_o|-|F_c|$ electron density omit maps are contoured at 3σ (light green mesh). (a). Intermediate state II: Cys160 forms a persulfide, as in the intermediate state I, whereas a more elongated electron density peak protrudes from the S^{γ} atom of Cys356 suggesting the formation of a trisulfide on Cys356 (green carbon atoms, magenta sulfur atoms). The redox-active Cys160 and Cys356 are not covalently connected. (b). Intermediate state III: Cys160 and Cys356 are covalently connected by an inserted trisulfide molecule thus forming a pentasulfide bridge. (c). Overlap of intermediate states I and III (corresponding conformations A and B). In the conformation B, a pentasulfide bridge containing an inserted trisulfide connects the two active site cysteines. A sulfide ion is close to the persulfide sulfur atoms (conformation A).

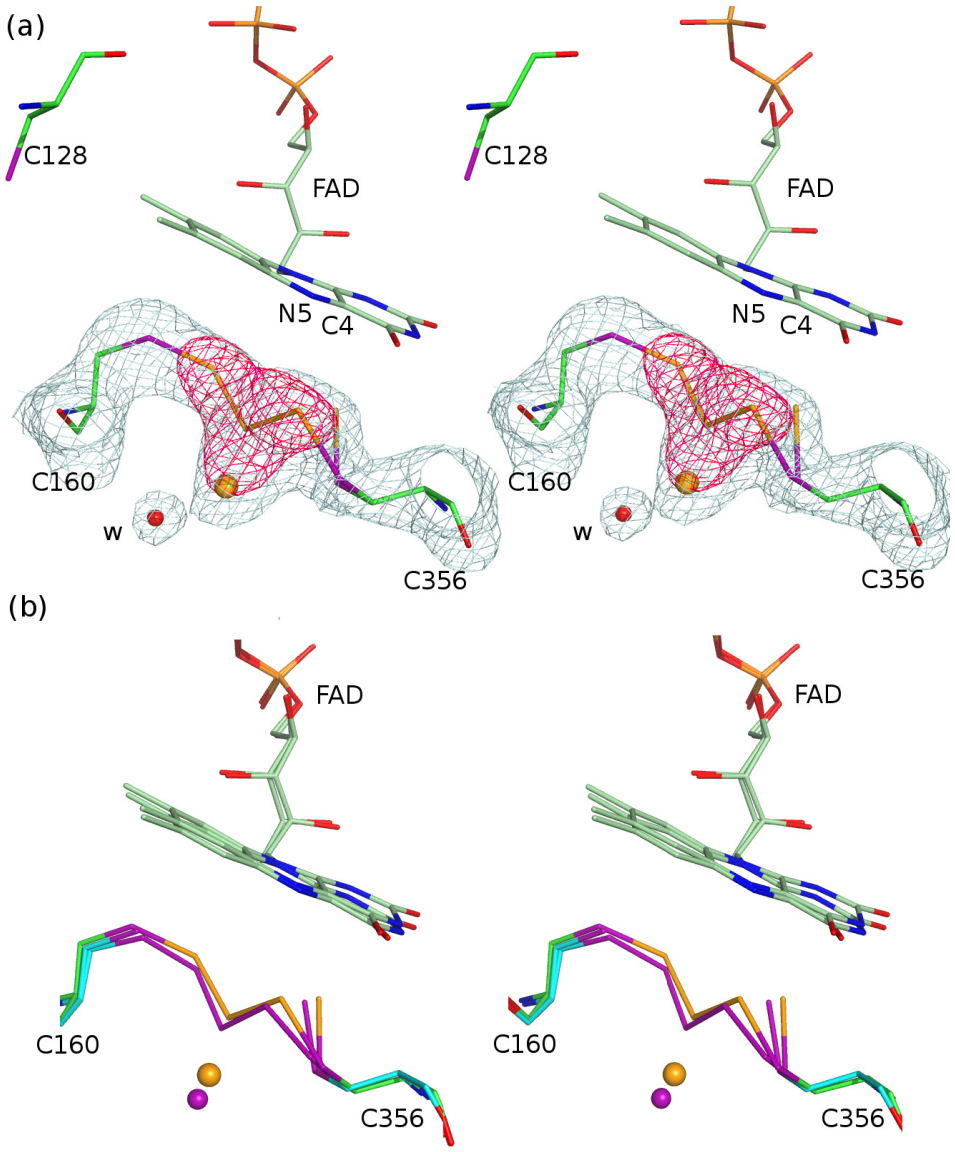

Figure 3.5. The active site of the wild-type SQR with bound triselenide (a) and superposition of the active sites of the wild-type SQR complexes containing sulfides and selenides (b).
(a). The active site of the wild-type SQR with bound triselenide (overlap of the intermediate states I-III). The $2|F_o|-|F_c|$ electron density omit map is contoured at 1σ (blue mesh); the anomalous difference map is contoured at 8σ (magenta mesh); it shows the presence of selenium atoms. Also shown are the catalytically active atoms of FAD, C^4 and N^5. In one conformation three selenium atoms form a triselenide bridge; in the alternate conformation the lone selenide ion is positioned close to the selenium atom bonded to S^{γ} of Cys356. (b). Superposition of the active sites of the wild-type SQR complexes containing sulfides (magenta sulfur atoms) and selenides (yellow selenium atoms).

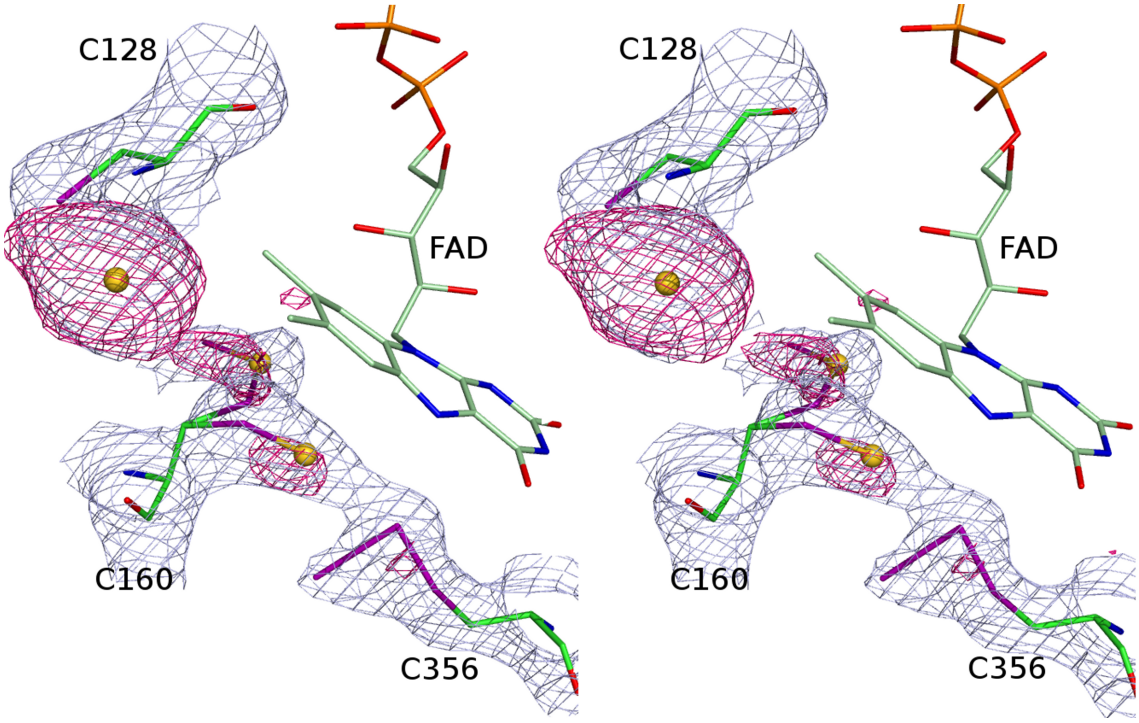

Figure 3.6. Binding of gold (I) cyanide to the active site of wild-type SQR.
The $2|F_o|-|F_c|$ electron density omit map is contoured at 1σ (blue mesh); the anomalous difference map contoured at 3σ (magenta mesh) shows gold (I) atoms. The largest anomalous density peak is for the gold bound to Cys128. Only a small anomalous electron density peak, split into two conformations is observed for the gold bound to Cys160. The Cys356 has an elongated density peak protruding from its S^{γ} atom forming a trisulfide.

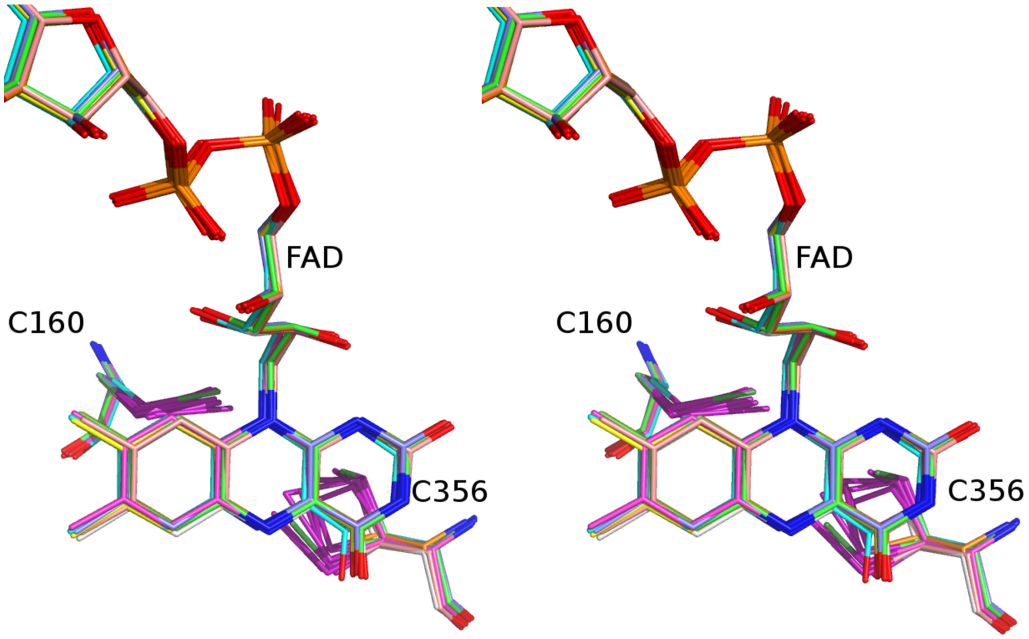

Figure 3.7. The projection of the Cys160 and Cys356 persulfides of different SQR variants onto the plane of the isoalloxazine ring. The Cys356 persulfide sulfur atoms are located under the C4 atom of FAD at an average distance of 3.2-3.5 Å.

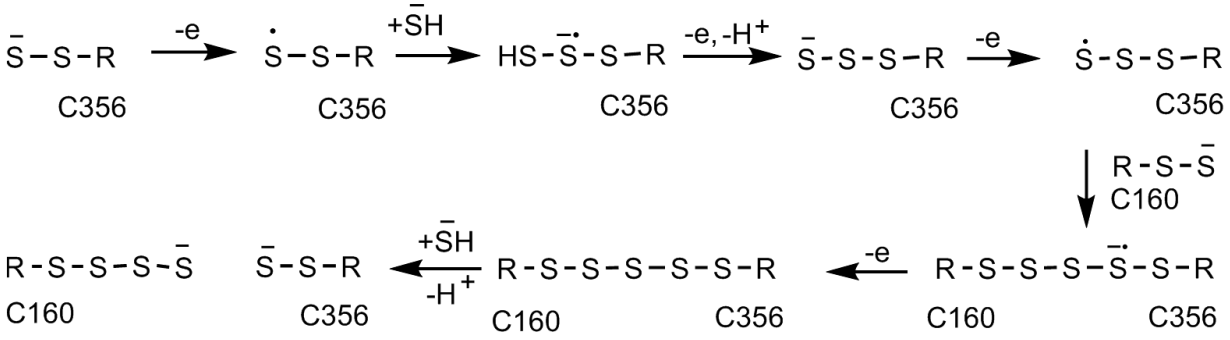

Figure 3.8. A schematic representation of the initial steps of an alternative electron transfer mechanism of SQR.
An electron from the persulfide group of Cys356 is transferred to the isoalloxazine ring of FAD. A Cys356-SS$^{\bullet}$ radical then reacts with a sulfide ion HS^{-} forming a radical anion from which a second electron is transferred to FAD. Each reaction with an HS^{-} ion results in two electrons transferred to FAD, one proton is released to solvent, and one sulfur atom is inserted into the polysulfide chain on Cys160. The scheme explains the formation of the three observed intermediate states (I-III).

3.7 Supplementary Tables

Supplementary Table 3.1. Data collection and refinement statistics for the Cys^{356Ala}, the Cys^{128Ala} and the Cys^{128Ser} variants

crystal/variant	Cys^{356Ala}	Cys^{128Ala}-DUQ (1)	Cys^{128Ala} (2)	Cys^{128Ala} (3)	Cys^{128Ser}-DUQ
Space group	$P6_222$	$P6_222$	$P6_222$	$P6_222$	$P6_222$
PDB accession codes	3SX6	3SXI	3T14	3T2K	3SZW
Cell dimensions *a*, (Å) *b*, (Å) *c,* (Å)	 149.83 149.83 81.51	 150.09 150.09 81.46	 149.70 149.70 81.40	 150.27 150.27 81.70	 149.91 149.91 81.39
α, β, γ (°)	90, 90, 120	90, 90, 120	90, 90, 120	90, 90, 120	90, 90, 120
Wavelength, (Å)	0.97949	0.97945	0.97945	0.97591	0.97945
Resolution, (Å)	50.0-1.80(1.86-1.80)	50.0-2.18 (2.26-2.18)	43.2-2.21(2.33-2.21)	55.3-2.35(2.48-2.35)	74.95-2.20(2.32-2.20)
R_{sym}	0.067 (0.749)	0.115 (0.889)	0.142 (0.978)	0.144 (0.789)	0.158(1.113)
$\langle I \rangle / \langle \sigma I \rangle$	32.2 (1.83)	22.1 (2.04)	9.5 (2.0)	6.5(1.5)	19.0(3.1)
Completeness (%)	92.2 (64.5)	99.1 (97.7)	89.1 (69.5)	92.5(100)	100(100)
Redundancy	11.8 (8.6)	11.8 (8.7)	9.8 (9.4)	4.5(4.6)	21.5(21.6)
Refinement					
Resolution (Å)	30.1-1.80	49.1-2.18	43.2-2.21	40.0-2.35	55.1-2.20
No. reflections	46540[a]	28457	45489[a]	39482[a]	49602[a]
R_{work} / R_{free}	17.9/22.0	16.7/22.0	17.3/23.3	19.5/25.0	16.7/21.6
No. atoms (a.u.)[b]	3711	3627	3517	3494	3641
Protein	3245	3232	3226	3223	3233
FAD	53	53	53	53	53
DDM	35	35	35	35	35
Sulfur	4	4	3	3	6
Decylubiquinone	23	23	-	-	23
Ions	10	5	15	5	5
Water	341	275	185	175	286
B-factors (Å^2)					
Protein	39.8	39.1	49.0	42.7	36.3
FAD	28.1	25.5	35.0	27.4	25.5
DDM	34.9	40.0	45.7	40.7	35.4
Sulfur	46.9	67.4	65.8	31.4	36.6
Decylubiquinone	100.2	89.8	-	-	82.6
Ions	86.1	100.2	118.0	84.8	93.6
Water	45.4	44.8	45.6	40.3	41.9
R.m.s. deviations					

Bond lengths (Å)	0.006	0.008	0.008	0.008	0.008
Bond angles (°)	1.08	1.20	1.12	1.18	1.09

Supplementary Table 3.2. Data collection and refinement statistics for the Ser^{126Ala} and His^{198Ser} variants and the wild-type complexes with selenide and gold (I) cyanide

crystal/variant	Ser^{126Ala}	Ser^{126Ala}	His^{198Ala}-DUQ	wild-type-H_2Se complex	wild-type-$NaAu(CN)_2$
Space group	$P6_222$	$P6_222$	$P6_222$	$P6_222$	$P6_222$
PDB accession codes	3SY4	3SYI	3SZF	3SZ0	3SZC
Cell dimensions *a*, (Å) *b*, (Å) *c,* (Å)	 149.77 149.77 81.73	 149.79 149.79 81.91	 150.23 150.23 81.89	 149.90 149.90 81.89	 149.54 149.54 81.74
α, β, γ (°)	90, 90, 120	90, 90, 120	90, 90, 120	90, 90, 120	90, 90, 120
Wavelength, (Å)	0.97949	1.77120	0.97949	0.97949	0.97949
Resolution, (Å)	81.6-1.91(2.01-1.91)	49.0-2.20 (2.32-2.20)	50-2.10(2.18-2.10)	49.07-2.15(2.27-2.15)	50.76-2.35
R_{sym}	0.088 (0.992)	0.098 (0.833)	0.086(0.642)	0.110(0.923)	0.126(0.992)
Mean($<I>/<\sigma I>$)	31.4 (1.7)	14.5 (1.3)	18.7 (1.46)	14.1(2.9)	12.6(2.9)
Completeness (%)	91.4 (64.7)	94.5 (69.2)	95.6(73.7)	90.5(76.1)	92.7(100)
Redundancy	32.3 (9.3)	12.2 (2.6)	8.4(3.1)	12.2(12.3)	14.4(14.5)
Refinement					
Resolution (Å)	69.1-1.91	42.1-2.20	43.4-2.10	43.3-2.15	48.9-2.35
No. reflections	69984[a]	48439[a]	30818	50666[a]	39496[a]
R_{work} / R_{free}	17.8/22.7	17.2/21.5	18.0/23.2	17.0/21.5	17.2/21.8
No. atoms (a.u.)[b]	3616	3426	3622	3546	3394
Protein	3224	3221	3218	3223	3223
FAD	53	53	53	53	53
DDM	35	35	35	35	-
Sulfur(selenium)	5	6	6	5	3
Decylubiquinone	-	-	23	-	23
Ions/Au	5	5	5	5	5/3
Water	294	106	282	225	84
B-factors ($Å^2$)					
Protein	41.1	53.4	34.4	46.9	56.8
FAD	25.8	36.5	23.4	28.8	40.2
DDM	40.8	52.7	34.0	44.1	-
Sulfur(Selenium)	56.4	68.2	39.7	59.8	65.6
Decylubiquinone	-	-	80.1	-	103.3
Ions/Au	59.2	116.9	44.5	114.7	135.6/65.6
Water	45.3	48.4	37.5	45.7	46.4
R.m.s. deviations					
Bond lengths (Å)	0.008	0.008	0.008	0.007	0.009

Bond angles (°)	1.15	1.16	1.15	1.13	1.18

Supplementary Table 3.3. Data collection and refinement statistics of the wild-type SQR and His132Ala variant

crystal/variant	wild-type-DUQ	His^{132Ala}
Space group	$P6_222$	$P6_222$
PDB accession codes	3T0K	3T2Y
Cell dimensions *a*, (Å) *b*, (Å) *c,* (Å)	 149.96 149.96 82.05	 150.07 150.07 81.86
α, β, γ (°)	90, 90, 120	90, 90, 120
Wavelength, (Å)	0.97949	0.97945
Resolution, (Å)	50.92-2.00(2.11-2.00)	50.9-2.50 (2.64-2.50)
R_{sym}	0.105 (0.953)	0.123 (0.893)
Mean(<*I*>/ <σ*I*>)	13.0 (2.9)	14.1(2.4)
Completeness (%)	90.1 (82.2)	79.4(89.2)
Redundancy	14.6 (14.7)	10.0(9.9)
Refinement		
Resolution (Å)	39.1-2.00	49.1-2.25
No. reflections	62829[a]	47105[a]
R_{work} / R_{free}	18.0/22.4	17.6/25.7
No. atoms (a.u.)[b]	3532	3264
Protein	3222	3104
FAD	53	53
DDM	-	35
Sulfur	5	3
Decylubiquinone	23	-
Ions	5	-
Water	224	69
B-factors ($Å^2$)		
Protein	55.8	53.4
FAD	34.4	41.9
DDM	-	48.8
Sulfur	60.2	82.0
Decylubiquinone	70.7	-
Ions	76.6	-
Water	56.0	44.9
R.m.s. deviations		
Bond lengths (Å)	0.007	0.008
Bond angles (°)	1.21	1.10

Values for the highest resolution shell are given in parentheses. R_{sym}= $\Sigma_h\Sigma_i(|\ I_i(h)-<I(h)>|)/\Sigma_h\Sigma_i I_i(h)$, where $I_i(h)$ is the ith intensity measurement and $<I(h)>$ is the weighted mean of all measurements of $I(h)$. R_{work} and R_{free} $=\Sigma_h(|F_o(h)| - |F_c(h)|)/|F_o(h)|$ for reflections in the working and test sets (5% of the data). [a] The Friedel pairs were separated to detect anomalous scattering. [b] Number of non-hydrogen atoms present in the asymmetric unit.

Chapter 4: Characterization of the kinetics and electron paramagnetic resonance spectroscopic properties of *Acidithiobacillus ferrooxidans* Sulfide:Quinone Oxidoreductase (SQR)

A version of this chapter has been published in Archives of Biochemistry and Biophysics.

Zhang, Y., and Weiner, J. H. (2014) Characterization of the kinetics and electron paramagnetic resonance spectroscopic properties of *Acidithiobacillus ferrooxidans* sulfide:quinone oxidoreductase (SQR). *Arch. Biochem. Biophys.* **564**, 110–119.

Acknowledgments The authors thank Justin G. Fedor for reviewing this manuscript and helpful discussions. This work was funded by the Canadian Institutes of Health Research (CIHR MOP89735). We thank Dr. Richard A. Rothery for help with the EPR analysis.

4.1 Introduction

Acidithiobacillus ferrooxidans is a motile, Gram-negative, acidophilic, chemolithotrophic bacterium which is usually found in acid environments such as acid mine drainage. This organism participates in one of the key industrial roles of microbial communities, *i.e.* the bacterial-chemical processes of bioleaching metal ores under mesophilic conditions [49]. It derives energy for growth mainly from oxidative respiration using reduced inorganic compounds such as Fe^{2+}, H_2S, S^{2-} and S^0, which are present in surrounding ores. Based on comparative genomic analysis, sulfur oxidation in *A. ferrooxidans* is catalyzed by the sulfide:quinone oxidoreductase (SQR) system and the initial step is the oxidation of sulfide (H_2S, HS^- and S^{2-}) to elemental sulfur (polysulfide or octasulfur rings) by SQR [53; 120]. The electrons released in the reaction reduce the membrane-bound ubiquinone pool. The sulfur may be further oxidized via $S_2O_3^{2-}$ and SO_3^{2-} to the final oxidation state +6 in SO_4^{2-} by other enzymes of the SQR system [53].

SQR is an ancient flavoprotein of the disulfide oxidoreductase family that is present in nearly all domains of life (from archaea to humans but not plants), serving multiple functions in addition to its original role in respiration. SQRs were first found in sulfidotrophic bacteria, later SQR-like enzymes were found in the mitochondria of some fungi, as well as in all animal species whose genomes have been sequenced [89; 121]. Based on phylogenetic analysis of completed bacterial genomes, SQR genes were classified into at least two clades: type I and type II SQRs. Type I SQRs occur in a diverse range of bacteria, including *A. ferrooxidans* [13; 62; 90]. They participate in respiration or in anaerobic photosynthesis and are characterized by high substrate affinities and high reaction rates [62; 90]. Type II includes SQRs from other bacteria, as well as the mitochondrial SQR-like

enzymes, and are mostly involved in detoxification [62] and heavy metal tolerance [65]. In animals SQR may participate in signaling by controlling the levels of H_2S in the brain [15; 16; 68; 69]. Additionally, mitochondrial ATP production with sulfides as electron donors was observed [27; 28].

Several SQRs have been purified and characterized by biochemical methods [62; 65; 73; 78; 81; 122]. They are considered to be integral monotopic membrane proteins, associating with the membrane through amphipathic helices. The monomeric molecular mass of the enzyme is around 50 kDa. The enzyme usually harbors a covalently-bound FAD cofactor in each monomer. However, FAD can also be non-covalently bound as in the SQR of *A. ferrooxidans* and some other organisms [37; 62; 79; 86].

Recently, we reported the heterologous expression of *A. ferrooxidans* SQR in *E. coli* that allowed us to prepare soluble, active enzyme suitable for X-ray crystallography. We have determined the three-dimensional structures of *A. ferrooxidans* SQR and several variants to 2.3 Å resolution (PDB id: 3T2Z, 3T31, 3KPK, 3SXI, 3T14, 3T2K, 3SZW, 3SX6, 3SY4, 3SY1, 3SZF and 3T2Y) [37; 86; 123]. We identified the sulfide reaction site, the ubiquinone-binding site and the amphipathic helices that are required for membrane attachment. Our structures are compatible with either a nucleophilic attack mechanism or a radical mechanism [37; 86; 123]. The sole cofactor involved in electron transfer is the non-covalently-bound FAD. Three conserved Cys residues in close contact with the FAD along with two conserved His residues are proposed to play key roles in catalysis. Although preliminary FAD reduction and steady state kinetics have been reported for SQR and the variants [23], herein we use a combination of pre-steady state and steady

state kinetics together with EPR spectroscopy to quantitate the role of the FAD and the conserved Cys and His residues.

4.2 Materials and Methods

4.2.1 Materials

Acidithiobacillus ferrooxidans ATCC 23270 was obtained from the American Type Culture Collection. *E. coli* TOP10 competent cells and *E. coli* strain BL21 (DE3) competent cells came from Invitrogen Life Technologies (Carlsbad, CA). Plasmid miniprep and gel extraction kits were obtained from Fermentas (Vilnius, Lithuania). Synthesized oligonucleotides were from Integrated DNA Technologies (Coraville, IA). Taq DNA polymerase, T4 DNA ligase and restriction enzymes came from Invitrogen (Carlsbad, CA). All other reagents were of research grade or better and were obtained from commercial sources.

4.2.2 Cloning of the *sqr* gene from *A. ferrooxidans* ATCC 23270

The *sqr* gene from *A. ferrooxidans* ATCC 23270 was cloned by PCR as reported previously [86]. Briefly, we added codons for three amino acids (Arg-Gly-Ser) between the initiating Met and Ala at the 5' end of the *sqr* gene and six continuous histidine codons to the 3' end and cloned the gene into a pLM1 [124] expression vector resulting in the pLM1::SQR plasmid (**Supplementary Figure 4.1**). The constructed pLM1::SQR plasmid was transformed into *E. coli* TOP10 competent cells for screening purposes. The positive colony was grown in LB medium containing ampicillin (100 mg L^{-1}), and the plasmid pLM1::SQR was isolated from harvested bacteria cells using a plasmid extraction kit. The isolated pLM1::SQR plasmid was confirmed by DNA-sequencing analysis and transformed into *E. coli* strain BL21(DE3) competent cells for expression purposes.

4.2.3 Construction of SQR *A. ferrooxidans* mutant plasmids

Construction of the site-directed mutants were carried out following the QuikChange method (Stratagene) using pLM1::SQR plasmid [86] as the template for mutagenesis. The oligonucleotides used are listed in Supplementary Table 1. Mutants were verified by DNA sequencing carried out at the Department of Biochemistry, DNA Core Facility at the University of Alberta.

4.2.4 Expression of soluble recombinant *A. ferrooxidans* SQR in *E. coli*

Wild-type and mutant plasmids were transformed into *E. coli* BL21(DE3) cells. The cells were grown at 37ºC in 2 L of Terrific Broth (TB) medium [109] containing ampicillin (100 mg L^{-1}) to an OD_{600} of 0.8. SQR expression was induced by the addition of 0.3 mM isopropyl β-D-1-thiogalactopyranoside (IPTG), and the cultures were incubated at 25ºC for 22 h with shaking at 180 rpm.

4.2.5 Purification of SQR_{His6}

The His-tagged SQR was purified by nickel affinity chromatography on a fast performance liquid chromatography (FPLC) system (ÄKTApurifier, GE Healthcare, Piscataway, NJ) as described previously [86]. All experiments utilized His_6 tagged protein. The protein fractions were buffer-exchanged (to remove imidazole) and concentrated to 5 mg mL^{-1} in buffer A (50 mM MOPS, 0.5 M NaCl, pH 7.0) using a YM-30 Centricon tube (Amicon) as soon as possible after the purification and stored at -80°C. All steps of protein purification were performed at 4°C.

The Bradford method [125] was used to determine the protein content with bovine serum albumin as the standard.

4.2.6 Determination of the FAD in SQR

The FAD content of SQR was calculated from the absorbance at 450 nm using the published molar extinction coefficient (ε_{450}=11.3 mM^{-1} cm^{-1} for the oxidized enzyme) [62]. Protein denaturation by cold 5% trichloroacetic acid (TCA) or 3 M KBr was used to determine if the FAD was covalently or non-covalently bound [126].

4.2.7 UV-Visible spectroscopy

UV-visible spectral scanning was carried out with a Hewlett Packard 8453 UV-VIS diode array spectrophotometer at 23°C.

4.2.8 Effect of pH and temperature on SQR activity

The pH optimum of SQR activity was determined between pH 2.7 and 9.5 using appropriate buffers (50 mM Bis-Tris Propane, 50 mM Bis-Tris, 50 mM MES, 50 mM Formate, 50 mM Citrate buffer and 50 mM Citrate-Phosphate buffer). Measurements were carried out using the decylubiquinone (DUQ) reduction assay at 23°C. The optimum pH value obtained from this assay was used in all the other experiments. The effect of temperature on SQR activity was measured between 10°C and 80°C. The activation energy (E_a) was calculated from an Arrhenius plot using the equation Slope=-E_a/R (approximate value for the gas constant R is 8.31 $J K^{-1}$ mol^{-1}). The temperature coefficient (Q_{10}) was calculated using the equation $Q_{10}=(v_2/v_1)^{(10/(T_2-T_1))}$, where v is the reaction rate, T is the temperature in Celsius.

4.2.9 Thermal stability of SQR

The influence of temperature on the stability of SQR was studied by incubating the enzyme solution (0.25 mg mL^{-1}, in 50 mM MOPS, 0.5 M NaCl, pH 7.0) at temperatures between 0°C and 45°C for varying periods of time in a temperature controlled water bath. 5 µL of enzyme solution was pipetted for the activity assay at 23°C.

The stability of the enzyme was expressed as a percentage of residual activity and was calculated by comparison with untreated enzyme.

4.2.10 Enzymatic activity assay based on the reduction of decylubiquinone

The DUQ reduction activity of SQR was measured by following the decrease of absorbance at 275 nm due to the reduction of DUQ as described previously [62; 110]. Measurements were carried out at 23 °C. The reaction mixture contained 1.25 μg mL^{-1} SQR in 50 mM Bis-Tris (pH 7.0), 20 mM glucose, 50 μM DUQ, 1 unit of glucose oxidase per mL and 10 units of catalase per mL. The 50 mM Bis–Tris (pH 7.0) and 20 mM glucose were first mixed and flushed with N_2 to establish anoxic conditions, and the reaction was started by the addition of 100 μM freshly prepared Na_2S. One unit of activity was defined as the amount of enzyme that catalyzed the reduction of 1 μmol of DUQ per minute [127]. The millimolar differential extinction coefficient at 275 nm (12.5 mM^{-1} cm^{-1}) was determined by the measurement of difference spectra of oxidized and reduced DUQ.

4.2.11 Determination of kinetic constants

V_{max} and Michaelis constant (K_m) for Na_2S and DUQ were determined by nonlinear fitting of data to the Michaelis-Menten equation using GraphPad Prism (GraphPad Software, San Diego, CA). Measurements were carried out using the DUQ reduction activity assay method at 23 °C. 1 mL anoxic reaction mixture contained 1.25 μg mL^{-1} SQR and varied concentrations of Na_2S at constant DUQ (50 μM) or varied concentrations of DUQ at constant Na_2S (100 μM).

4.2.12 Stopped-flow spectrophotometry and enzymatic activity assay based on the reduction of FAD

Stopped-flow experiments were performed using an Applied Photophysics SX.18MV stopped-flow instrument equipped with a multiwavelength photodiode array (PDA) detector and X-SCAN software (Applied Photophysics Ltd, Leatherhead, UK) at 23 °C. The optical path length was 1 cm. The dead time of the apparatus was 1.28 ms. The buffer (50 mM Bis-Tris, 20 mM glucose, 3 U mL^{-1} glucose oxidase and 10 units of catalase per mL, pH 7.0) and SQR in the same buffer were degassed with repeated cycles of vacuum and flushing with N_2. Na_2S was freshly dissolved and diluted in the degassed buffer before loading to the sample syringes. The flow system was flushed thoroughly with the anaerobic buffer prior to the experiments.

The FAD reduction assay was performed in the absence of DUQ by monitoring the reduction of FAD after rapidly mixing SQR (25 μM after mixing) with freshly prepared sulfide (125 μM after mixing) in 50 mM Bis-Tris buffer (pH 7.0) containing 20 mM glucose, 3 unit of glucose oxidase per mL and 10 units of catalase per mL. The buffer was degassed with repeated cycles of vacuum and flushing with N_2. Stopped-flow mixing chambers were washed with the deoxygenated buffer to establish the anoxic conditions. The reaction was monitored in the stopped-flow by multiwavelength absorption in the range of 300−700 nm. Temporal changes in absorbance at 448 nm were fitted to the double exponential equation (two-phase exponential decay equation) $\text{Abs} = A_1 e^{-k_{\text{Fast}} t} + A_2 e^{-k_{\text{Slow}} t} + b$ or the one-phase exponential decay equation $\text{Abs} = A_1 e^{-kt} + b$ with GraphPad Prism (GraphPad Software, San Diego, CA), where A_1 and A_2 are amplitudes, k_{Fast} and k_{Slow} (k for a one-phase decay) are the rate constants describing the observed rate at which the dependent variable is decreasing, expressed in s^{-1}, t is time, and b is the end point of the data trace. The rate constants k_{Fast} (for the two-

phase decay) or *k* (for the one-phase decay) obtained from fitting was used to indicate the FAD reduction activity.

4.2.13 Redox Potentiometry and Electron paramagnetic resonance (EPR) spectroscopy

"As is" air-oxidized SQR, samples contained 200 μL of purified SQR (5 mg mL^{-1}, 0.1 mM) in 50 mM MOPS, 0.5 M NaCl, pH 7.0. To reduce FAD, freshly prepared Na_2S was added to a final concentration of 5.5 mM or a crystal of sodium dithionite was added either sequentially or simultaneously with Na_2S to 200 μL of the same SQR sample and incubated at 23 °C for 10 min prior to freezing. Redox titrations were carried out anaerobically under argon at 25 °C on SQR wild-type and $SQR^{Cys160Ala}$ at a total protein concentration of 50 μM in 50 mM MOPS, 0.5 M NaCl, pH 7.0. The following redox mediators (dyes) were used at a concentration of 25 μM: quinhydrone (+287 mV), 2,6-dichlorophenolindolphenol (+217 mV), 1,2-naphthoquinone (+125 mV), toluylene blue (+115 mV), phenazine methosulfate (+80 mV), thionine (+60 mV), methylene blue (−11 mV), resorufin (−50 mV), indigo trisulfonate (−80 mV), indigo carmine (−125 mV), anthraquinone-2-sulfonic acid (−225 mV), phenosafranine (−255 mV), and neutral red (−329 mV). All samples were prepared in 3-mm internal diameter quartz EPR tubes, rapidly frozen in liquid nitrogen-chilled ethanol, and stored in liquid nitrogen until analyzed. EPR spectra were recorded using a Bruker Elexsys E500 spectrometer equipped with a Bruker liquid nitrogen-evaporating cryostat at 150 K, 20-milliwatt microwave power at 9.43 GHz. All spectra reported are the average of five scans using the modulation amplitude of 4.0 G_{pp} at 100 KHz modulation frequency. Potentiometric titration data were analyzed by plotting the signal height of peak-trough

amplitude versus E_h and fitting the data to two midpoint potential values (E_{m1} and E_{m2}) using the equation $SQ_{max} = C_{site}[1+2(10^{-2.3RT(E_{m1}-E_{m2})/2F})]^{-1}$ [128]; where C_{site} is the concentration of binding sites (assumed to equal the concentration of SQR), R is the gas constant, F is the Faraday constant, T is absolute temperature and 2.3 is the conversion factor for $\ln_e$ to $\log_{10}$. E_{m1} is defined as the potential of the quinone/semiquinone couple, and E_{m2} as the potential of the semiquinone/quinol couple. The highest radical signal would then be observed at E_m, the midpoint potential value of the E_{m1}/E_{m2} couple [$E_m = 0.5(E_{m1} + E_{m2})$]. E_m values were representative of two or three independent titrations with a S.D. value of ±5 mV.

4.3 Results

4.3.1 Expression and purification of *A. ferrooxidans* SQR in *E. coli*

SQR is a monotopic integral membrane protein that associates with the lipid bilayer through two C-terminal amphipathic helices [37; 80]. This association is fairly weak and over-expressed recombinant SQR can be found in the membrane and soluble fractions as well as insoluble inclusion bodies (**Supplementary Figure 4.2**). His-tagged SQR was purified from the soluble non-membrane fraction without the use of detergents using a nickel metal-affinity resin column as reported previously [86]. For the kinetic studies reported herein we eliminated the Superdex 200 gel filtration step that was previously used for preparing samples for crystallography and a summary of the revised purification procedure is given in Supplementary Table 2. The final purification yield of SQR was 50 mg from 10 liters of cell culture with a specific activity of 8.07 μmol mg^{-1} min^{-1} of decylubiquinone reduced. The purity of the recombinant SQR was examined by SDS-PAGE and a single band corresponding to the ~49 kDa protein was observed with ~98% purity (**Supplementary Figure 4.3**). The Cys and His variant enzymes utilized herein were purified by the same procedure with similar yields and purity.

4.3.2 Characterization of wild-type SQR

Effect of pH and temperature on SQR activity

Prior to analyzing the pre-steady state and steady state kinetics of SQR we optimized the experimental assay conditions. **Figure 4.1** presents the effects of varying the pH and temperature on the decylubiquinone reduction activity of purified SQR. The optimal pH range for SQR activity was found to be pH 6.5-7.0. This value was close to the optimal pH of SQR from *R. capsulatus* and *A. ferrooxidans* NASF-1 [78; 127]. The

activity decreased rapidly above pH 8.0 or below pH 5.0 and there was no activity below pH 2.0 or above pH 9.0 (**Figure 4.1a**).

The activity of SQR was measured at pH 7.0 at temperatures from 10°C to 80°C. Surprisingly, the enzyme showed the highest activity at 70°C (**Figure 4.1b**), which is much higher than the optimum growth temperature (30°C) for *A. ferrooxidans*. An Arrhenius plot of the logarithm of activity *versus* reciprocal temperature indicated the activation energy for wild-type SQR was 29.6 kJ mol^{-1} (insert **Figure 4.1b**). The purified protein activity had a temperature coefficient (Q_{10}) of 1.47 between 10°C and 40°C.

To test the thermal stability of SQR we incubated the enzyme at temperatures from 0°C to 45°C and assayed all samples for DUQ reduction activity at 23°C. The recombinant SQR was highly stable when incubated at 0°C, 4°C, 23°C or 30°C with >90% of the activity remaining after 7 h. It was less stable at 37°C and lost about 40% of the activity in the first 7.5 h. The activity of SQR decreased more rapidly at 45°C with a half-life of approximately 5 h (**Figure 4.1c**).

4.3.3 Kinetic characterization of wild-type SQR

a) Kinetics of the FAD reduction half reaction

The FAD is non-covalently bound as >95% of the flavin was released by cold 5% TCA or 3 M KBr treatment. The FAD-SQR stoichiometry was determined to be 0.72:1. Based on our X-ray crystallographic results [22], as well as quantitative measurements, *A. ferrooxidans* SQR contains 1 non-covalent FAD per monomer, similar to the recombinant SQR from *Oscillatoria limnetica* [73] and *Rhodobacter capsulatus* [30].

The FAD cofactor is essential to shuttle electrons between sulfide and quinone. In the reductive half reaction, oxidized FAD is reduced by electrons from sulfide. This

occurs via two 1-electron transfers with an intermediate and transient flavin semiquinone. The overall reduction of FAD can be followed by measuring the absorption spectrum (**Figure 4.2** and **Figure 4.5**). The visible absorption peaks of the FAD are at 379 and 448 nm [126].

In **Figure 4.2a** we monitored the pre-steady state kinetics of FAD reduction by Na_2S. SQR was only partially reduced by a 5-fold molar excess of Na_2S and partial formation of flavin semiquinone was observed during reduction. The decrease in absorbance at 379 nm and 448 nm was fitted to a two-phase exponential decay equation model (**Figure 4.2a, inset**). The observed rate constants (k_{Fast}) of SQR are 12.8 ± 1.19 s^{-1} and 11.7 ± 0.97 s^{-1}, respectively. The k_{Slow} (0.3 ± 0.02 and 0.2 ± 0.02 s^{-1}, respectively) are similar to the k obtained for photoreduction of the flavin (0.1 ± 0.05 s^{-1}, **Supplementary Figure 4.4**). At the same time, the broad absorbance between 520 nm and 660 nm increased slightly, which mirrored the formation of a small amount of neutral semiquinone [129]. The increase in absorbance at 550 nm was fit to the two-phase association model $\text{Abs} = A_1(1 - e^{-k_{\text{Fast}}t}) + A_2(1 - e^{-k_{\text{Slow}}t}) + b$ with the k_{Fast} value of 1.9 ± 0.35 s^{-1}. A transient absorption peak at 428nm was observed in both the Na_2S and dithionite reduced SQR (**Figure 4.2a, 4.2b and Supplementary Figure 4.5**). The isosbestic point shifted from 356 nm to 360 nm (**Figure 4.2a**), which indicates that the relative proportion of the oxidized, radical and the reduced FAD was changing during the reduction transition.

When dithionite was titrated into purified SQR, the visible absorption of the protein was bleached due to the reduction of FAD. An absorbance peak at 428 nm was also observed during the latter stage of the titration when over 0.5 equivalent dithionite

was added (**Figure 4.2b**). The 379 nm and 448 nm absorption peaks re-appeared when the FAD was oxidized by ferricyanide and the absorption is greater than the "as purified" SQR due to the absorption of ferricyanide at 250-450 nm (**Figure 4.2b**) [130].

b) Kinetics of the decylubiquinone reduction reaction

It was not possible to follow the oxidation of reduced FAD (the oxidative half-reaction) in the presence of decylubiquinone (DUQ) due to light scattering caused by inorganic sulfur accumulation. However, we could monitor the overall catalytic reaction (the transfer of two electrons from a sulfide ion via the FAD cofactor to the quinone) by following the Na_2S dependent reduction of DUQ to $DUQH_2$. DUQ was rapidly reduced by SQR under anoxic conditions and the k_{cat} was calculated (based on the specific activity, molecular weight of SQR and the amount of protein used in the assay) to be 6.5 ± 0.16 s^{-1} and the overall efficiency of the enzyme k_{cat}/K_m [Na_2S] was 2.19 $M^{-1}s^{-1}$ (**Table 4.1**). Based on nonlinear fitting of the Michaelis-Menten equation the Michaelis constant K_m values of SQR for Na_2S and DUQ are 2.97±0.28 μM and 3.43±0.43 μM, respectively (**Figure 3a and b, Table 1).** The poor fit in the 5-25 μM DUQ range indicates that the reaction might not follow Michaelis-Menten kinetics (**Figure 4.3b**).

1.1.1 4.3.4 Cys and His variants of SQR.

In SQR there are three absolutely conserved cysteine residues (Cys128, Cys160 and Cys356) [86] (**Figure 4.4**). The three Cys residues constitute the active site as determined by X-ray crystallography and are in close proximity to the FAD. Cys160 and Cys356 lie on the *re* side of the isoalloxazine ring of FAD, while Cys128 is located on the *si* side of the isoalloxazine ring of FAD [37] as shown in **Figure 4.4b**. In order to investigate the importance of the cysteines each was substituted with alanine and serine.

There are four highly conserved histidine residues (His3, His132, His198 and His334) in SQR (**Figure 4.4a**). From our X-ray crystallographic structure, His3 and His334 are located on the surface of the SQR molecule and probably do not participate in the catalytic mechanism. His132 and His198 residues are buried within the protein interior and are close to the sulfide oxidation site and FAD cofactor [37]. In order to investigate the importance of these interior histidine residues, both were substituted with alanine.

a) Kinetics of the FAD reduction half reaction

We monitored the pre-steady state reduction of FAD by Na_2S in the variants described above (**Figure 4.5**). Our results indicated that the $SQR^{Cys128Ala}$ and $SQR^{Cys128Ser}$ variants retained nearly complete FAD reduction activity. The observed rate constants (k_{Fast}) of $SQR^{Cys128Ala}$ and $SQR^{Cys128Ser}$ are 11.81 ± 1.39 s^{-1} and 11.73 ± 0.93 s^{-1}, respectively. The Cys160 and Cys356 variants displayed very low FAD reduction rates. The observed rate constants (k_{Fast}) of 0.05 to 0.08 s^{-1} are close to the rate constants obtained from photoreduction (0.1 ± 0.05 s^{-1}, **Supplementary Figure 4.4**). Overall this suggests that Cys160 and Cys356 play important roles in FAD reduction, whereas Cys128 does not participate in the reductive half reaction.

The $SQR^{His132Ala}$ variant retains intact FAD reduction activity with a k_{Fast} of 11.04 ± 1.6 s^{-1} (**Figure 4.5**), indicating that it does not participate in the reductive half reaction. The $SQR^{His198Ala}$ variant was significantly affected in its ability to reduce FAD as the k_{Fast} was reduced to 3.04 ± 0.87 s^{-1}.

b) Kinetics of the decylubiquinone reduction reaction

The $SQR^{Cys160Ala}$, $SQR^{Cys356Ala}$ and $SQR^{Cys356Ser}$ variants were inactive with k_{cat} values of 0 to 0.1 s^{-1} (**Table 4.1**). The $SQR^{Cys160Ser}$ variant retained minimal activity with a k_{cat} of 0.5 ± 0.04 s^{-1}. The $SQR^{Cys128Ala}$ and $SQR^{Cys128Ser}$ variants retained significant activity with k_{cat} values of 1.0 ± 0.09 s^{-1} and 1.6 ± 0.08 s^{-1}, respectively. The $SQR^{His132Ala}$ variant retained about 20% of wild-type activity (1.4 ± 0.16 s^{-1}) whereas the $SQR^{His198Ala}$ variant retained less then 5% of the wild-type activity (0.3 ± 0.06 s^{-1}).

4.3.5 Electron paramagnetic resonance (EPR) and redox potentiometry studies of FAD in wild-type SQR and $SQR^{Cys160Ala}$

Neutral and anionic flavin semiquinone forms have been found in flavoproteins. They can be distinguished by the different linewidths of their respective EPR spectra, which is defined as the separation, in gauss (G), between the peak and trough values [63]. A 19 G linewidth is characteristic for a neutral flavin semiquinone, while a 14-15 G linewidth is the trait of an anionic flavin semiquinone [63]. The semiquinone radical signal intensity in SQR was negligible in "as isolated" air-oxidized wild-type SQR (SQR-Wt, **Figure 4.6a**). In contrast, a strong neutral flavin semiquinone spectrum with a linewidth of 19.3 G was observed in the Na_2S reduced sample. The semiquinone radical signal doubled in intensity in the sodium dithionite reduced SQR-Wt sample with a shift of the linewidth to 14.6 G, which indicates the formation of anionic flavin semiquinone (**Figure 4.6a**). When wild-type SQR was reduced with a mixture of Na_2S and dithionite an intermediate linewidth between that of the individually reduced samples was observed.

We noted that pelleted *E. coli* cultures expressing wild-type SQR were light yellow in color whereas cultures of the $SQR^{Cys160Ala}$ variant were reddish brown. A possible explanation for this is that the flavin in the $SQR^{Cys160Ala}$ variant exists in the red

anionic semiquinone form under the ambient reducing conditions of the cytoplasm. We therefore investigated the EPR properties of the $SQR^{Cys160Ala}$ variant. The EPR spectrum of the purified "as isolated" air-oxidized $SQR^{Cys160Ala}$ variant was of very low intensity (C160A, **Figure 4.6b**). Following Na_2S reduction, the Cys160Ala variant exhibited an intense flavin semiquinone spectrum with a linewidth of 18.6 G, suggesting it arises from the formation of a neutral semiquinone. The signal intensity was three times higher than that monitored in the Na_2S reduced wild-type sample for an equivalent amount of enzyme (**Figure 4.6a**). In contrast to what was observed with the wild-type SQR, the intensity of the signal decreased in the presence of dithionite. In the presence of both dithionite and Na_2S, a slight diminution of intensity was observed, along with an intermediate linewidth of 15.7 G. These observations are consistent with the $SQR^{Cys160Ala}$ variant stabilizing the semiquinone.

In SQR, the FAD semiquinone signal was clearly detectable by EPR at neutral or basic pH values (**Figure 4.6, Supplementary Figure 4.6**). The EPR signal intensity detected at pH 8.0 in wild-type SQR was about two times more intense than that monitored at pH 7.0 in the as-isolated enzyme (**Supplementary Figure 4.6**). In the Na_2S reduced wild-type enzyme, however, the EPR signal intensity detected at pH 7.0 and 8.0 were similar. Therefore, the potentiometric titrations of the FAD semiquinone of the wild-type SQR and $SQR^{Cys160Ala}$ variant were performed at neutral pH (**Figure 4.7**). In both cases, the bell-shaped titration curve arises because only the intermediate FAD semiquinone form (when FAD accepts a single electron or $FADH_2$ donates a single electron) is EPR visible. Curve fitting of the FAD semiquinone signal revealed a midpoint potential of -139 ± 4 mV (E_{m1} = -58 ± 4 mV, E_{m2} = -220 ± 4 mV) at pH 7.0 for

the two-electron reduction of FAD to $FADH_2$ in wild-type SQR. The midpoint potential of the FAD in $SQR^{Cys160Ala}$ (E_m= -135 ± 5 mV; E_{m1} = -40 ± 5 mV, E_{m2} = -230 ± 5 mV) is similar to that in wild-type SQR. Close inspection of the EPR spectra of flavin semiquinone reveals that the major semiquinone formed during the reduction of wild-type SQR and $SQR^{Cys160Ala}$ variant by dithionite at pH 7.0 is the anionic flavin radical exhibiting a linewidth of ~14-15 G and ~13-15 G, respectively (**Figure 4.7c, d**).

4.4 Discussion

A. ferrooxidans SQR couples the oxidation of sulfide to quinone reduction and has been extensively characterized by X-ray crystallography [37; 86; 123]. Both a nucleophilic attack mechanism and a radical mechanism [37; 86; 123] have been proposed that are compatible with the structural data (**Supplementary Table 4.3**). SQR oxidizes sulfide to elemental sulfur by individually transferring two electrons from a sulfide ion to the FAD cofactor via a semiquinone radical and generating $FADH_2$. $FADH_2$ in turn transfers 2 electrons to the quinone pool in the membrane potentially via an intermediate semiquinone radical.

Three conserved cysteines (Cys 128, Cys160 and Cys356) and two histidines (His132 and His198) are implicated in the mechanism. Herein we determined the kinetic parameters for the pre-steady state reduction of FAD by Na_2S (the reductive half reaction) for wild-type SQR and variants of the conserved amino acids. Wild-type SQR and the variants of Cys128 and His132 exhibit a rate of approximately 11.7 s^{-1}, indicating that Cys128 and His132 do not participate in the reductive step. This rate is in the middle range of flavin reduction rates which can vary from 2.5 s^{-1} in human cytochrome P450 [131] to 38 s^{-1} in *E. coli* proline dehydrogenase [132]. Variants of Cys160 and Cys356 were unable to catalyze the reduction of FAD. In the published nucleophilic attack mechanisms (**Supplementary Table 4.3**) different catalytic cysteines have been proposed as nucleophiles; attacking different target atoms of FAD, C^{4A} or C^{8M} with the formation of a covalent adduct. We have proposed (**Figure 4.8**) that Cys356, in the form of a Cys356–$S^{\gamma-}$ thiol or a Cys356–S^{γ}–S^{-} disulfide, nucleophilically attacks the C^{4A} atom of the isoalloxazine ring of FAD with the polysulfide chain growing on Cys160 until it

cannot fit in the active site. The possible role of Cys128 is to release the polysulfur (or octasulfur) product by the nucleophilic attack from Cys128 disulfide (Cys128–S^{γ}–S^{-}) and accordingly to restart the redox reaction turnover. All Cys variants dramatically reduced the overall Na_2S-decylubiquinone reduction rate with only the $SQR^{Cys128Ala}$ and $SQR^{Cys128Ser}$ variants showing limited activity (~15% and ~ 25% of the wild-type k_{cat}, respectively). The low $SQR^{Cys128Ser}$ rate reflects the fact that Ser is a weaker nucleophile compared to Cys. The low $SQR^{Cys128Ala}$ rate may result from an alternate octasulfur release mechanism.

His132 and His198 are believed to catalyze protonation or deprotonation reactions in SQRs [62]. In *Rhodobacter capsulatus* SQR, His132 (in the *A. ferrooxidans* numbering) is proposed to be involved in the FAD oxidation half-reaction by protonating decylubiquinone in the neutral pH range [62]. In *A. ferrooxidans* SQR, His132 is unlikely to protonate decylubiquinone due to the distance (>20Å) between His132 and the decylubiquinone binding site (**Figure 4.4**). His132 is close to Cys128 and the entrance of the channel that is open to the negatively charged side of SQR. His132 is part of a hydrogen bonding network with Cys128 via a sulfide ion bound in the sulfide binding pocket close to Cys128 [37; 123]. We propose that the role of His132 is to abstract the proton from the protonated sulfide (H_2S and HS^-) and cysteine thiol and to take part in the reaction of releasing the polysulfur product. The $SQR^{His198Ala}$ variant maintained about 25% of the FAD reduction rate indicating that His198 has some effect (perhaps indirect) on flavin reduction but it is not essential. Additionally, His198 is ~21Å away from the decylubiquinone binding site and ~18 Å away from the isoalloxazine ring of FAD. So it is questionable whether His198 directly participates in the protonation or deprotonation

reactions of either decylubiquinone or FAD. It is possibly involved in the protonation or deprotonation reactions of sulfide ion (S^{2-} and SH^-). Moreover, His198 connects two loops along the channel via a hydrogen bond and a salt bridge with Glu310. Thus His198 may affect the overall stability of the protein. Further studies will be required to confirm the roles of His132 and His198.

The transient adduct to the C^{4A} atom of FAD (Cys356-S^{γ}-S-C^{4A}-FAD) shown in **Figure 4.8** was not observed in our crystallographic determinations which is understandable given the instability of the adduct [37; 123]. However, by EPR we observed a neutral semiquinone radical upon reduction of SQR with Na_2S. In contrast, dithionite reduction led to an anionic semiquinone radical resulting from the addition of an electron to FAD. We suggest that the neutral semiquinone radical reflects the Cys356-S^{γ}-S-C^{4A}-FAD intermediate in **Figure 4.8**. In support of this the neutral semiquinone radical was enhanced in the $SQR^{Cys160Ala}$ variant as expected from the proposed mechanism. Further work will be required to confirm this suggestion. Additionally, EPR allowed us to determine the midpoint potential of the flavin to be -139 mV, which is very similar to the E_m of the flavin in *E. coli* succinate dehydrogenase and fumarate reductase [133] and appropriate for transferring the electrons from sulfide ($E_{m,7}$= -260 mV) to the quinone pool (e.g. the $E_{m,7}$ of DUQ is +90 ± 10 mV) [6].

While the stopped flow experiments allowed us to determine the rates of flavin reduction in SQR and the variants, interpreting the spectral variations is complex. The broad absorbance observed between 520 nm and 660 nm upon Na_2S reduction increased slightly suggesting the formation of a small amount of neutral semiquinone in agreement with the EPR results. The transient peak at 428 nm observed in both the Na_2S and

dithionite reduced SQR requires further investigation. This absorbance is normally associated with a cytochrome b heme Soret band but this is very unlikely given the crystallographic purity of our SQR preparation. It may reflect an additional interaction of the reduced cysteines with the flavin and this remains to be investigated. Together our kinetic and EPR experiments shed new light on the mechanism of sulfide oxidation and the roles of the FAD cofactor and conserved Cys and His residues.

4.5 Tables

Table 4.1 Kinetic parameters of wild-type and SQR variants

Variant	*Specific activity* (µmol mg^{-1} min^{-1})	k_{cat} (s^{-1})	K_m[Na_2S] (µM)	K_m[DUQ] (µM)	k_{cat}/K_m[Na_2S] ($\times 10^6$ $M^{-1}s^{-1}$)	k_{cat}/K_m[DUQ] ($\times 10^6$ $M^{-1}s^{-1}$)
SQR	8.1±0.20	6.5±0.16	2.97±0.28	3.43±0.43	2.19	1.89
C128A	1.2±0.11	1.0±0.09	5.60±0.91	4.25±0.57	0.18	0.24
C128S	2.0±0.10	1.6±0.08	5.53±0.98	5.85±0.61	0.29	0.27
C160A	0.1±0.03	0.1±0.02	n.d	~8*	n.d	n.d
C160S	0.6±0.05	0.5±0.04	n.d	~7*	n.d	n.d
C356A	0	0	n.d.	n.d.	n.d.	n.d.
C356S	0.1±0.02	0.1±0.02	n.d	~11*	n.d	n.d
H132A	1.7±0.21	1.4±0.16	5.00±0.94	5.4±0.51	0.27	0.25
H198A	0.3±0.08	0.3±0.06	n.d	~10*	n.d	n.d

*The DUQ K_m values reported for the $SQR^{Cys160Ala}$, $SQR^{Cys160Ser}$, $SQR^{Cys356Ser}$ and $SQR^{His198Ala}$ variants are approximations due to the very low specific activity. n.d not determined

4.6 Figures

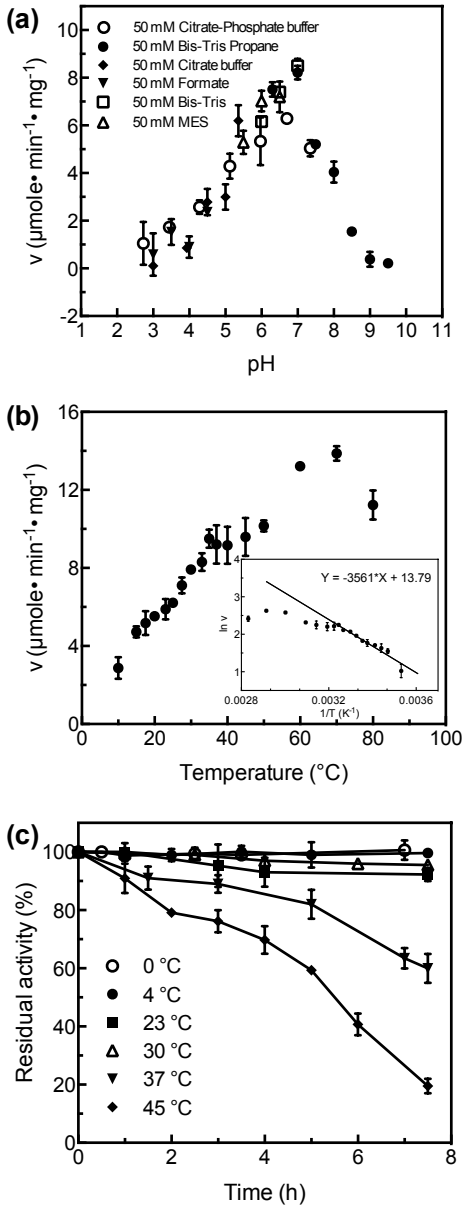

Figure 4.1. Effect of pH and temperature on SQR activity and stability.
The DUQ reduction activity of SQR was monitored as described in Methods; the reaction mixture contained 1.25 µg mL^{-1} SQR. (a) Effect of pH on SQR activity. A series of buffers (50 mM Bis-Tris Propane, 50 mM Bis-Tris, 50 mM MES, 50 mM Formate, 50 mM Citrate buffer and 50 mM Citrate-Phosphate buffer) covering a range of pH2.7-9.5 were utilized. (b) Effect of temperature on SQR activity. Assays were carried out at the indicated temperatures as described in Methods. Inset is the Arrhenius plot for calculation of the activation energy (E_a). (c) Thermal stability of SQR. Samples were incubated at the indicated temperatures as described in Methods. Aliquots were removed at the indicated times and assayed at 23°C. In all experiments the data are the mean values of three experiments; error bars indicate the standard deviation.

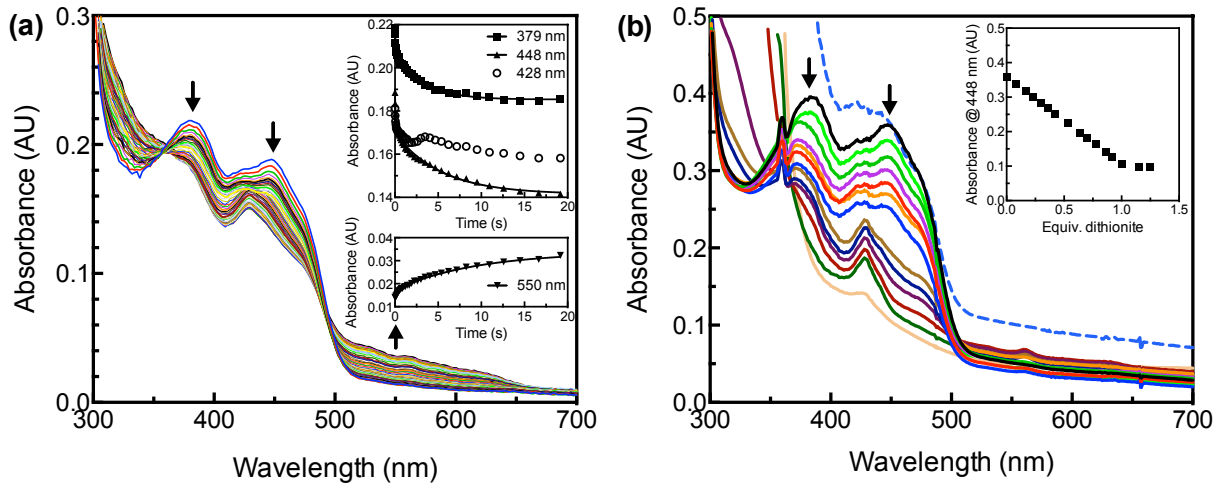

Figure 4.2. Spectral properties of the FAD in SQR.
(a) Stopped flow kinetics of flavin reduction by Na_2S. Purified SQR (25 μM after mixing) was rapidly mixed with 125 μM (after mixing) freshly prepared Na_2S in 50 mM Bis-Tris buffer (pH 7.0) containing 20 mM glucose, 1 unit mL^{-1} glucose oxidase and 10 units mL^{-1} catalase. The spectral changes were monitored with an Applied Photophysics SX.18MV stopped-flow instrument equipped with a multiwavelength photodiode array detector. The spectra shown were recorded at 0.00128−100 s after mixing. The arrows indicate the directions of spectral changes over time. Insets are the kinetics of absorbance changes observed at 379 nm, 428 nm, 448 nm and 550 nm, which were fitted to a two-phase exponential decay equation and to a two-phase association model, respectively. All fits were characterized by an R^2 better than 0.99. (b) Dithionite titration of SQR. Purified SQR (44 μM, in 50 mM Bis-Tris, pH 7.0, 20 mM glucose, 1 unit of glucose oxidase per mL and 10 units of catalase per mL) was titrated with 5 mM freshly prepared dithionite solution (in 50 mM Tris, pH 9.0). All buffers were argon-flushed before use. The spectra shown, in order of decreasing absorbance at 448 nm, correspond to the addition of different amount of dithionite. The blue dashed line was recorded after the addition of ferricyanide (1 mM) to the dithionite reduced SQR. The inset shows the absorbance change at 448 nm versus the amount of dithionite added.

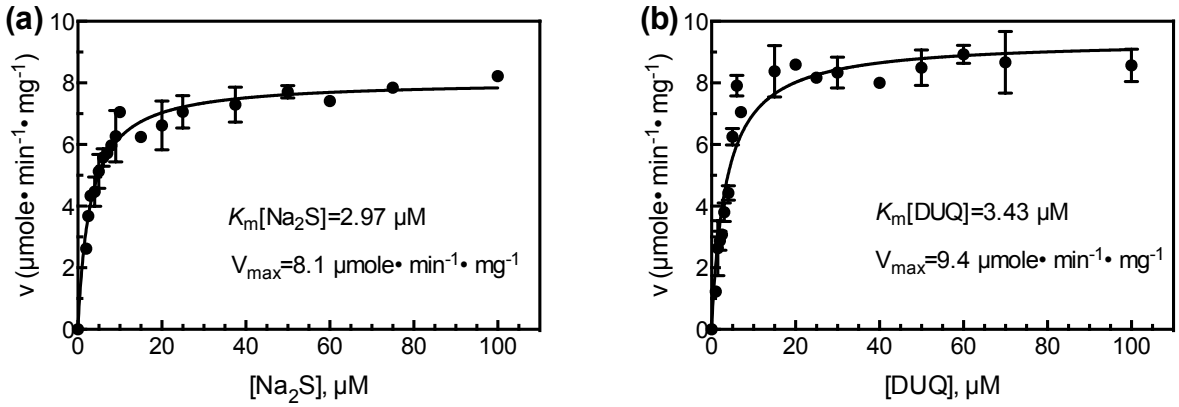

Figure 4.3. Kinetic analysis of SQR based on decylubiquinone reduction.
Measurements were carried out using the DUQ reduction activity assay method at 23°C as described in Methods. The reaction mixture contained 1.25 μg mL^{-1} SQR in 50 mM Bis-Tris, pH 7.0, 20 mM glucose, 1 unit of glucose oxidase per mL and 10 units of catalase per mL. The DUQ reduction rates observed at varying Na_2S concentration in the presence of 50 μM DUQ (a) and at varied DUQ concentration in the presence of 100 μM sulfide (b) were plotted and fitted to the Michaelis–Menten equation. The K_m and V_{max} values were determined by nonlinear regression using GraphPrism Software. The data are the mean values of three experiments; error bars indicate the standard deviation.

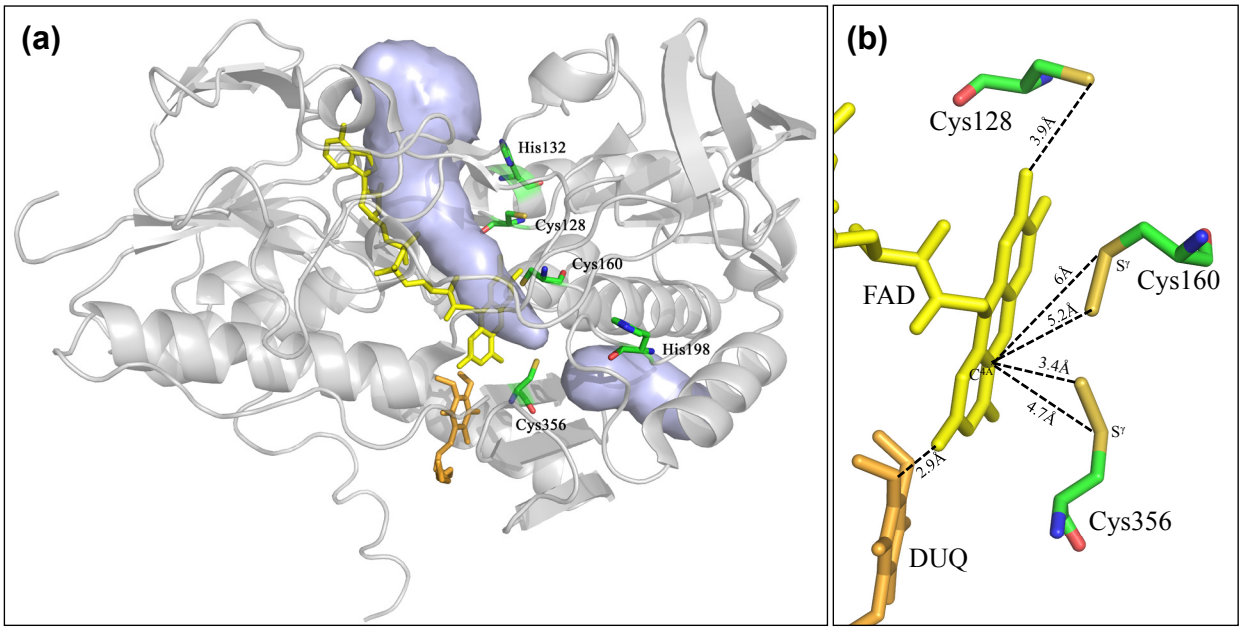

Figure 4.4. A cartoon representation of the SQR structure from PDB ID: 3T31 generated using PyMol [100].
The highly conserved Cys128, Cys160, Cys356, His132 and His198 are show as sticks. FAD is shown in yellow and DUQ in bright orange. (a) Potential channels predicted using CAVER [134] connecting the sulfide oxidation site to the outside environment are indicated in light blue. (b) The sulfide oxidation site in SQR. The distance between the C^{4A} atom of FAD and the S^{γ} atoms of Cys356 or Cys160 is 4.7 Å and 6.0 Å, respectively. Two sulfur atoms covalently attached to Cys356 and Cys160, respectively, were displayed. The distance between the C^{4A} atom of FAD and the S atoms of Cys356–S^{γ}–S^{-} disulfide or Cys160–S^{γ}–S^{-} disulfide is 3.4 Å and 5.2 Å, respectively. The Cys128 S^{γ} atom is 3.9 Å from C^{8M} atom of the isoalloxazine ring of the FAD cofactor. The benzoquinone head is also close to the isoalloxazine ring of FAD, the distance between the O^{2} atom of the DUQ and the O^{2} atom of FAD is 2.9 Å.

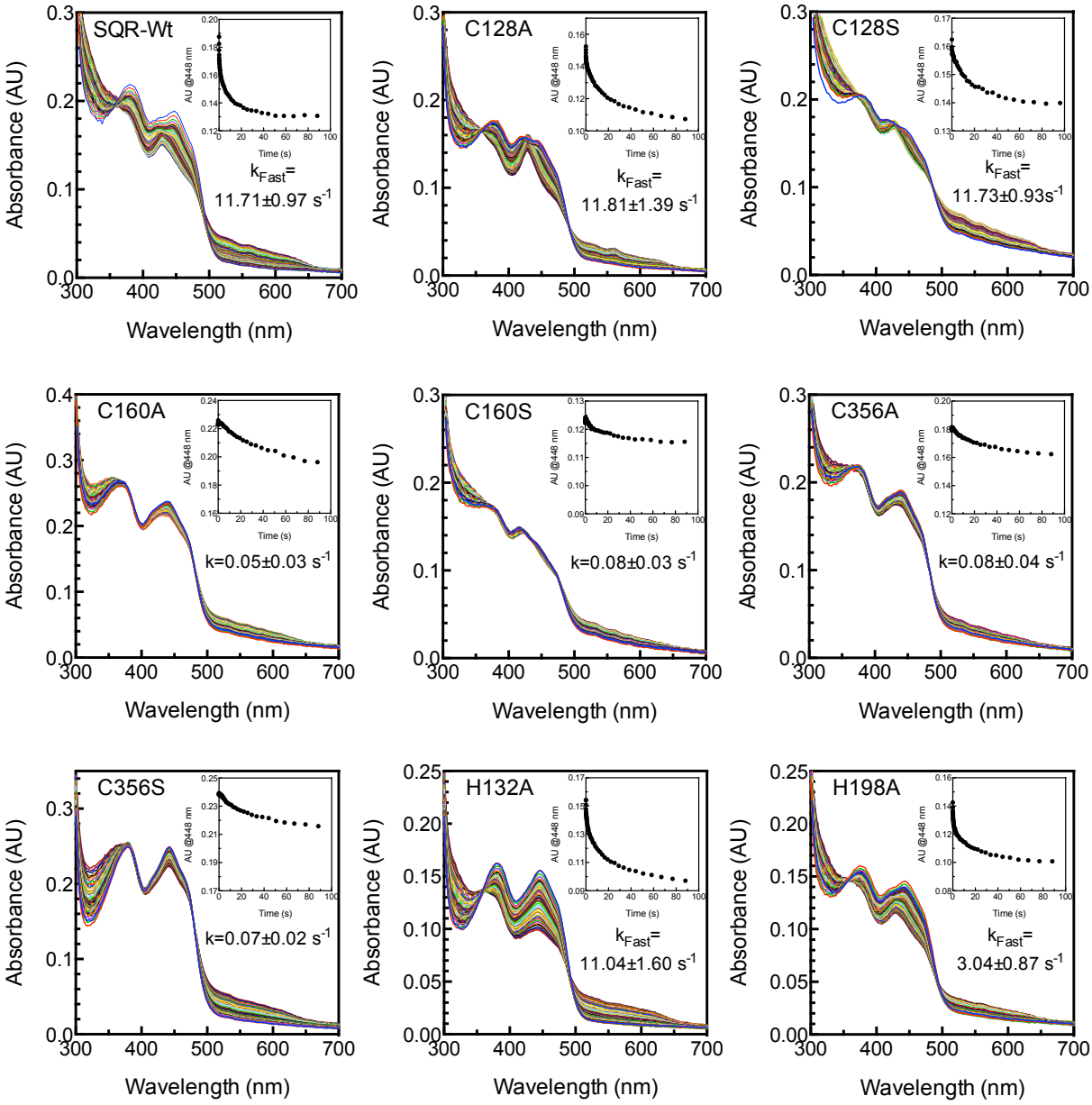

Figure 4.5. Pre-steady state reduction of FAD by Na_2S in wild-type and the variant SQR. Enzyme and substrate were mixed in the stopped-flow as described in Methods. The reaction was monitored by multiwavelength absorption in the range of 300−700 nm. The spectra shown were recorded at 0.00128−100 s after mixing. Insets are traces at 448 nm and the mean values (n=3) of the rate constants (k_{Fast} for the two-phase decay or k for the one-phase decay) obtained from fitting absorbance changes at 448 nm to the two-phase exponential decay equation model or the one-phase exponential decay equation which is it with GraphPad Prism (GraphPad Software, San Diego, CA). All fits were characterized by an R^2 better than 0.99.

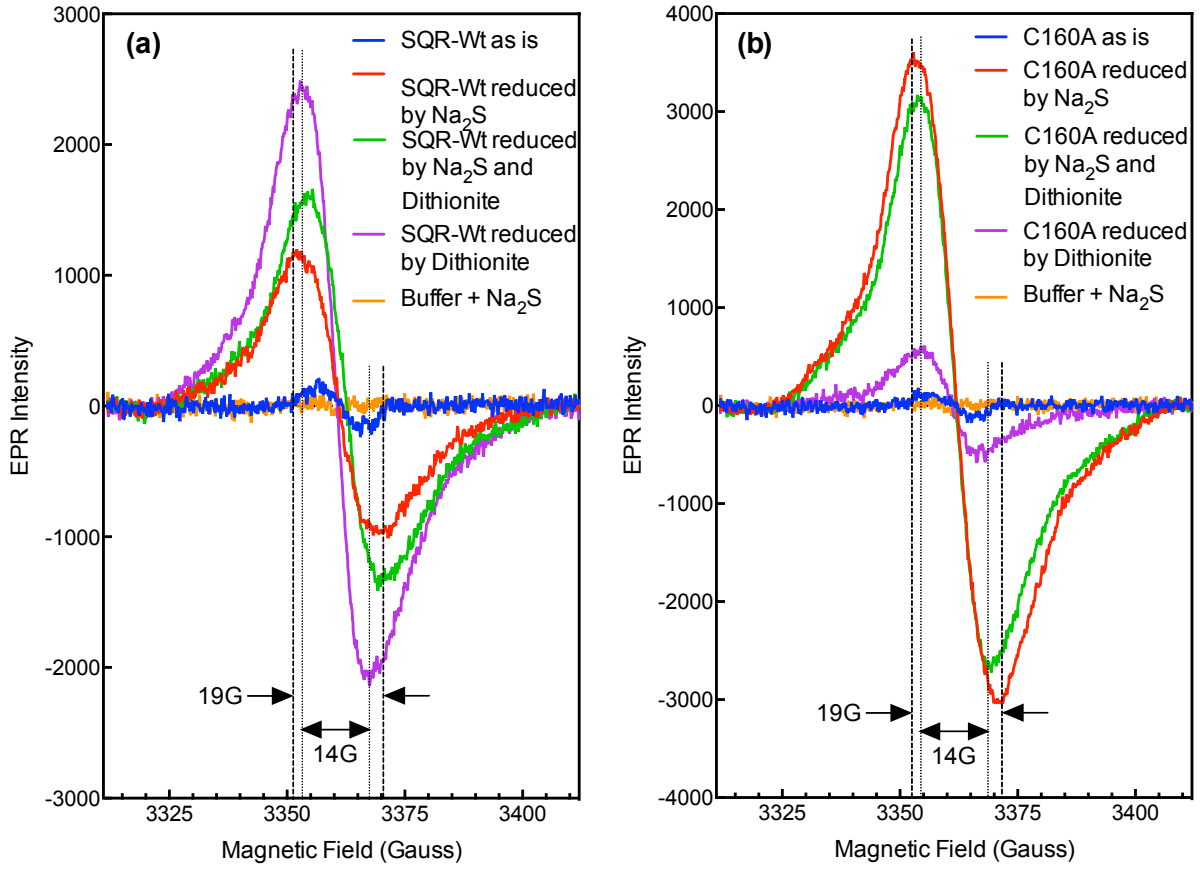

Sample	Linewidth of the spectrum (Gauss, G)
SQR-Wt as is (0.1 mM)	8.9
SQR-Wt reduced by 5.5 mM Na_2S	19.3
SQR-Wt reduced by 5.5 mM Na_2S and Dithionite	13.9
SQR-Wt reduced by Dithionite	14.6
Buffer +10 mM Na_2S	n.a.
C160A as is (0.1 mM)	11.1
C160A reduced by 5.5 mM Na_2S	18.6
C160A reduced by 5.5 mM Na_2S and Dithionite	15.7
C160A reduced by Dithionite	13.6

Figure 4.6. The EPR spectra of wild-type SQR (a) and $SQR^{Cys160Ala}$ variant (b) at pH 7.0. The "as is" air-oxidized (blue line), Na_2S reduced (red line), sodium dithionite reduced (green line) and Na_2S and Dithionite co-reduced (magenta line) samples were prepared in 3-mm internal diameter quartz EPR tubes and incubated at 23 °C for 10 min prior to freezing. The table below the figures summarizes the linewidths of the spectra. EPR spectra were recorded using a Bruker Elexsys E500 spectrometer equipped with a Bruker liquid nitrogen-evaporating cryostat at 150 K, 20-milliwatt microwave power at 9.43 GHz.

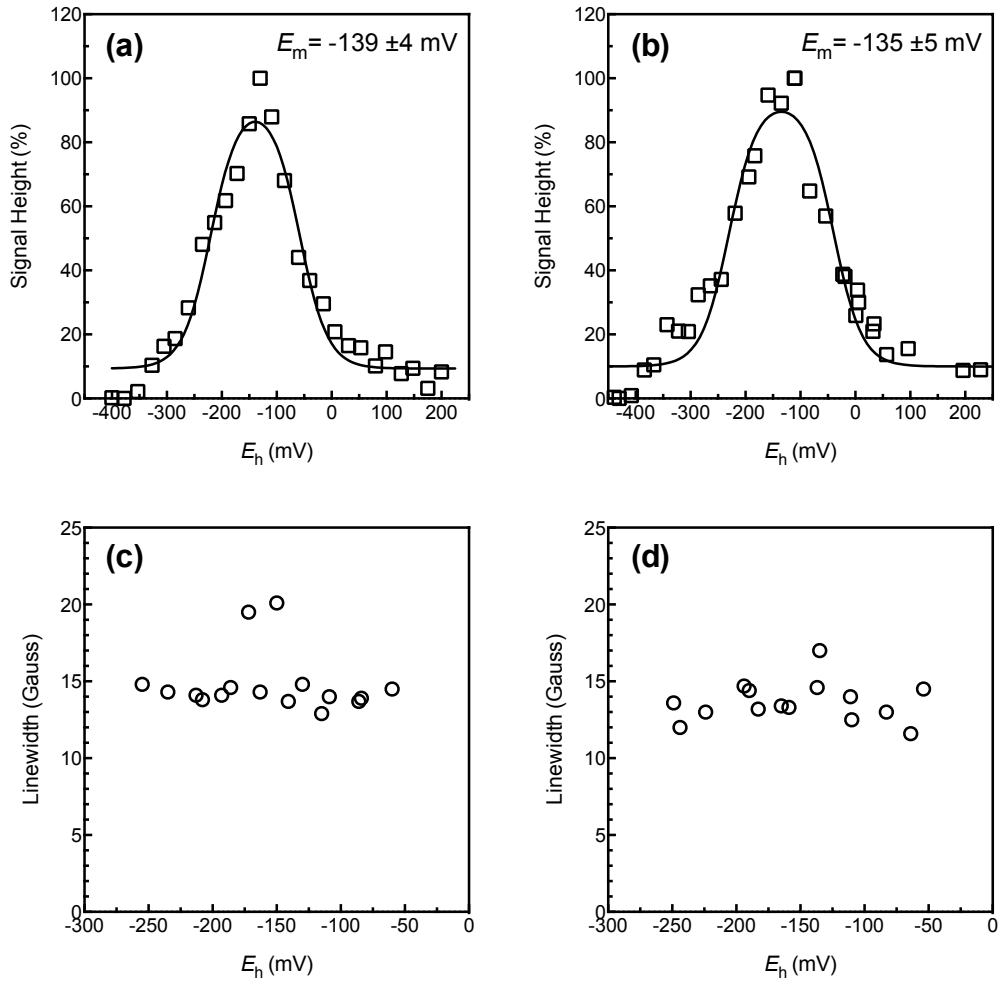

Figure 4.7. Potentiometric titration of the FAD radical signal in wild-type SQR and SQR^{Cys160Ala} variant at pH 7.0.

(a) Redox titration of wild-type SQR. (b) Redox titration of SQR^{Cys160Ala} variant. Peak-trough differentials were plotted as a function of E_h. Signal heights are normalized to 100%. (c) The linewidths (peak-trough separation) of the EPR spectra of flavin semiquinone in wild-type SQR. (d) The linewidths of the EPR spectra of flavin semiquinone in SQR^{Cys160Ala} variant. The linewidths of the flavin semiquinone EPR spectra with >30% normalized signal height among the titrated samples were analyzed and plotted. Presented data were gathered from two independent potentiometric titrations for both wild-type and variant enzyme.

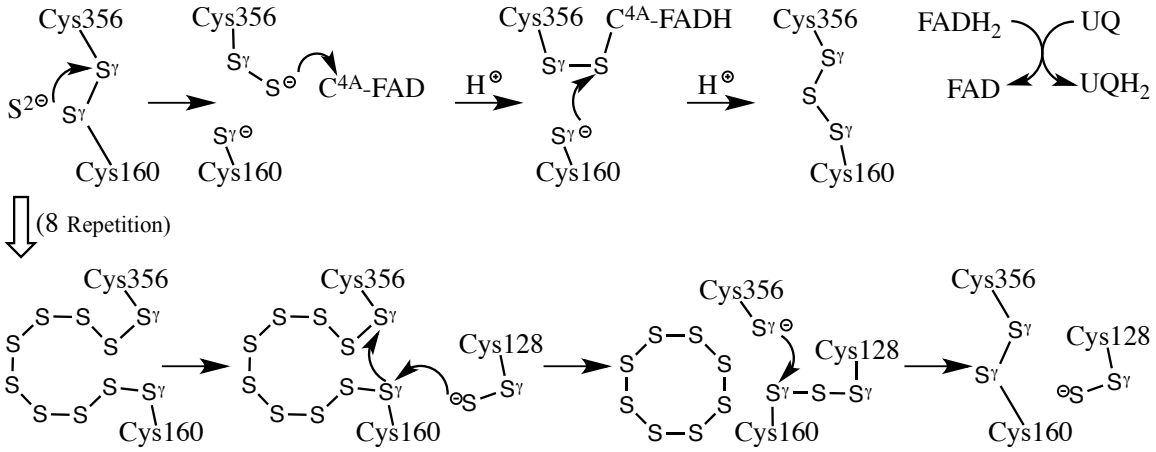

Figure 4.8 The proposed mechanism of sulfide oxidation of $SQR_{At,f}$.
Initially, a sulfide ion attacks the Cys356–S^{γ} breaks the sulfide bridge, consequently forming a Cys356–S^{γ}–S^{-} disulfide and a thiol on Cys160. Cys356–S^{γ}–S^{-} disulfide nucleophilically attacks the C^{4A} atom of FAD, forming a Cys356–S^{γ}–S–C^{4A}–FAD adduct, and one electron is transferred to FAD. Cys160 thiol then attacks the adduct and releases FAD and forming a trisulfide bridge. A second electron is transferred in this step. The fully reduced FAD then transfer the electrons to the ubiquinone pool in the membrane. Protons that are added to the reduced cofactor likely come from solvent. Eight repetitions of the steps described above lead to the polysulfide chain growing on Cys160 and forming an octasulfur ring, which is released by the nucleophilic attack from Cys128 disulfide (Cys128–S^{γ}–S^{-}). The mechanism proposed here is an update of our previously proposed sulfide oxidation mechanism based on the structure of $SQR_{At,f}$ [37]. In which, the active sites shows a branched tetrasulfide which was interpreted later as an overlap of intermediate states [123].

4.7 Supplementary Tables

Supplementary Table 4.1. List of mutagenic oligonucleotides.

Mutant	Mutagenic Oligonucleotide (5' to 3')
Cys^{128Ala}	GTCCATTGCTACGGTGGACC
Cys^{128Ser}	CAGTCCATTAGTACGGTGGAC
Cys^{160Ala}	CCATGGCCGGCGCAAGTGCCTTCGGACCGGCTT
Cys^{160Ser}	GCGCAAGTTCATTCGGACCG
Cys^{356Ala}	GGAATGCGGTGGCTTTTGCCGATATGG
Cys^{356Ser}	TGGAATGCGGTGAGCTTTGCCGATATG
His^{132Ala}	TTTGTACGGTGGACGCTGCGGAAC
His^{198Ala}	CCTACATCGGTGCTCTGGGCATTC

Supplementary Table 4.2. Purification of His-tagged SQR from recombinant *E. coli* BL21(DE3) harboring pLM1::SQR

Fraction	Protein (mg)	Specific activity (units mg^{-1})	Total activity (units)	Yield (%)	Purification (fold)
Cell-free extract	7339.5	0.092	675.23	100	1.0
Non-membrane	5814.0	0.102	593.03	87.8	1.1
Membrane	1323.7	0.047	62.21	9.2	0.5
Ni-Affinity Chromatography	50.0	8.07	403.50	59.8	87.7

Supplementary Table 4.3 Summary of proposed enzymatic mechanisms of SQR

Mechanism type	**Nucleophilic attack mechanism**					**Radical mechanism**
Source of SQR	*A. ferrooxidans*	*R. capsulatus*	*A. ambivalens*	*A. aeolicus*	*A. aeolicus*	*A. ferrooxidans*
Nucleophile	Cys356-S^{γ}-S^{-}	Cys160-$S^{\gamma-}$	Cys160-$S^{\gamma-}$	Cys160-S^{γ}-S^{-}	Cys128-S^{γ}-S^{-}	Not applicable*
Target atom of FAD	C^{4A}	C^{4A}	C^{4A}	C^{4A}	C^{8M}	Not applicable*
Residue on which the polysulfide chain grows	Cys160	Cys356	Cys356	Cys356	Cys356	Cys160
FAD bound form	Non-covalently	Non-covalently	Covalently	Covalently	Covalently	Non-covalently
Reference	This work	Griesbeck et al. (2002)	Brito et. al., (2009)	Marcia et. al. (2009)	Marcia et. al. (2009)	Cherney et. al. (2012)

*In radical mechanism, one electron from the persulfide anion Cys356-S^{γ}-S^{-} to the isoalloxazine ring of FAD with formation of a neutral radical Cys356-S^{γ}-$S^{\bullet}$. The Cys356-S^{γ}-$S^{\bullet}$ radical then reacts with a sulfide ion HS^{-} forming a radical anion from which a second electron is transferred to FAD. Each reaction with an HS^{-} ion results in two electrons transferred to FAD, one proton is released to solvent, and one sulfur atom is inserted into the polysulfide chain on Cys160.

4.8 Supplementary Figures

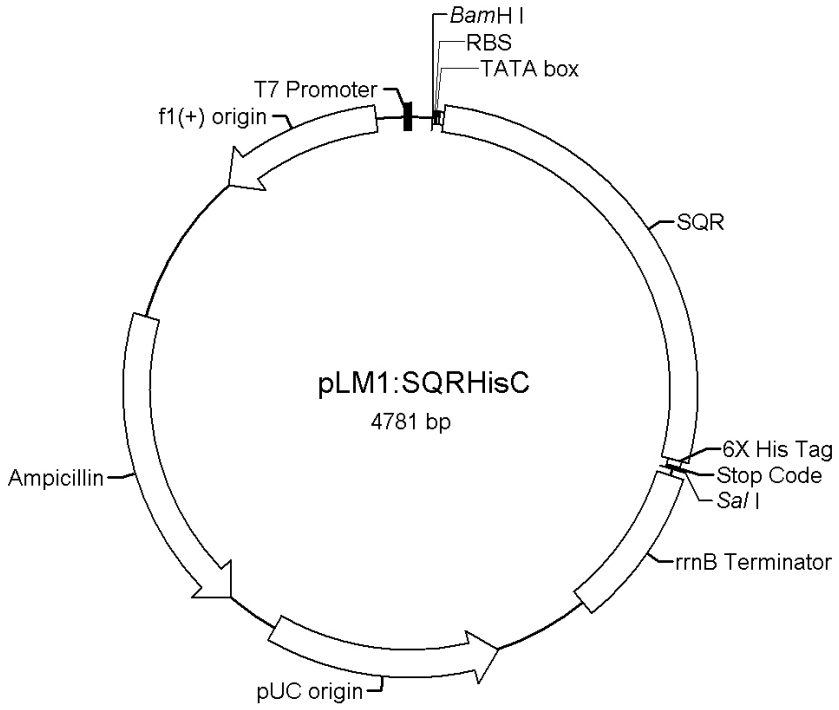

Supplementary Figure 4.1. Restriction map of pLM1::SQR_{His6} expression plasmid.

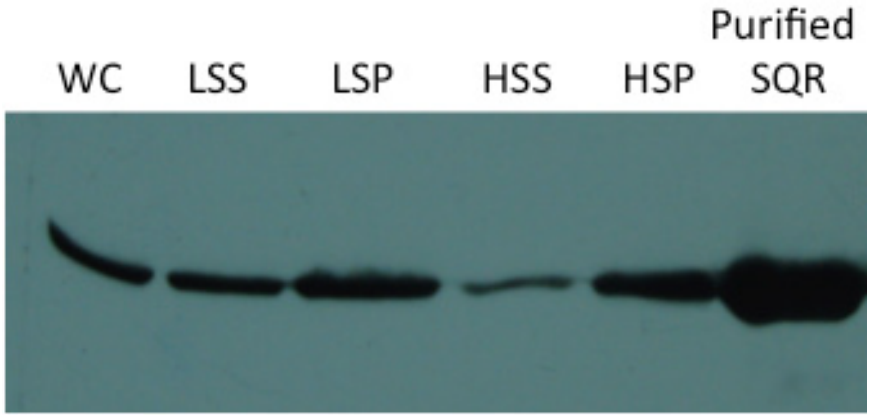

Supplementary Figure 4.2 Western blotting analysis of the fractions during the purification process of SQR.
WC: Whole cell, LSS: supernatant after low speed centrifuge, LSP: pellet after low speed centrifuge, HSS: supernatant after High speed centrifuge, HSP: pellet after High speed centrifuge, Purified SQR are used as a control. 20 μg of protein were loaded in each lane.

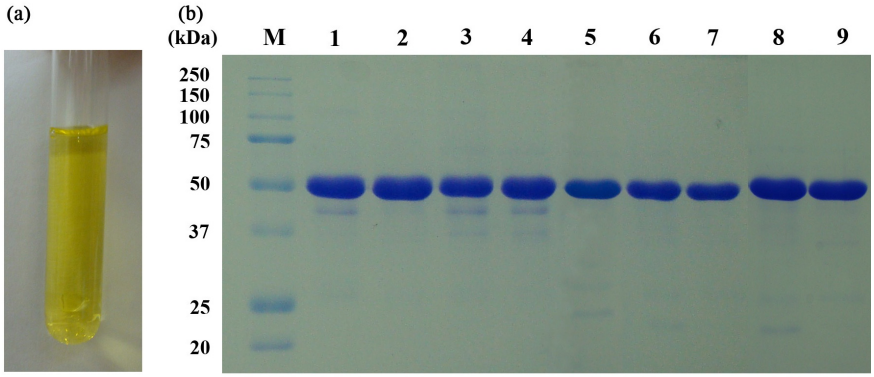

Supplementary Figure 4.3 Purified SQR showing the intense yellow color in visible light (a) and the Coomassie blue-stained SDS-PAGE of SQR (b).
Lane M, precision broad molecular weight standards (Bio-Rad); lane 1, purified recombinant SQR wild-type; lane 2, purified recombinant $SQR^{Cys128Ala}$; lane 3, purified recombinant $SQR^{Cys160Ala}$; lane 4, purified recombinant $SQR^{Cys356Ala}$; lane 5, purified recombinant $SQR^{Cys128Ser}$; lane 6, purified recombinant $SQR^{Cys160Ser}$; lane 7, purified recombinant $SQR^{Cys356Ser}$; lane 8, purified recombinant $SQR^{His132Ala}$; lane 9, purified recombinant $SQR^{His198Ala}$. 10 µg of protein were loaded in each lane. All proteins are tagged at the C-terminus with His_6.

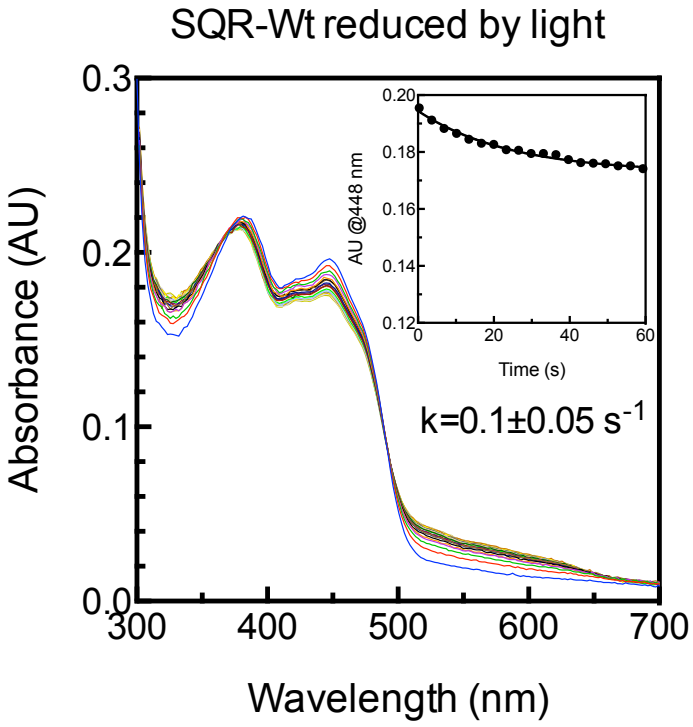

Supplementary Figure 4.4 Photoreduction of FAD in SQR wild-type during the stopped-flow multiwavelength absorption measurement.

Flavoproteins are light reducible. The FAD in SQR can be reduced slightly by the incident beam during the stopped-flow multiwavelength absorption measurement. The observed rate constants (k) of the light reduction of FAD in SQR was 0.1±0.05 s^{-1}. The measurement was performed in the same condition, without using Na_2S, descripted in the methods of enzymatic activity assay based on the reduction of FAD.

The reaction was monitored in the stopped-flow by multiwavelength absorption in the range of 300−700 nm. The spectra shown were recorded at 0.00128−100 s after mixing. Insets are single wavelength traces at 448 nm and the mean values (n=3) of the rate constants (k) obtained from fitting absorbance changes at 448 nm to the one-phase exponential decay equation model with GraphPad Prism (GraphPad Software, San Diego, CA). Goodness of all fit characterized by R-squared were better than 0.99.

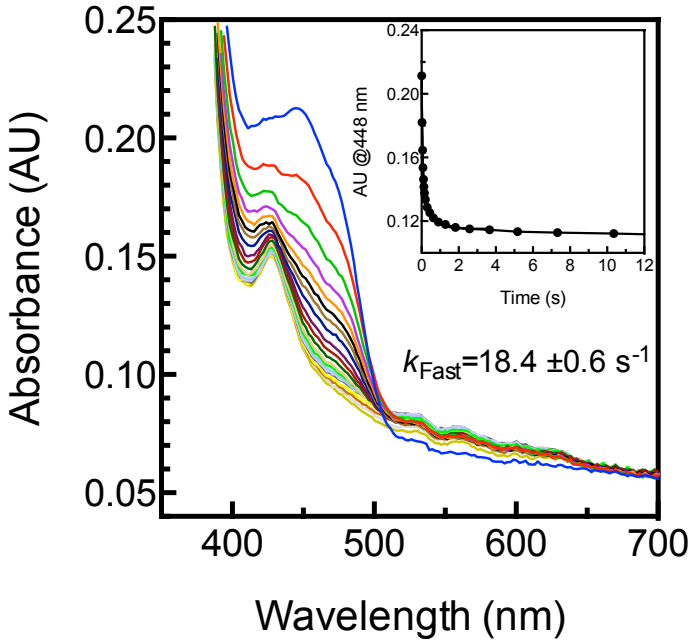

Supplementary Figure 4.5 Stopped flow kinetics study of flavin reduction by dithionite. Purified SQR (25 μM after mixing) was rapidly mixed with 2.5 mM (after mixing) freshly prepared dithionite in 50 mM Bis-Tris buffer (pH 7.0) containing 20 mM glucose, 1 unit mL^{-1} glucose oxidase and 10 units mL^{-1} catalase. The spectral changes were monitored with an Applied Photophysics SX.18MV stopped-flow instrument equipped with a multiwavelength photodiode array detector. The spectra shown were recorded at 0.00128−20 s after mixing. Inset is the kinetics of absorbance changes observed at 448 nm, which were fitted to a two-phase exponential decay equation. The observed rate constant (k_{Fast}) is 18.4 ± 0.6 s^{-1}. All fits were characterized by an R^2 better than 0.99.

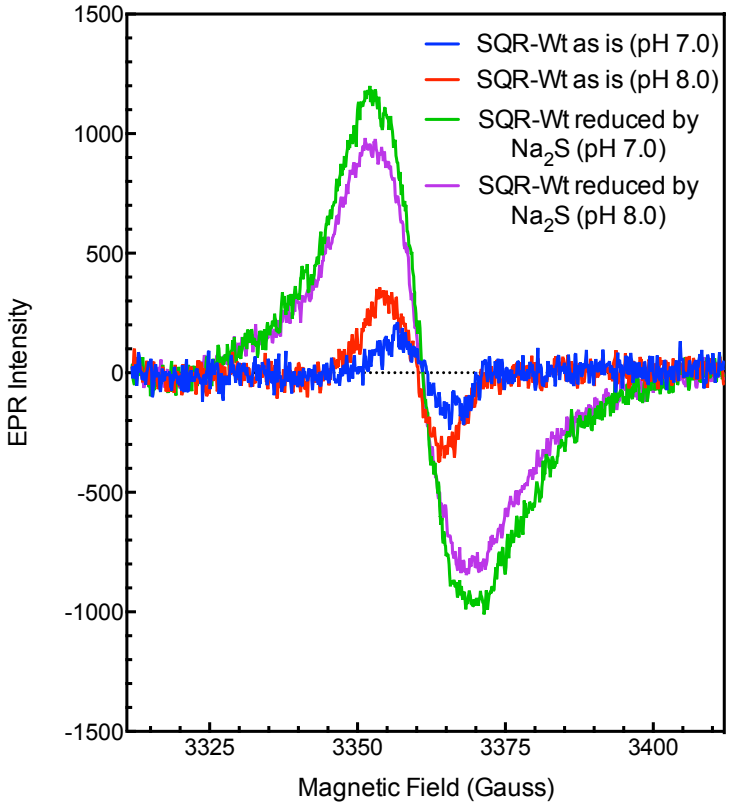

Supplementary Figure 4.6 The EPR spectra of wild-type SQR at pH 7.0 and pH 8.0. The "as is" air-oxidized and "Na_2S reduced" samples containing 200 µL of purified SQR (5 mg mL^{-1}, 0.1 mM) were prepared separately in 50 mM MOPS, 0.5 M NaCl, pH 7.0 (blue line and green line, respectively) and 50 mM Tricine, pH 8.0 (red line and magenta line, respectively).

Chapter 5: A simple semi-quantitative *in vivo* method using H_2S detection to monitor sulfide metabolizing enzymes

A version of this chapter has been published in BioTechniques.

Zhang, Y., and Weiner, J. H. (2014) A simple semi-quantitative in vivo method using H_2S detection to monitor sulfide metabolizing enzymes. *Biotech.* **57**, 208–210.

Acknowledgments This work was funded by the Canadian Institutes of Health Research (CIHR MOP89735).

5.1 Method summary:

We use lead acetate [$Pb(OAc)_2$] soaked filter paper to measure the *in vivo* activity of heterogeneously expressed sulfide:quinone oxidoreductase (SQR) based on the reaction of volatile H_2S with $Pb(OAc)_2$ to form insoluble PbS. The PbS stain is proportional to the amount of H_2S released from the culture. The *in vivo* H_2S oxidation activity was calculated based on the color density of the PbS stain formed by *E. coli* expressing SQR compared with cells harboring the empty vector pLM1.

5.2 Introduction

Sulfide (existing as three different forms: H_2S, HS^- and S^{2-})[a] is involved in a variety of biological processes. In mammals, it is considered a very toxic molecule, which inhibits mitochondrial ATP production [12]. However, it can be used as an energy source by microbes [89]. In recent years, sulfide has been identified as a signaling molecule and plays prominent roles in cellular physiology and pathophysiology including the regulation of vascular homeostasis, inflammation, apoptosis, and cellular stress response [15; 19; 135]. Several enzymes are involved in sulfide metabolism. Sulfide is produced from cysteine and/or homocysteine by sulfide-generating enzymes, e.g. cystathionine β-synthase (EC 4.2.1.22), cystathionine γ-lyase (EC 4.4.1.1), 3-mercaptopyruvate sulfurtransferase (EC 2.8.1.2) teamed with cysteine aminotransferase (EC 2.6.1.3), cysteine lyase (EC 4.4.1.10) and cysteine desulfurase (EC 2.8.1.7) [32; 33; 34; 35]. Sulfide is membrane permeable and highly diffusible in its gas form (H_2S) [3]. The produced sulfide can be removed (or stored) as sulfane-bound sulfur, which is the storage intermediate for sulfide and in turn may release sulfide when cells are under certain physiological conditions [36]. Sulfide:quinone oxidoreductase (SQR, EC 1.8.5.4), acting as a sulfide remover, catalyzes the oxidation of sulfide to elemental sulfur (polysulfide or octasulfur rings) [37]. Thiol S-methyltransferase (EC 2.1.1.9) and thiosulfate:cyanide sulfurtransferase (EC 2.8.1.1) are also involved in removing the sulfide via methylation and oxidation, respectively [38; 39].

Lead acetate, mercuric chloride or silver nitrate impregnated paper strips are widely used to qualitatively detect hydrogen sulfide in the atmosphere and solution with high sensitivity [136].

[a] In this paper the term "sulfide" will refer to the total sulfide present in solution including the three different forms: H_2S, HS^- and S^{2-}. The species H_2S, SH^- and S^{2-} will be named specifically as necessary.

These strips are also used for the qualitative detection of the microbial production of H_2S by inserting a lead acetate paper strip between the plug and inner wall of a culture tube, above the inoculated medium [137]. The major conventional methods for sulfide quantitative measurement in biological samples are colorimetric (e.g. the methylene blue method), electrochemical (sulfide-selective electrodes), gas chromatography, and sulfide precipitation–analysis [9]. However, these methods require sample homogenization and/or acidification prior to analysis. Fluorescent probe-based methods can be very suitable tools in detecting, measuring, and visualizing sulfide species in biological systems due to the high sensitivity, selectivity and real-time capability [138]. The *in vivo* activities of enzymes were normally examined by monitoring their abilities to support growth in minimal medium supplemented with corresponding substrates [139]. However, this method is not suitable for sulfide metabolizing enzymes as sulfide is a regulator and not necessary for cell growth.

5.3 Protocol

5.3.1 Reagents

Lead(II) acetate trihydrate (Catalog No. 32307; Sigma)

L-Cysteine (Catalog No. W326305; Sigma)

Ampicillin Sodium Salt (Catalog No. CA97061-440; VWR)

Isopropyl-B-D-thiogalactopyranoside (IPTG, catalog No. BP1755; Fisher)

Tryptone (Catalog No. CA1.07213.1000; VWR)

Yeast Extract, granulated (Catalog No. CA1.03753.0500; VWR)

Sodium Chloride (Catalog No. X0420-3; VWR)

5.3.2 Recipe

1. **2% Lead acetate [$Pb(OAc)_2$]**: dissolve 2% lead acetate in H_2O, filter through 0.22 μm filter.

2. **1000× Ampicillin stock solution (100 mg/mL):** Dissolve 1 g ampicillin in 10 ml of sterile Milli-Q water. Filter through a 0.22 um filter, Store at -20 °C.

3. **IPTG (isopropyl-beta-D-thiogalactopyranoside):** 0.5 M Stock solution in sterile H_2O, sterilize by filtration (0.22 um), Store at -20 °C.

4. **LB (Luria Bertani) Medium:** 10 g Tryptone, 5 g Yeast extract, and 10 g NaCl, 1 L H_2O, Autoclave immediately.

5. **LB $^{Amp+}$ agar plate:** 10 g Tryptone, 5 g Yeast extract, and 10 g NaCl, 15 g agar, add 1 L H_2O, Autoclave immediately. After removing the solution from the autoclave, allow the agar solution to cool to 55°C. Add 1 mL 1000x Ampicillin stock solution (100 mg/mL). Pour ~20mL of LB agar per 10 cm polystyrene Petri dish.

6. **L-cysteine stock solution (500 mM):** Dissolve 0.606 g L-cysteine in 10 mL of sterile Milli-Q water. Filter through a 0.22 um filter, make aliquots and store at -20 °C.

7. **2% lead acetate soaked filter paper:** (1) Cut Whatman qualitative filter paper to 123 mm × 82 mm rectangle with two rounded corners on one short side. Use the lid of the 24-well tissue culture plates as a template to cut the rounded rectangle filter paper. (2) Autoclave the rounded rectangle filter paper in an autoclave bag. (3) Soak the filter paper with 4 mL 2% lead acetate in a lid of the tissue culture plate, covered with the tissue culture plate and sit it at room temperature for 10 ~ 15 min.

5.3.3 Procedure

1. Streak stock cultures of *E. coli* DE3 (BL21)/pLM1, BL21/pLM1::sqr and variants on LB^{Amp+} agar plates, incubate at 37 °C overnight. Stock cultures are stored at -80 °C in 8 % DMSO.
2. Pick a single colony and transfer into 2 mL Luria Bertani (LB) medium containing 100 mg L^{-1} ampicillin, incubate at 37 °C overnight with shaking at 180 rpm.
3. Inoculate 0.2 mL of the overnight culture to 10 mL LB medium containing 100 mg L^{-1} ampicillin, incubate at 37 °C for 3 h with shaking at 180 rpm.
4. Soak the filter paper in 2% lead acetate solution.
5. Add 5 μL 500 mM freshly prepared L-cysteine to the 10 mL culture (final concentration is 250 μM).
6. Transfer 1 mL culture to a well of a flat-bottomed, 24-well tissue culture plate.

   A positive control (*E. coli* that harboured SQR wild-type) and a negative control (*E. coli* that harboured the empty vector pLM1) should be set in each plate. Make duplicates or triplicates for all samples.
7. Cover the inside of the lid with the lead acetate soaked filter paper. Place the plate in a 30°C shaker for 17 h with shaking at 180 rpm. Use tape and/or test tube rack to fix the position of the plate.
8. Measure the OD_{600} of the culture in each well using a spectrophotometer.
9. Scan the stained filter paper and save the color images in .tif, .jpg, .png or other image formats (a 16-bit .tif is the preferred format to retain the maximum amount of information in the original image).
10. Quantify the intensity of each stained disk on the filter paper by measuring the mean gray value (from 0 to 255) using ImageJ software (http://rsb.info.nih.gov/ij/). The mean gray

values were measured using consistent area selection and normalized to the OD_{600} of the culture.

H_2S oxidation activity was calculated based on the color density of the PbS stain formed by *E. coli* expressing SQR compared with cells harboring the empty vector pLM1. The relative activity compared to the wild-type was calculated using the OD_{600} normalized mean gray values. The relative activity (%) = (the mean gray value of stain X - the mean gray value of stain pLM1) × 100 / (the mean gray value of stain wild-type - the mean gray value of stain pLM1).

5.3.4 Equipment

Whatman qualitative filter paper, Grade 1 (Catalog No. 1001-185; GE Healthcare)

24-well tissue culture plates (Costar, catalog No. 3526, Costar, Cambridge, MA)

Tweezer

Laboratory shaker

Culture tube

Test tube rack

Tape

Scanner or All-In-One Printer

Spectrophotometer

Cuvette

5.4 Results

Herein, we present a simple *in vivo* activity assay method for recombinantly-expressed sulfide metabolizing enzymes in *E. coli*. *E. coli* metabolizing cysteine produces sulfide, which is highly diffusible in its gas form (H_2S) [3]. The released H_2S precipitates as lead sulfide (PbS) on lead acetate [$Pb(OAc)_2$] soaked filter paper. Cells expressing functional sulfide:quinone

oxidoreductase (SQR) can remove (or store) the sulfide by converting it to inorganic sulfur [35; 37] resulting in less PbS precipitate. A detailed protocol is available in the Supplementary Material. Briefly, a 2% overnight culture of *E. coli* BL21(DE3) transformed with empty vector, a vector expressing His-tagged wild-type SQR or SQR variants with reduced activity, was inoculated into Luria Bertani (LB) medium, containing 100 mg L^{-1} ampicillin and 300 μM isopropyl-beta-D-thiogalactopyranoside (IPTG), and grown at 37°C for 3 h with shaking at 180 rpm. 250 μM freshly prepared cysteine was added to the culture and 1 mL was transferred to a well of a 24-well tissue culture microtiter plate. The lid was covered with a piece of filter paper soaked in $Pb(OAc)_2$ (2%). The plate was placed in a 30°C shaker for 17 h with shaking at 180 rpm. The H_2S gas released from cysteine metabolism reacts with the $Pb(OAc)_2$ in the moistened filter paper to form a brown PbS stain. The PbS stain is proportional to the amount of H_2S released from the culture. The stained paper was scanned and quantified by measuring the mean gray value using ImageJ software [140]. The results were normalized to the OD_{600} of the culture. H_2S oxidation activity was calculated based on the color density of the PbS stain formed by *E. coli* expressing SQR compared with cells harboring the empty vector pLM1. The relative activity compared to the wild-type was calculated using the OD_{600} normalized mean gray values. The relative activity (%) = (the mean gray value of stain X - the mean gray value of stain pLM1) × 100 / (the mean gray value of stain wild-type - the mean gray value of stain pLM1). **Figure 5.1** summarizes the results which reflect the *in vitro* activity of SQR measured by decylubiquinone (DUQ) reduction assays [115]. *E. coli* BL21(DE3) expressing wild-type SQR completely oxidized endogenously-produced H_2S during growth thus preventing the precipitation of PbS on the lead acetate soaked paper. In contrast, H_2S released from *E. coli* BL21(DE3) harboring the empty vector pLM1 reacted with $Pb(OAc)_2$ soaked filter paper and formed insoluble PbS stain. A

variant, $SQR^{Cys128Ala}$, that retained 30% DUQ reduction activity displayed similar activity based on PbS precipitation. Inactive $SQR^{Cys160Ala}$ and $SQR^{Cys36Ala}$ variants were inactive in both assays. The differences in the *in vivo* sulfide oxidation activity of the overexpressed SQR mutants were not due to different expression levels, as indicated by western blotting (**Figure 5.2**).

In conclusion, the method described here provides a simple and efficient way to measure the *in vivo* activity of the recombinantly-expressed sulfide metabolizing enzymes in *E. coli*. It is simple and can be used for sulfide metabolizing enzymatic studies, mutant screening and high-throughput inhibitor screens. The limit range for released sulfide is 0.0625 - 3 μmole (**Figure 5.3**). The PbS stain reaches saturation when there are more than 3 μmole H_2S released from each well of a 24-well tissue culture microtiter plate.

5.5 Figures

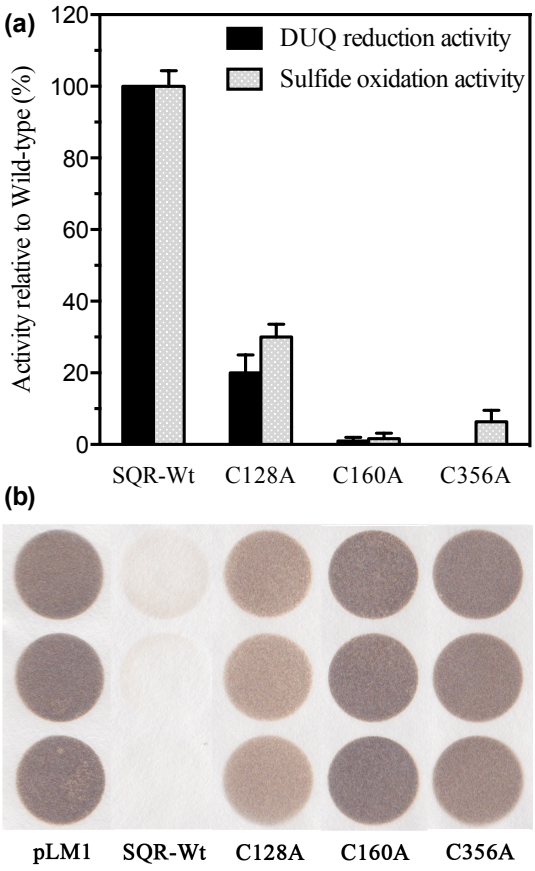

Figure 5.1 Comparison of DUQ reductase activity with PbS precipitation.
(a) Relative enzyme activities and PbS stain formed by wild-type (Wt) and variant SQR. 100% of DUQ reduction activity is 8.07 μmol mg^{-1} min^{-1} [115]. 100% H_2S oxidation activity is the differential density (differential mean gray value=56.91±3.74) of the PbS stain formed by *E. coli* BL21(DE3) that harboured wild-type SQR and the empty vector, pLM1. The mean gray values were measured using consistent area selection and normalized to the OD_{600} of the culture. The relative activity compared to the wild-type SQR was calculated using the OD_{600} normalized mean gray values. The relative activity (%) = (the mean gray value of stain X - the mean gray value of stain pLM1) × 100 / (the mean gray value of stain wild-type - the mean gray value of stain pLM1). The data are the mean values of three experiments (shown); error bars indicate standard deviation. (b) PbS stain formed by *E. coli* BL21(DE3) that harboured the empty vector pLM1, SQR-Wt and SQR variants. As the *in vivo* H_2S oxidation activity assay is not measured as a function of time, activity of 10% or less of wild-type was considered as a total loss of activity.

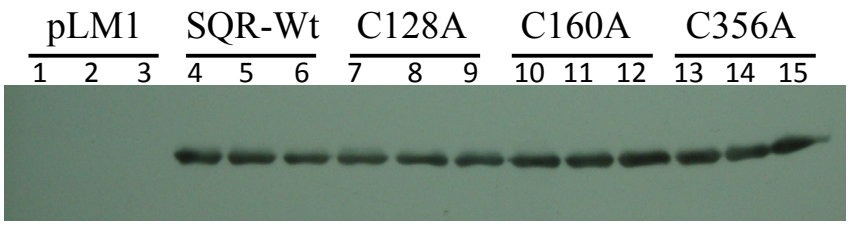

Figure 5.2 Western blot analysis of the expression levels of the His-tagged SQR in the culture of *E. coli* BL21(DE3) transformed with empty vector, a vector expressing wild-type SQR or SQR variants.

Culture samples of 0.2 mL each were taken from each well and pelleted by centrifugation at 10000 rpm. The pellets were suspended in 80 μL 1× protein sample loading buffer supplemented with fresh dithiothreitol (DTT). The suspended samples were boiled for 10 min and centrifuged at 10000 rpm for 2 min. 10 μL supernatant of each sample was analyzed with western blot immunodetection of the His-tag using monoclonal mouse antibody (Qiagen) and anti-mouse secondary IgG (Qiagen).

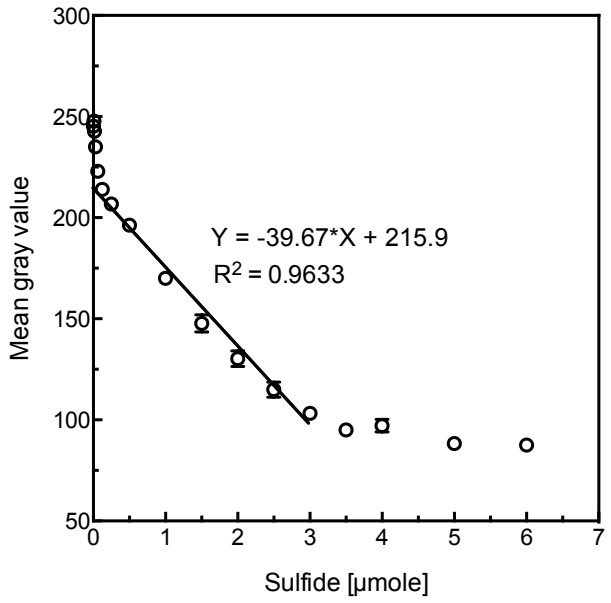

Figure 5.3 Calibration curve for sulfide.
20 µL Na_2S solutions, with varying concentrations from 0 to 300 mM, were dripped on the pre-dried 2% $Pb(OAc)_2$ soaked filter paper. The PbS stains formed were scanned and quantified by measuring the mean gray value with ImageJ software [140] using consistent area selection. The mean grey values were plotted against the amount of sulfide (in moles) dripped onto the lead acetated paper. Linear relationship was obtained over the range of 0.0625 - 3 µmole. The correlation coefficient (R^2) was found to be 0.9633.

Chapter 6: The Quinone-Binding Site of *Acidithiobacillus ferrooxidans* Sulfide:Quinone Oxidoreductase Controls both Flavin and Quinone Reduction

A version of this chapter has been submitted for publication as Zhang, Y., Qadri, A. and Weiner, J. H. (2014) The Quinone-Binding Site of *Acidithiobacillus ferrooxidans* Sulfide:Quinone Oxidoreductase Controls both Flavin and Quinone Reduction.

Acknowledgements The authors thank Justin G. Fedor and Dr. Richard A. Rothery for reviewing this manuscript and helpful discussions. This work was funded by the Canadian Institutes of Health Research (CIHR MOP89735). JinYang (Peter) Xu aided in constructing the site-directed variants.

6.1 Introduction

Sulfide (existing as three different forms: H_2S, HS^- and S^{2-}) is involved in a variety of biological processes. In mammals, it is considered a very toxic molecule, which inhibits mitochondrial ATP production [12]. However, it can be used as an energy source by microbes, such as the acidophilic chemolithotrophic bacterium *Acidithiobacillus ferrooxidans* [46; 47; 89]. Recently sulfide has been identified as a signaling molecule and plays prominent roles in cellular physiology and pathophysiology, including the regulation of vascular homeostasis, inflammation, apoptosis, and cellular stress response [15; 19; 135].

A key enzyme in maintaining the sulfide homeostasis is sulfide:quinone oxidoreductase (SQR), an ancient flavoprotein that is present in all domains of life (although it is absent in the plant kingdom). SQR is a peripheral membrane protein and catalyzes the oxidation of sulfide species to elemental sulfur by transferring two electrons from a sulfide ion via the FAD cofactor to the quinone pool in the membrane. SQR interacts with the membrane via two amphipathic helices and the quinone-pool through a conserved hydrophobic domain [37]. Quinones, the most important lipophilic electron and proton carriers, can undertake $2e^-/2H^+$ oxidation-reduction reactions and shuttle electrons and protons between respiratory enzymes via the membrane-bound quinone pool. Different types of natural quinones, comprising mainly benzoquinones, naphthoquinones, anthraquinones and polycyclic quinones, are widely distributed in different organisms. Animals and plants use ubiquinones (1,4-benzoquinones or *p*-benzoquinone) in their mitochondrial membrane quinone-pool, while bacteria use a mixture of quinones including ubiquinones, naphthoquinones and the derivatives menaquinone and rhodoquinone for the bioenergetic reactions. The distribution in the redox potentials ($E_{m,7}$) of quinones and the derivatives

ranges from ~ -400 mV for the non-physiological anthraquinones to ~ +110 mV for the physiological ubiquinones [42]. A significant shift of the redox potential can be caused by hydroxylation or methylation on the quinone motif. e.g. duroquinone ($E_{m,7}$ = +7 mV), menadione ($E_{m,7}$ = -12 mV), lawsone ($E_{m,7}$ = -119 mV) and plumbagin ($E_{m,7}$ = -40 mV) [43].

In SQR, quinone shuttles electrons from the FAD cofactor to the membrane-bound quinone pool. The site of quinone binding has been determined from the cocrystallized $SQR_{At,f}$-decylubiquinone (DUQ) complex structure [37]. The binding site of decylubiquinone (DUQ) is confined in the hydrophobic region that is close to the two C-terminal amphipathic helices (α9 and α10, residues 321-427). The benzoquinone ring of DUQ is sandwiched between the two benzene rings of Phe357 and Phe394 with the center-to-center distance of 3.4 Å and 3.8 Å respectively (**Figure 6.1**). Out of a total of 47 atom-atom interactions with DUQ within a distance of 3.9 Å, 24 are made to these two phenylalanine residues (**Supplementary Table 6.1**). The other interacting residues Phe41, Pro43, Gly322, Tyr323, Asn353, Ile368, Lys391 and Tyr411, together with Phe357 and Phe394, form a hydrophobic pocket (**Figure 6.1**). The benzoquinone head is also located close to the isoalloxazine ring of FAD; the distance between the O2 atom of the quinone and the O2 atom of FAD is less than 3 Å (**Figure 6.1c**). The hydrophobic quinone tail (decyl chain) points away from the amphipathic helices. It interacts with the protein via the side chains of Tyr323, Asn353, Ile368, and Tyr411, which are located at the entrance of the hydrophobic pocket. Sequence conservation analysis indicated that these four amino acids are not conserved, however, the other six amino acids out of the total ten quinone site corresponding residues are highly conserved and potentially necessary for either structural integrity and/or biological activity (**Supplementary Figure 6.1**).

In this study we have examined the quinone-binding site using quinone analogues and quinone site inhibitors. Computational approaches combined with pre-steady state and steady state kinetics have been applied to wild-type SQR and variants of amino acids comprising the quinone binding site. Our results show that the quinone-binding site also plays an important role in flavin reduction.

6.2 Materials and Methods.

6.2.1 Bacterial Strains and Plasmids

E. coli strain DH10B (F^- *end*A1 *rec*A1 *gal*E15 *gal*K16 *nup*G *rps*L Δ*lac*X74 Φ80*lac*ZΔM15 *ara*D139 Δ(*ara,leu*)7697 *mcr*A Δ(*mrr-hsd*RMS-*mcr*BC) λ^-; Invitrogen) was used for mutagenesis. *E. coli* BL21(DE3) (F^- *omp*T *gal dcm lon hsd*S_B(r_B^- m_B^-) λ(DE3 [*lac*I *lac*UV5-T7 gene 1 *ind*1 *sam*7 *nin*5])) was used for all enzyme expression. Wild-type SQR was expressed from plasmid pLM1::SQR under the control of the T7 promoter [86].

6.2.2 Quinones, Quinone analogs and Inhibitors

Decylubiquinone (DUQ), ubiquinone Q0 (UQ0), 2,3,5,6-tetramethylcyclohexa-2,5-diene-1,4-dione (Duroquinone), 2,5-dihydroxy-1,4-benzoquinone (DHBQ), 1,4-naphthoquinone (NQ), 2-hydroxy-1,4-naphthoquinone (Lawsone), 5-hydroxy-1,4-naphthoquinone (Juglone), anthraquinone-2-sulfonic acid sodium salt monohydrate (ANSO), 5-hydroxy-2-methyl-1,4-naphthoquinone (Plumbagin), 2-methyl-1,4-naphthoquinone (Menadione), pentachlorophenol (PCP), 4,4,4-trifluoro-1-(2-thienyl)-1,3-butanedione (TTFA), 6-methyl-N-phenyl-2,3-dihydro-1,4-oxathiine-5-carboxamide (Carboxin) and antimycin A were obtained from Sigma–Aldrich (St Louis, MO). 2-*n*-heptyl 4-hydroxyquinoline-*N*-oxide (HOQNO) was purchased from Alexis Biochemicals (San Diego, CA).

6.2.3 Site-directed Mutagenesis of quinone site Mutants

Construction of the site-directed variants was carried out following the QuikChange method (Stratagene) using pLM1::SQR plasmid as the template for mutagenesis [86; 115]. The oligonucleotides used are listed in **Supplementary Table 6.2** and were obtained from

Integrated DNA Technologies (Coraville, IA). All recombinant plasmids were verified by DNA sequencing (DNA core facility, University of Alberta).

6.2.4 Enzyme Expression and Purification

Enzyme expression and purification was performed as previously described [86]. The protein fractions were buffer-exchanged (to remove imidazole) and concentrated to 5 mg/ml in buffer (50 mM MOPS, 0.5 M NaCl, pH 7.0) using a YM-30 Centricon tube (Amicon) as soon as possible after the purification and flash-frozen as aliquots with liquid N_2 before being stored at -80°C prior to use [115]. All steps of protein purification were performed at 4°C.

6.2.5 Protein Assays

Protein concentrations were determined by the Bradford method with bovine serum albumin as the standard [125]. 10 μg of purified wild-type and variants were analyzed by 12% SDS-polyacrylamide gel electrophoresis (SDS-PAGE) [141]. Low-molecular-mass markers were obtained from Bio-Rad. Gel electrophoresis was run at 200 V for 45 min, and the gel was stained with Coomassie Brilliant Blue.

6.2.6 Measurement of Enzyme Activity

The quinone reduction activity of SQR was measured as described previously [115]. Measurements were carried out with a Hewlett Packard 8453 UV-VIS diode array spectrophotometer at 23°C. The standard reaction mixture contained 50 mM Bis-Tris (pH 7.0) and 20 mM glucose. To establish anoxic conditions, the 50 mM Bis–Tris (pH 7.0) and 20 mM glucose were first mixed and flushed with N_2; 1 unit of glucose oxidase per mL and 10 units of catalase per mL were added to the assay medium when needed. The reaction was started by the addition of 100 μM freshly prepared Na_2S. The sulfide-decylubiquinone

(DUQ) reduction activity of SQR was measured in the presence of varying concentrations of DUQ. The reaction was followed by the decrease of absorbance at 275 nm (ε_{275}= 12.5 mM^{-1} cm^{-1}) as described previously [110; 127]. The sulfide-UQ_0 reduction activity was determined in the presence of varying concentrations of UQ_0 (ε_{275}= 12 mM^{-1} cm^{-1}). The sulfide-duroquinone reduction activity was determined by the decrease of absorbance at 275 nm (ε_{275}= 12.5 mM^{-1} cm^{-1}) in the presence of varying concentrations of duroquinone. The sulfide-DHBQ reduction activity was monitored by following the loss of absorbance at 340 nm (ε_{340}= 2.89 mM^{-1} cm^{-1}) [142]. The sulfide-naphthoquinone reduction activity was determined in the presence of varying concentrations of 1,4-naphthoquinone (ε_{265}= 4.01 mM^{-1} cm^{-1}), lawsone (ε_{275}= 15.17 mM^{-1} cm^{-1}), juglone (ε_{420}= 1.96 mM^{-1} cm^{-1}), plumbagin (ε_{275}= 10.3 mM^{-1} cm^{-1}) or menadione (ε_{275}= 2.38 mM^{-1} cm^{-1}), respectively.

6.2.7 Determination of Kinetic Constants

V_{max} and Michaelis constant (K_m) for Na_2S, DUQ and quinone analogs were determined by nonlinear fitting of the Michaelis-Menten equation using GraphPad Prism (GraphPad Software, San Diego, CA). Measurements were carried out using the quinone reduction activity assay method as described above at 23°C. 1 mL anoxic reaction mixture contained 1.25 μg/mL wild-type SQR (or 12.5 μg/mL or 25 μg/mL SQR variant) and varying concentration of Na_2S at constant DUQ (50 μM) or varying concentration of quinone or quinone analog at constant Na_2S (100 μM). The k_{cat} was calculated based on the specific activity, molecular weight of SQR and the amount of protein used in the assay.

6.2.8 Inhibition of SQR

The half maximal inhibitory concentration (IC_{50}) for selected inhibitors was determined at varying concentrations of the inhibitors at a constant concentration of DUQ

(50 μM) in the quinone reduction activity assay described above. All inhibitor stock solutions were prepared in ethanol. The final concentration of ethanol did not exceed 1.5 % (v/v) in the assays. The IC_{50} values were determined by plotting residual enzyme activity against drug concentrations and extrapolated graphically. The *in vitro* inhibition constants (K_i) were calculated assuming a competitive inhibition model and applying the Cheng-Prusoff equation for competitive inhibition (K_i=IC_{50}/(S/K_m+1) [143], where substrate concentration [S] is 50 μM, Michaelis-Menten constant K_m is 3.43 μM.

6.2.9 Stopped-flow spectrophotometry and enzymatic activity assay based on the reduction of FAD

Stopped-flow experiments were performed using an Applied Photophysics SX.18MV stopped-flow instrument equipped with a multiwavelength photodiode array (PDA) detector and X-SCAN software (Applied Photophysics Ltd, Leatherhead, UK) at 23°C. The optical path length was 1 cm. The dead time of the apparatus was 1.28 ms. The buffer (50 mM Bis-Tris, 20 mM glucose, 3 U mL^{-1} glucose oxidase and 10 units of catalase per mL, pH 7.0) and SQR in the same buffer were degassed with repeated cycles of vacuum and flushing with N_2. Na_2S was freshly dissolved and diluted in the degassed buffer before loading to the sample syringes. The flow system was flushed thoroughly with the anaerobic buffer prior to the experiments.

The FAD reduction assay was performed in the absence of DUQ by monitoring the reduction of FAD after rapidly mixing SQR (25 μM after mixing) with freshly prepared sulfide (125 μM after mixing) in 50 mM Bis-Tris buffer (pH 7.0) containing 20 mM glucose, 3 unit of glucose oxidase per mL and 10 units of catalase per mL. The buffer was degassed with repeated cycles of vacuum and flushing with N_2. Stopped-flow mixing

chambers were washed with the deoxygenated buffer to establish the anoxic conditions. The reaction was monitored in the stopped-flow by multiwavelength absorption in the range of 300−700 nm. Temporal changes in absorbance at 448 nm were fitted to the double exponential equation (two-phase exponential decay equation) $\text{Abs} = A_1 e^{-k_{\text{Fast}} t} + A_2 e^{-k_{\text{Slow}} t} + b$ or the one-phase exponential decay equation $\text{Abs} = A_1 e^{-kt} + b$ with GraphPad Prism (GraphPad Software, San Diego, CA), where A_1 and A_2 are amplitudes, k_{Fast} and k_{Slow} (k for a one-phase decay) are the rate constants describing the observed rate at which the dependent variable is decreasing, expressed in s^{-1}, t is time, and b is the end point of the data trace. The rate constants k_{Fast} (for the two-phase decay) or k (for the one-phase decay) obtained from fitting was used to indicate the FAD reduction activity.

6.2.10 Quinone docking

The crystal structure of SQR in complex with decylubiquinone (PDB ID: 3T31) was used for docking. Bound DUQ, DDM (n-dodecyl-ß-D-maltoside) and all crystallized water molecules were removed from the PDB file. Polar hydrogen atoms were added using AutoDockTools (ADT) [144].

Autodock vina 1.1.2 [145] was used for docking and relative binding free energy calculations. A docking box of 60 × 60 × 60 points with a grid spacing of 0.375 Å was used in the calculations. The docking box was centered on the mass center (center_x =45, center_y =-7, center_z =6) of the crystallographic ligand and encompassing all active site atoms. All rotatable bonds within the ligand were allowed to rotate freely. All other parameters were set as defaults. The resulting docking poses were analyzed with PyMol [100] to verify the orientation of the ligand within the binding site.

6.2.11 Redox Potentiometry and Electron paramagnetic resonance (EPR) spectroscopy

Redox titrations were carried out anaerobically under argon at 25 °C on wild-type SQR and the $SQR^{Phe357Ala/Phe394Ala}$ variant at a total protein concentration of 50 μM in 50 mM MOPS, 0.5 M NaCl, pH 7.0. The following redox mediators (dyes) were used at a concentration of 25 μM: quinhydrone (+287 mV), 2,6-dichlorophenolindolphenol (+217 mV), 1,2-naphthoquinone (+125 mV), toluylene blue (+115 mV), phenazine methosulfate (+80 mV), thionine (+60 mV), methylene blue (−11 mV), resorufin (−50 mV), indigo trisulfonate (−80 mV), indigo carmine (−125 mV), anthraquinone-2-sulfonic acid (−225 mV), phenosafranine (−255 mV), and neutral red (−329 mV). All samples were prepared in 3-mm internal diameter quartz EPR tubes, rapidly frozen in liquid nitrogen-chilled ethanol, and stored in liquid nitrogen until analyzed. EPR spectra were recorded using a Bruker Elexsys E500 spectrometer equipped with a Bruker liquid nitrogen-evaporating cryostat at 150 K, 20-milliwatt microwave power at 9.43 GHz. All spectra reported are the average of five scans using the modulation amplitude of 4.0 G_{pp} at 100 KHz modulation frequency. Potentiometric titration data were analyzed by plotting the signal height of peak-trough amplitude versus E_h and fitting the data to two midpoint potential values (E_{m1} and E_{m2}) using the equation $SQ_{max} = C_{site}[1+2(10^{-2.3RT(Em1-Em2)/2F})]^{-1}$ [128]; where C_{site} is the concentration of binding sites (assumed to equal the concentration of SQR), R is the gas constant, F is the Faraday constant, T is absolute temperature and 2.3 is the conversion factor for $\ln_e$ to $\log_{10}$. E_{m1} is defined as the potential of the quinone/semiquinone couple, and E_{m2} as the potential of the semiquinone/quinol couple. The highest radical signal would then be observed at E_m, the midpoint potential value of the E_{m1}/E_{m2} couple [$E_m = 0.5(E_{m1} +$

E_{m2})]. E_m values were representative of two or three independent titrations with a S.D. value of ± 5 mV.

6.3 Results.

6.3.1 SQR can use both benzoquinone and naphthoquinone as electron acceptors.

SQR catalyzes the oxidation of sulfide and the reduction of ubiquinone via a non-covalent FAD cofactor. In previous publications we have utilized decylubiquinone as an artificial electron acceptor to monitor catalytic activity [115]. Additionally, a crystal structure of decylubiquinone bound in the quinone site has been published [37]. To further our understanding of the quinone site we used a computational docking method (Autodock vina 1.1.2) to calculate the binding affinity (binding free energy) of analogues of benzoquinone, naphthoquinone and anthraquinone. Analogues were chosen with a range of redox potentials varying from -225 mV to +110 mV. The docking results showed that all of the quinones and derivatives examined herein were positioned into the quinone binding site with predicted binding affinity values within a narrow range of -6.1 to -10.5 kcal/mol (**Table 6.1**). Anthroquinone bound most tightly with a predicted affinity of -10.5 kcal/mol. All the naphthoquinone analogues bound within a narrow range of -8.8 to -9.2 kcal/mol. The benzoquinone analogues showed the weakest binding with affinities in the -6.1 to -8.8 kcal/mole range.

We measured the efficiency of each quinone analogue to serve as an electron acceptor for SQR-mediated Na_2S oxidation by determining k_{cat}/K_m at steady state. As shown in Table 1, SQR was able to use benzoquinones and naphthoquinones but not water soluble anthraquinone sulfonate. All of the analogues except DUQ (K_m 3.4 ± 0.4 μM) had very high K_m values varying from 26.0 ± 6.0 μM for 5-hydroxy-1,4 naphthoquinone to 193 ± 15.6 μM for UQ_0. There was no correlation between predicted binding efficiency and K_m. UQ_0 and 1,4-naphthoquinone had the highest k_{cat} values but DUQ was the most efficient

acceptor with a k_{cat}/K_m of 2.2 $\mu M^{-1}s^{-1}$ due to its low K_m although it had a low k_{cat} of 7.6 ± 0.2 s^{-1}. All the other quinones had much lower k_{cat}/K_m values in the 0.0 to 0.4 range. There was no obvious correlation between redox potential, binding affinity K_m or k_{cat} although acceptors with higher redox potentials were somewhat better.

6.3.2 Quinone inhibitors of SQR

Five well-studied quinone inhibitors (pentachlorophenol (PCP), 2-(n-heptyl-4-hydroxyquinolone N-oxide (HOQNO), theonyltrifluoroactone (TTFA), carboxin and antimycin A) were tested for their inhibitory potency on SQR activity. The half maximal inhibitory concentrations (IC_{50}) were determined and the *in vitro* inhibition constants (K_i) were then calculated using the Cheng-Prusoff equation (**Table 6.2**). PCP and HOQNO were effective inhibitors with IC_{50} values are 7.1 ± 1.8 μM and 9.1 ± 1.6 μM, respectively. Their apparent inhibition constants (K_i) were 0.46 μM and 0.58 μM, respectively. In contrast, TTFA, carboxin and antimycin A showed weak inhibition with the IC_{50} values of 200 ± 9 μM, 260 ± 11 μM and 350 ± 25 μM, respectively. The apparent inhibition constants (K_i) were 13 μM, 17 μM and 22 μM, respectively.

6.3.3 Kinetic analysis of the variants involved in quinone binding and reduction in SQR

The quinone binding pocket of SQR comprises six conserved amino acids. Two Phe residues (Phe357 and Phe394) sandwich the benzoquinone ring and Phe41, Pro43, Gly322, and Lys391 interact with the ring. Tyr323, Asn353, Ile368 and Tyr411 interact with the hydrophobic isoprenoid side chain of the quinone but are not highly conserved. To investigate the role of each of these amino acids in quinone binding and SQR catalysis,

variants were constructed and characterized by pre-steady state and steady state kinetic assays. For each variant the enzyme was assembled, and contained the FAD cofactor in approximately 0.7:1 molar ratio. Each variant was purified by FPLC Ni-affinity chromatography prior to enzymatic analysis. Two kinetic assays were used to characterize the variants. A pre-steady state reaction follows the Na_2S dependent reduction of FAD (**Figure 6.2 and Supplementary Figure 6.2)** and a Na_2S dependent reduction of DUQ measures the overall catalytic activity of the variants (**Table 6.3 and Supplementary Figure 6.3)**.

6.3.4 Phe357 and Phe394 sandwich the benzoquinone ring

The benzoquinone ring of the DUQ is sandwiched between the aromatic rings of Phe357 and Phe394 [37]. Phe357 is situated next to the essential cysteine (Cys356) and interacts with the O4 atom of FAD through its main-chain nitrogen and oxygen atoms at a distance of 3.42 Å and 3.18 Å, respectively [37]. In contrast, Phe394 is ~7 Å away from FAD. Alanine variants were generated at these positions to verify that the hydrophobic "sandwiching" of the benzoquinone head group is critical for activity. Both variants retained less than 10% wild-type steady-state activity with k_{cat} values of 0.3 ± 0.01 s^{-1} and 0.6 ± 0.02 s^{-1}, respectively (**Table 6.3**). Surprisingly, for the $SQR^{Phe357Ala}$ variant the K_m for DUQ was not altered but the K_m for Na_2S increased 13-fold. The $SQR^{Phe394Ala}$ variant also had an unaltered K_m for DUQ and the K_m for Na_2S showed a slight increase. When both Phe residues were converted to Ala the enzyme was totally inactive. We also examined the Na_2S dependent pre-steady state reduction of FAD in the $SQR^{Phe357Ala}$, $SQR^{Phe394Ala}$ and $SQR^{Phe357Ala/Phe394Ala}$ variant enzymes. No bleaching was detectable within the time frame monitored (**Figure 6.2**). To examine if alteration of these Phe residues affects the redox

potential of FAD in SQR, potentiometric titrations of the FAD semiquinone of the wild-type SQR and $SQR^{Phe357Ala/Phe394Ala}$ variant were performed at neutral pH (**Figure 6.3**). Curve fitting of the FAD semiquinone signal revealed a midpoint potential of -136 ± 5 mV (E_{m1} = -71 ± 5 mV, E_{m2} = -200 ± 5 mV) at pH 7.0 in $SQR^{Phe357Ala/Phe394Ala}$ variant, which is similar to that in wild-type SQR (E_m= -139 ± 5 mV; E_{m1} = -58 ± 5 mV, E_{m2} = -220 ± 5 mV).

6.3.5 Phe41, Pro43, Gly322 and Lys391 encompass the quinone binding pocket

Phe41, Pro43, Gly322 were substituted with alanine and Lys391 was substituted with Ala, Asp, Glu and Arg. In the steady state assay, $SQR^{Phe41Ala}$ and $SQR^{Pro43Ala}$ variants retained about 15% activity with k_{cat} values of 1.2 ± 0.04 s^{-1} and 1.3 ± 0.03 s^{-1}, respectively and Michaelis constants for Na_2S and DUQ similar to the wild-type enzyme. However, the $SQR^{Gly322Ala}$ variant was totally inactive (**Table 6.3**) indicating that placing a side chain in this position was highly disruptive.

In the pre-steady state kinetic assay, the $SQR^{Phe41Ala}$ variant retained about 75% of FAD reduction activity with an observed rate constant (k_{Fast}) of 8.8 ± 1.8 s^{-1}. In contrast, the $SQR^{Pro43Ala}$ and $SQR^{Gly322Ala}$ variants exhibited no appreciable activity, with observed rate constants (k_{Fast}) of 0.15 ± 0.01 s^{-1} and 0.12 ± 0.02 s^{-1}, respectively, which are only marginally greater than the rate constants obtained for FAD photoreduction (0.1 ± 0.05 s^{-1}) [115].

Lys391 is located within hydrogen-bonding distance of both DUQ and FAD in SQR. Its side chain ζ-amine group could interact with the C-4 keto oxygen (the O4 atom) of FAD and/or of DUQ, and participate in proton transfer (**Supplementary Table 6.1 and 6.3**). In order to identify the function of Lys391, Ala, Glu, Asp and Arg variants were generated. The $SQR^{Lys391Ala}$, $SQR^{Lys391Asp}$ and $SQR^{Lys391Glu}$ variants were totally inactive in both the

pre-steady state and steady state kinetic assays (**Figure 6.2 and Table 6.3**). In contrast, the $SQR^{Lys391Arg}$ variant retained 62.5% of FAD reduction activity in the pre-steady state kinetic assay (**Figure 6.2 and Supplementary Figure 6.2**), but only 1% DUQ reductase activity with a k_{cat} value of 0.1 ± 0.01 s^{-1} (**Table 6.3 and Supplementary Figure 6.3**). Overall this suggests that Lys391 participates in both quinone and FAD reduction.

6.3.6 Tyr323, Asn353, Ile368 and Tyr411 interact with the hydrophobic quinone tail

Tyr323, Asn353, Ile368 and Tyr411 are situated around the entrance of the quinone binding pocket in SQR and are not highly conserved. Based on our crystal structure of DUQ bound to SQR (PDB ID: 3T31), all interact with the hydrophobic quinone tail [37]. To examine the catalytic role of these residues, each was substituted with alanine. Additionally Tyr411 was converted to Phe.

In the steady state kinetic assay, all of the variants retained minimal activity with k_{cat} values of 0.2 to 0.9 s^{-1}, corresponding to 3-13% of the activity of wild-type SQR. The K_m values of $SQR^{Tyr323Ala}$, $SQR^{Ile368Ala}$ and $SQR^{Tyr411Ala}$ variants for DUQ and Na_2S are similar to those of the wild-type SQR. The $SQR^{Asn353Ala}$ and $SQR^{Tyr411Phe}$ variants have elevated K_m values (13.89 ± 2.99 μM and 13.07 ± 3.26 μM, respectively) for DUQ. The $SQR^{Tyr411Phe}$ variant also has a very high K_m of 42.38 ± 2.42 μM for Na_2S, which is about 14 times of that of the wild-type SQR. When we examined the pre-steady state kinetics, $SQR^{Tyr323Ala}$, $SQR^{Ile368Ala}$ and $SQR^{Tyr411Ala}$ variants showed a complete loss of FAD reduction activity whereas $SQR^{Asn353Ala}$ and $SQR^{Tyr411Phe}$ variants retained 53.8% and 91.2% activity.

These results suggest that the Ala substitution of Asn353 affects the affinity for DUQ as well as turnover. The Phe substitution of Tyr411 has no effect on the FAD

reduction, but dramatically decreases DUQ reduction due to increased DUQ and Na_2S K_m values.

6.4 Discussion.

Acidithiobacillus ferrooxidans SQR couples the oxidation of sulfides such as H_2S, HS^- and S^{2-} to the reduction of ubiquinone via a non-covalent FAD cofactor with an $E_{m,7}$ (FAD) of -139 mV [115]. SQR is relatively small and the three-dimensional structure of SQR indicates that the quinone binding site is very close to the FAD which in turn is close to the catalytic sulfide oxidation site consisting of Cys160, Cys356 and FAD. Thus one could predict that mutations of conserved amino acids in the quinone binding site could have profound effects not only on quinone reduction but also on sulfide mediated FAD reduction. Inspection of structurally characterized quinone sites in many dehydrogenases and reductases does not provide a well-defined structural binding motif but some general features can be discerned [146; 147]. Quinone-binding sites are hydrophobic and normally have several aromatic residues (Phe, Tyr, His or Trp) within 4 Å of the quinone molecule. In the quinone site of SQR three aromatic residues (Phe41, Phe357 and Phe394) interact with the quinone ring and an additional two aromatic residues (Tyr323 and Tyr411) interact with the quinone tail. We investigated the role of the quinone binding site in SQR catalysis and showed that the enzyme could use both benzoquinones and naphthoquinones and that there was no obvious correlation between predicted binding energy, K_m or k_{cat} and activity although there was a rough correlation between the redox potential ($E_{m,7}$) of quinone and activity (*i.e.* quinones with a more positive $E_{m,7}$ than -139 mV exhibited greater activity).

At.f SQR was inhibited by PCP and HOQNO. These inhibitors have been shown to bind to the quinone binding site of nitrate reductase, succinate dehydrogenase and fumarate reductase [148; 149]. The apparent IC_{50} value of HOQNO (9.1 μM) for $SQR_{At.f}$ is close to that for SQRs from *Aquifex aeolicus* and *Rhodobacter capsulatus* (12 μM and 5.6 μM,

respectively) [77; 127]. Interestingly, antimycin A, a strong inhibitor of the SQRs from *Aquifex aeolicus*, *Paracoccus denitrificans* and *Rhodobacter capsulatus* with the apparent IC_{50} values of 10 µM, 15 µM and 50 µM, respectively [76; 77; 127] was inactive towards *At.f* SQR.

Computational docking is a widely used tool to gain an understanding of protein–ligand interactions. It computationally predicts the positioning and binding affinity of the ligand in the binding pocket of the protein. The predicted binding affinity values of the examined quinone substrate and inhibitor candidates vary from 6 to 10 kcal/mol (**Table 6.2**), but have no correlation to the measured Michaelis constants (K_m) and inhibition constants (K_i). The weak inhibitors TTFA, Carboxin and Antimycin A had similar predicted binding affinity value to that of the potent inhibitors HOQNO and PCP, but showed weak inhibition with about 20-40 fold higher K_i values. The AutoDock positions of the inhibitors (**Supplementary Figure 6.4**) reveal that the weak inhibitors TTFA, Carboxin and Antimycin do not fit well into the quinone binding site when compared to DUQ, PCP and HOQNO. This might explain the lack of inhibition.

We employed a site-directed mutagenesis approach of the quinone binding site to create variants of residues that interact with the benzoquinone ring and hydrophobic tail of the quinone and subjected the variant enzymes to steady state kinetic analysis of Na_2S dependent reduction of DUQ and pre-steady state kinetic analysis of Na_2S-dependent flavin reduction.

Conversion of either of the two Phe residues (Phe357 and Phe394) that sandwich the benzoquinone ring to Ala resulted in no affect on the midpoint potential of FAD in SQR, but a 90% loss of DUQ activity. In these variants we could not observe Na_2S-dependent flavin bleaching. This suggests these Phe residues also result in conformational changes at

the catalytic Na_2S oxidation site consisting of Cys160, Cys356 and FAD. However we cannot rule out that very limited residual activity might result from flavin independent direct DUQ reduction by Na_2S within the enzyme. This is supported by the lack of FAD bleaching and the increased K_m of Na_2S in the variants.

Four additional conserved amino acids are found within the quinone binding site. Mutation of Phe41 to Ala had minimal effect on FAD reduction but reduced the overall reaction rate by 85%. Given that Phe41 is 6.5 Å from the FAD this is not unexpected. Mutation of Pro43 or Gly322 to Ala reduced both FAD and DUQ reduction to very low levels. As these two amino acids are within 4 Å of both FAD and DUQ, this indicates close conformational coupling between the active site and the quinone site. As noted above we cannot rule out direct Na_2S reduction of DUQ in the enzyme. Lys391 hydrogen bonds to both the quinone and FAD. Mutation to Arg had only a small effect on FAD reduction but eliminated DUQ reduction. Mutation to Ala, or acidic residues Asp or Glu eliminated both FAD and DUQ reduction. Thus mutation to another positive amino acid was tolerated for the FAD reduction step but not DUQ reduction. Placing a neutral or acidic residue in this position was not tolerated.

Tyr323, Asn353, Ile368 and Tyr411 make up the isoprenoid binding channel for the quinone and interact with the DUQ decyl chain. Mutation of any of these amino acids to Ala eliminated DUQ reduction. A similar perturbation of the isoprenoid binding channel has been observed in SQR from the archaea *Caldivirga maquilingensis* [80]. Mutation of Tyr323, Ile368 or Tyr411 to Ala also eliminated Na_2S reduction of FAD. This was unexpected as these residues are physically distant from the FAD and Na_2S catalytic site. Mutation of Asn353 to Ala or Tyr411 to Phe retained significant FAD reduction activity.

The two ketone oxygens (O1 and O4) of oxidized quinone are hydrogen bond acceptors. The typical hydrogen bond partners include the polar/ionizable residues Glu, Asp, Lys; the polar residues His, Ser, Tyr, Arg, backbone NH and water molecules [150]. In SQR, a Tyr (Tyr411) is located within hydrogen-bonding distance of the DUQ C-1 ketone oxygen (O1); the distance between the O1 atom of DUQ and the OH of Y411 is 3.4 Å (**Supplementary Table 6.1 and Supplementary Figure 6.2**). The conserved Lys391 has a long flexible side-chain with a positively-charged amine that could be more inclined to interact with the FAD C-4 carbonyl oxygen within a distance of 3.6 Å. The distance between N_{ζ} atom of Lys391 and the O4 atom of DUQ is 4.5 Å. The hydrogen bonding between Lys391 and DUQ may need the assistance of a water molecule or a rotation of the side-chain of Lys391. Such interactions are commonplace in the quinone sites of enzymes such as *Escherichia coli* menaquinol:fumarate and menaquinol:nitrate oxidoreductases [148; 151; 152]. The backbone nitrogen of Gly322 is distant from the DUQ ketone group (>5 Å), but is able to hydrogen bond to the FAD C-2 carbonyl oxygen within a distance of 2.4 Å.

The quinone site of *Aquifex aeolicus* SQR is the only other structurally characterized SQR quinone site [153]. *A. ferrooxidans* SQR has 40% sequence identity with *Aq. aeolicus* SQR. The superposition of the *A. ferrooxidans* SQR structure with the structure of *Aq. aeolicus* SQR (PDB ID: 3HYW) shows high similarity with a root-mean-square deviation (RMSD) value of about 1.3 Å for 401 Cα atoms (**Figure 6.4**). Both of the quinone sites are located in the hydrophobic region and close to the isoalloxazine ring of FAD. The amino acids (Phe41, Pro43, Lys391 and Phe394; in the *A. ferrooxidans* numbering) interacting with the benzoquinone head are similar except that the aromatic ring is bound between the benzene ring of Phe385 and the side chain of Ile346 in *Aq. aeolicus* SQR. In contrast, the

amino acids that interact with the hydrophobic quinone tail are varied due to the high flexibility of the amphipathic helices in the C-terminal domain (**Figure 6.3**).

Overall our computational and kinetic analysis show that there is an intimate conformational connection between the catalytic Na_2S oxidation site and the quinone reduction site; and shed new light on the understanding of the quinone site of *A. ferrooxidans* SQR.

6.5 Tables

Table 6.1 Redox potential, predicted binding energy and steady-state kinetic parameters of SQR with quinone homologues and analogs

Name	Rings	Redox Potential ($E_{m,7}$= mV)	Predicted binding affinity (kcal/mol)	K_m (μM)	k_{cat} (s^{-1})	k_{cat}/K_m ($\mu M^{-1} s^{-1}$)
Decylubiquinone (DUQ)	1	~ +110	-8.3	3.4 ± 0.4	7.6 ± 0.2	2.2
Ubiquinone-0 (UQ0)	1	+100	-7.4	193.0 ± 15.6	47.7 ± 4.7	0.2
Tetramethyl-1,4-benzoquinone (Duroquinone)	1	+7	-8.1	31.4 ± 3.4	11.3 ± 0.9	0.4
2,5-Dihydroxy-1,4-benzoquinone (DHBQ)	1	-60	-6.1	n.d.	0.0	n.d
1,4-Naphthoquinone (NQ)	2	+60	-8.8	76.9 ± 7.1	33.8 ± 2.2	0.4
2-Methyl-1,4-naphthoquinone (Menadione)	2	-12	-9.2	71.6 ± 11.9	19.5 ± 2.6	0.3
2-Hydroxy-1,4-naphthoquinone (Lawsone)	2	-139	-9.2	72.1 ± 13.6	1.2 ± 0.3	0.0
5-Hydroxy-1,4-naphthoquinone (Juglone)	2	+33	-9.1	26.0 ± 6.1	6.3 ± 1.4	0.2
5-Hydroxy-2-methyl-1,4-naphthoquinone (Plumbagin)	2	-40	-9.1	44.7 ± 5.3	3.4 ± 0.3	0.1
Anthraquinone sulfonate (ANSO)	3	-225	-10.5	n.d.	n.d.	n.d.

n.d. : not determined

Table 6.2 Inhibition of SQR activity.

Name	Predicted binding affinity (kcal/mol)	IC_{50} (μM)	K_i* (μM)
Pentachlorophenol (PCP)	-6.7	7.1 ± 1.8	0.46
2-(n-heptyl)-4-hydroxyquinoline N-oxide (HOQNO)	-7.3	9.1 ± 1.6	0.58
Thenoyltrifluoroacetone (TTFA)	-7.2	200 ± 9	12.84
Carboxin	-7.3	260 ± 11	16.69
Antimycin A	-8.6	350 ± 25	22.47

* Apparent inhibition constant values (K_i) were calculated using the Cheng-Prusoff equation ($Ki = IC_{50} / (1+[S]/K_m)$), where substrate (DUQ) concentration [S] = 50 μM. Michaelis constant K_m = 3.43 μM.

Table 6.3 Steady-state kinetic parameters of wild-type SQR and variants

Variant	Specific Activity (μmol $mg^{-1}min^{-1}$)	k_{cat} (s^{-1})	K_m[Na_2S] (μM)	K_m[DUQ] (μM)	k_{cat}/K_m[Na_2S] ($\times 10^6$ $M^{-1}s^{-1}$)	k_{cat}/K_m[DUQ] ($\times 10^6$ $M^{-1}s^{-1}$)
SQR	9.4 ± 0.28	7.6 ± 0.22	2.97 ± 0.28	3.43 ± 0.43	2.55	2.20
F41A	1.5 ± 0.05	1.2 ± 0.04	4.78 ± 1.18	2.05 ± 0.45	0.25	0.59
P43A	1.6 ± 0.04	1.3 ± 0.03	2.67 ± 0.58	2.88 ± 0.35	0.48	0.44
G322A	0.0	0.0	n.d.	n.d.	n.d.	n.d.
Y323A	0.3 ± 0.01	0.2 ± 0.01	2.16 ± 0.72	2.31 ± 0.54	0.09	0.09
N353A	0.6 ± 0.04	0.5 ± 0.03	3.37 ± 0.73	13.89 ± 2.99	0.15	0.04
F357A	0.4 ± 0.02	0.3 ± 0.01	40.80 ± 3.50	3.55 ± 0.52	0.01	0.08
I368A	0.5 ± 0.03	0.4 ± 0.02	8.05 ± 2.48	4.94 ± 1.28	0.05	0.07
K391A	0.0	0.0	n.d.	n.d.	n.d.	n.d.
K391D	0.0	0.0	n.d.	n.d.	n.d.	n.d.
K391E	0.0	0.0	n.d.	n.d.	n.d.	n.d.
K391R	0.1 ± 0.01	0.1 ± 0.01	7.31 ± 2.47	2.39 ± 0.74	0.01	0.03
F394A	0.8 ± 0.03	0.6 ± 0.02	7.50 ± 1.30	3.46 ± 0.44	0.08	0.18
Y411A	0.7 ± 0.03	0.6 ± 0.02	2.84 ± 0.96	3.80 ± 0.81	0.20	0.15
Y411F	1.2 ± 0.09	0.9 ± 0.07	42.38 ± 2.42	13.07 ± 3.26	0.02	0.07
F357A/F394A	0.0	0.0	n.d.	n.d.	n.d.	n.d.

n.d. : not determined

6.6 Figures

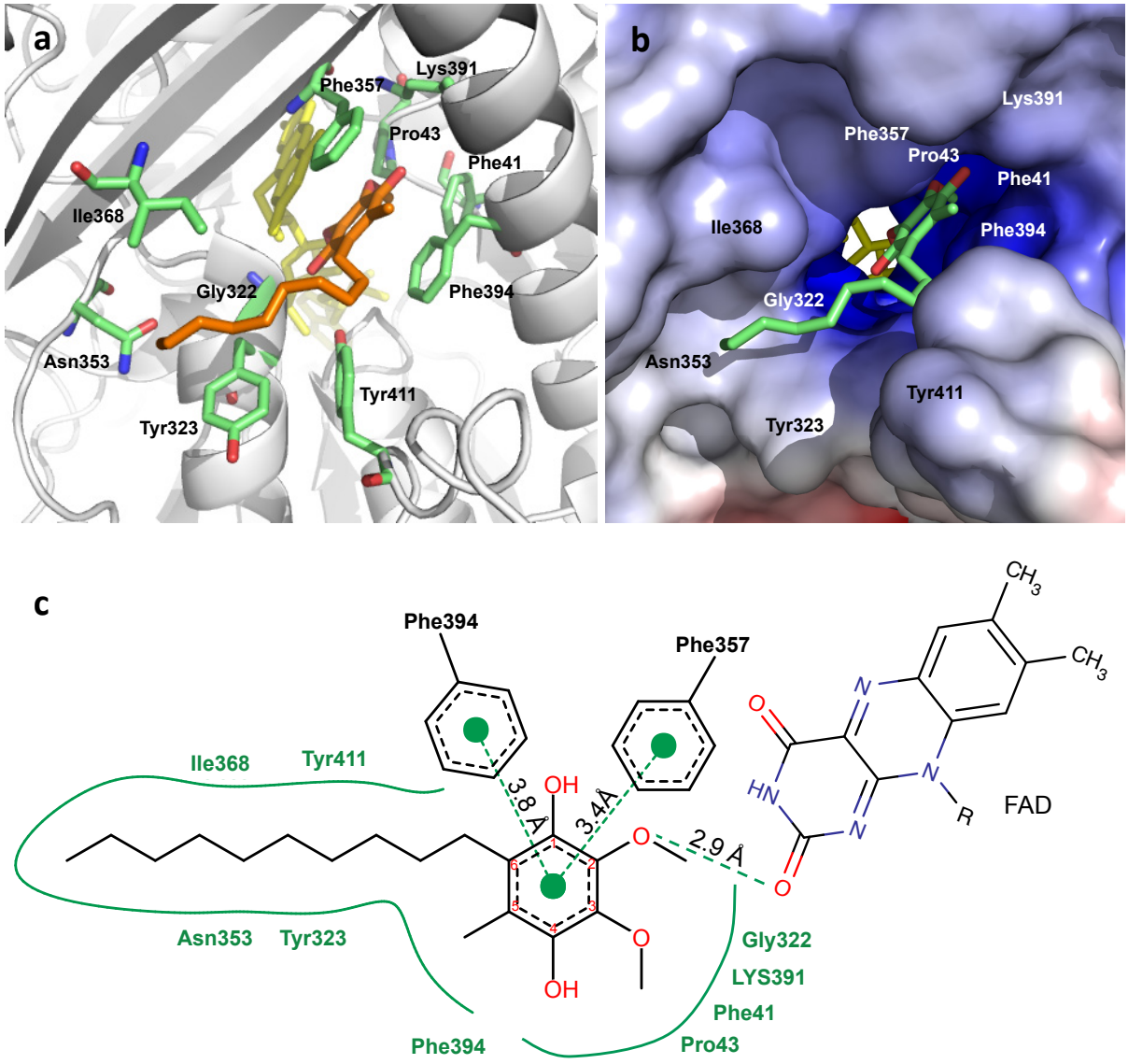

Figure 6.1 The quinone binding site of *A. ferrooxidans* SQR (PDB ID: 3T31).
The highly conserved amino acids surrounding the quinone site are shown as sticks in the cartoon representation (a) and labeled in surface representation (b). DUQ and FAD (yellow) are shown as sticks in Figure (a) and (b); (c) The 2D sketch of the SQR-DUQ-FAD complex was generated using the online software tool PoseView (http://poseview.zbh.uni-hamburg.de).

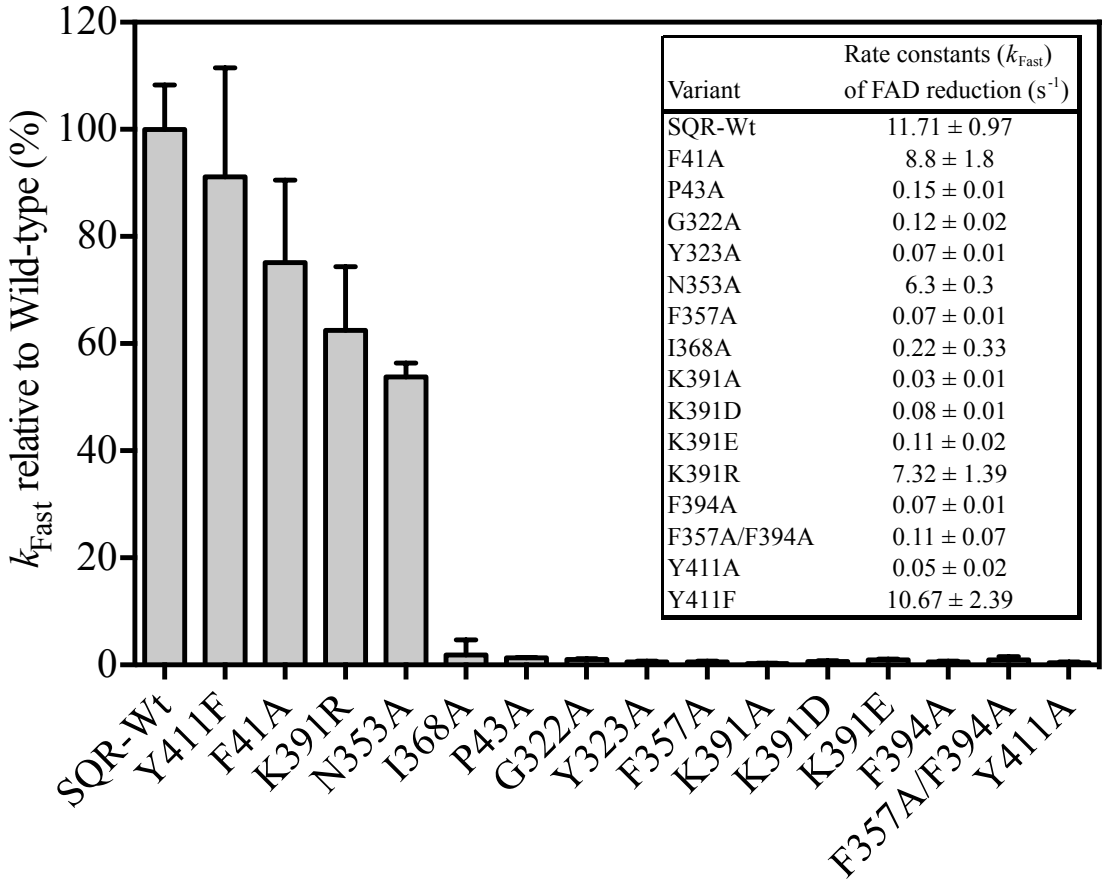

Variant	Rate constants (k_{Fast}) of FAD reduction (s^{-1})
SQR-Wt	11.71 ± 0.97
F41A	8.8 ± 1.8
P43A	0.15 ± 0.01
G322A	0.12 ± 0.02
Y323A	0.07 ± 0.01
N353A	6.3 ± 0.3
F357A	0.07 ± 0.01
I368A	0.22 ± 0.33
K391A	0.03 ± 0.01
K391D	0.08 ± 0.01
K391E	0.11 ± 0.02
K391R	7.32 ± 1.39
F394A	0.07 ± 0.01
F357A/F394A	0.11 ± 0.07
Y411A	0.05 ± 0.02
Y411F	10.67 ± 2.39

Figure 6.2 The relative rate constants (k_{Fast}) of SQR and variants in pre-steady state reduction of FAD by Na_2S.
100% of the k_{Fast} is 11.71 ± 0.97 s^{-1}. Insert is the apparent rate constants (k_{Fast}) of SQR and variants in pre-steady state reduction of FAD by Na_2S. The data are the mean values of three experiments; error bars indicate the standard deviation.

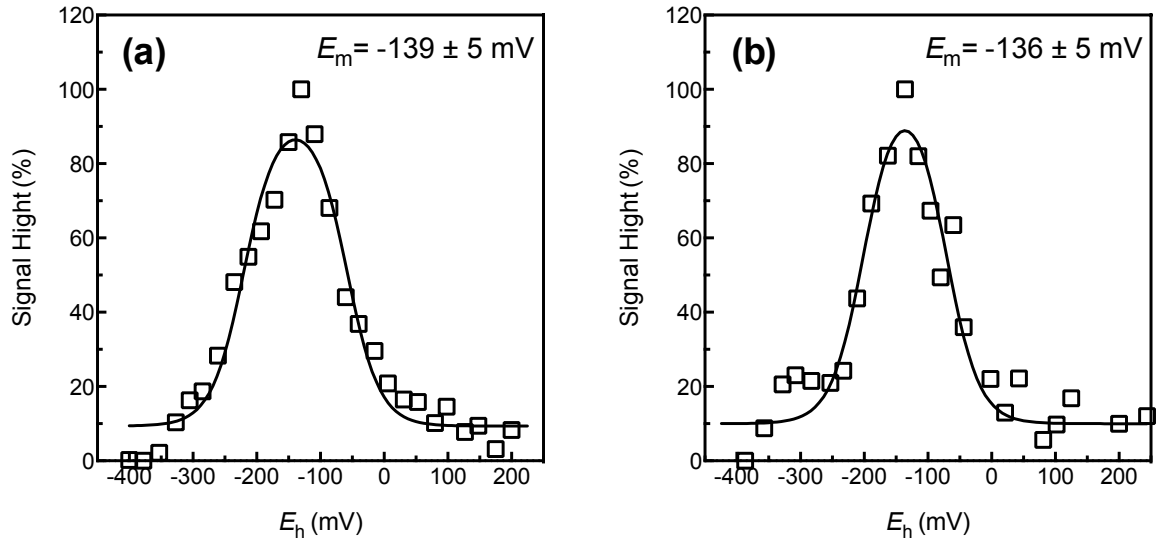

Figure 6.3 Potentiometric titration of the FAD radical signal in wild-type SQR (a) and $SQR^{Phe357Ala/Phe394Ala}$ variant (b) at pH 7.0.
Peak-trough differentials were plotted as a function of E_h. Signal heights are normalized to 100%. Presented data were gathered from two independent potentiometric titrations for both wild-type and variant enzyme.

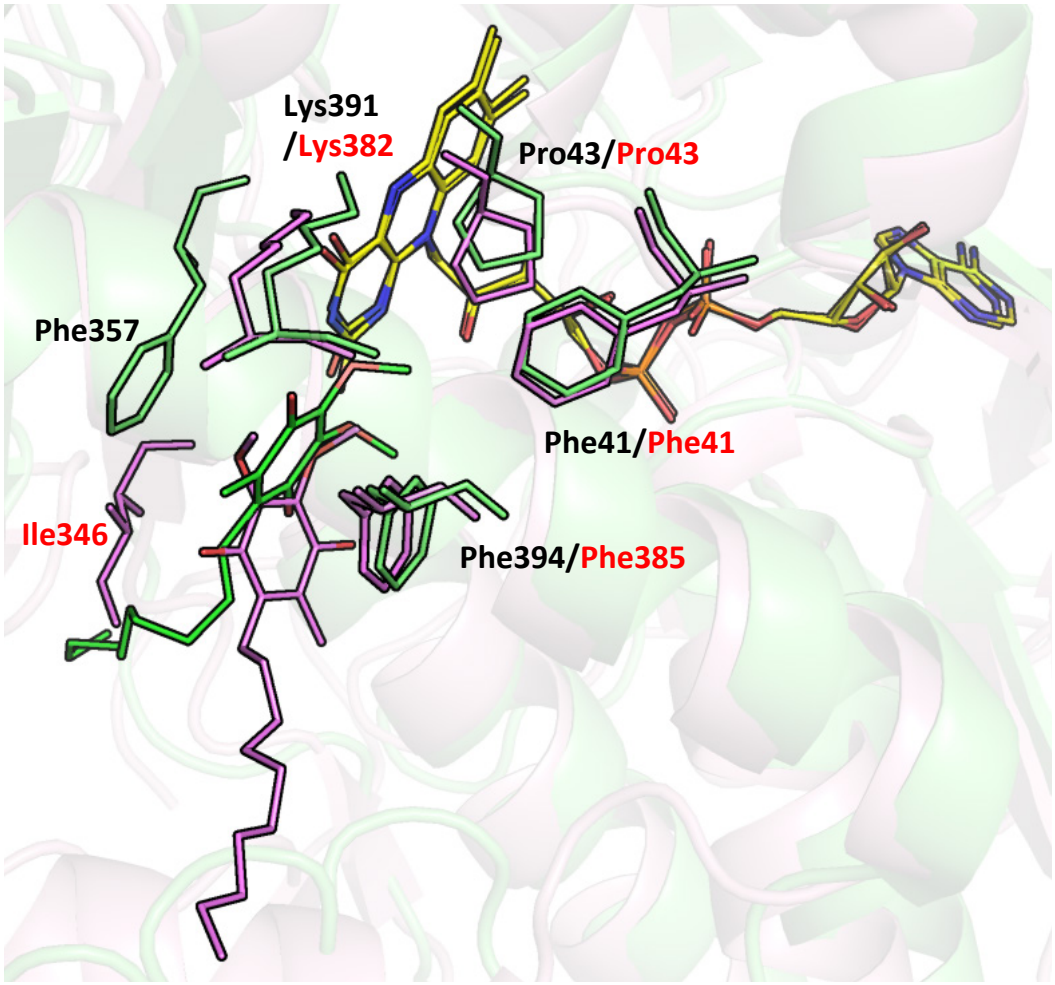

Figure 6.4 Superposition of the structures of the quinone binding sites of *A. ferrooxidans* SQR (green, PDB ID: 3T31) and *Aquifex aeolicus* SQR (magenta, PDB ID: 3HYW).
The atoms of the FAD cofactors (yellow) were used for this superposition. DUQ and the amino acids surrounding the quinone binding sites are represented by sticks. The amino acids are labeled in black (for *A. ferrooxidans* SQR) and in red (for *Aquifex aeolicus* SQR) respectively.

6.7 Supplementary Tables

Supplementary Table 6.1. Interaction partners for DUQ. The distances listed are between the atoms of DUQ and the indicated partners.
The structure of *A. ferrooxidans* SQR (PDB ID: 3T31) was used for analysing.

Atom of DUQ	Interaction partner	Distance (Å)
O1	OH, Tyr411	3.42
C2	$C_{\varepsilon 2}$, Phe394	3.79
O2	C2, FAD	3.20
	N3, FAD	3.01
	O2, FAD	2.86
C2M	C_{α}, Gly322	3.68
	$C_{\varepsilon 2}$, Phe394	3.69
	OH, Tyr411	3.70
	C2, FAD	3.77
	O2, FAD	3.25
C3	$C_{\delta 2}$, Phe394	3.54
	$C_{\varepsilon 2}$, Phe394	3.71
O3	C4, FAD	3.88
	N3, FAD	3.64
	O4, FAD	3.51
C3M	$C_{\varepsilon 2}$, Phe41	3.88
	C_{ζ}, Phe41	3.23
	C_{γ}, Pro43	3.55
	$C_{\delta 2}$, Phe394	3.31
	$C_{\varepsilon 2}$, Phe394	3.44
C4	$C_{\delta 2}$, Phe357	3.55
	C_{γ}, Phe357	3.80
	$C_{\delta 2}$, Phe394	3.50
	C_{γ}, Phe394	3.69
O4	C_{γ}, Phe357	3.56
	C_{β}, Phe394	3.54
	C_{α}, Lys391	3.76
C5	$C_{\delta 2}$, Phe357	3.56
	$C_{\varepsilon 2}$, Phe357	3.41
	C_{ζ}, Phe357	3.86
	C_{γ}, Phe394	3.88
C5M	$C_{\varepsilon 1}$, Phe357	3.67
	$C_{\varepsilon 2}$, Phe357	3.46
	C_{ζ}, Phe357	3.32
C6	$C_{\varepsilon 2}$, Phe357	3.72
C8	$C_{\varepsilon 2}$, Tyr411	3.90
C14	$C_{\delta 1}$, Ile368	3.83
C15	C_{ε}, Lys417	3.36
C16	$C_{\delta 2}$, Tyr323	3.72
	C_{β}, Asn353	3.78
	C_{γ}, Asn353	3.43
	$O_{\delta 1}$, Asn353	3.48
	C_{ε}, Lys417	3.34
Plane (C1, C2, C3, C4, C5, C6)	Plane ($C_{\delta 1}$, $C_{\delta 2}$, $C_{\varepsilon 1}$, $C_{\varepsilon 2}$, C_{γ}, C_{ζ}), Phe394	3.83/20°
Plane (C1, C2, C3, C4, C5,	Plane (C_{β}, $C_{\delta 1}$, $C_{\delta 2}$, $C_{\varepsilon 1}$, $C_{\varepsilon 2}$, C_{γ}, C_{ζ}), Phe357	3.44/6°
C5M, C6, C7, O1, O2, O3, O4)	Plane (C_{β}, $C_{\delta 1}$, $C_{\delta 2}$, $C_{\varepsilon 1}$, $C_{\varepsilon 2}$, C_{γ}, C_{ζ}), Phe394	3.80/20°
	Plane ($C_{\delta 1}$, $C_{\delta 2}$, $C_{\varepsilon 1}$, $C_{\varepsilon 2}$, C_{γ}, C_{ζ}), Phe394	3.84/20°

Supplementary Table 6.2. List of mutagenic oligonucleotides.

Mutant	Mutagenic Oligonucleotide (5' to 3')
Phe41Ala	TTATTTCCAGgcaGTTCCGTCCAACCCG
Pro43Ala	CCAGTTCGTTgcaTCCAACCCGT
Gly322Ala	CCAAGACCgctTATATGATCGAATCCAT
Tyr323Ala	CAAGACCGGTgctATGATCGAATCCATGGTGTCGGCGGCG
Asn353Ala	GGGCACCTGGgctGCGGTGTGTTTTG
Phe357Ala	ATGCGGTGTGTGCTgccGATATG
Ile368Ala	CGCGGCATTTgcaGCCTTGCCCC
Lys391Ala	CATCTGGCGgctGTGGCCTTTGAA
Lys391Asp	GCATCTGGCGgatGTGGCCTTTGAAAAATACTTTATCC
Lys391Glu	GCATCTGGCGgagGTGGCCTTTG
Lys391Arg	GCATCTGGCGagaGTGGCCTTTGAAAAATACTTTATCCGC
Phe394Ala	GCGAAGGTGGCCgctGAAAAATACT
Tyr411Ala	CGAGCCCTTCgctGAGAAGGTGC
Tyr411Phe	CGAGCCCTTCtttGAGAAGGTGC
Phe41Ala	TTATTTCCAGgcaGTTCCGTCCAACCCG
Pro43Ala	CCAGTTCGTTgcaTCCAACCCGT
Gly322Ala	CCAAGACCgctTATATGATCGAATCCAT
Tyr323Ala	CAAGACCGGTgctATGATCGAATCCATGGTGTCGGCGGCG

Supplementary Table 6.3. The interactions between FAD and DUQ and between FAD and the residues involved in quinone site of SQR.
The distances listed are between the atoms of FAD and the indicated partners. The structure of *A. ferrooxidans* SQR (PDB ID: 3T31) was used for analysing.

Atom of FAD	Neighbour	Distance (Å)
N1	C_{γ}, Pro43	5.00
	C_{α}, Gly322	4.67
	N, Gly322	3.86
	C4M, DUQ	4.71
	O4, DUQ	4.42
C2	N, Gly322	3.58
	C4M, DUQ	3.77
	O4, DUQ	3.20
	Cα, Gly322	4.31
	C3, DUQ	4.98
	C4, DUQ	4.34
	O3, DUQ	4.66
O2	N, Gly322	2.43
	C_{α}, Gly322	3.17
	C4M, DUQ	3.25
	O4, DUQ	2.86
	C, Gly322	4.32
	C4, DUQ	4.05
	C5, DUQ	4.69
	O5, DUQ	4.34
N3	O4, DUQ	3.01
	C_{γ}, Pro43	4.66
	N, Gly322	4.85
	N, Phe357	4.39
	C3, DUQ	4.10
	C3M, DUQ	4.22
	C4, DUQ	3.81
	C4M, DUQ	3.95
	C5, DUQ	4.91
	O3, DUQ	3.64
C4	C_{β}, Pro43	4.06
	C_{γ}, Pro43	3.95
	N, Phe357	4.25
	O, Phe357	4.49
	N_{ζ}, Lys391	4.81
	C3, DUQ	4.71
	C3M, DUQ	4.34
	C4, DUQ	4.80
	O3, DUQ	3.88
	O4, DUQ	4.14
O4	N, Phe357	3.42
	O, Phe357	3.18
	C_{α}, Pro43	4.82
	C_{β}, Pro43	3.76
	C_{γ}, Pro43	4.13
	C, Phe357	4.04
	C_{α}, Phe357	4.12
	C_{β}, Phe357	4.31
	C_{δ}, Lys391	4.96

	C_{ε}, Lys391	4.29
	N_{ζ}, Lys391	3.55
	C3, DUQ	4.45
	C3M, DUQ	4.18
	C4, DUQ	4.92
	O3, DUQ	3.51
	O4, DUQ	4.64
C4A	C_{γ}, Pro43	3.76
	C_{α}, Pro43	4.51
	C_{β}, Pro43	3.97
	C_{δ}, Pro43	4.90
N5	C_{α}, Pro43	3.68
	C_{β}, Pro43	3.57
	Plane (C_{α}, C_{β}, C_{δ}, C_{γ}, N), Pro43	3.31
	C, Pro43	4.89
	C_{δ}, Pro43	4.70
	C_{γ}, Pro43	3.78
	N, Pro43	4.37
	N_{ζ}, Lys391	4.89
C5A	C_{α}, Pro43	3.94
	C_{β}, Pro43	4.32
	C_{δ}, Pro43	4.90
	C_{γ}, Pro43	4.38
	N, Pro43	4.35
C6	Cα, Pro43	3.87
	C, Pro43	4.75
	C_{β}, Pro43	4.67
	N, Pro43	4.38
	O, Pro43	4.86
C7	C_{α}, Pro43	4.81
C9A	C_{α}, Pro43	4.91
	C_{γ}, Pro43	4.90
	N, Pro43	4.95
N10	C_{γ}, Pro43	4.90
C10	C_{β}, Pro43	4.91
	C_{γ}, Pro43	4.33
Plane (C10,C4A,C5A,C9A,N10,N5)	Plane (C_{α},C_{β} ,C_{δ}, C_{γ}, N), Pro43	3.98/42°
Plane (C10, C2, C4, C4A, C5A, C6, C7, C7M, C8, C8M, C9, C9A, N1, N10, N3, N5, O2, O4)	Plane (C_{α}, C_{β}, C_{δ}, C_{γ}, N), Pro43	3.97/41°

6.8 Supplementary Figures

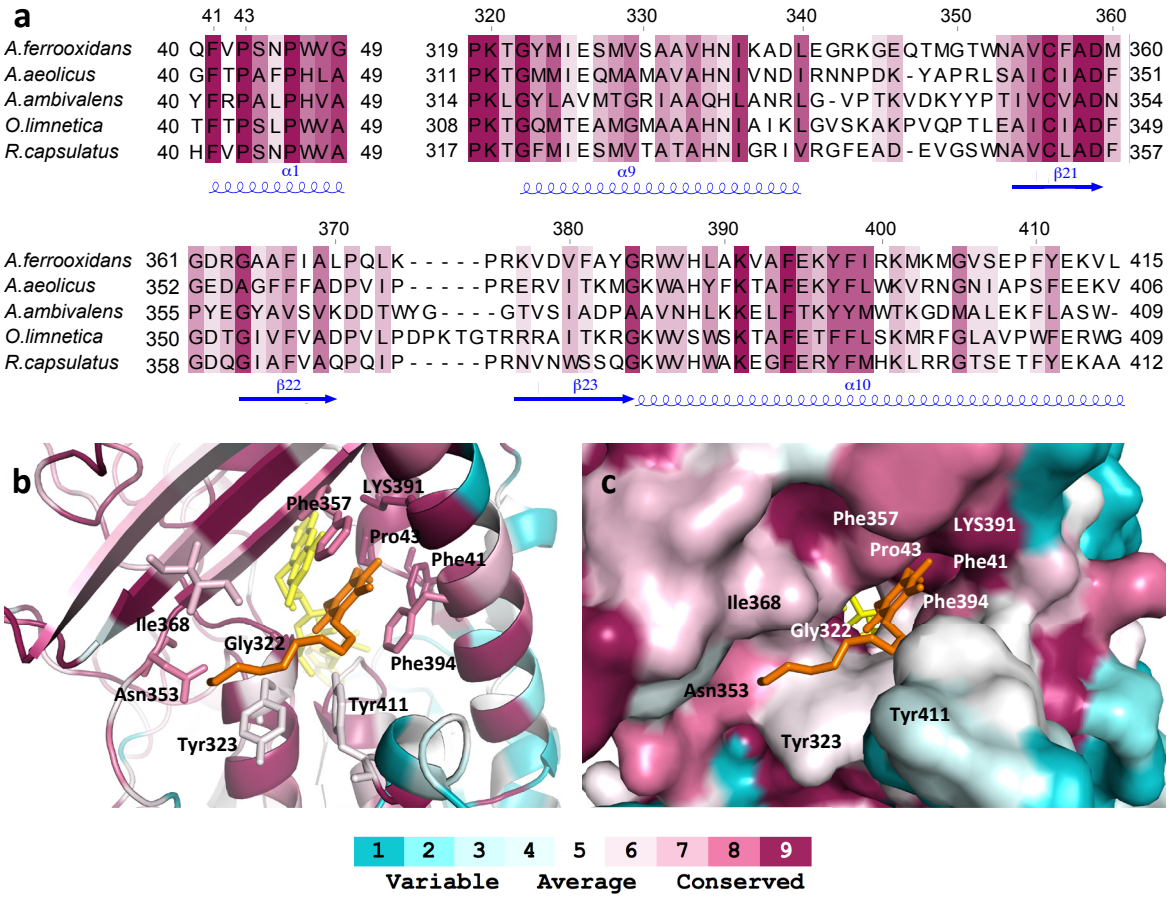

Supplementary Figure 6.1. Sequence conservation at the quinone binding site of SQR.
(a) Multiple sequence alignment of corresponding peptides of *Acidithiobacillus ferrooxidans* SQR (residues 40-49 and residues 319-415) and SQRs from *Aquifex aeolicus, Acidianus ambivalens, Oscillatoria limnetica* and *Rhodobacter capsulatus*. Residues in the four most conserved levels are highlighted. The corresponding secondary structural elements are shown. (b, c) ConSurf analysis of the sequence conservation at the quinone site of SQR. Conservation mappings in cartoon (b) and surface (c) are analyzed by ConSurf server (http://consurf.tau.ac.il/) and colored according to degree of conservation. The multiple sequence alignment used for the ConSurf analysis was composed of 150 sequences. Five representative sequences illustrate the degree of conservation (a).

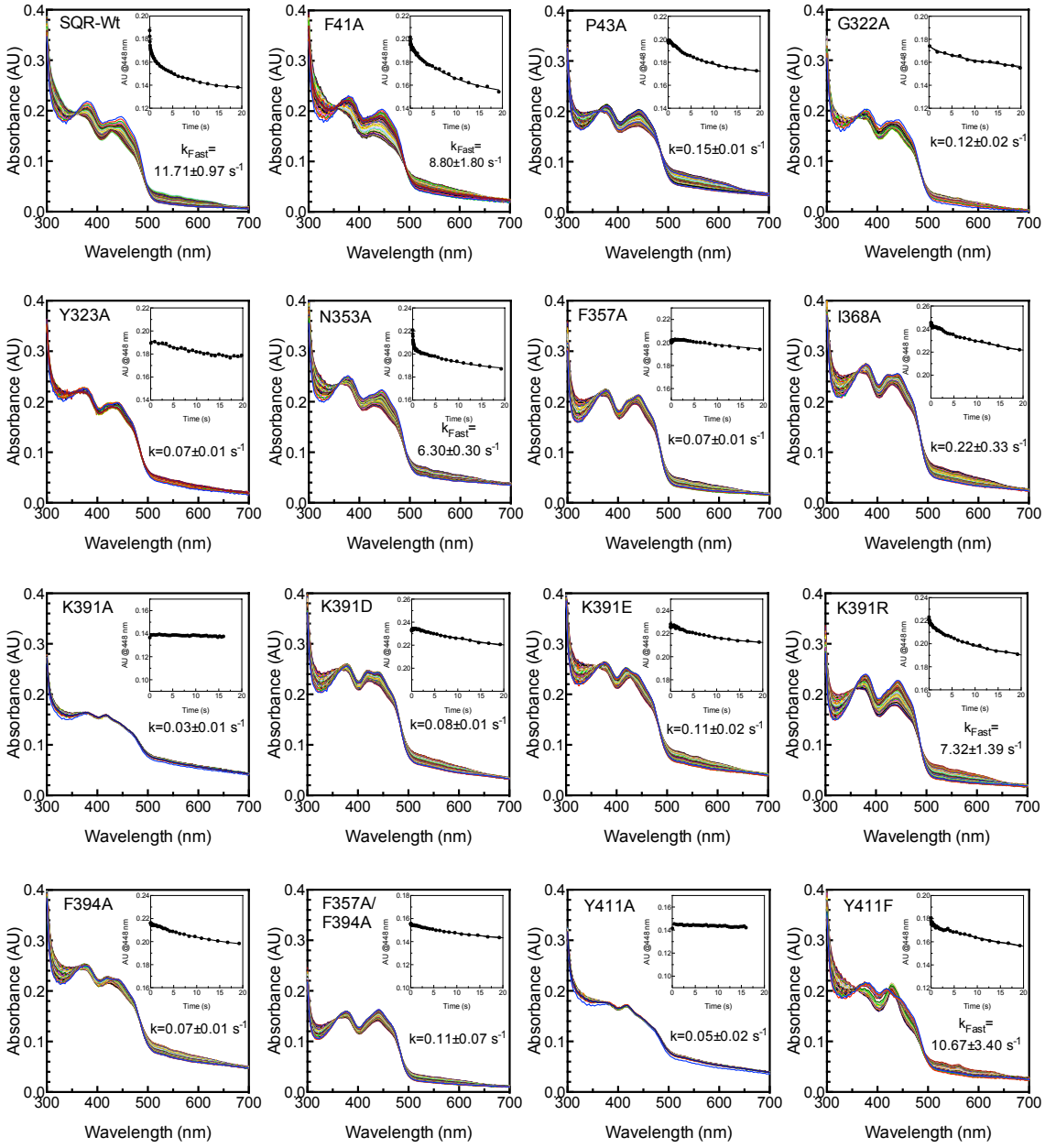

Supplementary Figure 6.2. Pre-steady state reduction of FAD by Na_2S in wild-type and the variant SQR.

Enzyme and substrate were mixed in the stopped-flow as described in Methods. The reaction was monitored by multiwavelength absorption in the range of 300−700 nm. The spectra shown were recorded at 0.00128−100 s after mixing. Insets are traces at 448 nm and the mean values (n=3) of the rate constants (k_{Fast} for the two-phase decay or k for the one-phase decay) obtained from fitting absorbance changes at 448 nm to the two-phase exponential decay equation model or the one-phase exponential decay equation which is it with GraphPad Prism (GraphPad Software, San Diego, CA). All fits were characterized by an R^2 better than 0.99.

Supplementary Figure 6.3. Kinetic analysis of SQR and variants based on decylubiquinone reduction.

Measurements were carried out using the DUQ reduction activity assay method at 23°C as described in Methods. The reaction mixture contained 1.25 µg mL^{-1} SQR in 50 mM Bis-Tris, pH 7.0, 20 mM glucose, 1 unit of glucose oxidase per mL and 10 units of catalase per mL. The DUQ reduction rates observed at varied DUQ concentration in the presence of 100 µM sulfide (a) and at varying Na_2S concentration in the presence of 50 µM DUQ (b) were plotted and fitted to the Michaelis–Menten equation. The K_m and V_{max} values were determined by nonlinear regression using GraphPrism Software. The data are the mean values of three experiments; error bars indicate the standard deviation.

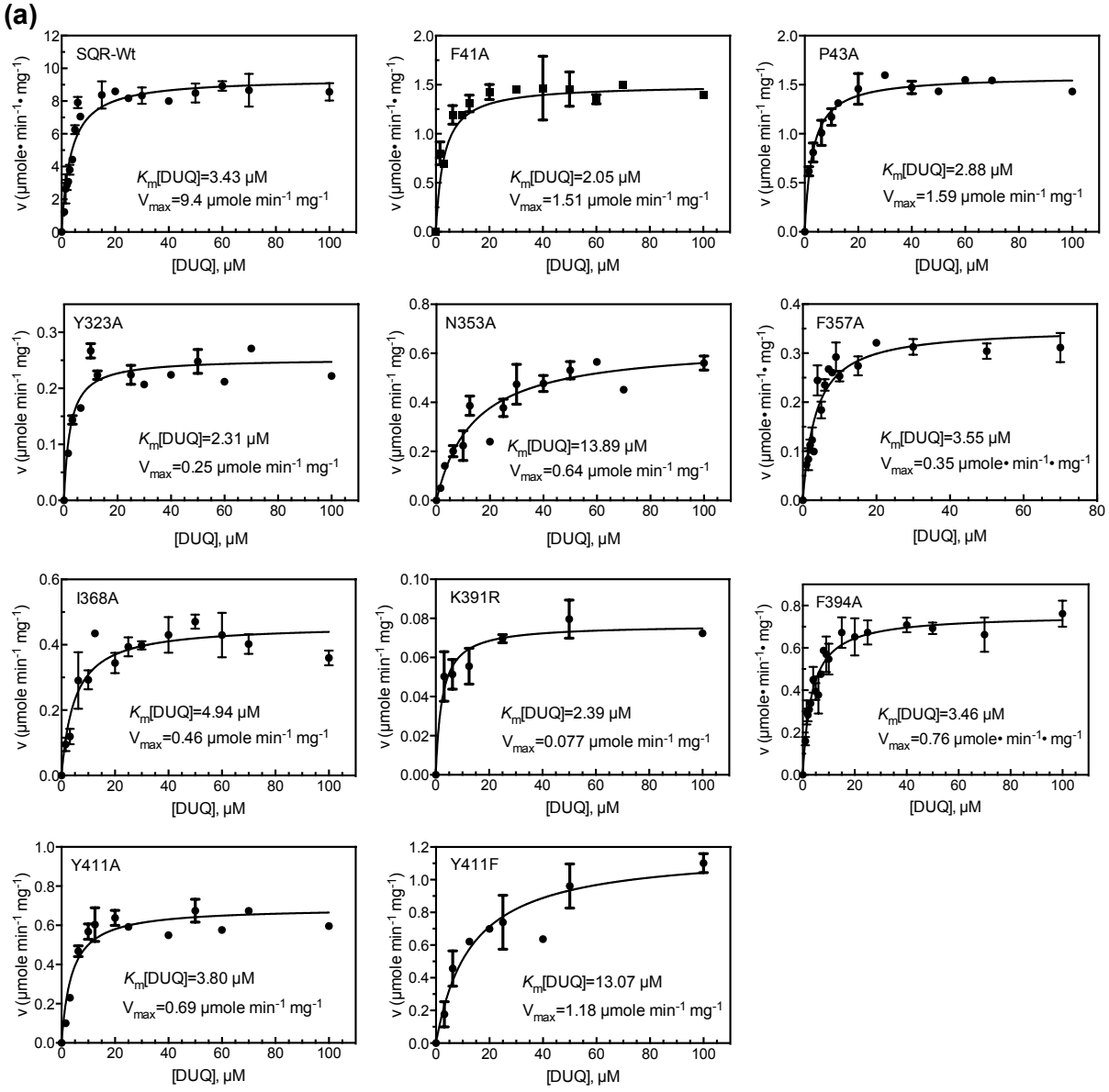

(b)

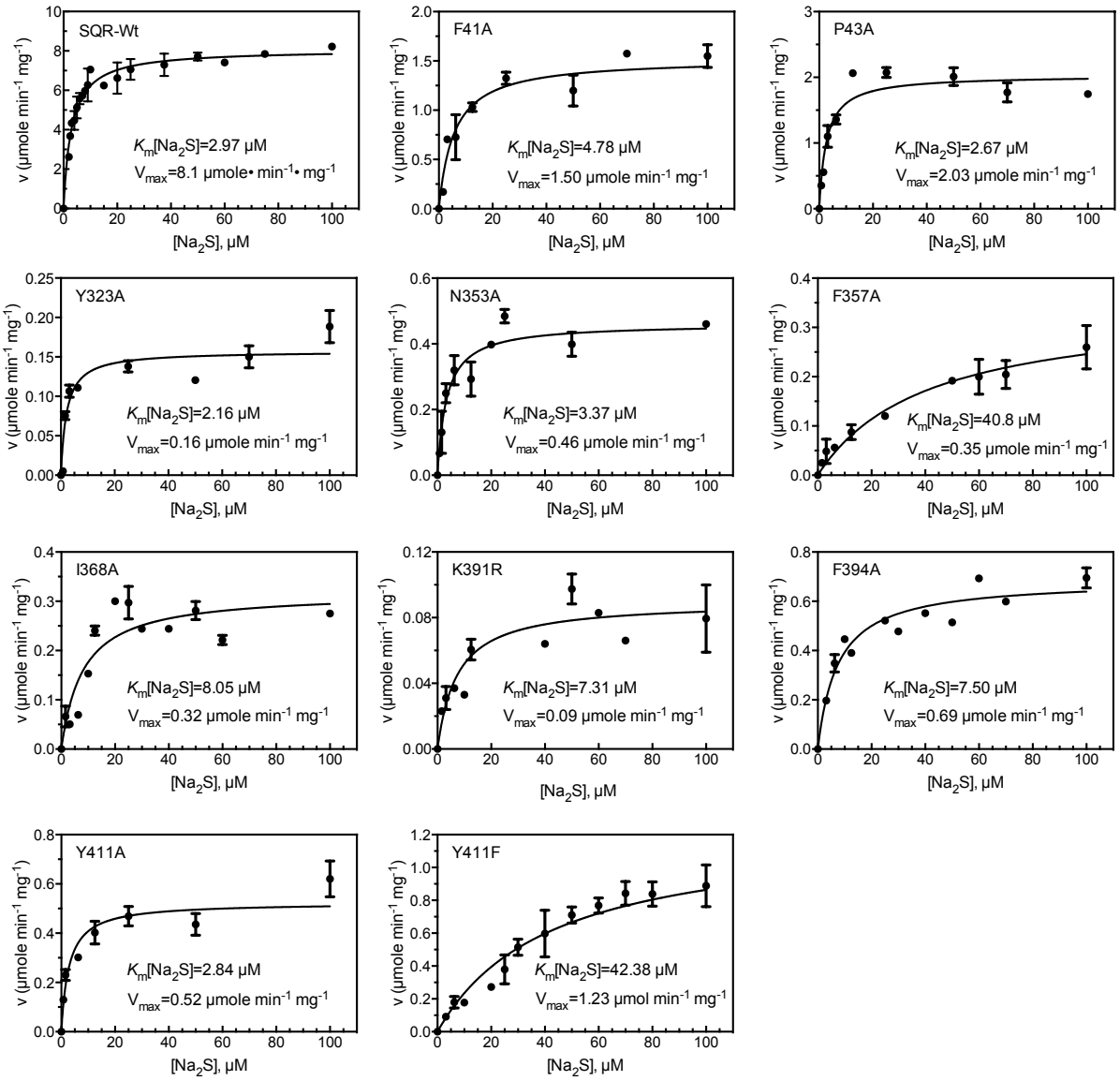
SQR-Wt
K_m[Na$_2$S]=2.97 μM
V_{max}=8.1 μmole• min^{-1}• mg^{-1}
F41A
K_m[Na$_2$S]=4.78 μM
V_{max}=1.50 μmole min^{-1} mg^{-1}
P43A
K_m[Na$_2$S]=2.67 μM
V_{max}=2.03 μmole min^{-1} mg^{-1}
Y323A
K_m[Na$_2$S]=2.16 μM
V_{max}=0.16 μmole min^{-1} mg^{-1}
N353A
K_m[Na$_2$S]=3.37 μM
V_{max}=0.46 μmole min^{-1} mg^{-1}
F357A
K_m[Na$_2$S]=40.8 μM
V_{max}=0.35 μmole min^{-1} mg^{-1}
I368A
K_m[Na$_2$S]=8.05 μM
V_{max}=0.32 μmole min^{-1} mg^{-1}
K391R
K_m[Na$_2$S]=7.31 μM
V_{max}=0.09 μmole min^{-1} mg^{-1}
F394A
K_m[Na$_2$S]=7.50 μM
V_{max}=0.69 μmole min^{-1} mg^{-1}
Y411A
K_m[Na$_2$S]=2.84 μM
V_{max}=0.52 μmole min^{-1} mg^{-1}
Y411F
K_m[Na$_2$S]=42.38 μM
V_{max}=1.23 μmol min^{-1} mg^{-1}
v (μmole min^{-1} mg^{-1})
[Na$_2$S], μM

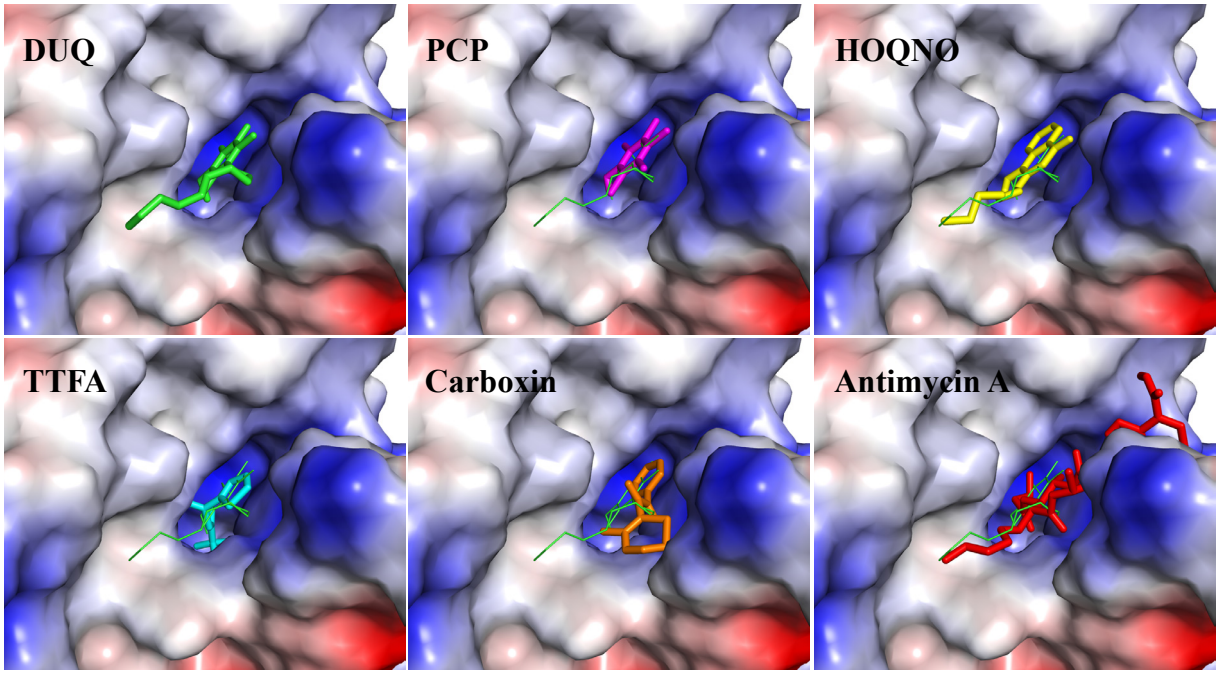

Supplementary Figure 6.4. Crystal structure of the quinone binding site of SQR shown in space filling with basic residues in blue, acidic residues in red and other residues in white.
DUQ is shown in green in the top left panel. The other panels show AutoDock Vina-predicted positions of inhibitors: PCP (magenta), HOQNO (yellow), TTFA (cyan), Carboxin (orange) and Antimycin A (red). The position of DUQ in thin green lines model is shown in the docked structures for comparison.

Chapter 7: Summary, Concluding Remarks and Future Direction

7.1 General Conclusions and Discussion

The goal of the thesis project was to elucidate more detailed insight of the enzymology, structure and oxidation-reduction reaction mechanism of SQR. In addition to this, redox potentiometry and electron paramagnetic resonance (EPR) spectroscopy have been utilized to further study the FAD radical signal in wild-type SQR and several variants. Furthermore, we have developed a simple semi-quantitative method using H_2S detection to measure the *in vivo* activity of heterogeneously expressed SQR. Overall, this thesis shed light on the structure and the complex mechanism of electron transfer in SQR. All of the foundations allow us to use $SQR_{At.f}$ as a model system to further investigate the sulfide-FAD-quinone redox reaction mechanisms.

In Chapter 2 and 3, we successfully expressed the wild-type *sqr* gene from *Acidithiobacillus ferrooxidans,* as well as several variants of conserved, catalytically important amino acids in *E. coli* BL21(DE3) and purified soluble, active, His-tagged SQR. The purified wild-type SQR and the variants were subjected to catalytic activity and structural analysis.

The recombinant SQR was crystallized and its X-ray structure was determined to 2.3 Å resolution. The overall structure of *At.f* SQR comprises two tandem Rossmann fold domains and a very flexible C-terminal domain containing two amphipathic helices that are thought to provide for membrane binding; there is also one FAD cofactor that is noncovalently bound in the first Rossmann fold domain in the N-terminal domain. The active site of SQR includes three cysteines (Cys160, Cys356 and Cys128) and the FAD cofactor. The FAD cofactor plays a central role in the catalytic mechanism. It accepts electrons from a sulfide and transfers them to quinone. Cys160 and Cys356 lie on the *re* side of the isoalloxazine ring of FAD; these two cysteine residues are positioned in a line that is almost parallel with the plane of the isoalloxazine ring.

The distance between the C^{4A} atom of the isoalloxazine ring of the FAD cofactor and the S^{γ} atoms of Cys160 or Cys356 is ~5 Å. Cys128 is located on the *si* face of the isoalloxazine ring of FAD. Its S^{γ} atom is 3.86 Å from C^{8M} of the isoalloxazine ring of FAD. The quinone-binding site has been determined from the cocrystallized $SQR_{At.f}$-DUQ complex structure. The binding site of DUQ is confined in the hydrophobic region that is close to the two C-terminal amphipathic helices (α9 and α10, residues 321-427). The benzoquinone ring of DUQ is sandwiched between the two benzene rings of Phe357 and Phe394 with the center-to-center distance of 3.4 Å and 3.8 Å respectively (**Figure 1**). DUQ is located on the *si* face of the isoalloxazine ring of FAD. The benzoquinone head is also close to the isoalloxazine ring (less than 3 Å). In addition, as selenides are homologous to sulfides in chemical properties, we questioned whether SQR can interact with selenides. The wild-type SQR was co-crystallized with Na_2Se, with and without DUQ. The determined structure revealed the selenium atoms form a tri-selenide bridge that is covalently inserted between the S^{γ} atoms of both active site cysteines (Cys160-S^{γ}-Se-Se-Se-S^{γ}-Cys356). The structure of this complex confirms that selenide is a substrate involved in the same redox reactions as sulfide. Selenide ions are considerably larger than sulfides so it is easier to identify selenides in the crystal structure. Moreover, they also give an anomalous signal at a wavelength that is usually used for data collection at synchrotrons (around 1 Å).

To gain further insights into the reaction mechanism and the role of the catalytically essential residues in the enzymatic mechanism, we further investigated the crystal structures of different batches of wild-type SQR and the selected variants, and observed three different sulfide oxidation intermediate states. They likely represent three different stages in the catalytic reaction. In intermediate state I, the persulfide group presents on both redox-active cysteines. The electron density between the persulfide groups is not continuous, so they are not covalently bonded. A

free hydrogen sulfide ion is proximal to both persulfide groups, but it is not covalently connected to either of them. The distance between the sulfide ion and the persulfide sulfur of Cys356 is 3.1 to 3.2 Å, whereas the distance from the sulfide ion to the persulfide sulfur of Cys160 is longer, in the range of 3.6 to 4.0 Å. In intermediate state II, a third sulfur atom is covalently attached to the persulfide group at Cys356, thus forming a trisulfide group; the Cys160 residue remains as the persulfide. Cys160 and Cys356 are not connected as can be seen by the non-continuous electron density. In intermediate state III, a pentasulfide bridge covalently connects the two redox-active cysteines, in which two sulfur atoms belong to the redox-active cysteines and a trisulfide is inserted into the bridge. In all of these intermediate states the sulfur atom that makes a covalent bond to the thiol of Cys356 is also very close to the N^5 and C^4 atoms of the isoalloxazine ring (3.2-3.8 Å).

Our catalytic activity analysis and structural determination led us to propose two alternative mechanisms: (1) A nucleophilic attack mechanism that involves Cys356–S–S^- as a nucleophile which attacks the C^{4A} atom of FAD; or (2) A radical mechanism of direct electron transfer from Cys356 disulfide to FAD. The growing polysulfide is held between Cys160 and Cys356. The role of Cys128 (most likely in the form of a disulfide) is confined to the release of the polysulfur product.

In Chapter 4, we use a combination of pre-steady state and steady state kinetics together with EPR spectroscopy to quantitate the role of the FAD cofactor and the conserved Cys and His residues that are proposed to play key roles in catalysis.

The properties of the enzyme were compared with alanine and/or serine variants of conserved cysteine residues (Cys128, Cys160, Cys356) which are structurally close to the FAD cofactor and histidine residues (His132, His198) implicated in function. When the pre-steady

state reduction of FAD was monitored using stopped flow spectrophotometry, variants of Cys128 and His132 had similar rates (11.7 s^{-1}) to wild-type enzyme confirming that Cys128 and His132 do not participate in the reductive half reaction. Whereas, variants of Cys160, Cys356 and His198 had greatly reduced activity. Using steady state kinetics of Na_2S-dependent DUQ reduction we measured a k_{cat} of 6.5 s^{-1} and a Michaelis constant K_m (Na_2S) of 3.0 mM and a K_m (DUQ) of 3.4 mM. Variants of Cys160, Cys356 and His198 had greatly diminished DUQ reduction activity whereas variants of Cys128 and His132 were less affected. We propose that the role of His132 is to abstract the proton from the protonated sulfide (H_2S and HS^-) and cysteine thiol and to take part in the reaction of releasing the polysulfur product. His198, moreover, may affect the overall stability of the protein. However, further studies will be required to confirm the roles of His132 and His198.

Potentiometric titrations of the FAD semiquinone revealed a midpoint potential of -139 ± 4 mV (E_{m1} = -58 ± 4 mV, E_{m2} = -220 ± 4 mV) at pH 7.0 for the two-electron reduction of FAD to $FADH_2$ in wild-type SQR, which is appropriate for transferring the electrons from sulfide ($E_{m,7}$= -260 mV) to the quinone pool (e.g. the $E_{m,7}$ of DUQ is +90 ± 10 mV). The midpoint potential of the FAD in $SQR^{Cys160Ala}$ (E_m= -135 ± 5 mV; E_{m1} = -40 ± 5 mV, E_{m2} = -230 ± 5 mV) is similar to that in wild-type SQR. Close inspection of the EPR spectra of flavin semiquinone reveals that the major semiquinone formed during the reduction of wild-type SQR and $SQR^{Cys160Ala}$ variant by dithionite at pH 7.0 is the anionic flavin radical exhibiting a linewidth of ~14-15 G and ~13-15 G, respectively. In contrast, a neutral flavin semiquinone was observed in the EPR spectrum of wild-type SQR reduced with Na_2S. The EPR intensity of this neutral flavin radical was enhanced in the Cys^{160Ala} variant. We suggest that the neutral semiquinone radical reflects the Cys356-S^{γ}-S-C^{4A}-FAD adduct intermediate in the proposed nucleophilic attack mechanism. In

support of this, the observation of the broad absorbance between 520 nm and 660 nm increased slightly upon Na_2S reduction in the stopped flow experiments suggesting the formation of a small amount of neutral semiquinone in agreement with the EPR results.

We used the DUQ reduction based enzymatic activity assay to determine the steady state kinetic constants and turnover numbers of SQR and the variants. Stopped-flow spectrophotometry and enzymatic activity assay based on the reduction of FAD allowed us to measure the pre-steady state kinetics of flavin reduction in SQR *in vitro*. Additionally, in Chapter 5, we used lead acetate [$Pb(OAc)_2$] soaked filter paper to measure the *in vivo* activity of heterogeneously expressed SQR and variants, in *E. coli,* based on the reaction of volatile H_2S with $Pb(OAc)_2$ to form insoluble PbS. The PbS stain is proportional to the amount of H_2S released from the culture. The *in vivo* H_2S oxidation activity was calculated based on the color density of the PbS stain formed by *E. coli* expressing SQR compared with cells harboring the empty vector pLM1. This assay method is simple and can be applied for *in vivo* sulfide metabolizing enzymatic studies, mutant screening and high-throughput inhibitor (drug) screens for sulfide metabolizing enzymes.

In Chapter 6, we combined computational docking and kinetic approaches to analyze quinone binding in SQR using quinone analogues and quinone site inhibitors. The results indicated SQR can reduce both benzoquinones and naphthoquinones. The alkyl side chain of ubiquinone derivatives enhances binding to SQR but limits the enzyme turnover. Pentachlorophenol (PCP) and 2-*n*-heptyl-4-hydroxyquinoline-*N*-oxide (HOQNO) are potent inhibitors of SQR with apparent inhibition constants (K_i) of 0.46 μM and 0.58 μM, respectively.

To study the roles of the highly conserved amino acids surrounding the quinone binding site, we employed a site-directed mutagenesis approach of the quinone binding site to create

variants of residues that interact with the benzoquinone ring and hydrophobic tail of the quinone and subjected the variant enzymes to steady state kinetic analysis of Na_2S dependent reduction of DUQ and pre-steady state kinetic analysis of Na_2S-dependent flavin reduction. The phenyl side chains of Phe357 and Phe391 sandwich the benzoquinone head group and are critical for quinone binding. Conversion of either of the two Phe residues (Phe357 and Phe394) that sandwich the benzoquinone ring to Ala resulted in no affect on the midpoint potential of FAD in SQR, but a 90% loss of DUQ activity. In these variants we could not observe Na_2S-dependent flavin bleaching. This suggests these Phe residues also result in conformational changes at the catalytic Na_2S oxidation site consisting of Cys160, Cys356 and FAD. Four additional conserved amino acids (Phe41, Pro43, Gly322 and Lys391) encompass the quinone binding pocket and play a role in conformational coupling between the active site and the quinone site. Lys391, located within hydrogen-bonding distance of both DUQ and FAD in SQR, participates in both quinone and FAD reduction. Tyr323, Asn353, Ile368 and Tyr411 make up the isoprenoid binding channel for the quinone and interact with the DUQ decyl chain.

Overall, our computational and kinetic analysis on the highly conserved amino acids surrounding the quinone binding site show that there is an intimate conformational connection between the catalytic Na_2S oxidation site and the quinone reduction site; and shed new light on the understanding of the quinone site of *A. ferrooxidans* SQR.

7.2 Remaining Questions and Future Directions

"The more I learn, the more I realize how much I don't know." With the light shed on SQR in this thesis, several remaining big questions arise: (1) What is the real product of sulfide oxidation catalyzed by SQR, —— Cyclooctasufur or polysulfide? (2) How is SQR translocated

through the cytoplasmic membrane? (3) How does SQR bind to the membrane and interact with quinone in the lipid bilayer? (4) How does the quinone-binding site control both FAD and quinone reduction in SQR? and (5) Does SQR play other roles other than sulfide homeostasis in sulfide signaling? To partially answer the above questions, the following research directions are worth pursuing.

Probing the species of sulfur present in the product of sulfide oxidation catalyzed by SQR

SQR oxidizes sulfide to zero-valent sulfur **(ZVS)**, which is then released from the protein. However, it has not been determined whether the released product of SQR is cyclic octasulfur or a more soluble linear polysulfide. ZVS can exist in various forms, including the dissolved cyclooctasulfur (S_8), soluble linear polysulfides (S_n^{2-} and protonated forms), and crystalline rhombic cyclooctasulfur (α-S_8) [154]. The bonding energy of the S-S bounds in linear polymeric sulfur is 2.4 kJ mol^{-1} weaker than that in cyclooctasulfur [155]. Thus, the linear polysulfides might be more easily used for further oxidation in the cell. Urich *et al*. [156] reported that sulfur oxygenase only use linear polysulfides rather than cyclooctasulfur.

The key function of SQR is acquiring electrons from sulfide for respiration. However, another function of SQR consequently is maintaining sulfide/sulfur homeostasis by governing the sulfur species in the product of the sulfide oxidation reaction. The sulfur can either be stored inside the cell for further usage or be exported to the extracellular environment. Sulfur chains have been found in anaerobically grown bacteria [157; 158], while sulfur rings and polythionates present in aerobically grown organisms [159; 160; 161]. In our previous study, we did not find octasulfur rings in any of our $SQR_{At,f}$ structures. However, the octasulfur ring was observed in the structure of SQR from *Aquifex aeolicus* [162].

Distinguishing the sulfur product in SQR reaction is helpful for understanding the mechanism and function of SQR. I propose to apply sulfur K-edge X-ray absorption spectroscopy (**XAS**) to probe the species of the sulfur product catalyzed by SQR. Sulfur K-edge XAS is a powerful technique for probing the forms of sulfur in intact cells and tissues.

First, It is necessary to analyze the sulfur species that is present in intact cells and in the different subcellular fractions (periplasm and spheroplast) of *At.f* and *E. coli* BL21(DE3) with and without expression of wild-type and mutant SQR. I postulate that either cyclooctasulfur or linear polysulfide will be detected in *At.f* and *E. coli* with expression of wild-type SQR, but not in the negative control sample —*E. coli* without expression of SQR. If dominant short polysulfide chains are observed in *E. coli* with expression of mutant SQR (presumably in C160A and C356A), the number of sulfur atom in the chain could be used for studying the sulfide oxidation mechanism of SQR.

Furthermore, probing the form of sulfur product of the SQR reaction *in vitro* using purified SQR and variants is another direction to study the products and the mechanism of sulfide oxidation in SQR. The sulfur species detected in the product could easily answer the question about the real product of sulfide oxidation catalyzed by SQR. Meanwhile, sulfur K-edge XAS can provide quantitative information on the chemical identities of the sulfur species that are present in a sample. It will allow us to track the extension of polysulfide by adding different amount of DUQ to the SQR reaction with abundant sulfide. In our proposed sulfide oxidation mechanism of SQR, the polysulfide chain grows on Cys160, and is released by Cys128. I postulate that the variant C160A will only generate short linear polysulfide chain, while variant C128A will dominantly accumulate longer linear or ring sulfur due to lacking of the product release ability.

The location, membrane attachment and the translocation pathway of SQR

SQRs are generally considered to be peripheral membrane proteins [62]. However, its membrane topology is still in debate. In the past three decades, all of the reported directly-purified SQRs were isolated from the membrane. Some bacterial SQRs are loosely bound to the membrane, and can be easily washed out by chaotropes NaBr [62; 76; 163]. SQRs from cyanobacteria and eukaryotes are tightly membrane-bound, and need detergent (Triton X-100 or DDM) to extract them [161; 164; 165; 166; 167].

Several SQRs were also heterologously expressed and purified in active form. SQR from the purple nonsulfur bacterium *Rhodobacter capsulatus* was expressed in *E. coli* and purified from the membrane fraction[168]. Surprisingly, a relatively high proportion (30–50%) of soluble SQR was obtained from the non-membrane fraction of *E. coli*. Alkaline phosphatase **(PhoA)** fusion study indicated that the SQR of *R. capsulatus* functions at the periplasmic side of the cytoplasmic membrane and that this flavoprotein is translocated by an unknown mechanism.

Subcellular localization prediction based on the sequence of $SQR_{At.f}$ indicates that SQR has multiple locations in *At.f*. In our preliminary study, SQR was detected in periplasm, cytoplasm and cytoplasmic membrane fractions in *At.f* by western blot analysis using anti-SQR antiserum. Similarly, heterologously expressed SQR was obtained from both the soluble and membrane fraction in *E. coli* BL21(DE3) /pLM1::sqr [37]. Interestingly, the recombinant SQR was also found in the periplasmic space in *E. coli* BL21(DE3) /pLM1::sqr. However, the amino acid sequence of SQR lacks an N-terminal signal peptide for translocation. Therefore, a signal peptide that is different from N-terminal Tat and Sec signal peptides must be present in the amino acid sequence of SQR; or SQR may be cotranslocated with a protein bearing such a signal, as was found for the catalytic subunits of several periplasmic redox proteins (eg. DmsAB) [169; 170].

Therefore, the questions need be answered are: (1) how is SQR translocated through the cytoplasmic membrane and (2) how does it become attached to the membrane and interact with quinone in lipid bilayer. The following experiments can be attempted to answer the questions related in this topic.

In order to accurately determine its location, western blot analysis needs to be performed to inspect all the subcellular fractions of *At.f* using anti-SQR antibody. The control antibodies against the specific location-identified protein in *At.f* will be used in the western blot analysis [171]. Additionally, nanoscale liquid chromatography mass spectrometry (LC-MS/MS) can be utilized to investigate the presence of SQR in different subcellular fractions of *At.f*.

The X-ray structures indicate that the very flexible C-terminal domain of *At.f* SQR contains two amphipathic helices that are thought to provide for membrane binding. The amphipathic helices motif is suited for relatively weak and non-specific membrane binding, which is driven by hydrophobic forces to drive the binding. In order to study the interaction between SQR and the cytoplasmic membrane, different concentrations of NaCl (from 0 mM to 500 mM) can be used in the buffers for subcellular fractionation. Relative binding affinity can be verified through western blots using anti-SQR antibody. Higher concentrations of salt can increase the hydrophobic effect and should increase the affinity of the membrane for SQR.

In order to detect the distribution of the heterologously expressed His-tagged SQR in *E. coli* BL21(DE3), the western blot analyses for different subcellular fractions using both anti-His and anti-SQR antibodies are necessary to be performed. Meanwhile, we have made two constructs incorporating the 6×His tag at the N- and C- termini of SQR, respectively. This should reveal if either terminus is cleaved after translocation by comparing the results of western blots using anti-His and anti-SQR antibodies, respectively. We can use the antibody against the

cytoplasmic marker cAMP receptor protein (anti-CRP) and against the periplasmic marker β-lactamase (anti-β-lactamase) as controls for the purity of the *E. coli* subcellular fractions [172].

To verify the translocation of SQR to the periplasmic space, PhoA fusion and ß-lactamase fusion techniques can be used. Alkaline phosphatase **(PhoA)** and TEM ß-lactamase are only functional in the periplasm. Additionally, we can make truncated SQR-PhoA fusions (or truncated SQR-ß-lactamase fusion) and combine these with site-directed mutagenesis to determine which amino acid residues are critical for translocation. Furthermore, if we confirm the periplasmic location of SQR in both *At.f* and *E. coli*, and target the translocation related signal peptide, we can use diverse knockout and mutant strains, e.g. Tat knock-out strain [173] and temperature-sensitive Sec mutant strain [174; 175], to analyze how SQR is translocated across the cytoplasmic membrane. I postulate that SQR may use a Sec-independent and Tat-independent pathway to perform the translocation.

It is also possible that SQR can cross the cytoplasmic membrane by interacting with a second protein participating in translocation. To test this hypothesis, we can fish out the candidate proteins from *At.f* and *E. coli* using a His-tagged SQR pull-down method. The pull-down proteins can be identified by SDS-PAGE and Mass spectrometry.

Investigation on how does the quinone-binding site control both FAD and quinone reduction in SQR

We proposed in Chapter 4 that the quinone-binding site of *A. ferrooxidans* SQR controls both FAD and quinone reduction. Hypothetically, the control could be processed either through the occupation of the quinone binding site or by the effects of the proton relay, and so on.

To further study the effect on the FAD reduction by the quinone binding site, the following aspects can be approached. First, it is worth determining if the occupation of the

quinone binding site will affect the redox potential of FAD in wild-type SQR, as well as the reaction rate of FAD reduction by sulfide. The inhibitor PCP can be utilized instead of DUQ for potentiometric titrations and stopped-flow experiments. Furthermore, testing if membrane environment, e.g. adding liposomes in the reaction buffer, will cause any effect on both quinone binding and FAD reduction may reveal some new information on this topic.

In addition, the proton transfer pathways in SQR are still unclear. Several potential proton relay pathways are involved in or in the vicinity of the quinone binding site. Lys391 was proposed to participate in proton transfer via interacting with the C-4 keto oxygen (the O^4 atom) of FAD and/or of DUQ. However, more evidence is needed to support this hypothesis on Lys391. Moreover, based on the analysis on the structures of wide-type SQR and the variants, O^4-Tyr411-H_2O-H_2O-Glu326 could be another proton transfer relay in SQR. This also needs to be proved by further experimental results.

Reference

1. Scheele, C. W. & Bergman, T. (1777). *Carl Wilhelm Scheele's d. Königl. Schwed. Acad. d. Wissenschaft Mitgliedes, Chemische Abhandlung von der Luft und dem Feuer*, Verlegt von Magn. Swederus ... zu finden bey S.L. Crusius.
2. Partington, J. R. (1970). *A history of chemistry*, Macmillan, London.
3. Cuevasanta, E., Denicola, A., Alvarez, B. & Moller, M. N. (2012). Solubility and permeation of hydrogen sulfide in lipid membranes. *PLoS One* **7**, e34562.
4. Li, Q. & Lancaster, J. R., Jr. (2013). Chemical foundations of hydrogen sulfide biology. *Nitric Oxide* **35**, 21-34.
5. Kabil, O. & Banerjee, R. (2010). Redox biochemistry of hydrogen sulfide. *J Biol Chem* **285**, 21903-7.
6. Harris, D. C. (2010). *Quantitative chemical analysis*, W. H. Freeman and Company, New York.
7. Pearson, R. G., Sobel, H. R. & Songstad, J. (1968). Nucleophilic reactivity constants toward methyl iodide and trans-dichlorodi(pyridine)platinum(II). *Journal of the American Chemical Society* **90**, 319-326.
8. Fukuto, J. M., Carrington, S. J., Tantillo, D. J., Harrison, J. G., Ignarro, L. J., Freeman, B. A., Chen, A. & Wink, D. A. (2012). Small molecule signaling agents: the integrated chemistry and biochemistry of nitrogen oxides, oxides of carbon, dioxygen, hydrogen sulfide, and their derived species. *Chem Res Toxicol* **25**, 769-93.
9. Nagy, P., Palinkas, Z., Nagy, A., Budai, B., Toth, I. & Vasas, A. (2014). Chemical aspects of hydrogen sulfide measurements in physiological samples. *Biochim Biophys Acta* **1840**, 876-91.
10. Mustafa, A. K., Gadalla, M. M., Sen, N., Kim, S., Mu, W., Gazi, S. K., Barrow, R. K., Yang, G., Wang, R. & Snyder, S. H. (2009). H2S signals through protein S-sulfhydration. *Sci Signal* **2**, ra72.
11. Stasko, A., Brezova, V., Zalibera, M., Biskupic, S. & Ondrias, K. (2009). Electron transfer: a primary step in the reactions of sodium hydrosulphide, an H2S/HS(-) donor. *Free Radic Res* **43**, 581-93.
12. Cooper, C. E. & Brown, G. C. (2008). The inhibition of mitochondrial cytochrome oxidase by the gases carbon monoxide, nitric oxide, hydrogen cyanide and hydrogen sulfide: chemical mechanism and physiological significance. *J Bioenerg Biomembr* **40**, 533-9.
13. Griesbeck, C., Hauska, G. & Schütz, M. (2000). Biological sulfide oxidation: sulfide-quinone reductase (SQR), the primary reaction. *Recent research developments in microbiology* **4**, 179–203.
14. Hildebrandt, T. M. & Grieshaber, M. K. (2008). Three enzymatic activities catalyze the oxidation of sulfide to thiosulfate in mammalian and invertebrate mitochondria. *FEBS J* **275**, 3352-61.
15. Wang, R. (2002). Two's company, three's a crowd: can H2S be the third endogenous gaseous transmitter? *The FASEB journal : official publication of the Federation of American Societies for Experimental Biology* **16**, 1792-1798.

16. Goubern, M., Andriamihaja, M., Nubel, T., Blachier, F. & Bouillaud, F. (2007). Sulfide, the first inorganic substrate for human cells. *The FASEB journal : official publication of the Federation of American Societies for Experimental Biology* **21**, 1699-706.
17. Tang, G., Wu, L. & Wang, R. (2010). Interaction of hydrogen sulfide with ion channels. *Clinical and Experimental Pharmacology and Physiology* **37**, 753-763.
18. Bouillaud, F. & Blachier, F. (2011). Mitochondria and sulfide: a very old story of poisoning, feeding, and signaling? *Antioxidants & redox signaling* **15**, 379-391.
19. Li, L., Rose, P. & Moore, P. K. (2011). Hydrogen sulfide and cell signaling. *Annu Rev Pharmacol Toxicol* **51**, 169-187.
20. Petersen, L. C. (1977). The effect of inhibitors on the oxygen kinetics of cytochrome c oxidase. *Biochim Biophys Acta* **460**, 299-307.
21. Nicholls, P., Marshall, D. C., Cooper, C. E. & Wilson, M. T. (2013). Sulfide inhibition of and metabolism by cytochrome c oxidase. *Biochem Soc Trans* **41**, 1312-6.
22. Yong, R. & Searcy, D. G. (2001). Sulfide oxidation coupled to ATP synthesis in chicken liver mitochondria. *Comparative Biochemistry and Physiology Part B: Biochemistry and Molecular Biology* **129**, 129-137.
23. Leschelle, X., Goubern, M., Andriamihaja, M., Blottiere, H. M., Couplan, E., Gonzalez-Barroso, M. D., Petit, C., Pagniez, A., Chaumontet, C., Mignotte, B., Bouillaud, F. & Blachier, F. (2005). Adaptative metabolic response of human colonic epithelial cells to the adverse effects of the luminal compound sulfide. *Biochim Biophys Acta* **1725**, 201-12.
24. Hughes, M. N., Centelles, M. N. & Moore, K. P. (2009). Making and working with hydrogen sulfide: The chemistry and generation of hydrogen sulfide in vitro and its measurement in vivo: a review. *Free Radic Biol Med* **47**, 1346-53.
25. Dopson, M. & Johnson, D. B. (2012). Biodiversity, metabolism and applications of acidophilic sulfur-metabolizing microorganisms. *Environ Microbiol* **14**, 2620-31.
26. Brierley, J. A. (2008). A perspective on developments in biohydrometallurgy. *Hydrometallurgy* **94**, 2-7.
27. Parrino, V., Kraus, D. W. & Doeller, J. E. (2000). ATP production from the oxidation of sulfide in gill mitochondria of the ribbed mussel Geukensia demissa. *The Journal of experimental biology* **203**, 2209-18.
28. Yong, R. & Searcy, D. G. (2001). Sulfide oxidation coupled to ATP synthesis in chicken liver mitochondria. *Comparative biochemistry and physiology. Part B, Biochemistry & molecular biology* **129**, 129-37.
29. Stein, A. & Bailey, S. M. (2013). Redox Biology of Hydrogen Sulfide: Implications for Physiology, Pathophysiology, and Pharmacology. *Redox Biol* **1**, 32-39.
30. Kolluru, G. K., Shen, X. & Kevil, C. G. (2013). A tale of two gases: NO and H2S, foes or friends for life? *Redox Biol* **1**, 313-8.
31. Schreier, S. M., Muellner, M. K., Steinkellner, H., Hermann, M., Esterbauer, H., Exner, M., Gmeiner, B. M., Kapiotis, S. & Laggner, H. (2010). Hydrogen sulfide scavenges the cytotoxic lipid oxidation product 4-HNE. *Neurotox Res* **17**, 249-56.
32. Zeng, J., Zhang, Y., Liu, Y., Zhang, X., Xia, L., Liu, J. & Qiu, G. (2007). Expression, purification and characterization of a cysteine desulfurase, IscS, from Acidithiobacillus ferrooxidans. *Biotechnology letters* **29**, 1983-1990.
33. Stipanuk, M. H. & Beck, P. W. (1982). Characterization of the enzymic capacity for cysteine desulphhydration in liver and kidney of the rat. *Biochem J* **206**, 267-77.

34. Chiku, T., Padovani, D., Zhu, W., Singh, S., Vitvitsky, V. & Banerjee, R. (2009). H2S biogenesis by human cystathionine gamma-lyase leads to the novel sulfur metabolites lanthionine and homolanthionine and is responsive to the grade of hyperhomocysteinemia. *J Biol Chem* **284**, 11601-12.
35. Kabil, O. & Banerjee, R. (2014). Enzymology of H2S biogenesis, decay and signaling. *Antioxid Redox Signal* **20**, 770-82.
36. Ogasawara, Y., Isoda, S. & Tanabe, S. (1994). Tissue and subcellular distribution of bound and acid-labile sulfur, and the enzymic capacity for sulfide production in the rat. *Biol Pharm Bull* **17**, 1535-42.
37. Cherney, M. M., Zhang, Y., Solomonson, M., Weiner, J. H. & James, M. N. G. (2010). Crystal structure of sulfide:quinone oxidoreductase from *Acidithiobacillus ferrooxidans*: insights into sulfidotrophic respiration and detoxification. *J Mol Biol* **398**, 292-305.
38. Picton, R., Eggo, M. C., Merrill, G. A., Langman, M. J. & Singh, S. (2002). Mucosal protection against sulphide: importance of the enzyme rhodanese. *Gut* **50**, 201-5.
39. Roediger, W. E., Babidge, W. & Millard, S. (1996). Methionine derivatives diminish sulphide damage to colonocytes--implications for ulcerative colitis. *Gut* **39**, 77-81.
40. Pluth, M. D., Bailey, T. S., Hammers, M. D. & Montoya, L. A. (2013). Chemical Tools for Studying Biological Hydrogen Sulfide. *Biochalcogen Chemistry: The Biological Chemistry of Sulfur, Selenium, and Tellurium. American Chemical Society, Washington, DC*, 15-32.
41. Hellwinkel, D. (2001). *Systematic Nomenclature of Organic Chemistry: A Directory to Comprehension and Application on Its Basic Principles ; with 35 Tables*, Springer Berlin Heidelberg.
42. Clark, W. M. (1960). *Oxidation-reduction potentials of organic systems*, Williams and Wilkins Co, Baltimore.
43. Ratasuk, N. & Nanny, M. A. (2007). Characterization and quantification of reversible redox sites in humic substances. *Environ Sci Technol* **41**, 7844-50.
44. Lennarz, W. J. & Lane, M. D. (2004). *Encyclopedia of biological chemistry*. 1st edit. 4 vols, Elsevier Academic Press, Amsterdam; Boston.
45. Kelly, D. P. & Wood, A. P. (2000). Reclassification of some species of Thiobacillus to the newly designated genera Acidithiobacillus gen. nov., Halothiobacillus gen. nov. and Thermithiobacillus gen. nov. *International Journal of Systematic and Evolutionary Microbiology* **50**, 511-516.
46. Zhang, Y. F., Yang, Y., Liu, J. S. & Qiu, G. Z. (2013). Isolation and characterization of *Acidithiobacillus ferrooxidans* strain QXS-1 capable of unusual ferrous iron and sulfur utilization. *Hydrometallurgy* **136**, 51-57.
47. Temple, K. L. & Delchamps, E. W. (1953). Autotrophic bacteria and the formation of acid in bituminous coal mines. *Appl Microbiol* **1**, 255-8.
48. Margalith, P., Silver, M. & Lundgren, D. (1966). Sulfur oxidation by the iron bacterium Ferrobacillus ferrooxidans. *Journal of Bacteriology* **92**, 1706.
49. Olson, G. J., Brierley, J. A. & Brierley, C. L. (2003). Bioleaching review part B: progress in bioleaching: applications of microbial processes by the minerals industries. *Appl Microbiol Biotechnol* **63**, 249-257.
50. Tano, T. & Lundgren, D. (1978). Sulfide oxidation by spheroplasts of Thiobacillus ferrooxidans. *Appl Environ Microbiol* **35**, 1198-205.

51. Rohwerder, T., Gehrke, T., Kinzler, K. & Sand, W. (2003). Bioleaching review part A: progress in bioleaching: fundamentals and mechanisms of bacterial metal sulfide oxidation. *Appl Microbiol Biotechnol* **63**, 239-248.
52. Duquesne, K., Lebrun, S., Casiot, C., Bruneel, O., Personne, J. C., Leblanc, M., Elbaz-Poulichet, F., Morin, G. & Bonnefoy, V. (2003). Immobilization of arsenite and ferric iron by Acidithiobacillus ferrooxidans and its relevance to acid mine drainage. *Appl Environ Microbiol* **69**, 6165-73.
53. Valdés, J., Pedroso, I., Quatrini, R., Dodson, R., Tettelin, H., Blake, R., Eisen, J. & Holmes, D. (2008). *Acidithiobacillus ferrooxidans* metabolism: from genome sequence to industrial applications. *BMC genomics* **9**, 597-620.
54. González-Toril, E., Martínez-Frías, J., Gómez Gómez, J. M., Rull, F. & Amils, R. (2005). Iron meteorites can support the growth of acidophilic chemolithoautotrophic microorganisms. *Astrobiology* **5**, 406-414.
55. Leathen, W. W. & Braley, S. A. (1954). A new iron-oxidizing bacterium: Ferrobacillus ferrooxidans. *Bacteriol. Proc* 44.
56. Braley, S. A., Sr., Kinsel, N. A. & Leathen, W. W. (1956). Ferrobacillus ferrooxidans: a chemosynthetic autotrophic Bacterium. *J Bacteriol* **72**, 700-4.
57. Chi, A., Valenzuela, L., Beard, S., Mackey, A. J., Shabanowitz, J., Hunt, D. F. & Jerez, C. A. (2007). Periplasmic proteins of the extremophile Acidithiobacillus ferrooxidans: a high throughput proteomics analysis. *Mol Cell Proteomics* **6**, 2239-51.
58. Nieto, P. A., Covarrubias, P. C., Jedlicki, E., Holmes, D. S. & Quatrini, R. (2009). Selection and evaluation of reference genes for improved interrogation of microbial transcriptomes: case study with the extremophile Acidithiobacillus ferrooxidans. *BMC Mol Biol* **10**, 63.
59. Quatrini, R., Appia-Ayme, C., Denis, Y., Jedlicki, E., Holmes, D. S. & Bonnefoy, V. (2009). Extending the models for iron and sulfur oxidation in the extreme acidophile *Acidithiobacillus ferrooxidans*. *BMC genomics* **10**, 394-412.
60. Nicholls, D. G. & Ferguson, S. (2013). *Bioenergetics*, Academic Press.
61. Rohwerder, T. & Sand, W. (2003). The sulfane sulfur of persulfides is the actual substrate of the sulfur-oxidizing enzymes from Acidithiobacillus and Acidiphilium spp. *Microbiology* **149**, 1699-710.
62. Griesbeck, C., Schutz, M., Schodl, T., Bathe, S., Nausch, L., Mederer, N., Vielreicher, M. & Hauska, G. (2002). Mechanism of sulfide-quinone reductase investigated using site-directed mutagenesis and sulfur analysis. *Biochemistry* **41**, 11552-11565.
63. Murataliev, M. B. (1999). Application of electron spin resonance (ESR) for detection and characterization of flavoprotein semiquinones. In *Flavoprotein Protocols*, pp. 97-110. Springer.
64. Alberts, B., Bray, D., Johnson, A., Lewis, N., Raff, M., Roberts, K. & Walter, P. (1998). *Essential Cell Biology*, Garland Publishing Inc., New York.
65. Vande Weghe, J. G. & Ow, D. W. (1999). A fission yeast gene for mitochondrial sulfide oxidation. *J Biol Chem* **274**, 13250-7.
66. Vande Weghe, J. G. & Ow, D. W. (2001). Accumulation of metal-binding peptides in fission yeast requires hmt2+. *Mol Microbiol* **42**, 29-36.
67. Nagy, C. I., Vass, I., Rakhely, G., Vass, I. Z., Toth, A., Duzs, A., Peca, L., Kruk, J. & Kos, P. B. (2014). Coregulated genes link sulfide:quinone oxidoreductase and arsenic metabolism in Synechocystis sp. strain PCC6803. *J Bacteriol* **196**, 3430-40.

68. Boehning, D. & Snyder, S. H. (2003). Novel neural modulators. *Annual review of neuroscience* **26**, 105-31.
69. Kimura, H. (2002). Hydrogen sulfide as a neuromodulator. *Molecular Neurobiology* **26**, 13-19.
70. Arieli, B., Padan, E. & Shahak, Y. (1991). Sulfide-induced sulfide-quinone reductase activity in thylakoids of Oscillatoria limnetica. *J Biol Chem* **266**, 104-11.
71. Theissen, U., Hoffmeister, M., Grieshaber, M. & Martin, W. (2003). Single eubacterial origin of eukaryotic sulfide:quinone oxidoreductase, a mitochondrial enzyme conserved from the early evolution of eukaryotes during anoxic and sulfidic times. *Mol Biol Evol* **20**, 1564-74.
72. Shahak, Y., Arieli, B., Padan, E. & Hauska, G. (1992). Sulfide quinone reductase (SQR) activity in Chlorobium. *FEBS Lett* **299**, 127-30.
73. Arieli, B., Shahak, Y., Taglicht, D., Hauska, G. & Padan, E. (1994). Purification and characterization of sulfide-quinone reductase, a novel enzyme driving anoxygenic photosynthesis in Oscillatoria limnetica. *J Biol Chem* **269**, 5705-11.
74. Schutz, M., Shahak, Y., Padan, E. & Hauska, G. (1997). Sulfide-quinone reductase from Rhodobacter capsulatus. Purification, cloning, and expression. *J Biol Chem* **272**, 9890-4.
75. Schutz, M., Maldener, I., Griesbeck, C. & Hauska, G. (1999). Sulfide-quinone reductase from Rhodobacter capsulatus: requirement for growth, periplasmic localization, and extension of gene sequence analysis. *J Bacteriol* **181**, 6516-23.
76. Schutz, M., Klughammer, C., Griesbeck, C., Quentmeier, A., Friedrich, C. G. & Hauska, G. (1998). Sulfide-quinone reductase activity in membranes of the chemotrophic bacterium Paracoccus denitrificans GB17. *Archives of Microbiology* **170**, 353-360.
77. Nubel, T., Klughammer, C., Huber, R., Hauska, G. & Schutz, M. (2000). Sulfide:quinone oxidoreductase in membranes of the hyperthermophilic bacterium Aquifex aeolicus (VF5). *Arch Microbiol* **173**, 233-44.
78. Wakai, S., Tsujita, M., Kikumoto, M., Manchur, M. A., Kanao, T. & Kamimura, K. (2007). Purification and Characterization of Sulfide:Quinone Oxidoreductase from an Acidophilic Iron-Oxidizing Bacterium, Acidithiobacillus ferrooxidans. *Biosci Biotechnol Biochem* **71**, 2735-42.
79. Brito, J. A., Sousa, F. L., Stelter, M., Bandeiras, T. M., Vonrhein, C., Teixeira, M., Pereira, M. M. & Archer, M. (2009). Structural and functional insights into sulfide:quinone oxidoreductase. *Biochemistry* **48**, 5613-22.
80. Lencina, A. M., Ding, Z., Schurig-Briccio, L. A. & Gennis, R. B. (2013). Characterization of the Type III sulfide:quinone oxidoreductase from Caldivirga maquilingensis and its membrane binding. *Biochim Biophys Acta* **1827**, 266-75.
81. Theissen, U. & Martin, W. (2008). Sulfide : quinone oxidoreductase (SQR) from the lugworm Arenicola marina shows cyanide- and thioredoxin-dependent activity. *FEBS J* **275**, 1131-9.
82. Shahak, Y. & Hauska, G. (2008). Sulfide Oxidation from Cyanobacteria to Humans: Sulfide–Quinone Oxidoreductase (SQR), Vol. 27, pp. 319-335.
83. Ma, Y. B., Zhang, Z. F., Shao, M. Y., Kang, K. H., Tan, Z. & Li, J. L. (2011). Sulfide:quinone oxidoreductase from echiuran worm Urechis unicinctus. *Mar Biotechnol (NY)* **13**, 93-107.

84. Jackson, M. R., Melideo, S. L. & Jorns, M. S. (2012). Human sulfide:quinone oxidoreductase catalyzes the first step in hydrogen sulfide metabolism and produces a sulfane sulfur metabolite. *Biochemistry* **51**, 6804-15.
85. Marcia, M., Ermler, U., Peng, G. & Michel, H. (2009). The structure of Aquifex aeolicus sulfide:quinone oxidoreductase, a basis to understand sulfide detoxification and respiration. *Proc Natl Acad Sci U S A* **106**, 9625-30.
86. Zhang, Y., Cherney, M. M., Solomonson, M., Liu, J., James, M. N. & Weiner, J. H. (2009). Preliminary X-ray crystallographic analysis of sulfide:quinone oxidoreductase from Acidithiobacillus ferrooxidans. *Acta Crystallogr Sect F Struct Biol Cryst Commun* **65**, 839-42.
87. Shibata, H., Takahashi, M., Yamaguchi, I. & Kobayashi, S. (1999). Sulfide oxidation by gene expressions of sulfide-quinone oxidoreductase and ubiquinone-8 biosynthase in Escherichia coli. *J Biosci Bioeng* **88**, 244-9.
88. Brasseur, G., Levican, G., Bonnefoy, V., Holmes, D., Jedlicki, E. & Lemesle-Meunier, D. (2004). Apparent redundancy of electron transfer pathways via bc(1) complexes and terminal oxidases in the extremophilic chemolithoautotrophic Acidithiobacillus ferrooxidans. *Biochim Biophys Acta* **1656**, 114-26.
89. Shahak, Y. & Hauska, G. (2008). Sulfide oxidation from cyanobacteria to humans: Sulfide–Quinone Oxidoreductase (SQR). *Sulfur Metabolism in Phototrophic Organisms*, 319-335.
90. Pham, V. H., Yong, J. J., Park, S. J., Yoon, D. N., Chung, W. H. & Rhee, S. K. (2008). Molecular analysis of the diversity of the sulfide : quinone reductase (sqr) gene in sediment environments. *Microbiology* **154**, 3112-21.
91. Grieshaber, M. K. & Volkel, S. (1998). Animal adaptations for tolerance and exploitation of poisonous sulfide. *Annu Rev Physiol* **60**, 33-53.
92. Chen, Z. W., Koh, M., Van Driessche, G., Van Beeumen, J. J., Bartsch, R. G., Meyer, T. E., Cusanovich, M. A. & Mathews, F. S. (1994). The structure of flavocytochrome c sulfide dehydrogenase from a purple phototrophic bacterium. *Science* **266**, 430-2.
93. Otwinowski, Z., Minor, W. & W Jr, C. C. (1997). Processing of X-ray diffraction data collected in oscillation mode.
94. Kabsch, W. (1993). Automatic processing of rotation diffraction data from crystals of initially unknown symmetry and cell constants. *Journal of Applied Crystallography* **26**, 795-800.
95. Vagin, A. & Teplyakov, A. (1997). MOLREP: an Automated Program for Molecular Replacement. *Journal of Applied Crystallography* **30**, 1022-1025.
96. McCoy, A. J., Grosse-Kunstleve, R. W., Adams, P. D., Winn, M. D., Storoni, L. C. & Read, R. J. (2007). Phaser crystallographic software. *J Appl Crystallogr* **40**, 658-674.
97. Afonine, P., Grosse-Kunstleve, R. & Adams, P. (2005). The Phenix refinement framework. *CCP4 newsletter* **42**.
98. Emsley, P. & Cowtan, K. (2004). Coot: model-building tools for molecular graphics. *Acta Crystallogr D Biol Crystallogr* **60**, 2126-32.
99. Laskowski, R. A., MacArthur, M. W., Moss, D. S. & Thornton, J. M. (1993). PROCHECK: a program to check the stereochemical quality of protein structures. *Journal of applied crystallography* **26**, 283-291.
100. Schrodinger, L. (2010). The PyMOL Molecular Graphics System. Version 1.3r1.

101. Krissinel, E. & Henrick, K. (2007). Inference of macromolecular assemblies from crystalline state. *J Mol Biol* **372**, 774-97.
102. Shahak, Y., Klughammer, C., Schreiber, U., Padan, E., Herrman, I. & Hauska, G. (1994). Sulfide-quinone and sulfide-cytochrome reduction in Rhodobacter capsulatus. *Photosynth Res* **39**, 175-81.
103. Johnson, J. E. & Cornell, R. B. (1999). Amphitropic proteins: regulation by reversible membrane interactions (review). *Mol Membr Biol* **16**, 217-35.
104. White, S. H. & Wimley, W. C. (1994). Peptides in lipid bilayers: structural and thermodynamic basis for partitioning and folding. *Current Opinion in Structural Biology* **4**, 79-86.
105. Flint, D. H. (1996). Escherichia coli contains a protein that is homologous in function and N-terminal sequence to the protein encoded by the nifS gene of Azotobacter vinelandii and that can participate in the synthesis of the Fe-S cluster of dihydroxy-acid dehydratase. *Journal of Biological Chemistry* **271**, 16068-16074.
106. Lagoutte, E., Mimoun, S., Andriamihaja, M., Chaumontet, C., Blachier, F. & Bouillaud, F. (2010). Oxidation of hydrogen sulfide remains a priority in mammalian cells and causes reverse electron transfer in colonocytes. *Biochim Biophys Acta* **1797**, 1500-11.
107. Lavu, M., Bhushan, S. & Lefer, D. J. (2011). Hydrogen sulfide-mediated cardioprotection: mechanisms and therapeutic potential. *Clin Sci (Lond)* **120**, 219-29.
108. Marcia, M., Langer, J. D., Parcej, D., Vogel, V., Peng, G. & Michel, H. (2010). Characterizing a monotopic membrane enzyme. Biochemical, enzymatic and crystallization studies on Aquifex aeolicus sulfide:quinone oxidoreductase. *Biochim Biophys Acta* **1798**, 2114-23.
109. Sambrook, J., Maniatis, T. & Fritsch, E. F. (1989). *Molecular cloning: a laboratory manual*, Cold Spring Harbor Laboratory.
110. Morton, R. A. (1965). *Spectroscopy of quinones and related substances.* Biochemistry of Quinones (Morton, R. A., Ed.), Academic Press Inc, London.
111. Leslie, A. G. (2006). The integration of macromolecular diffraction data. *Acta Crystallogr D Biol Crystallogr* **62**, 48-57.
112. Evans, P. (2006). Scaling and assessment of data quality. *Acta Crystallogr D Biol Crystallogr* **62**, 72-82.
113. Adams, P. D., Afonine, P. V., Bunkoczi, G., Chen, V. B., Davis, I. W., Echols, N., Headd, J. J., Hung, L. W., Kapral, G. J., Grosse-Kunstleve, R. W., McCoy, A. J., Moriarty, N. W., Oeffner, R., Read, R. J., Richardson, D. C., Richardson, J. S., Terwilliger, T. C. & Zwart, P. H. (2010). PHENIX: a comprehensive Python-based system for macromolecular structure solution. *Acta Crystallogr D Biol Crystallogr* **66**, 213-21.
114. Jacob, C., Giles, G. I., Giles, N. M. & Sies, H. (2003). Sulfur and selenium: the role of oxidation state in protein structure and function. *Angew Chem Int Ed Engl* **42**, 4742-58.
115. Zhang, Y. & Weiner, J. H. (2014). Characterization of the kinetics and electron paramagnetic resonance spectroscopic properties of Acidithiobacillus ferrooxidans sulfide:quinone oxidoreductase (SQR). *Arch Biochem Biophys* **564**, 110-9.
116. Steudel, R. (1996). Mechanism for the formation of elemental sulfur from aqueous sulfide in chemical and microbiological desulfurization processes. *Industrial & engineering chemistry research* **35**, 1417-1423.

117. Hadley, J. H., Jr. & Gordy, W. (1974). Nuclear coupling of 33S and the nature of free radicals in irradiated crystals of cystine dihydrochloride: Part II, charged radicals. *Proc Natl Acad Sci U S A* **71**, 4409-13.
118. Lawrence, C. C., Bennati, M., Obias, H. V., Bar, G., Griffin, R. G. & Stubbe, J. (1999). High-field EPR detection of a disulfide radical anion in the reduction of cytidine 5'-diphosphate by the E441Q R1 mutant of Escherichia coli ribonucleotide reductase. *Proc Natl Acad Sci U S A* **96**, 8979-84.
119. Ishikita, H. (2007). Influence of the protein environment on the redox potentials of flavodoxins from Clostridium beijerinckii. *J Biol Chem* **282**, 25240-6.
120. Holmes, D. S. & Bonnefoy, V. (2007). Genetic and bioinformatic insights into iron and sulfur oxidation mechanisms of bioleaching organisms. In *Biomining*, pp. 281-307. Springer.
121. Theissen, U., Hoffmeister, M., Grieshaber, M. & Martin, W. (2003). Single eubacterial origin of eukaryotic sulfide: quinone oxidoreductase, a mitochondrial enzyme conserved from the early evolution of eukaryotes during anoxic and sulfidic times. *Molecular biology and evolution* **20**, 1564-1574.
122. Shibata, H. & Kobayashi, S. (2006). Characterization of a HMT2-like enzyme for sulfide oxidation from Pseudomonas putida. *Can J Microbiol* **52**, 724-730.
123. Cherney, M. M., Zhang, Y., James, M. N. & Weiner, J. H. (2012). Structure-activity characterization of sulfide:quinone oxidoreductase variants. *J Struct Biol* **178**, 319-328.
124. Sodeoka, M., C. J. Larson, L. Chen, K. P. LeClair, and G. L. Verdine. (1993). A Multifunctional Plasmid for Protein Expression by ECPCR: Overproduction of the p50 Subunit of NF-kB. *Bioorg. Med. Chem. Lett.* **3**, 1089-1094.
125. Bradford, M. M. (1976). A rapid and sensitive method for the quantitation of microgram quantities of protein utilizing the principle of protein-dye binding. *Anal Biochem* **72**, 248-254.
126. Weiner, J. H. & Dickie, P. (1979). Fumarate reductase of Escherichia coli. Elucidation of the covalent-flavin component. *J Biol Chem* **254**, 8590-8593.
127. Shahak, Y., Klughammer, C., Schreiber, U., Padan, E., Herrman, I. & Hauska, G. (1994). Sulfide-quinone and sulfide-cytochrome reduction in *Rhodobacter capsulatus*. *Photosynthesis Research* **39**, 175-181.
128. Hastings, S. F., Kaysser, T. M., Jiang, F., Salerno, J. C., Gennis, R. B. & Ingledew, W. J. (1998). Identification of a stable semiquinone intermediate in the purified and membrane bound ubiquinol oxidase-cytochrome bd from Escherichia coli. *Eur J Biochem* **255**, 317-23.
129. Müller, F., Brüstlein, M., Hemmerich, P., Massey, V. & Walker, W. H. (1972). Light‐Absorption Studies on Neutral Flavin Radicals. *European Journal of Biochemistry* **25**, 573-580.
130. Chakrabarti M.H. & E.P.L., R. (2008). Analysis of mixtures of ferrocyanide and ferricyanide using UV–visible spectroscopy for characterization of a novel redox flow battery. *Journal of The Chemical Society of Pakistan* **30**, 817–823.
131. Gutierrez, A., Lian, L. Y., Wolf, C. R., Scrutton, N. S. & Roberts, G. C. (2001). Stopped-flow kinetic studies of flavin reduction in human cytochrome P450 reductase and its component domains. *Biochemistry* **40**, 1964-75.
132. Moxley, M. A. & Becker, D. F. (2012). Rapid reaction kinetics of proline dehydrogenase in the multifunctional proline utilization A protein. *Biochemistry* **51**, 511-20.

133. Maklashina, E., Iverson, T. M., Sher, Y., Kotlyar, V., Andrell, J., Mirza, O., Hudson, J. M., Armstrong, F. A., Rothery, R. A., Weiner, J. H. & Cecchini, G. (2006). Fumarate reductase and succinate oxidase activity of Escherichia coli complex II homologs are perturbed differently by mutation of the flavin binding domain. *J Biol Chem* **281**, 11357-65.
134. Chovancova, E., Pavelka, A., Benes, P., Strnad, O., Brezovsky, J., Kozlikova, B., Gora, A., Sustr, V., Klvana, M., Medek, P., Biedermannova, L., Sochor, J. & Damborsky, J. (2012). CAVER 3.0: a tool for the analysis of transport pathways in dynamic protein structures. *PLoS Comput Biol* **8**, e1002708.
135. Szabó, C. (2007). Hydrogen sulphide and its therapeutic potential. *Nature Reviews Drug Discovery* **6**, 917-35.
136. Natusch, D. F., Sewell, J. R. & Tanner, R. L. (1974). Determination of hydrogen sulfide in air--an assessment of impregnated paper tape methods. *Anal Chem* **46**, 410-5.
137. MacFaddin, J. F. (2000). *Biochemical tests for identification of medical bacteria*. 3rd ed. edit, Lippincott Williams & Wilkins, Philadelphia.
138. Pluth, M. D., Bailey, T. S., Hammers, M. D. & Montoya, L. A. (2013). Chemical Tools for Studying Biological Hydrogen Sulfide.
139. Sambasivarao, D. & Weiner, J. H. (1991). Differentiation of the multiple S-and N-oxide-reducing activities ofEscherichia coli. *Current Microbiology* **23**, 105-110.
140. Abràmoff, M. D., Magalhães, P. J. & Ram, S. J. (2004). Image processing with ImageJ. *Biophotonics international* **11**, 36-42.
141. Laemmli, U. K. (1970). Cleavage of structural proteins during the assembly of the head of bacteriophage T4. *Nature* **227**, 680-685.
142. Sirdeshmukh, D. B., Sirdeshmukh, L. & Subhadra, K. G. (2006). Micro- and macro-properties of solids thermal, mechanical and dielectric properties. In *Springer series in materials science,*, pp. xvii, 403 p. Springer-Verlag, Berlin.
143. Brandt, R. B., Laux, J. E. & Yates, S. W. (1987). Calculation of inhibitor Ki and inhibitor type from the concentration of inhibitor for 50% inhibition for Michaelis-Menten enzymes. *Biochem Med Metab Biol* **37**, 344-9.
144. Morris, G. M., Huey, R., Lindstrom, W., Sanner, M. F., Belew, R. K., Goodsell, D. S. & Olson, A. J. (2009). AutoDock4 and AutoDockTools4: Automated docking with selective receptor flexibility. *Journal of computational chemistry* **30**, 2785-2791.
145. Trott, O. & Olson, A. J. (2010). AutoDock Vina: improving the speed and accuracy of docking with a new scoring function, efficient optimization, and multithreading. *J Comput Chem* **31**, 455-61.
146. Rich, P. R. (1996). Quinone binding sites of membrane proteins as targets for inhibitors. *Pesticide Science* **47**, 287-296.
147. Fisher, N. & Rich, P. R. (2000). A motif for quinone binding sites in respiratory and photosynthetic systems. *Journal of Molecular Biology* **296**, 1153-1162.
148. Bertero, M. G., Rothery, R. A., Boroumand, N., Palak, M., Blasco, F., Ginet, N., Weiner, J. H. & Strynadka, N. C. (2005). Structural and biochemical characterization of a quinol binding site of *Escherichia coli* nitrate reductase A. *J Biol Chem* **280**, 14836-43.
149. Maklashina, E. & Cecchini, G. (1999). Comparison of catalytic activity and inhibitors of quinone reactions of succinate dehydrogenase (Succinate-ubiquinone oxidoreductase) and fumarate reductase (Menaquinol-fumarate oxidoreductase) from *Escherichia coli*. *Arch Biochem Biophys* **369**, 223-32.

150. Zheng, Z., Dutton, P. L. & Gunner, M. (2010). The measured and calculated affinity of methyl ‐ and methoxy ‐ substituted benzoquinones for the QA site of bacterial reaction centers. *Proteins: Structure, Function, and Bioinformatics* **78**, 2638-2654.
151. Rothery, R. A., Seime, A. M., Spiers, A. M., Maklashina, E., Schroder, I., Gunsalus, R. P., Cecchini, G. & Weiner, J. H. (2005). Defining the Q-site of *Escherichia coli* fumarate reductase by site-directed mutagenesis, fluorescence quench titrations and EPR spectroscopy. *FEBS J* **272**, 313-26.
152. Maklashina, E., Hellwig, P., Rothery, R. A., Kotlyar, V., Sher, Y., Weiner, J. H. & Cecchini, G. (2006). Differences in protonation of ubiquinone and menaquinone in fumarate reductase from *Escherichia coli*. *J Biol Chem* **281**, 26655-64.
153. Marcia, M., Ermler, U., Peng, G. & Michel, H. (2009). The structure of *Aquifex aeolicus* sulfide: quinone oxidoreductase, a basis to understand sulfide detoxification and respiration. *Proceedings of the National Academy of Sciences* **106**, 9625-9630.
154. Dahl, C. & Prange, A. (2006). Bacterial sulfur globules: occurrence, structure and metabolism. *Inclusions in Prokaryotes*, 21-51.
155. Steudel, R. (1996). Mechanism for the Formation of Elemental Sulfur from Aqueous Sulfide in Chemical and Microbiological Desulfurization Processes. *Industrial & Engineering Chemistry Research* **35**, 1417-1423.
156. Urich, T., Gomes, C. M., Kletzin, A. & Frazão, C. (2006). X-ray Structure of a self-compartmentalizing sulfur cycle metalloenzyme. *Science* **311**, 996-1000.
157. Prange, A., Chauvistré, R. & Modrow, H. (2002). Quantitative speciation of sulfur in bacterial sulfur globules: X-ray absorption spectroscopy reveals at least three different species of sulfur. ....
158. Prange, A., Arzberger, I., Engemann, C., Modrow, H., Schumann, O., Trüper, H. G., Steudel, R., Dahl, C. & Hormes, J. (1999). In situ analysis of sulfur in the sulfur globules of phototrophic sulfur bacteria by X-ray absorption near edge spectroscopy. *Biochimica et biophysica acta* **1428**, 446-454.
159. Prange, A., Dahl, C., Trüper, H. G., Behnke, M., Hahn, J., Modrow, H. & Hormes, J. (2002). Investigation of S-H bonds in biologically important compounds by sulfur K-edge X-ray absorption spectroscopy. *The European Physical Journal D* **20**, 589-596.
160. Pasteris, J., Freeman, J. & Goffredi, S. (2001). Raman spectroscopic and laser scanning confocal microscopic analysis of sulfur in living sulfur-precipitating marine bacteria 10.1016/S0009-2541(01)00302-3 : Chemical Geology | ScienceDirect.com. *Chemical Geology*.
161. Reinartz, M., Tschäpe, J., Brüser, T., Trüper, H. & Dahl, C. (1998). Sulfide oxidation in the phototrophic sulfur bacterium Chromatium vinosum. *Archives of Microbiology* **170**, 59-68.
162. Marcia, M., Ermler, U., Peng, G. & Michel, H. (2009). The structure of Aquifex aeolicus sulfide: quinone oxidoreductase, a basis to understand sulfide detoxification and respiration. *Proceedings of the National Academy of Sciences* **106**, 9625.
163. Wakai, S., Tsujita, M., Kikumoto, M., Manchur, M. A., Kanao, T. & Kamimura, K. (2007). Purification and characterization of sulfide:quinone oxidoreductase from an acidophilic iron-oxidizing bacterium, Acidithiobacillus ferrooxidans. *Bioscience, biotechnology, and biochemistry* **71**, 2735-2742.

164. Arieli, B., Shahak, Y., Taglicht, D., Hauska, G. & Padan, E. (1994). Purification and characterization of sulfide-quinone reductase, a novel enzyme driving anoxygenic photosynthesis in Oscillatoria limnetica. *The Journal of biological chemistry* **269**, 5705.
165. Bronstein, M., Schutz, M., Hauska, G., Padan, E. & Shahak, Y. (2000). Cyanobacterial sulfide-quinone reductase: cloning and heterologous expression. *Journal of Bacteriology* **182**, 3336.
166. Theissen, U. & Martin, W. (2008). Sulfide: quinone oxidoreductase (SQR) from the lugworm Arenicola marina shows cyanide-and thioredoxin-dependent activity. *FEBS Journal* **275**, 1131-1139.
167. Shibata, H. & Kobayashi, S. (2006). Characterization of a HMT2-like enzyme for sulfide oxidation from Pseudomonas putida. *Canadian Journal of Microbiology* **52**, 724-730.
168. Griesbeck, C., Schütz, M., Schödl, T., Bathe, S., Nausch, L., Mederer, N., Vielreicher, M. & Hauska, G. (2002). Mechanism of sulfide-quinone reductase investigated using site-directed mutagenesis and sulfur analysis. *Biochemistry* **41**, 11552-11565.
169. Cheng, V. W. T., Rothery, R. A., Bertero, M. G., Strynadka, N. C. J. & Weiner, J. H. (2005). Investigation of the environment surrounding iron-sulfur cluster 4 of Escherichia coli dimethylsulfoxide reductase. *Biochemistry* **44**, 8068-8077.
170. Rothery, R., Workun, G. & Weiner, J. (2008). The prokaryotic complex iron-sulfur molybdoenzyme family. *Biochimica et Biophysica Acta (BBA)-Biomembranes* **1778**, 1897-1929.
171. Castelle, C., Guiral, M., Malarte, G., Ledgham, F., Leroy, G., Brugna, M. & Giudici-Orticoni, M.-T. r. s. (2008). A new iron-oxidizing/O2-reducing supercomplex spanning both inner and outer membranes, isolated from the extreme acidophile Acidithiobacillus ferrooxidans. *The Journal of biological chemistry* **283**, 25803-25811.
172. Ishikawa, T., Sabharwal, D., Broms, J., Milton, D. L., Sjostedt, A., Uhlin, B. E. & Wai, S. N. (2012). Pathoadaptive conditional regulation of the type VI secretion system in Vibrio cholerae O1 strains. *Infect Immun* **80**, 575-84.
173. Wexler, M., Sargent, F., Jack, R. L., Stanley, N. R., Bogsch, E. G., Robinson, C., Berks, B. C. & Palmer, T. (2000). TatD is a cytoplasmic protein with DNase activity - No requirement for TatD family proteins in Sec-independent protein export. *Journal of Biological Chemistry* **275**, 16717-16722.
174. Ito, K., Hirota, Y. & Akiyama, Y. (1989). Temperature-sensitive sec mutants of Escherichia coli: inhibition of protein export at the permissive temperature. *J Bacteriol* **171**, 1742-3.
175. Fandl, J. P., Cabelli, R., Oliver, D. & Tai, P. C. (1988). SecA suppresses the temperature-sensitive SecY24 defect in protein translocation in Escherichia coli membrane vesicles. *Proc Natl Acad Sci U S A* **85**, 8953-7.